Experimental and Computational Analysis of Various Design Parameters of Automotive Component Using Rapid Prototyping

THESIS

Submitted in Delhi Technological University
for the award of the degree of

DOCTOR OF PHILOSOPHY
in
ENGINEERING

By

NAGENDRA KUMAR MAURYA
(2K14/PH.D/ME/11)

Under the Supervision of

Prof. Vikas Rastogi
Department of Mechanical, Industrial
Production and Automobile Engineering

Dr. Pushpendra Singh
Department of Mechanical, Industrial
Production and Automobile Engineering

DELHI TECHNOLOGICAL UNIVERSITY
DELHI - 110042 (INDIA)

NOVEMBER 2019

DELHI TECHNOLOGICAL UNIVERSITY
Shahabad Daulatpur, Main Bawana Road
Delhi-110042 (India)

DECLARATION

I hereby declare that the thesis entitled **"Experimental and Computational Analysis of Various Design Parameters of Automotive Component Using Rapid Prototyping"** submitted by me for the award of the degree of ***Doctor of Philosophy*** to **Delhi Technological University (Formerly Delhi College of Engineering)** is a record of *bonafide* work carried out by me under the guidance of Prof. Vikas Rastogi, DTU & and Dr. Pushpendra Singh, DTU

I further declare that the work reported in this thesis has not been submitted and will not be submitted, either in part or in full, for the award of any other degree or diploma in this Institute or any other Institute or University.

Nagendra Kumar Maurya
Reg No: 2K14/Ph.D/ME/11
Department of Mechanical, Industrial,
Production and Automobile Engineering
Place: New Delhi
Date:

DELHI TECHNOLOGICAL UNIVERSITY
Shahabad Daulatpur, Main Bawana Road
Delhi-110042 (India)

CERTIFICATE

This is to certify that the thesis entitled **"Experimental and Computational Analysis of Various Design Parameters of Automotive Component Using Rapid Prototyping"** submitted by **Mr. Nagendra Kumar Maurya** to **Delhi Technological University (Formerly Delhi College of Engineering)**, for the award of the degree of "*Doctor of Philosophy*" in Mechanical engineering is a record of *bona fide* work carried out by him. Nagendra Kumar Maurya has worked under our guidance and supervision and has fulfilled the requirements for the submission of this thesis, which to our knowledge has reached requisite standards.

The results contained in this thesis are original and have not been submitted to any other university or institute for an award of any degree or diploma.

Prof. Vikas Rastogi
Professor
Department of Mechanical, Industrial
Production and Automobile Engineering
Delhi Technological University (DTU)
Bawana, Delhi-110042

Dr. Pushpendra Singh
Associate Professor
Department of Mechanical, Industrial
Production and Automobile Engineering
Delhi Technological University (DTU)
Bawana, Delhi-110042

ACKNOWLEDGEMENTS

I would like to express my special appreciation and thanks to my advisors Prof. Vikas Rastogi and Dr. Pushpendra Singh, Department of Mechanical, Industrial, Production and Automobile Engineering, Delhi Technological University. They have been tremendous mentors for me. Perseverance, exuberance, positive approaches are just some of the traits they have imprinted on my personality. These lines are dedicated to my guides:

"गुरुर्ब्रह्मागुरुर्विष्णुर्गुरुर्देवोमहेश्वरः
गुरुः साक्षातपरब्रह्मातस्मैश्रीगुरवेनमः"

They steered me through this journey with their invaluable advice, positive criticism, stimulating discussions and consistent encouragement. If I would stand proud of my achievements, they are the main creditors undeniably. It is my privilege to be under their tutelage. Their advice on both research as well as on my career have been priceless. I would like to thank them for encouraging my research.

I would like to express my gratitude to Prof. Yogesh Singh, Vice chancellor, Delhi Technological University, Delhi for providing this opportunity to carry out this work in this prestigious institute.

I would like to thanks Prof. R.S. Mishra, DRC Chairman and Prof. Vipin Kumar, Head of the department of Mechanical Engineering, for their support to accomplish this work.

I wish to record my thank and gratitude to our all internal and external SRC experts, Prof. Anup Kumar Saha (NIT Durgapur), Late Prof. R.K. Srivastava (MNNIT Allahabad) and Prof. Atul Agrawal (Delhi Technological University) for their valuable guidance, critical and constructive discussion during this work.

I would like to thank my fellow lab mates especially Dr. Ashish Gupta, Anuj Sharma, Aakash and Yamika for helping and encouraging me throughout my research.

I also convey my sincere thanks to my faculty colleague Dr. Shashi Prakash Dwivedi, Dr. Ashish Kumar Srivastava, Dr. Ambuj Saxena, Mr. Manish Maurya, Mr. Avdhesh Tyagi, Mr. Rohit Sahu, Mr Pankaj Pachauri and Mr. Pramod Singh for their active support.

My sincere thanks to anonymous reviewers whose insightful and constructive comments and suggested revisions improved the organization and clarity of the research

I am greatly indebted to my parents for their love and blessings to see me scaling greater heights of life. I truly appreciate the support which I got from my elder brother Mr. Harikesh Maurya throughout my career. Without his motivation and encouragement, pursuit of this Ph.D. work would have never been possible.

With immense pleasure and delight, I would like to thank my wife Mrs. Ruby Maurya for giving me the mental and moral support in my highs and lows during this Ph. D. journey. I appreciate my baby, my little son Ojasav Maurya for abiding my ignorance and patience he showed during my Ph.D. Words can never say how grateful I am to both of you.

Finally, I would like to express my thanks to Almighty 'ॐ for giving me patience and strength to overcome all types of hindrances. The words of my inspiration during this journey:

"उद्यमेनहिसिध्यन्तिकार्याणिनमनोरथैः।
नहिसुप्तस्यसिंहस्यप्रविशन्तिमुखेमृगाः।।"

(Nagendra Kumar Maurya)

ABSTRACT

Manufacturing is one of the most vital wheel cogs for the developing country like India. Government of India is planning to increase the manufacturing capacity of the country and place the India as a manufacturing hub in the world map. India is planning to increase share of the manufacturing industry of the gross domestic product GDP. Prototyping is an important step for the conceptualization of any design and mould making process. Nowadays, several prototyping processes are available. Among all the available prototyping processes, rapid prototyping process takes minimum time to make the prototype model from the 3D CAD model. However, the quality of prototype model produced through rapid prototyping process is inferior over the traditional methods of prototyping. Several reports and published articles are available in the international and national journal & which show that the quality of prototype model produced through the rapid prototyping process is depends upon the printing process parameters.

The main focus of this research is to propose the methodology to improve the quality of prototype model developed through the commonly used rapid prototyping technology namely FDM and PolyJet. In this thesis, initially a comparison is being made for FDM and PolyJet technology. Comparative study are carried out on the basis of flatness, cylindricity, roundness, percentage errors in the linear dimension, percentage error in the radial dimension, surface roughness and cost of the prototype model developed via FDM and PolyJet process. For the comparative study of FDM and PolyJet technology, a complex shaped product, radial engine connecting rod was considered. The selected automotive component has cylindrical, linear, radial dimensions and flat surface.

FDM technology is the most widely used for the printing of prototype parts because of low cost. The quality of printed prototype parts through FDM process depends on the number of process parameters viz., layer thickness, infill pattern, orientation, raster angle, infill density, raster width, number of couture etc. Several studies have been conducted to get an optimum level of process parameters for the FDM process. However, very limited studies are available related to impact of process parameters i.e. infill pattern and infill density on dimensional accuracy, flatness and cylindricity of the fabricated component.

In this work, an attempt is being made to investigate the impact of important FDM process parameters i.e. layer thickness, orientation, infill pattern and infill density on flatness, cylindricity, percentage error in the linear dimension, percentage error in the radial domination. Taguchi's approach was applied for the selection of optimum level of process parameters. A regression model is also developed for the selected response factors in terms of process parameters. The developed models are good enough to predict the response factors within the experimental domain. For evaluating the goodness of fit of the model, *F-test* has been applied. Analysis of variance is employed to get the percentage contribution of individual process parameters. A multi Objective optimization 'Utility theory' is successfully applied to get the best level of process parameters which optimize all the selected response. International tolerance grades for the components fabricated through FDM process are investigated. It was found that tolerance grades of the fabricated samples are consistent.

Another focus of this work is to obtain an optimum level of process parameters for the PolyJet process. This study deals with the effect of process parameters viz.,

raster angle, orientation and type of surface finish on dimensional accuracy, flatness and surface roughness of the component fabricated through PolyJet process. Some research works have been reported few studies related to impact of PolyJet process parameters on surface roughness parameter R_a only. However, this work contains all the surface roughness parameters i.e. R_a, R_q and R_z are being considered as response variables. Regression models for the flatness, dimensional accuracy and roughness parameters are also developed. The main outcomes of these models are that they are well within the experimental domain.

It is generally noticed that strength of the component fabricated through rapid prototyping is less as compared to the traditional manufacturing process. In this work, a new methodology is presented to improve the tensile strength of the ABS and PLA component fabricated by FDM process. High strength PETG material is used as the reinforcement to improve the unidirectional tensile strength of the material. For validation of the experimental results, a computational model of the unidirectional reinforcement process is also developed. From experimental and computational study, it can be further concluded that due to reinforcement of high strength material, tensile strength of ABS and PLA materials are significantly improved. SEM analysis of the component printed along flat orientation and on-edge orientation is performed to visualize the surface of the fabricated components. Results illustrate that the component printed along flat orientation has less voids and air gaps in comparison to edge orientation.

There are some research work have been reported related to elastic deformation behavior of RGD840 material manufactured via PolyJet process. However, no attempt

is made to investigate the plastic strain in the material. This study also focus on experimental investigation of effect of process parameters on elastic modulus, fracture strength and percentage elongation of the component. Further, calculation of true stress, true strain and plastic strain are also carried out. The value of strength coefficient *(K)* and strain hardening coefficient (n_1) are calculated through graphical method from true stress and plastic strain curve. Numerical simulation is also performed to validate the experimental value of plastic strain. Results revealed that the numerical simulation of plastic strain is a close approximation of the experimental result.

Finally, the thesis contains a methodology for improving the clearance between matting parts. In this section, clearance analysis between matting part is calculated, which is based on model developed through archival literature. An assembly joint of automotive components are fabricated through the FDM process. It is observed that the shrinkage phenomena in the solid and hollow parts are different. Shrinkage in the hollow section was more as compared to the solid part.

Keywords: Analysis of variance, Automotive component, Cylindricity, Dimensional accuracy, Rapid prototyping, Flatness, Mechanical properties, Multi Objetive optimization, Signal to noise ratio, Tolerance grade, Taguchi approach, Plastic strain

TABLE OF CONTENTS

LIST OF FIGURES

LIST OF TABLES

LIST OF ABBREVIATIONS

ABS	Acrylonitrile Butadiene Styrene
AM	Additive Manufacturing
ANN	Artificial Neural Network
ANOVA	Analysis of Variance
BT	Build Time (Min)
CB	Carbon Black
CAD	Computer Aided Design
CAA	Computer Aided Accuracy
CI	Confidence Interval
CCD	Central Composite Design
CMM	Coordinate Measuring Machine
CT	Computed Tomography
DA	Dimensional Accuracy
df	Degree of Freedom
DFM	Dynamic Flexural Modulus (Mpa)
DPM	Degree of Particle Melt
DS	Dynamic Stiffness (Mpa)
FDM	Fused Deposition Modelling
FMC	Feedstock Material Consumption
FFF	Fused Filament Fabrication
GA	Genetic Algorithm
GRA	Grey Relational Analysis
GMDH	Group Method of Data Handling
HIPS	High Impact Polystyrene
IT	International Tolerance
LDM	Low-Temperature Deposition Manufacturing
LOM	Laminated Object Manufacturing
MRI	Magnetic Resonance Imaging
MSD	Mean-Square Deviation
OAs	Orthogonal Array

PLA	Polylactic Acid
PCA	Principal Component Analysis
PMMA	Polymethyl Methacrylate
PETG	Polyethylene Terephthalate Glycol
RP	Rapid Prototyping
RSM	Response Surface Methodology
SEM	Scanning Electron Microscope
SLA	Stereo-Lithography Apparatus
SLS	Selective Laser Sintering
SLM	Selective Laser Melting
SR	Surface Roughness
VC	Vacuum Casting

NOMENCLATURES

A_b	amount of build material consumed in (Kg)
A_s	amount of support material consumed in (Kg)
C_{lc}	labour cost in (INR)
C_m	machine cost in (INR)
C_b	unit cost per kg of build material in (INR)
C_s	unit cost per kg of support material in (INR)
Cy	cylindricity value in (mm)
Cy_{opt}	optimum value of cylindricity (mm)
D	geometric mean range of nominal size
D_m	measured dimension
D_n	nominal dimension
E	modulus of elasticity
Fy	flatness value in (mm)
Fy_{opt}	optimum value of flatness (mm)
f_j	degree of freedom of j^{th} parameter
F_j	F-ratio of j^{th} factor
F_1	raster angle
F_2	orientation on PolyJet platform
F_3	surface finish
i	fundamental tolerance in (μm)
K	strength coefficient (MPa)
% ΔL	percentage error in linear dimension
$\%\Delta L_{opt}$	optimum value of percentage error in linear dimension
n	tolerance unit
n_1	strain hardening exponent
R_a	average roughness height
R_q	mean roughness height
R_z	average peak to valley height

R_p	peak roughness height
R_v	peak valley height
R_t	peak height to peak valley height
$\%\Delta R$	percentage error in radial dimension
$\%\Delta R_{opt}$	optimum value of percentage error in radial dimension
S_T	total sum of square
SS_j	sum of square deviation of j^{th} factor
T_c	total cost in (INR)
t_{pre}	preprocessing time in (hrs)
t_{post}	post processing time in (hrs)
$U_i(Z_i)$	utility of the i^{th} attribute
V_j	variance of j^{th} parameter
V_e	variance of error
W_i	weight function
X_1	layer thickness (μm)
X_2	infill pattern
X_3	orientation
X_4	infill density (%)
Y	response function
Y_i	output response
$Y_{ave,}$	average value of data point
Y_0	target value
Z_i	measure of effectiveness of quality characteristics
Z_1	minimum acceptable value of quality characteristics
Z*	optimal value of quality characteristics

Greek Symbols

η	S/N ratio
η_0	overall mean
$\overline{\eta}$	average value of S/N ratio
σ^2	variance

$\% \Delta_t$	percentage error in dimensional accuracy along perpendicular direction from build tray in PolyJet process
σ_T	true stress (N/mm^2)
σ_E	engineering stress(N/mm^2)
ε_E	engineering strain (mm/mm)
ε_T	true strain (mm/mm)
ε_E	engineering strain (mm/mm)
ε_p	plastic strain
μ	poisson's ratio

Chapter 1
Introduction

Chapter 1
Introduction

1.1 Motivation

The incessant quest for better productivity and efficiency across the entire spectrum of manufacturing industries has ensured that products are subjected to manufacturing processes keeping a close relationship between rates of production and cost of product [1]. Manufacturing has always been considered as one of the most vital cogs in the wheel of development and industrial revolution. According to World Economic Forum (WEF), in global manufacturing index, India ranked 30^{th} position in January 2018 [2]. In 2014, Our Honourable Prime minister of India *Mr Narendra Modi* had taken an initiative of 'Make in India' drive. The purpose of this drive isto present India as a manufacturing hub for global recognition. With this drive, Government of India plans to enhance the sharing of manufacturing sector from *16%* to *25%* of gross domestic product (GDP) by 2022. It is anticipated that by 2020, India will become the 5^{th} largest manufacturing nation globally [3].

According to the NITI Aayog report (2018) published by Government of India, by 2022-23, India should be among the top 50 countries in global Innovation index. For this India is planning to spend *2%* of GDP on research and development activity with equal share of public and private sectors. India is promoting to advance manufacturing technology and innovation like industry *4.0* through which growth of manufacturing sector can be double by 2022. India is progressing to become hi-tech manufacturing hub. The possibilities in Indian market are attracting the Global giants such as Siemens, Boeing, HTC, Toshiba and GE. These organisations have either set up or are in the process of setting up manufacturing plants in India.

The primary motivation of this research work came from the recent trends in development of product variety and reduction of lead time for product development cycle. Making a prototype model is one of the critical steps in the development of a new product. Rapid prototyping has become a solution for making prototype models globally. Rapid prototyping (RP) is an innovation in which components are generated in layer-by-layer arrangement. It is one of the fastest-growing technologies by which prototypes model of any component can be built in just a few hours from 3D CAD design. Complexity of shape is not an issue in the RP process. It provides the designer opportunity of verifying shapes of the product and validate if it fits into an assembly with the desired functions. It is used in mechanical design, aerospace, medical application, arts and architecture etc.The next subsection will provide an overview of various rapid prototyping processes.

1.2 Overview of the rapid prototyping process

Prototypes are most important for the conceptualisation of design, manufacturing and analysis of design. Among all the available prototyping techniques, rapid prototyping takes minimum time to fabricate physical model from 3D CAD data. Rapid prototypes are commonly used for the reduction of lead time at various stages of product development cycle [4-5]. RP process was initially started to make prototypes, which were deemed very costly for the final products. However, recently with the introduction of numerous inexpensive desktop printers, it is used for the low volume production [6]. Nowadays, several rapid prototyping technologies are commercially available like Stereolithography (SL), Selective Laser Sintering (SLS), Fused Deposition Modeling (FDM), Laminated Object Manufacturing (LOM) etc. [7]. Each technology is working

on a different principle of operation. RP technology has a limitation that most of the available materials are not suitable for RP technology. This limitation can be overcome by evolution of new materials in future [8-9]. The next sub-section will provide the evolution of rapid prototyping process.

1.3 Evolution of rapid prototyping process

Rapid prototype technologies are fully automated systems, which requires 3D CAD model only. 3D CAD models are sliced into number of small layers with the help of software associated with printers. Sometimes these technologies are also refereed as layered manufacturing or solid freeform fabrication [10]. Additive manufacturing builds physical models in two-dimensional layers. Rapid prototype has potential to make complex shape models in a single component.

In 1983, Charles (Chuck) Hull has invented the first Stereolithography (SLA) machine, patented in 1986 and commercially available in 1988. It is a rapid manufacturing technology, which can be used for the development of physical models, pattern making, prototype/scaled model in layer-by-layer fashion using photo-polymerization process. In 1987, Carl Deckard developed powder-based rapid prototyping technology known as Selective Laser Sintering (SLS) and patent was issued to him in1989 by the US government. Scott crump has developed a solid-based rapid prototype in 1989 known as Fused Deposition Modeling(FDM) and got patent in 1992 to Stratasys company. In 1993 Inkjet technology was launched by Massachusetts Institute of Technology (MIT) and Z Corporation has got a license. The historical developments of rapid prototyping process are shown in Figure 1.1. The next section will provide the classification of various methods used for the prototyping process.

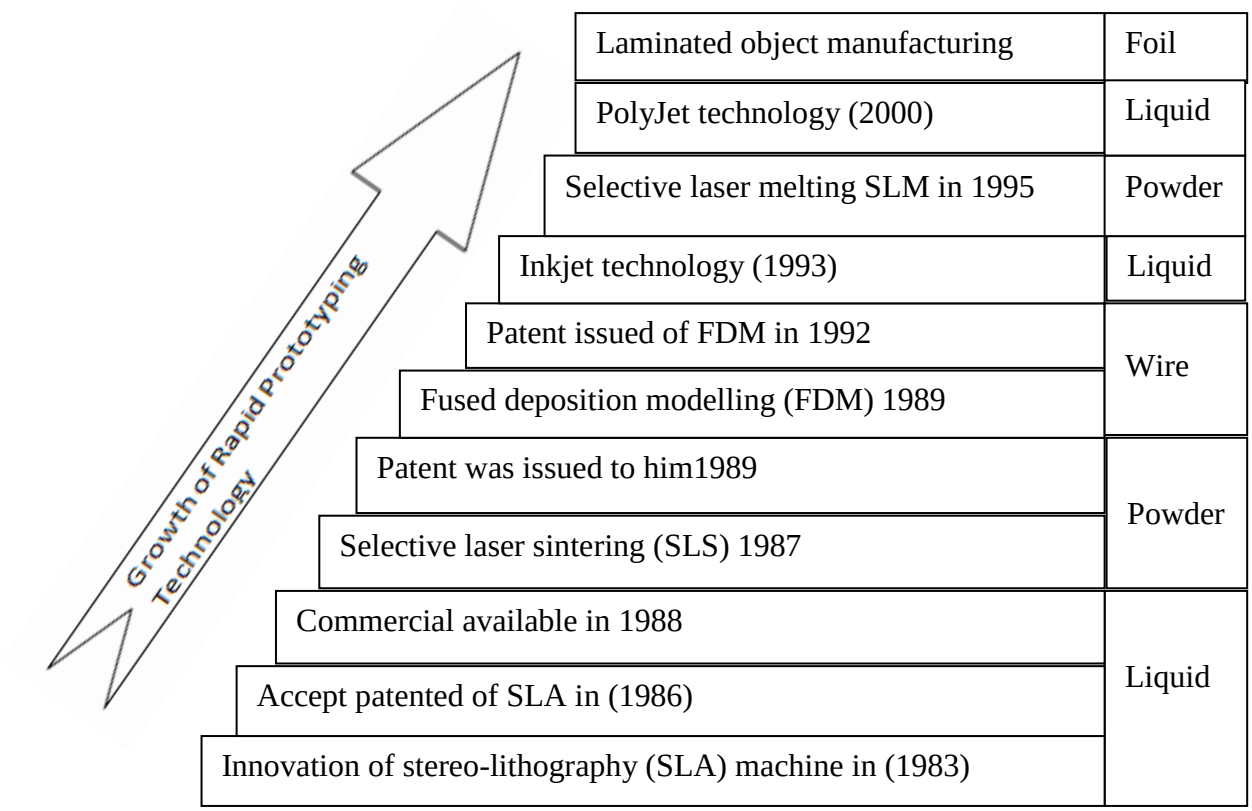

Figure 1.1: Historical development of rapid prototyping technology

1.4 Classification of the prototyping process

Currently, several methods are used for the manufacturing of prototype model. Figure 1.2 demonstrates the classification of fabrication techniques used for the development of a prototype component. Among all the available prototyping process, a rapid prototyping technique takes minimum duration for creating physical prototype model from the 3D CAD data. Rapid prototyping process can be further classified based on types of material supply used for the fabrication of component. Each technology works on different principle. Each technology has its advantage and disadvantage. Depending on technology material can be used in the form of powder, liquid, foil and wire. In this work, methods of prototyping are classified based on different processes used for the manufacturing of prototype models.

Further, rapid prototyping technologies are classified based on material used for the manufacturing of physical models. The next sub-section will provide the working procedure ofcritical rapid prototyping processes used for the manufacturing of physical model.

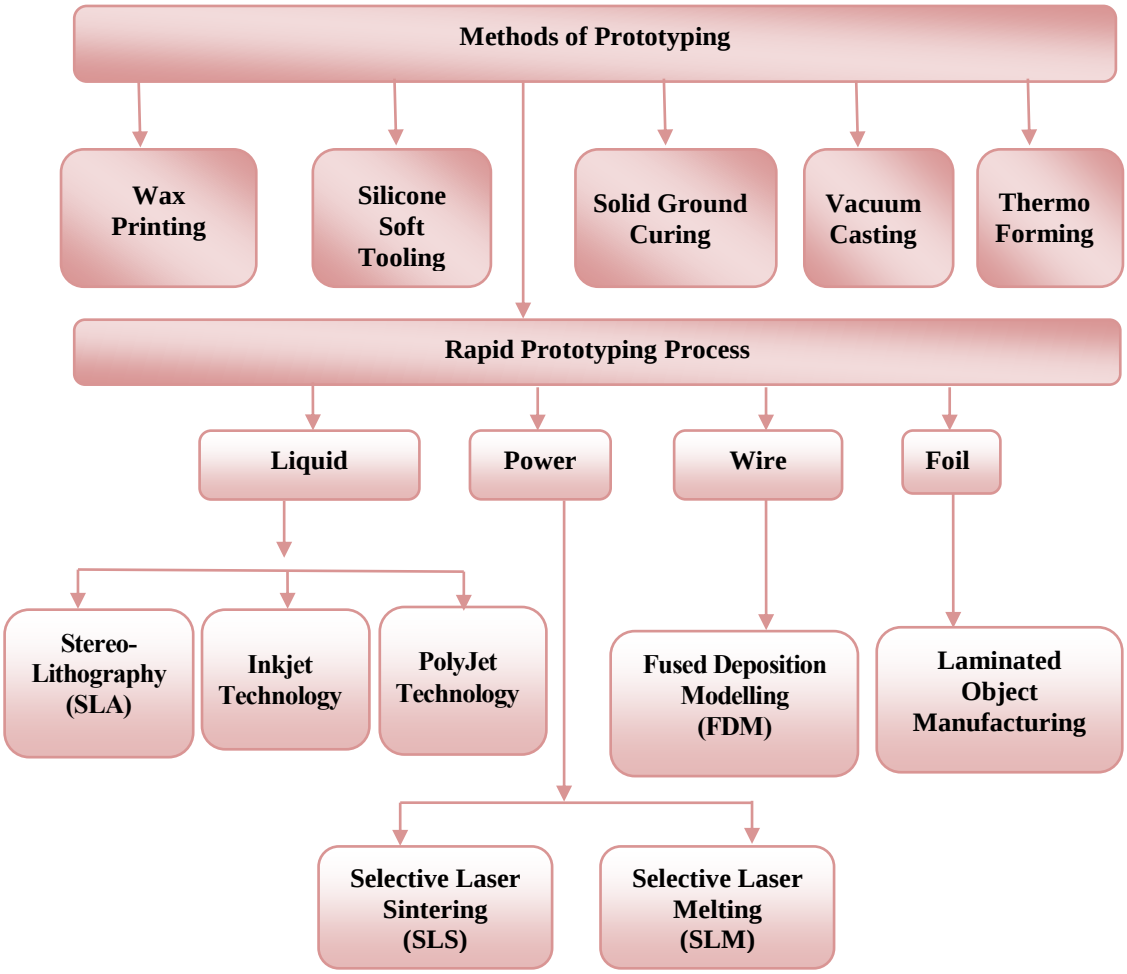

Figure 1.2: Classification of prototyping methods

1.4.1 Stereolithography

Stereolithography (SLA) was the first RP technology, developed in 1986 and become commercially available in1988. In this process, a perforated platform is used just below the surface of a vat of liquid photocurable polymer [11]. In SLA process, UV laser

beams were used to trace the first slice of the component to be fabricated and hardened thin layer of photopolymer material. The platform is lowered one layer thickness after tracing, and this process will be contained until the fabrication completed. The schematic block diagram of SLA process is as shown in Figure 1.3.

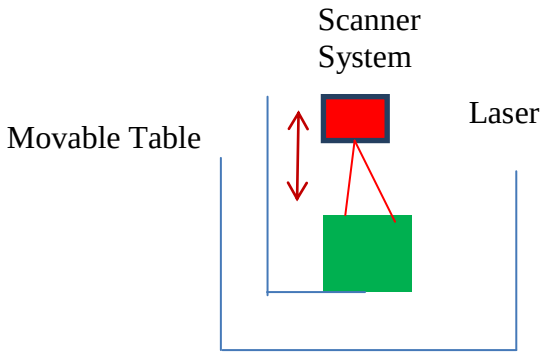

Figure 1.3: Stereolithography system

1.4.2 Fused deposition modeling

FDM technology was developed in 1988 and commercially available in 1992. In recent days FDM technology are in huge demand due to low cost and fast manufacturing rate. In the FDM process, a plastic filament is supplied to the extrusion nozzle, and the nozzle is heated to melt the material. There are mechanisms, which allow the flow of the melted material to be turned on and off. X-Y plotter type mechanism is used to trace the geometry as per the sliced CAD data. There is a provision of another nozzle, which is used to supply the support material. Support materials are used for providing support in the hollow structure. The entire system is attached within an adjacent chamber and maintains a constant chamber temperature below the melting point of the material. The schematic block diagram of FDM process is as shown in Figure 1.4.

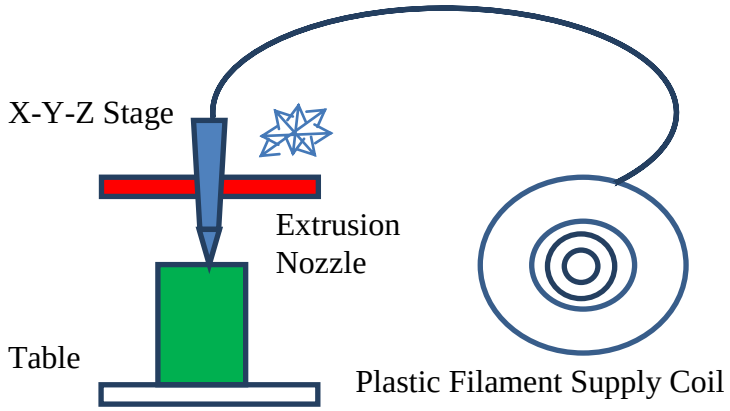

Figure 1.4: Fused deposition modelling system

1.4.3 Selective laser sintering (SLS)

SLA technology was developed in 1988. The schematic line diagram of SLS technology is shown in Figure1.5. In the SLS process, a roller is used to spread the power of build material over the surface of build cylinder. Piston in the cylinder moves down one layer thickness to form a new layer of powder. In material supply cylinder, piston moves in upward direction of one layer height to supply the measured quantity of powder for each layer. A laser beam is used to trace the surface of rigidly compacted powder, which melt and join the grains together to form a solid object. It is required to maintain the temperature of the fabrication chamber below the melting point of the powder.

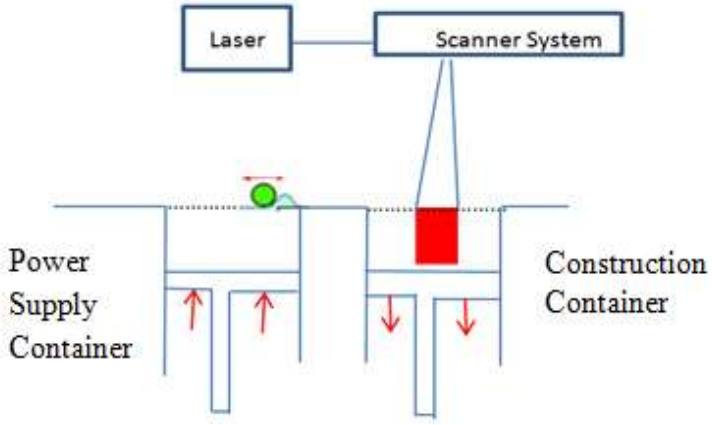

Figure 1.5: Selective laser sintering system

1.4.4 Inkjet 3D printing

MIT has developed the Inkjet technology in 1993.The schematic level block diagram for Inkjet printing is, as shown in Figure 1.6. In this method, single jet is used for each plastic build materials and support materials [12]. The liquids are fed to the jetting heads, which squirt tiny droplets of the materials when they are moved in X-Y direction in the specified pattern to generate a layer of the object. Material becomes hard due to the rapidly dropping in temperature. A milling head is passed over the layer after entire layer of the object is built to make it a uniform thickness. The process is continued until the complete object is built. After completion of object wax support material is either melted or dissolved away.

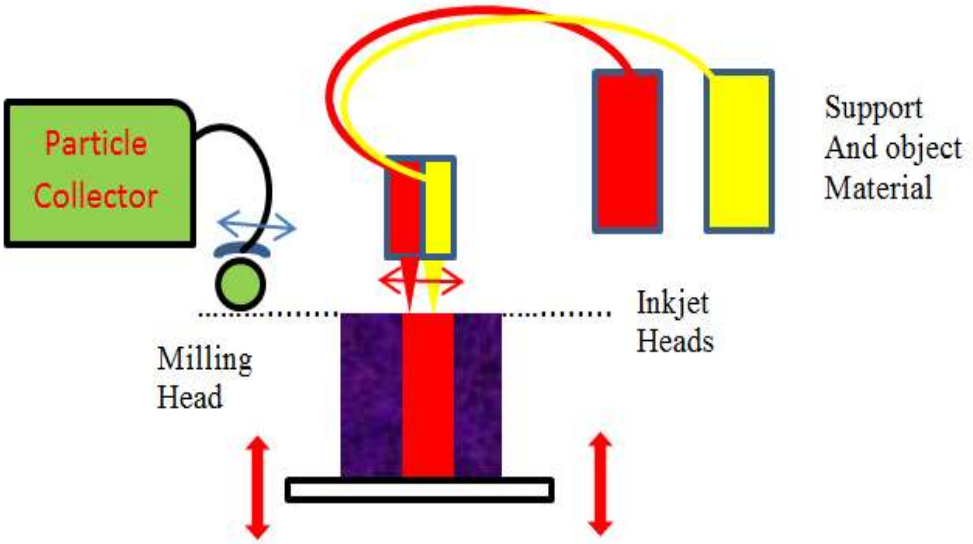

Figure 1.6: Inkjet technology

1.4.5 PolyJet 3D printing

Israeli company Objet geometries Ltd have developed the PolyJet 3D printing technology in 2000. It has the capability to replace the stereolithography (SLA) technology. In this method photopolymers are used for both builds as well as support.

Inkjet head is used to deposit build material as well as support material according to the predefined program. A UV flood lamp is attached with the print head to complete cure after depositing each layer of the build material. Pressurised water is used to remove the support material from the surface of the building geometry. The resolution of parts printed by PolyJet process equals to the SLA systems. There are several materials suitable available for PolyJet technologies. The major drawback of this technology is that print heads are costly and need to be replaced regularly. The schematic diagram for PolyJet system is shown in Figure 1.7.

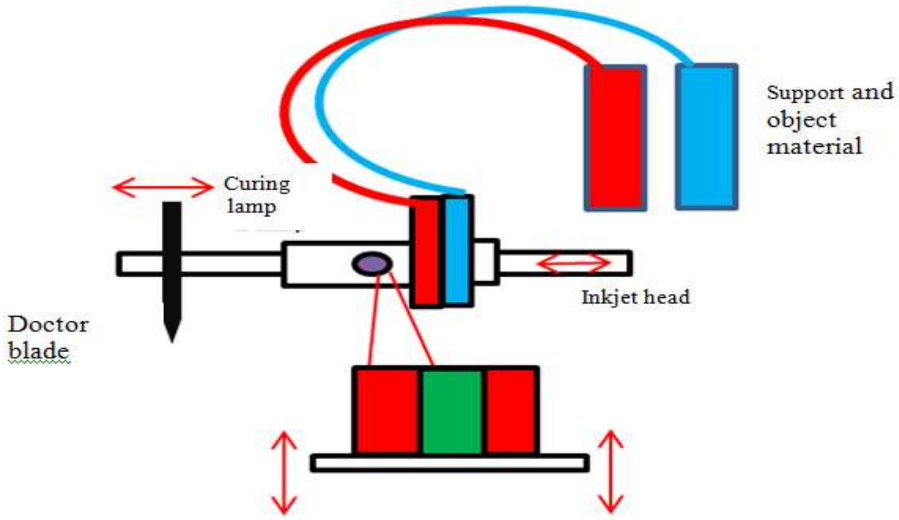

Figure 1.7: PolyJet 3D printing system

1.4.6 Laminated object manufacturing

LOM was developed in 2000 and Helisys is the commercial provider of LOM. In this technology, the laser is used to cut the profiles of object from paper or web materials. There is a provision of heating, which melts the plastic coating on the bottom side of the paper and first layer bonded to the previous layer. This process is continued until the complete object is built. An optics system is mounted to X-Y stage that traces the

profile of the object. Scrape paper is cut away after the cutting of each layer and separate the paper rolls. There is no requirement of support materials in this technology. In general, the accuracy of LOM object is not as good as compared to the other RP methods. However, the material cost is meagre as compared to other RP technology. Therefore, this method can be employed for physical visualisation of the design. The schematic diagram for LOM process is demonstrated in Figure 1.8.

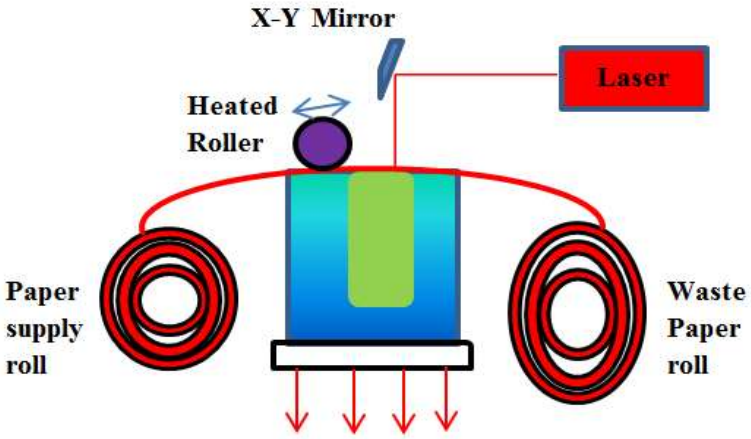

Figure 1.8: Laminated object manufacturing process

1.5 3D CAD modelling and STL file generation

Nowadays, several computer-aided design software (CAD) are available, which works on different algorithms to generate the solid object. Therefore to establish compatibility, a standard file format is required. A standard file format .STL (stereolithography) is adopted for all the rapid prototyping process. For creating 3D CAD model, most popular CAD software's are Auto CAD with mechanical desktop, CATIA, I-DEAS, Pro/Engineer, Unigraphics, Solid Works, and Solid Edge etc. In rapid prototyping process, components are fabricated in layer-by-layer, so CAD models are being sliced into small height thin layers. Slicing software is associated with every 3D printing

process, which converts CAD model into number of slice model and finally sliced model is saved in .STL file format. The next section will provide the classification of prototyping process.

1.6 Applications of rapid prototyping process

At present, RP process is extensively used for various engineering and medical application. RP process is used in the stage of conceptualization of new design, mould making, pattern making etc. In automotive industries often designers used scaled model of automotive component via additive manufacturing for aerodynamic testing. Prototyping of automotive components in-house through RP allows control of any Intellectual Property (IP) infringements and information leaks [13].The next subsection will provide the application of RP in the rapid tooling application.

1.6.1Application of rapid prototyping in rapid tooling

Recently, the manufacturing industries have major attention to reduce the lead time of the product development cycle. For the development of any new product, mould design plays a vital role and consumes lots of time. In modern-day rapid, prototyping is becoming a solution for making mould in less time and low cost. Some of the rapid tooling applications of RP are reported in literatureis reproduced here.

Lusic et al. [14] have manufactured CFRP-laminated moulds by using FDM technique. Authors have focused on minimizing the manufacturing cost, material consumption and lightweight design. CFRP-laminated mould was designed with maintaining stiffness in order to withstand deformation. This method of mould design reduces up-to 84% time of the mould design in comparison to conventional method. *Afonso et al. [15]* have highlighted the application of rapid prototyping in rapid tooling.

A sheet metal tool was manufactured by RP process. This sheet metal tool has sufficient strength and stiffness to withstand the low-pressure manufacturing process and moulding force. The surface quality and accuracy of the component was compatible with the large number of component. *Noble et al. [16]* have compared three moulding technique viz, CNC machining of plastic, 3D printing of plasticand CNC machining of aluminium for the injection moulding application. Fabricated moulds were compared based on quality, speed and difficulty. Results of measurement depict that resin-coated 3D printed moulds were better than other selected methods of rapid moulding technique.

Rahmati et al. [17] have fabricated injection tool for the injection moulding through Stereolithography (SLA) technology to minimize the time and fabrication cost. SL resin has the capability to withstand injection temperature, pressure and 500 injections were achieved. Failure mechanisms during injections were also investigated. It was suggested that failure of tools occurs either due to excessive flexural stress or shear stress induced in the injection tool. *Ding et al. [18]* have highlighted the integration of different methods of mould design to reduce the time and cost. System consists of four moulds viz., virtual prototyping, physical prototyping, digital prototyping and rapid tooling. Results depicted that intricate system had reduced the time required for the mould design.

Jiang et al. [19] have conducted theoretical and experimental study to evaluate the threshold overhang angle for the FDM process through which component can be fabricated without support material. It was observed that extrusion temperature and print speed had greatly influenced the printable threshold overhang angle. Strong

correlations between theoretical and experimental results were found.*Chen et al. [20]* have explored the processability of the overhanging structure through SLM method, which was challenging to process. The response of downward-facing surface morphology and melt pool dynamics process under various conditions were presented. Numerical simulations ware carried out to evaluate the underlying thermal physical mechanism in the dross formation phenomenon while SLM manufacturing overhanging surface. Results depicted that both low and high laser volume energy density had poor surface quality. A strong correlation between experimental and simulation results were observed. *Allaire et al. [21]* have evaluated shape optimization under overhang constraint condition. Components were fabricated through Fused Filament Fabrication methods and Electron Beam Melting technology. Results revealed that angle between build direction and structural boundary had influenced the quality of processed shape.

1.6.2 Medical application of RP

The demand for the rapid prototyping in the medical industry is increasing very rapidly due to its capability to fabricate 3D physical model from cloud point (CT scan or MRI) data. The first steps of the printing any medical model is to acquire high-resolution images. The image quality of MRI is better than CT scan image. Nowadays, low-resolution images are also getting available from ultrasound and being used for the printing of abnormal anatomies of a fetus *(Van Koevering et al.) [22]*.Medical images are being captured in the form of DICOM file format. DICOM image can be used as 2D sliced data set. Second step is to create a 3D surface from the 2D data set. This process is known as segmentation of data. It is done by the software. The next step is to prepare .STL file, required for all the 3D printing technology *Durfee et al. [23]*. Currently, RP is frequently used in several medical applications like Cardiac 3D printing, Low-cost

limb prosthetics and orthotics, printing of scaffolds, tissue-engineering etc. Some of the medical applications of RP reported by various researchers are presented in this section.

Santis et al. [24] have prepared scaffolds through the RP process for osteochondral tissue regeneration to evaluate the viscoelastic properties of magnetic nanocomposite. Poly (ε-caprolactone) and poly (ethylene glycol) materials were used for the fabrication scaffolds by using stereolithography approaches. Results depicted that poly (ethylene glycol) and poly (ε-caprolactone) based scaffolds was adequately reproduced articular cartilage tissues and viscoelastic properties of subchondral bone respectively. By combining SLA and FDM it was possible to manufacture a hybrid scaffold.

Nizam et al. [25] have optimized the dimensional accuracy of the model of the skull by using SLA process. Eight linear measurements of the four adult's skulls were measured by using the digital calliper. To check the accuracy of fabricated model, five replicates were manufactured, and average value of each measurement was selected. The absolute difference between actual human skulls and replica model was 0.23 mm found. The percentage error in the linear dimension was *0.08%*. *Vazquez et al. [26]* have prepared Si-doped Hydroxyapatite/Gelatine scaffolds by using RP process for application of drug delivery and bone regeneration. Results of microscopic study show that scaffolds produced by RP process were highly homogeneous. Mechanical properties of RP bone was found to be approximately equal to the tubular bone. *Inokoshi et al. [27]* fabricated dentures models by using RP technology to compare with conventional fabrication process. Results depicted that RP models were more accurate in comparison to the conventional process. *Bustamante et al. [28]* have fabricated a tracheobronchial tree by using RP technology to teach bronchoscopic anatomy. For this purpose, computed tomographic (CT) data were used for the

generation of physical model. *Boyer et al. [29]* have highlighted the application of additive manufacturing for patient-specific devices. Authors have demonstrated the antimicrobial properties, feasibility, CT scan imaging characterization etc. It was suggested that PVA printing with iodine, represent a unique platform to manufacture an antimicrobial and high-visibility devices.

Zopf et al. [30] have fabricated bioresorbable airway splint through the RP process and successfully implanted in a five-month-old baby in which a collapsed bronchus blocks the airflow to the lungs. CT scan data was used to design the splint, and polycaprolactone material was used to fabricate the patient's airway. *Salmi et al. [31]* have fabricated medical models (skulls) by using three different RP technique namely PolyJet, 3DP and SLS. The measurement was carried out by using the CMM. Results revealed that the DA of PolyJet model was best. The average dimensional accuracy in PolyJet component was found to be $0.18 \pm 0.12\%$.

Liu et al. [32] have used the LDM process to fabricate blood vessel, nerve tissue regenerations, tissue-engineered scaffolds for bone and cartilage. Biomedical applications, control parameters and challenges were discussed. Results depicted that for fabrication of vascular scaffold LDM process is better as compared to other traditional methods of making scaffold. The next subsection will provide the rapid tooling application of RP process.

1.7 Thesis scope

Keeping in view the worldwide scenario on rapid prototyping, the present research work has been undertaken to fulfil the following broad objective set for the present research work.

- Comparative studies of PolyJet techniques and FDM methods for printing prototype automotive parts
- Experimental analysis for the DA and SR by using various parameters and develop a mathematical model for the same
- Experimental analyses of flatness and cylindricity by both PolyJet and FDM methods
- Experimental investigations for improving part strength on FDM and PolyJet 3D printed parts
- Experimental investigations for clearance between mating parts.

1.8 Contribution of the thesis

The focus of the thesis is mainly directed towards experimental and computational analysis of design parameters of automotive components. The thesis contributesto analyses of the design parameters through rapid prototyping in the following aspects.

(a) **Comparative study of FDM and PolyJet technology:** Previously, many studies have been carried out to examine the products quality of the component manufactured by the FDM and PolyJet technology. The main focuses of the studies carried out in the archival literature are to analyses the effect of various process parameters on form errors and mechanical behaviour of the manufactured component. In this thesis, comparative study of FDM and PolyJet process was carried out for the manufacturing of prototype automotive component (connecting rod).

(b) **Experimental analysis of flatness, cylindricity and dimensional accuracy of the component fabricated through FDM process:** In this *chapter* of the

thesis, an attempt was made to evaluate the influence of variable on flatness, cylindricity and DA of the component fabricated through FDM process. A regression model was developed to forecast the form errors present in the component fabricated through the FDM process. In addition, a multi-objective optimization technique was also applied to find out the optimum level of process variable.

(c) **Investigation of dimensional accuracy, flatness and surface roughness of PolyJet component:**Impact of process parameters on DA, flatness and SR of the component fabricated component by Objet-30 (PolyJet) printer has been experimentally investigated. Taguchi approach was applied to perform experiments andobtained optimum level of process variable, with minimum number of experiments. All the surface roughness parameters were investigated. Furthermore, regression model in terms of process parameter were also developed.

(d) **Methodology for improving part strength:** A methodology for improving part strength of the component generated by FDM and PolyJet process were presented. For improving unidirectional tensile strength of ABS and PLA material, a high strength material (PETG) was used as reinforcement. Further, computational studies were also carried out to validate the experimental result.

Analysis of impact of process variables, on tensile strength and elastic modulus of RGD 840 material, manufactured by PolyJet process were highlighted. Various studies have been reported for the investigation of elastic behaviour of component generated through PolyJet process. However, no attempt was made to explore the plastic behaviour of RGD 840 material in the archival literature. In this work,

experimental and computational studies were carried out to illustrate the plastic strain, true stress and true strain of the material. Finally, a methodology for clearance analysis between mating pars were also presented.

1.9 Organization of thesis

The present thesis has been organized into *seven chapters*. The *first chapter* is introductory. It gives the fundamental goal with data and figures, which motivate author to persuade this research work. Further, a brief introduction about rapid prototyping and historical development of various RP techniques are well presented. It also illustrates the classification, working principle and various application of rapid prototyping. *Second chapter* is the literature review related to flatness, cylindricity, DA, SR and mechanical properties of important RP technology. A summary table of research work carried out related to form error, and mechanical properties are also presented.

Third chapter presents the comparative analysis of FDM and PolyJet technology. Automotive components were fabricated through MakerBot and Ultimaker FDM printer, and Objet30 PolyJet printer at optimum level of process parameters. Comparison was made based on various form errors present during fabrication and post-processing process & cost of the fabricated component. *Fourth chapter* presents experimental analysis of flatness, cylindricity and dimensional accuracy of the FDM components (connecting rod). Experiments were performed according to Taguchi theory. Further, multi-objective optimization and international tolerance grades were also calculated. *Fifth chapter* provides an insight into an experimental investigation of flatness and SR of PolyJet components. All the roughness parameters, i.e. R_a, R_z and R_q

were evaluated. *Sixth chapter* presents experimental and computational analysis of part strength of FDM and PolyJet components. Effect of PETG reinforcement on tensile strength of ABS and PLA material has been investigated. In addition, effect of process parameters on tensile strength and elastic modulus of RGD material was also discussed. Finally, a methodology for clearance analysis between mating parts of automotive components fabricated through FDM process was discussed. *Seventh chapter* presents conclusionof thesis. It concludes the primary outcomes of entire thesis and presents future direction of the research.

Chapter 2
Literature Review

Chapter 2
Literature Review

2.1 Introduction

The work embodied in the present thesis is the experimental and computational analysis of various design parameters of automotive components. A large number of works are available covering different aspects of form errors like dimensional accuracy, flatness, cylindricity and surface roughness. So, following subsection are mainly focused on discussing the literature available on investigation of surface roughness, flatness and cylindricity, characterization of mechanical properties and optimization of process parameters.

2.2 Investigation of form error

Various research works have been reported related to improvement of form errors in the component fabricated by RP technology. The major work was carried out to improve surface roughness, dimensional accuracy, flatness, cylindricity, roundness etc. The details of reported works related to form errors are highlighted in the next sub-sections.

2.2.1 Investigation of surface roughness

Kumar et al. [33] have conducted theoretical and experimental evaluation of SR of PolyJet additive manufacturing system. Process variable consist of the influence of final finishing, orientation of local surface and thickness of layer. It was observed that the orientation of local surface and final surface finishing are the most influencing process variables for the SR in the component fabricated through PolyJet process. The study revealed that SR distribution for PolyJet parts was different from the parts generated by

other AM technology. *Ahn et al. [34]* have conducted analytical and experimental study to determine the effect of local surface orientation and layer thickness in laminated object manufacturing (LOM) component. Further, an observation had been made that SR is increased with an increase in the height of layer, in all orientation. There was good agreement between the proposed analytical model and experimental value of surface roughness R_a.

Kechagias et al. [35] have fabricated tensile specimen of LPH042 and LPH080 prepared by LOM 1015 Helisys machine to investigate the surface roughness. Experiments were conducted by using Taguchi technique. The temperature and speed of heater, thickness of the layer and the speed of feeder, platform and laser are the process parameters which are employed for statistical analysis. A regression model was developed to relate the process variables and response factor. Statistical results revealed that the thickness of layer, speed of laser and temperature of heater is the main influencing parameters. *Galantucci et al. [36]* have analyzed the surface roughness in ABS component generated by FDM process. Measurement of surface roughness was performed in two-phase. In first phase, surface roughness was measured without chemical treatment, and in the second phase, SR was measured after the chemical treatment. Result shows that chemical treatment had significantly reduced the value of surface roughness. In this investigation process parameters considered were raster width, tip size and slice height.

Galantucci et al. [37] have fabricated a tensile specimen of ABS material to investigate the mechanical properties and surface roughness. Central composite designs (CCDs) were used for conducting the experiment. Surface roughness & mechanical

properties (flexural strength and tensile strength) were evaluated before and after chemical treatment. 10 % water and90% dimethylketone solution was used for the chemical treatment. The value of SR was significantly reduced after the chemical treatment in the post-processing stage. Mechanical properties of the ABS component were slightly reduced after chemical treatment. *Guerra et al. [38]* have fabricated microfluidic devices by using four different 3D printers namely FDM, SLA, FFF and PolyJet. A low-cost non-destructive system (photogrammetric scanning system) was applied for the measurement.

Kent et al. [39] have investigated the DA and surface roughness in the component fabricated by Objet 260 (PolyJet) printer. The selected component has both positive and negative features. Three different types of materials (RGD835, RGD525 & MED 610) were used for the investigation. It was found that DA and surface roughness in the PolyJet component were significantly affected by orientation. *Sachdeva et al. [40]* have used CCD design to optimize the roughness parameters, i.e. R_a, R_q and R_z in the component manufactured by SLS process. Four important process parameters viz., laser power (W), bed temperature (°C), scan spacing (mm) and hatch length (mm) was used for the investigation. Optimization results show that the optimum condition of process parameters for the surface roughness were laser power (24 W), bed temperature 175.02 °C, scan spacing 0.2 mm and hatch length 120 mm. *Singh et al. [41]* have fabricated master pattern by FDM process, which was required for the silica mould in vacuum casting (VC). In this investigation three response factor viz., linear dimension, radial dimension and surface roughness (R_a) was considered for the investigation. The tolerance grades of the selected dimensions were evaluated by using the ISO standard

UNI EN 20286-I and (1995) DIN16901. Total fifteen samples were fabricated at the optimum levels of process variable, which show that tolerance grades were consistent.

Shi et al. [42] have highlighted the application of robot for the post-processing of the 3D component manufactured by SLS process. It was observed that post-processed components had a better surface finish and dimensional accuracy. However, this technique cannot be applied for post-processing where the component has internal cavity or small inner radius whose curvature is smaller than tip radius.

2.2.2 Investigation of dimensional accuracy

Satyanarayana et al. [43] have manufactured replicated keys of ABS material by using FDM technology. Profile projector was used for the measurement of dimensions of the original key and key manufactured by RP process. Result of measurement shows that the dimensions of RP keys were close to the dimensions of original key. *Chen et al. [44]* have developed a five-axis hybrid RP system and low-cost FDM machine. In this process physical prototype model can be manufactured without using the support material. It can conduct five-axis machining. This hybrid system has better dimensional accuracy and surface finishing.

Pohit et al. [45] have manufactured plastic gears by FDM methods; the dimensions of these actual solid models were compared with the virtual gears. It was observed that dimensions of the RP gears matches quite well with their typical values obtained from software. Manufacturing processes of three different types of gears, namely helical, spur and bevel gears was simulated in a virtual environment. *Senthilkumaran et al. [46]* have demonstrated a new methodology to calculate shrinkage compensation in SLS process, which has improved the accuracy. In addition a mathematical model was also developed.

*Jain et al. [47]*use fused deposition modeling (FDM) for investment casting. Middle disc of Oldham coupling was made by sand casting and new investment casting. It was found that ABS pattern made by RP was strong then wax pattern. It was able to withstand rough handling. Wax pattern has excellent surface finish then ABS pattern. ABS pattern can be created faster comparatively. Wax pattern takes long lead times of up to 12 weeks. *Garrett et al. [48]* have highlighted the impact of process variables on DA and mechanical behaviour of PLA material fabricated by MakerBot replicator-2 3D desktop printer. Process variables, i.e. print orientation, layer thickness and infill density were used in the investigation. *Singh et al. [49]* have experimentally investigated the DA in the component fabricated by PolyJet technology. Three different types of materials viz., Full cure 720, Vero blue and Vero white were used for fabricating component. Dimensions were measured by using the CMM. IT grades were also calculated in this study. Results revealed that horizontal position was the most cost-effective condition for DA of Vero white' material.

Panda et al.[50] have suggested new methods to calculate volumetric error based on computer-aided design. It has capability to compute volumetric error present in the .CAT file before the fabrication. Effect of orientation and layer thickness on volumetric error was investigated. Several FDM components were fabricated to verify the purposed method. *Brajlih et al. [51]* have conducted comparative analysis in terms of speed and achievable accuracy of four different printers (EDEN330, EOSINT P385, SLA 3500 and prodigy plus). Similar components were fabricated by all the printers. Result shows that EOSINT P385 machine has highest manufacturing speed. Prodigy plus machine achieved lowest manufacturing speed. It was suggested that different mechanisms can be used within a certain range of speed. *Dimitrov et al. [52]* have fabricated components of ZP14

(starch-based powder), ZP100 (plaster-based powder) and infiltrated with wax and Zi580 agent. Dimensional accuracy and international tolerance (IT) grades were calculated for each dimension. Experiment was designed statistical techniques. Results revealed that DA of the fabricated components was within the 95% confidence interval (CI). IT grades of the fabricated component vary from IT9-IT16.

Chang et al. [53] have fabricated ABS component by using FDM technology to investigate the profile error and extruding features. Taguchi method was applied for conducting experiment. Process parameters contour depth, raster width and contour width were used for the investigation. Results revealed that contour width was the most significant process parameters for the profile errors in the RP component. *Chaudhari et al. [54]* have fabricated ABS component to evaluate the influence of process variables on SR, built time and cost of the manufactured parts. Taguchi L_9 orthogonal array was employed for conducting the experiment. The optimum process parameter condition viz., orientation YZ0, infill density 100%, layer thickness 0.3 mm and post-processing (paper polishing method).

2.2.3 Investigation of flatness and cylindricity

Senthilkumaran [1] has experimental investigated to check the impact of process variables viz., laser power, temperature, laser scanning speed and orientation on flatness & cylindricity of the component generated through SLS process. ASME Y14.5M-1994 codes were used for the measurement of flatness and cylindricity. Post-processing of the cloud point data was carried out by using polyworks software. For checking the goodness of the developed model for the flatness and cylindricity, ANOVA analysis was carried out. It was noticed that in case of cylindricity interaction effect was more dominant than special effect.

Knoop et al. [55] have evaluated the geometrical accuracy of holes and cylinders in the FDM component. Specimens were design ranging 3- 80 mm diameters. CMM was employed to measure the cylindricity of the inner and outer cylinders. Different filling pattern and shrink factors were used to improve the DA of the fabricated components. It was observed that the roundness in the component fabricated along XY-plane was better as compared to Z direction. The use of support material significantly affects the DA in Z alignment. *Paul et al. [8]* have suggested voxel-based approach to optimize the flatness and cylindricity with minimum utilization of support materials. Effect of orientation was investigated theoretically as well as experimentally. About 29-35% volume of the support material was reduced by using voxel-based approach. Furthermore a combined model for form error function and support volume function was developed, which minimised the volume of support material around 11-26%. *Saqib et al. [56]* have fabricated cope and drag casting components by using FDM technology. The effect of process parameters on distortion in manufactured component was analysed. Selected component have thick wall and thin wall features. Response was assessed in terms of flatness, perpendicularity and cylindricity. Results depict that forms and features have more impact on geometrical accuracy than process parameters.

2.3 Characterization of mechanical properties

The main drawback of all the rapid prototyping technologies is the poor mechanical properties as compared to other fabrication methods. In archival literature, several attempts were made for strength the mechanical properties of RP components. The next sub-section will provide the review of research work for improvement of mechanical properties for various RP techniques.

2.3.1 Characterization of mechanical properties of FDM component

Durgun and Ertan [57] have conducted experimental procedure for optimization of cost of ABS component fabricated and mechanical properties prepared with FDM process. The process parameters raster angle and orientation were used in this investigation. The result shows that process parameter raster angle '0' degree and orientation '0' degree were optimum conditions for mechanical properties. *Anna and Guceri [58]* have conducted experimental and computational investigation to examine the mechanical behaviour of ABS component generated by FDM process. Results revealed that material shows anisotropic behaviour. The process parameters, i.e. road, road to road interaction and path strongly affect the components mechanical behaviour. *Cantrell et al. [59]* have evaluated the tensile and shear properties of ABS component generated through FDM technology. It was found that process parameter, i.e. orientation and raster angle do not affect the tensile strength of material. However, shears strength varied up-to 33%. Result implies that tensile properties were not indicative of shear strength.

Mohamed et al. [60] have investigated the impact of process variables viz., number of contours, road width, raster angle, build orientation, layer thickness and air gap on the viscoelastic behaviour of the component manufactured by FDM technology.RSM was adopted for the conduction of experiment. Experimental results depicted that process parameters viz., number of contours, layer thickness and air gap were impartment process variables for the FDM technology. The optimal process parameters were found air gap of 0.0 mm, layer thickness of 0.3302 mm, number of contours 10, build orientation of 90°, raster angle of 0° and road width of 0.4572 mm. *Raut et al.[61]* have highlighted the impact of orientation on mechanical behaviour and fabrication cost of ABS material. The results revealed thatat 0° orientation tensile strength was maximum.

Ravari et al. [62] have fabricated cellular lattices through FDM process to examine the compressive strength and elastic modulus of PLA cellular lattice structure. *Onwubolu and Rayegani [63]* have evaluated the impact of process variables, namely raster width, air gap, raster angle, orientation and layer height on tensile strength of ABS material. Results revealed that minimum raster width and layer thickness had improved the tensile strength of material. *Dawoud et al.[64]* have highlighted the mechanical behaviour of ABS components, which were fabricated through FDM process. Further, a comparison of FDM printed component with injection moulded parts was carried out for both static and dynamic loading. Process parameters air gaps and raster angle was considered for the investigation. Results show that raster angle -45/+45(degree) have maximum tensile strength. However, flexural strength was maximum at 0/90° degree orientation. *Wu et al. [65]* have suggested the optimum process parameters condition for fabrication of component of polyether-ether-ketone material by FDM technology. The process parameters layer thickness and raster angle were used for investigation. Result shows that the optimal process conditions were layer thickness 300 μm and raster angle '0' degree.

Mohamed et al. [66] highlighted the effect of process variables on creep behaviour of the PC and ABS component fabricated by FDM process. A relationship was established between the process parameters viz., air gap, layer thickness, part print direction, bead width and number of shells with response variable creep. Result showed that the value of creep displacement was decreased by decreasing the value of the parameters, i.e. slice height, raster fill angle and air gaps. The optimum process parameter condition for the creep was found, i.e. layer height of 0.2540 mm, bead

width of 0.4572 mm, air gap of 0 mm, 8 shells, print direction of 20° and rater fill angle of 0°.

Espin et al.[67] have conducted an experimental investigation to find out 9 elastic constants for the orthotropic properties of FDM printed components and compare the model with simulation results. Results revealed that within the elastic region material behave isotropic and after yield stress material shows anisotropic behaviour. Results were also affected by some other process parameters like layer thickness, nozzle diameter and diameter of extruded filament. *Espin et al. [68]* have investigated the impact of building parameters on the dynamic behaviour of component fabricated through FDM process. Three essential building parameters, i.e. number of contours nozzle diameter and raster - to - raster air gap were used in the investigation. Experiments were designed based on the Taguchi method. *Szykiedans and Credo [69]* have evaluated the tensile strength and elastic modulus of ABS material by using FDM and SLA process. Result shows that properties of different printers were not uniform. *Chacon et al. [70]* have evaluated the impact of process variables viz. layer height, orientation and feed rate on mechanical behaviour of PLA component fabricated via FDM process. The experimental results revealed that selected process parameters were significantly affecting the mechanical properties. Results of the experimental study depicted that, tensile strength of recycled samples were decreased by 10.9%, shear strength increased by 6.8% and hardness decreased by 2.4%. The overall mechanical behaviour of the recycled PLA component was approximately equal to the virgin PLA.

Table 2.1: Summary of the characterization of mechanical properties in FDM technology

Investigator Name	**Material**	**Raster angle**	**Other process parameters**	**Mechanical properties**
Durgun et al. [57]	ABS	*0°, 30°, 45°, 60°,90°*	Orientation (horizontal, vertical and perpendicular)	Tensile strength
Cantrell et al.[59]	ABS, PC	*45/-45, 30/-60, 15/-75, 0/90)*	Orientation (flat, on-edge, upright)	Tensile strength, poisson's ratio, shear strength and shear modulus
Mohamed et al. 2017[60]	PC-ABS	*0°, 45°* and *90°*	Part print direction, number of shells, slice height, air gap, and bead width	Creep displacement (μm)
Raut et al.[61]	ABS		Orientation, cost	Tensile strength, bending strength
Ravari et al.[62]	PLA	Constant		Compressive strength, collapse stress
Onwubolu et al.[63]	ABS	Constant	Layer height, part orientation, raster widthand air gap raster angle	Tensile strength
Dawoud et al.[64]	ABS	*0/−90, 15/−75, 30/−60, 45/−45*	Raster gap	Tension, bending, impact
Wu et al.[65]	PEEK, ABS	*0°, 30°, 45°,*	Layer thickness	Tensile, compressive and bending strengths
Mohamed et al. [66]	PC-ABS	*0°,15°, 30°, 45°, 60°, 75°, 90°*	Number of contours, air gap, road width, layer thickness andbuild orientation	Complex modulus and dynamic viscosity
Espin et al.[67]	PC	Constant	Orientation	Young's modulus, ultimate strength, elastic constants, poission's ratio, shear modulus
Szykiedans et al. [69]	ABS		-	Tensile strength, young's modulus
Chacon et al. [70]	PLA		Layer thickness, build orientation and feed rate	Tensile strength and bending strength

Anderson [71] has carried out an experimental study to compare the mechanical behaviour of recycled PLA material with virgin PLA. Mechanical behaviour, i.e. tensile strength, shear strength and hardness were used for the comparative analysis. Results of the experimental study depicted that, tensile strength of recycled samples were decreased by 10.9 %, shear strength increased by 6.8 % and hardness decreased by 2.4 %.

The overall mechanical properties of the recycled PLA component were approximately equal to the virgin PLA. *Vicente et al. [72]* have examined the effect of process variables viz., infill pattern and infill density on mechanical properties of ABS material, manufactured by FDM technology. It was observed that mechanical properties varied by only 5% because of variation in different infill pattern. Table 2.1shows the summary of the characterizations of mechanical properties in FDM technology.

2.3.2 Characterization of mechanical properties of SLS component

Kashdan et al. [73] have designed a meso-scale negative stiffness system to measure dynamic transmissibility of a system. A bistable structure in the form of pre buckled beam/pre-compressed beam was used in investigation. Experimental result shows that pre-compression induced negative stiffness, which increases the damping and sift frequency of unconstrained beam. *Athreya et al. [74]* have evaluated the mechanical properties (tensile strength, tensile modulus, flexural modulus and flexural strength) of Nylon-12 reinforced with 4 wt.% of carbon black (CB) fabricated by SLS process and compared the results with injection moulded components. Results depict that Nylon-12 made by SLS process have 35% higher tensile strength and 25% higher flexural modulus. However, in addition of CB, both tensile strength and flexural modulus were decreased due to high porosity and poor dispersion of nanoscale CB in SLS component.

Bassoli et al. [75] have highlighted the joining mechanism and evaluated mechanical properties of SLS component. Primary and secondary anisotropy were evaluated. Results proved that samples fabricated parallel to the growth direction had different responses in another direction. *Spierings et al. [76]* have investigated the

experimental works to find out the influence of particle size on mechanical properties and surface quality of SLS component. Result shows that fine particle improves the mechanical properties. However, the coarse particles should remain to increase the layer thickness for better productivity. *Sudarmadji et al. [77]* have conducted the experimental study to investigate porosity and mechanical behavior relationship in SLS polyhedral for FGS. Scaffolds of different structural configurations were designed using CASTS. The properties, yield strength, compressive stiffness and porosity of the scaffolds varied in the range of *2.74 –55.95MPa*, *0.17–5.03 MPa* and *40–84%* respectively.

*Starr et al.[78]*evaluated that mechanical behaviour of SLS processed nylon which was affected by the different process variables. The process parameters like laser properties (power, speed and scan capacity), orientation of building and thickness of layer were used to optimize mechanical properties like; yield strength, ultimate tensile strength, modulus and elongation of the material. Result shows that if adequate energy is supplied to melted powder, the modulus and strength of the material can be increased. Elongation was maximum corresponding to the higher energy density. Build orientation has significant effect on the elongation. *Song et al. [79*] have fabricated Ti6Al4V parts by using the SLS method. Different melting mechanisms were used in this investigation. Surface roughness, microstructure, microhardness and densification of Ti_6Al_4V parts were evaluated. The scanning speed of process parameters and laser power were used for the investigation. At scanning speed 0.4m/s and laser power 100W, perfect Ti_6Al_4V part was successfully manufactured by SLM process. In Ti6Al4V part produced by continuous melting mechanism highest value of surface roughness 2.1µm and microhardness 450 HV were observed.

Majewski et al.[80] have used differential scanning calorimetry curve for indicating the level of melting within semicrystalline SLM parts or degree of particle melt (DPM). Result shows that DPM increases as the energy input increases. Tensile strength and elongation at break also increases as DPM increases. DPM does not affect the young's modulus. *Shi et al. [81]* have used high impact polystyrene (HIPS) material for the fabrication of part by SLS process. The sintering process parameters and mechanical properties were evaluated. The epoxy resin was used to filtering process of fabricated parts. After the post-processing, properties were re-evaluated.

Zheng et al. [82] have fabricated reinforced polystyrene-based composite by using the SLS process. In this study, the effects of treated and untreated nanoparticles on mechanical properties were investigated. It was observed that in treated specimens notched impact strength increased up-to *50%* while an increment up-to *300%* was recorded for tensile strength which is *31.2MPa*. Further, the maximum value of impact strength *12.kJ/m*^{2} was obtained. *Jain et al. [83]* have carried out experimental works to improve the part strength in SLS process. Experiments were conducted based on the Taguchi method. Investigation revealed that at part bed temperature was less than *175°C,* the curling phenomenon occurred. After *178°C,* caking problem was identified. The layer with *150 mm* thickness showed the maximum tensile strength with *60%* refresh rate and *178 °C* temperature.

Farzadia et al. [84] have studied the effect of layer printing delay. Further, its effect on three dimensional printed porous prototypes geometrical accuracy, mechanical behaviour in the field of bone tissue applications was evaluated. Tangent modulus, compressive strength and toughness of specimen printed with 300ms delay period was observed higher value as compared to other samples.

Santos et al. [85] have fabricated pure titanium by using the SLS method. Microstructures including mechanical properties of the fabricated components were tested. The optical and SEM image of the fabricated component shows that pore structure depends on the peak power, hatching pitch and scan speed. The value of Vickers hardness of the fabricated samples was nearly 240 HV. Table 2.2 shows the characterizations of mechanical properties in SLS technology in a summarized way.

Table 2.2: Summary of the characterizations of mechanical properties in SLS technology

Investigator Name	**Material**	**Other process parameters**	**Mechanical properties**
Kashdan et al.[73]	Nylon 11	Layer thickness, laser power, part bed temperature, layer time, roller speed	Negative stiffness of beam, dynamic behaviour
Athreya et al.[74]	Nylon-12 with 4% CB	Laser scan spacing, laser power, powder feed temperature setpoint, laser scan speed, powder layer thickness, roller speed	Flexural modulus, flexural strength and tensile strength
Bassoli et al.[75]	Polyamide 12, aluminium-filled polyamide 12, alumina-filled Polyamide 12 composite	Orientation	Yield strength, ultimate strength, hardness, microstructure
Spierings et al.[76]	316L power with different grade D10 µm, D50 µm,D90µm	Layer thickness, orientation, laser power, scanning speed, hatch distance	Yield tensile strength, ultimate tensile strength
Sudarmadji et al.[77]	PCL powder with average particle size 100 µm	Laser power, part bed temperature, scan speed	Porosity, mechanical stiffness
Song et al.[79]	Ti6Al4V	Laser power, scanning speed	Microhardness, microstructure
Majewski et al.[80]	Nylon-12	Heater set point, scan spacing, laser power	Tensile strength, elastic modulus
Shi et al.[81]	HIPS powders particle range 75 to 100 µm	Thickness of layer, scanning spacing scanning speed, laser power	Tensile strength, impact strength, young's modulus
Zheng et al.[82]	Nano-Al_2O_3/polystyrene composite	Laser power	Impact strength, tensile strength
Jain et al.[83]	PA 2200 with an average grain size of 60µm	Layer thickness, Refresh rate, part bed temp, hatch pattern	Ultimate tensile strength
Farzadia et al.[84]	ZP150, ZB63	Layer printing delay	Compressive strength, toughness and tangent modulus
Santos et al.[85]	Pure titanium powder grade 1	Scan speed, laser power	Hardness, torsional fatigue strength

2.3.3 Characterization of mechanical properties of PolyJet component

Sugavaneswaran et al. [86] have fabricated multi-materials reinforced composite by using PolyJet technology to investigate the stiffness of component. The rule of mixture was employed for mixing materials. The effect of orientation concerning reinforcement direction was investigated to enhance stiffness of fabricated component. Result shows that reinforcement significantly improved the elastic modulus of component. Elastic modulus was improved between 6.79 - 21.03% concerning change in orientation.

Moore et al. [87] have fabricated a fatigue specimen of tango black plus material by using PolyJet technology. Microstructure of the fabricated component was examined by using the optical microscope. Results of fatigue test shows that reduction in cross-section area, like necking on specimen samples was significantly reduced the fatigue life of the component. A relationship between fatigue life and strain was established. However, this study was limited to examine the tensile fatigue only. *Blanco et al. [88]* have fabricated specimen to check the time dependence of load application on RGD240 mechanical properties generated by PolyJet process.

Further, the orientation influence also evaluated on mechanical properties. Results indicate that a mechanical property of material was time-dependent. Properties were evaluated in terms of relaxation modulus *E(t)*. The value of relaxation modulus was maximum at '0' degree orientation and gradually decreased on increase of orientation. At 60°-75° minimum value of *E(t)* was observed and at 90° orientation relaxation modulus suddenly increased.

Cazon et al. [89] have fabricated tensile test specimen using Objet Eden 330 PolyJet printer to investigate the tensile properties and surface roughness of RGD240

component. Tensile test was performed using the Instron model 4467 machine that has 30 kN load cell. Surface roughness was investigated using Mitutoyo SJ 301 portable roughness machine. Experimental results revealed that sample fabricated in the X-direction was maximum ultimate tensile strength 42 MPa. Maximum elongation in the component of RGD240 material 54% was observed. Glossy surface was minimum surface roughness in XY-plane. *Yapa et al. [90]* have experimentally investigated the effect of shape recovery on 3D printed polymeric honeycomb structure. Polymer specimens with honeycomb structure were prepared by using the polypropylene with the PolyJet system. The accuracy of part produced by PolyJet was 0.2 mm for smooth surface. Table 2.3 shows the summary of characterizations of mechanical properties in PolyJet technology.

Table 2.3: Summary of the characterizations of mechanical properties in PolyJet technology

Investigator Name	**Material**	**Other process parameters**	**Mechanical properties**
Sugavaneswaran et al.[86]	Vero black and darus white	Reinforcement and orientation	Elastic modulus
Moore et al.[87]	Tango black plus	Surface type	Cyclic fatigue and microstructure
Blanco et al.[88]	RGD240	Orientation	Relaxation modulus E(t)
Cazon et al.[89]	Fullcure 720	Orientation and surface type	Tensile strength
Yapa et al.[90]	RGD-430	Honeycomb design shape, number of compressions, and loading rate	Compressive strength

2.3.4 Characterization of mechanical properties of stereolithography component

Chockalingam et al. [91] have conducted an experimental study to investigate the influence of layer thickness on mechanical properties in Stereolithographic process. Specimen samples were prepared as per the ASTM slandered. It was observed that the strength of epoxy resin depends on bonds between molecules. For examine the fracture

surface of the tensile specimens and impact test specimen, microstructures were taken by using SEM. It was concluded that ultimate tensile strength and impact strength were maximum in lower layer thickness due to better bonding between the molecular chains.

Mansour et al. [92] have conducted the experimental studies to analyze the influence of short-term ageing on mechanical behaviour of the epoxy resin accuraSI40. *Sabree et al. [93]* have fabricated porous ceramic scaffolds to analyse the influence of internal size on mechanical behaviour. Scaffolds of 70% SiO_2–30% CaO glass powder materials were fabricated by using Stereolithography technology at constant porosity 42%. Fabricated samples were further sintered at high temperature 1200°C. The mechanical properties of fabricated scaffolds manufactured by SLA process were similar to the other ceramic and glass scaffold structures. In order to check the effect of sintering, SEM test was performed and found that in sintered scaffolds microstructure contain fractions of wol-lastonite and a pseudo-woll astonite phase.

Alharbi et al. [94] have highlighted the influence of orientation on compressive strength in the component fabricated by DW028D 3D-printer. Results of compressive test depicted that compressive strength of the components fabricated in vertical orientation were higher than horizontal orientation. For checking the leading mechanism for the variation of mechanical properties, SEM test were conducted. It was noticed that horizontal oriented fabricated specimen have higher creaks as compared to the vertical orientation.

Weng et al. [95] have fabricated composite by using the SLA method. In this investigation, nanocomposites were fabricated by adding nanoSiO_2, ATP and OMMT into SLR. It was observed that due to addition of nanofiller, viscosity was increased

around 10%. Addition of nano $SiO_2$was increased the curing speed. However, addition of ATP and OMMT decreases curing speed. It was noticed that addition of all nanofiller material had enhanced the elastic properties of SLR. It was suggested that among all three considered nanofiller, SiO_2 shows best properties. *Wu et al. [96] h*ave fabricated defect-free Al_2O_3-Z_rO_2 composite via SLA method to analyse the influence of sintering temperature on the mechanical behaviour of sintered composite. The results depicted that, fracture toughness increases on increase of sintering temperature. It was also observed that sample density was increased on increase of sintering temperature and had maximum density of 4.27 g/cm^3 at 1600 °C. *Vayrynen et al. [97]* have fabricated specimens of epoxy-based resin (Somos watershed XC 11122; DSM) material by SLA process to investigate the fractural strength and elastic modulus. In this analysis, influence of orientation of nozzle on mechanical behaviour was carried out. Results depict that elastic modulus and flexural strength of the fabricated SLA component have anisotropic properties.

Table 2.4: Summary of the characterization of mechanical properties in stereolithography

Investigator Name	**Material**	**Process parameters**	**Mechanical properties**
Chockalingam et al.[91]	SL5530	Layer thickness	Tensile, yield and impact tests
Mansour et al.[92]	Accura SI40	Short-term ageing	Impact strength, ultimate tensile strength, flexural strength
Sabree et al. [93]	70% SiO_2–30% CaO glass powder	Effect of pore size pore sizes	Mean crushing strength
Alharbi et al.[94]	Composite resin restorative material	Effect of orientation	Compressive strength, Microstructure
Weng et al.[95]	Nano SiO_2, ATP and OMMT	Effect of different nanofiller material	Elastic properties, tensile strength
Wu et al. [96]	Al_2O_3-Z_rO_2 composite	Effect of sintering temperature	Fracture toughness, density and Vickers hardness
Vayrynen et al. [97]	Epoxy-based resin	Effect of nozzle orientation	Flexural strength and elastic modulus
Galeta et al. [98]	zp130	Different type of structure	Tensile strength at fracture point.

Galeta et al. [98] have prepared samples according to ISO 527:2012 standard to check the effect of different type of structure on mechanical properties. Results show that hexagonal structure has the maximum tensile strength. Table 2.4 illustrates the summary of characterization of mechanical properties of Stereolithography component.

2.4 Optimization of process parameters

Mechanical properties and form errors of the component fabricated through rapid prototyping were greatly influenced by process parameters. Researchers have conducted several studies to find out the optimum process parameters condition for the various RP technologies. The main focus of this study was to highlight the optimization technique used by researchers for optimization of process variables. The details of optimization work reported by the researchers were discussed below.

Rong-Ji et al. [99] have designed an experiment by using the neural network to find the optimum value of process parameters to manufacture component through SLS process. The principal focus of the study was to minimise the shrinkage error in the fabricated component. The process parameters used in analysis were hatch spacing, thickness of layer, scanning speed, laser power, surroundings temperature, scanning mode and interval time. To find the global minima genetic algorithm based on neural network optimization tool was adopted. The values of optimum process parameters conditions were found, i.e. hatch spacing 0.12 mm, layer thickness 0.2 mm, 93°Cworking surrounding temperature, laser power 18 W, interval time 1s and 1,800 mm/s scanning speed.

Sajan et al. [100] have applied grey relational analysis (GRA) to optimize the surface roughness and circularity error in the component of ABS material fabricated by

FDM process. The process variables viz., nozzle temperature, temperature of bed, loop number, infill percentage, speed of print and thickness of layer were used in the investigation. Grinder blade including three axes holes was used as specimen. Results depicted that the optimum process parameters conditions for the minimum circularity error and roughness error were nozzle temperature 220 ℃, print speed of 35 mm/s, 0.4mm layer height, three loops number, 110 ℃ bed temperature and infill of 30%. It was suggested that surface roughness and circularity error was minimum and maximum at XY and XZ-plane respectively.

Srivastava et al. [101] have fabricated ABS component by using the FDM process to optimize the built material, support material, and manufacturing time. Experiments were conducted according to full factorial central composite design (CCD). Process parameters viz., raster width, width of contour, gap of air, height of slice, orientation and raster angle were used to optimize the response factors. RSM based optimization technique was used for optimization. The optimum process parameters conditions, i.e. raster width 0.4mm, air gap 0.9mm, contour width 0.56 mm, slice height 0.3302mm, orientation 0 degrees and raster angle 0 degree were found. *Casalino et al. [102]* have fabricated 18Ni300 maraging steel component by using SLS process to optimize the hardness, strength, surface roughness, porosity and part density. Process parameters viz., laser power, scanning speed and laser density were used in the investigation. Statistical technique was employed to optimize above process parameters.

Calignano et al. [103] have fabricated AlSi10Mg and Ti6Al4V component by using the SLS process to optimize the overhang features by minimising the support

material. Process parameters viz., scan speed (mm/s), hatching distance (mm), laser power (W), layer height (μm) and laser spot size (mm) were used in the investigation. For aluminium alloy, the optimum supports conditions were found, i.e. hatching was 0.5 mm, teeth base interval 0.10mm and teeth height 0.43 mm. However, Zoffsets values were no effect on distortion of structure. For titanium alloy, optimum condition were found viz., hatching 0.75 mm, teeth height 0.43 mm, base interval 0.10 mm and Zoffsets of 0.03 mm. *Peng et al. [104]* have conducted experiment by using RSM to find the optimum process condition for the ABS material fabricated by FDM method. Fuzzy inference system was employed to find the multi-response factors. Fuzzy interface was used to relate each output response in terms of process variables. Finley second-order RSM was applied to combined single response factors to find single objective function in terms of input response factors. Developed model was validated by ANN and GA. There was a good agreement between RSM model, and ANN & GA model. *Velu et al. [105]* have conducted experimental analysis to examine the effect of process parameters on porosity and mechanical properties of PMMA material, which is suitable for biomedical application. Specimen samples were fabricated by using SLS process. MATLAB function was employed for the image processing in surface morphology. It was suggested that scanning speed and laser power were the significant process parameters.

Onwubolu et al.[106] have applied the GMDH technique to develop a functional relationship between process parameters and tensile strength. A mathematical model was developed to forecast the tensile strength of ABS material

corresponding to process parameters condition. Process parameters were used in the investigations viz., raster angle, part orientation, air gap and raster width. There was a good agreement between the proposed model and experimental results. The optimum process parameters conditions were found viz., part orientation '0' degree, raster angle 50°, raster width 0.2034 mm and air gap of 0.0025 mm. *Sood [107]* has investigated effect of process parameters viz., orientation, layer height, raster width, air gap and raster angle on tensile, bending and impact strength of the material. Optimization technique Principal Component Analysis (PCA) was employed to formulate single response factor, which optimized all the output response factors. The optimum process parameters were found viz., layer height 0.254 mm, orientation 30°, raster angle '0' degree, air gap 0mm and raster width 0.4063 mm. *Villalpando et al. [108]* have conducted experimental and computational study to investigate the impact of internal structure and orientation on mechanical properties. Global optimization technique GA was used to find the optimum process condition.

Wang et al. [109] have integrated Taguchi design with GRA to find the optimum process parameters condition for fabrication of component of ABS material through FDM technology. Response factors viz., ultimate tensile strength, DA and SR were used for the investigation. A relationship between process parameters viz., layer thickness, support style Z direction, support style X direction, deposition style, DO_X, build location and response factors were established. Table 2.5 shows the summary of optimization technique used by the researchers.

Table 2.5: Summary of the optimization work

Investigator name	Material	Machine	Process parameters	Optimized response factors	Optimization technique
Rong-Ji et al.[99]	Composite of polystyrene	SLS	Surroundings temperature, hatch spacing, layer thickness, interval time and laser power	Shrinkage error	ANN and GA
Sajan et al.[100]	ABS	FDM	Nozzle temperature, bed temperature, number of loops, infill percentage and print speed	Circularity error, surface roughness	GRA
Srivastava et al.[101]	ABS	FDM	Slice height, raster width, air gap and contour width	Built material, support material and manufacturing time	RSM
Casalino et al.[102]	18Ni300 maraging steel	SLS	Laser density, laser power and scanning speed	Hardness, surface roughness, porosity, part density	Taguchi
Calignano [103]	AlSi10Mg, Ti6Al4V	SLS	Laser spot size, Scan speed, laser power, hatching distance and layer thickness	Supports material	Taguchi
Peng et al.[104]	ABS	FDM	Filling velocity, line width compensation and layer thickness	Warp deformation dimensional error, and built	FIS, ANN
Velu et al. [104]	PMMA powder	SLS	Energy density, scan speed and laser power	Density, porosity, mechanical properties	MATLAB function
Rayegani et al.[106]	ABS	FDM	Raster width, raster angle, part orientation and air gap	Tensile strength	GMDH
Sood[107]	ABS	FDM	Raster width, Orientation, air gap and layer height	Impact strength, tensile strength and bending	PCA
Villalpando [108]	ABS	FDM	Build orientations and parametric structures	Interior geometry, build time, Tensile strength and material usage	GA
Wang et al.[109]	ABS	FDM	Layer thickness, support style Z direction, support style X direction, deposition style, DO_X, build location	Ultimate tensile strength, DA and SR	GRA With Taguchi
Vosniakos et al.[110]	Thermo-setting polymer	wax modelling machine	Slice thickness constitutes and model orientation and	Volumetric accuracy, building time	ANN and GA
Lee et al.[111]	ABS	FDM	Raster width, layer height, raster angle and air gap	Elastic modulus	Taguchi

2.5 Outcome of literature review

Various studies had been conducted in the area of rapid prototyping, in which researchers were made attempts for enhancing the process parameters of rapid prototyping. Several computational models were available, but there was a wide gap between a complete framework of computational analysis and experimental framework.

- The results of measurements shows that the performance of PolyJet was better than other 3D printing process as regard dimensional accuracy (DA) and surface roughness. Using a factorial plan based on the input variable like layer thickness, raster angle raster width and air gap a mathematical model can be developed.
- Other researchers use simple parts, for better understanding and comparative analysis with other manufacturing techniques, automotive parts like piston rings, connecting rods, piston, gear etc. can be used.
- Study of clearance between mating parts is one of the critical parameters, but no attempts were made for the analysis of clearance between mating parts.
- In a literature review, researchers have made effort to improve the mechanical properties through optimizing the process parameter only. However, only very few literatures are available related to effect of reinforcement on the mechanical behaviour of ABS and PLA material.
- The optimum selection of process parameters for the PolyJet process cannot be identified from the literature.
- Very few research works were carried out for the investigation of flatness and cylindricity analysis of FDM process.

- Very few researchers were made an effort to find out influence of process variable on mechanical properties for the PolyJet process.
- The optimum level of process parameter for the dimensional accuracy, flatness and cylindricity were different. No attempt was made to optimize the dimensional accuracy, flatness and cylindricity by using multi-objective optimization technique.

Chapter 3

Comparative Study of PolyJet and FDM Technology

Chapter 3

Comparative Study of PolyJet and FDM Technology

3.1 Introduction

Prototyping is the most criticalrealisation process in the design analysis and manufacturing process. Prototyping is the first steps in product development process. In the present investigation, a comparative study has been present regarding PolyJet and FDM technology. The next sub-section presents the details of experimental plan and 3D printers used for the generation of prototype automotive components.

3.2 Experimental setup of the RP machine and data analysis

In this research work, a comparative study of FDM and PolyJet technique was carried out based on SR, DA, flatness,cylindricityand costanalysis of the component. For this purpose, a scaled radial engine connecting rod was selected as a specimen. The selected component has linear, radial and cylindrical dimensions along with flat surface. In metrology, CMM is being used to automate the process of inspection, which has tremendously increased inspection capabilities. CONTURA G-2 coordinate measuring machine was used to measure the flatness, cylindricity, linear dimensions and radial dimensions. All axes of CONTURA G-2 are equipped with 4-sided Carl Zeissair bearings, which provide precise measurement. CONTURA G-2 is also equipped with C99 controller, which offers CAA for real-time dynamic correction for exceptionally accurate results. The probe size 3 mm was used for the measurement.

The value of SR was measured by using MicroXAM-100 3D optical surface profiler. The next sub-section will provide the details of FDM and PolyJet machine& process parameter used for the fabrication of a connecting rod.

3.2.1 Overview of FDM machine and PolyJet machine

In the current study, two FDM printers namely MakerBot Replicator 2and Ultimaker printers were used for the fabrication of connecting rod. The level of process variables considered for manufacturing of component through FDMprocess are shown in Table 3.1. PLA plastic material was used for both build as well as support geometry. Support material was removed after the fabrication of the component. Specially designed hand tools were used for the removal of support material.

Table 3.1: Level of process parameter

S.N	Process Parameter	Level
1	Layer thickness (µm)	200
2	Orientation	Flat
3	Infill pattern	Hexagonal
4	Infill density (%)	60
5	Number of contours	6
6	Nozzle diameter (mm)	0.4 mm
7	Print temperature (°C)	210
7	Bed temperature (°C)	110
8	Number of shells	4

Objet 30, a 3D desktop printer was chosen for the fabrication of connecting rod through PolyJet process. The maximum build size of the printer along X, Y and Z direction are 294 mm × 192 mm ×148.6 mm respectively. The resolution of printer in X-direction is 600 dpi, in the Y-axis 600 dpi and Z-axis 900 dpi. The accuracy of fabricated component depends on the number of process variables like raster angle, orientation, material type, part geometry, materials and the methods of post-processing process. However, layer thickness for Objet 30 printer has a fixed value, i.e. 28 µm. It can be operated in the surrounding temperature of 18°C to 25°C.

Figures 3.1(a-b) illustrate the diagram of PolyJetand FDM machine used for the fabrication of samples. The details of working principle are discussed in *chapter 1*.

Specimen samples were prepared by using RGD 840 (Vero blue) material. It is a cartridge containing ink, which can be used under normal condition. The substance is released only from the cartridge inside the printing system. Hence, external exposure is limited. Material SUP 705 was used as a support material. After printing the component, nontoxic support material was removed from the surface of build geometry through pressurised water. Fabricated model can be used directly without additional post-processing. In industry RGD 840 (Vero blue) material is used for the checking of form and fit testing, moving and assembly parts, fabrication of exhibition models, silica moulding, and assembly of electronic component etc. The 3D modelling of radial engine connecting rod is presented in next sub-section.

Figure 3.1(a): Experimental setup of PolyJet machine

Figure 3.1(b): Experimental setup of FDM printer

3.2.2 3D modelling of the scaled model radial engine connecting rod

In recent years, digital fabrication has slowly infiltrated the field of prototype making. At present, there are more than twenty different types of 3D printers are available for rapid

prototyping. In order to analyse the DA, shape error, SR and cost of prototype component printed by FDP and PolyJet process, a scaled model of radial engine connecting rod was considered as a case study. For creating the geometry 3D CAD software CATIA V6 was used. Figure 3.2 shows the dimensions of the selected component. 3D CAD model of specimen used in the experiment is demonstrated in Figure 3.3 (a). RP used standard.STL file format only. The sliced model is as shown in Figure 3.3 (b).

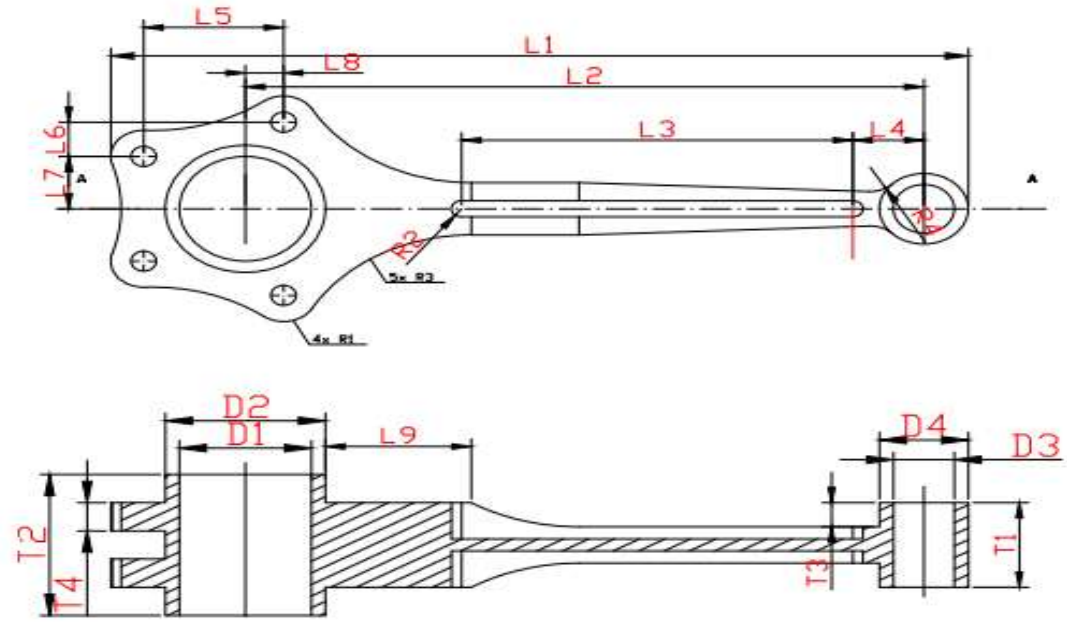

Figure 3.2: Dimensions of the component

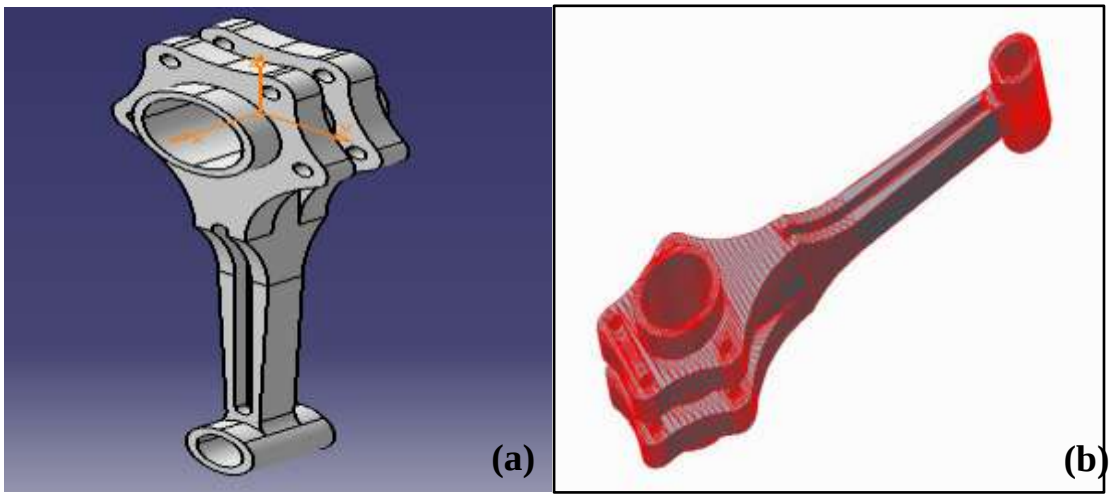

Figure 3.3: (a) CAD model of connecting rod (b) Sliced model of connecting rod

3.2.3 Digital fabrication of the component

For comparing the process capability of the selected RP printers (Objet-30, Ultimaker and MakerBot), a component (connecting rod) was fabricated at the optimum process parameters condition of each printer. RGD840 was used as the build material and SUP705 as support material for the Objet-30 printer. For Ultimaker and MakerBot printers, polylacticacid *(*PLA) was used for both build and support material. Figure 3.4 (a) illustrates the fabricate component by Objet-30 printer, Figure 3.4 (b) shows the fabricated component through MakerBot printer and Figure 3.4 (c) illustrates the fabricated component by Ultimaker printer.

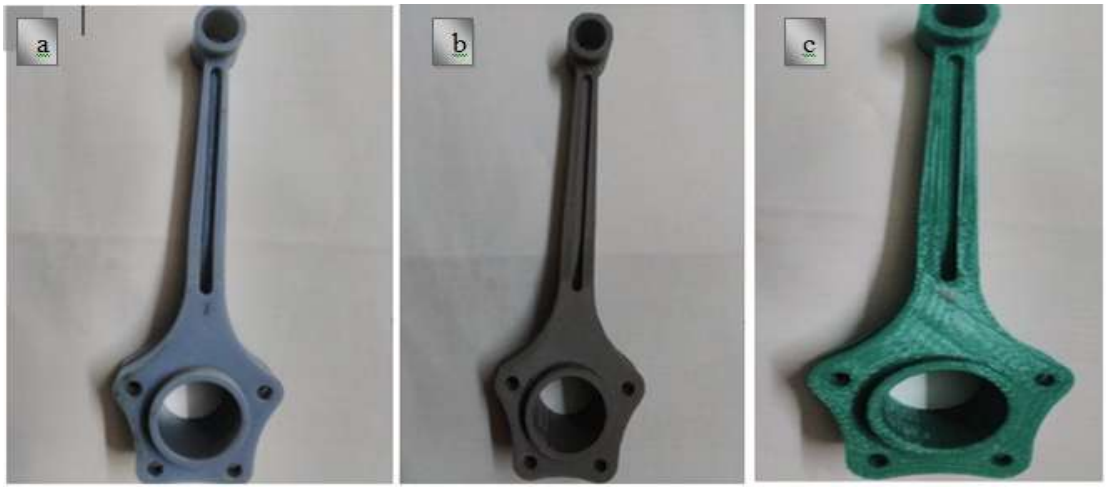

Figure 3.4: Fabricated prototype model of connecting rod (a) Objet30 (PolyJet) printer. (b) MakerBot (FDM) printer (c) Ultimaker (FDM) printer.

3.2.4 Measurement of dimensions

The coordinate measuring machine (CMM) shown in (Figure 3.5) was used for the measurement of linear as well as a radial dimensions of the automotive component (connecting rod). For connecting rod total 12 linear dimensions,4 radial dimensions and 4 circular dimensions were measured. Total 9 linear dimensions were measured along the print bed (X-Y axis) and 3linear dimensions were measured perpendicular to the

print bed (Y-Z axis) as shown in Table 3.2 and Table 3.3 respectively. Table 3.4 shows the circular dimensions and Table3.5 shows the radial dimensions for the connecting rods.

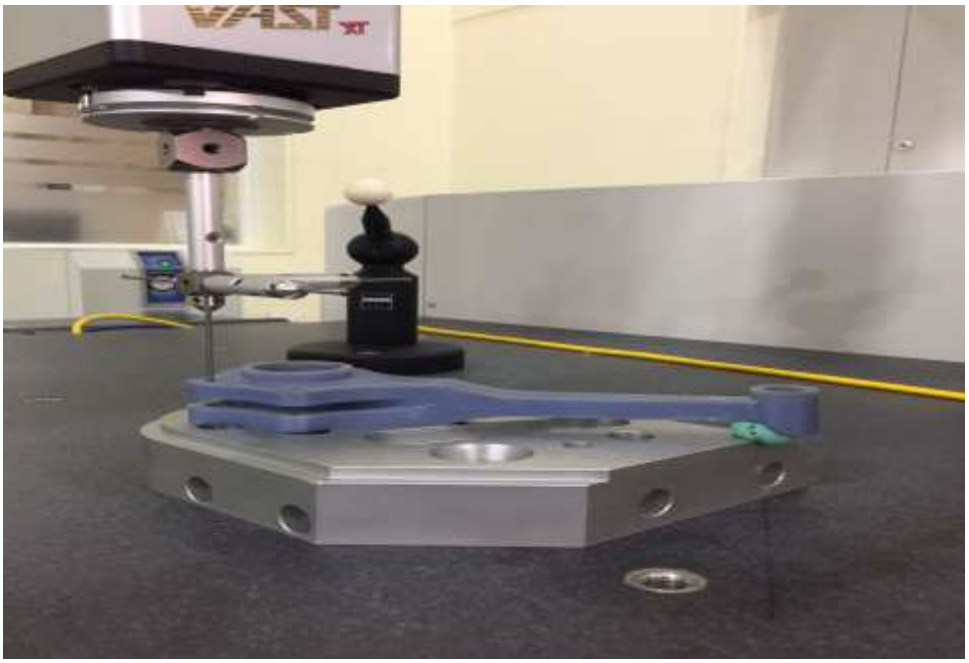

Figure 3.5: Measurement of the dimensions of connecting rod

Table3.2: Linear dimensions along XY plane

Dimension	**CAD dimension**	**Objet 30**	**Ultimaker**	**MakerBot**	**%Error Objet 30**	**%Error Ultimaker**	**%Error MakerBot**
L_1	202.56	200.75	200.69	200.09	0.89	0.92	1.22
L_2	160.26	160.10	160.30	159.03	0.10	0.02	0.77
L_3	92.40	92.07	92.00	91.38	0.36	0.43	1.10
L_4	16.80	16.91	17.15	16.81	0.64	2.10	0.03
L_5	33.00	32.21	33.25	32.35	2.41	0.77	1.97
L_6	10.20	10.27	10.12	9.69	0.65	0.82	5.05
L_7	15.60	15.26	15.30	16.00	2.18	1.93	2.55
L_8	9.00	8.89	8.86	9.17	1.25	1.58	1.91
L_9	33.00	32.86	30.82	32.98	0.43	6.61	0.06
Average %error					0.99	1.69	1.63
Maximum % error					2.41	6.61	5.05
STDEV (%)					0.81	1.97	1.54

Table 3.3: Linear dimensions along YZ plan

Dimension	CAD dimension	Objet30 dimension	Ultimaker	MakerBot dimension	%Error Objet 30	%Error Ultimaker	%Error MakerBot
T_1 (mm)	25.2	26.156	25.341	25.37	3.79	0.56	0.67
T_2 (mm)	42	42.36	41.564	41.79	0.86	1.04	0.50
T_3 (mm)	9.7	9.9	9.4	9.49	2.06	3.09	2.16
Average % error					2.24	1.56	1.11
Maximum % error					3.79	3.09	2.16
STDEV (%)					1.48	1.35	0.92

Table 3.4: Circular dimensions of connecting rod

Dimension	CAD dimension	Objet30 dimension	Ultimaker dimension	MakerBot dimension	%Error Objet 30	%Error Ultimaker	%Error MakerBot
D_1(mm)	14.4	14.62	13.887	14.02	1.53	3.56	2.64
D_2(mm)	21	21.1	20.657	20.71	0.48	1.63	1.38
D_3(mm)	31.2	31.39	30.373	30.64	0.61	2.65	1.79
D_4(mm)	37.8	37.67	37.233	37.19	0.34	1.5	1.61
Average % error					0.74	2.34	1.86
Maximum % error					1.53	3.56	2.64
STDEV (%)					0.54	0.97	0.54

Table 3.5: Radial dimensions of connecting rod

Dimension	CAD dimension	Objet30 dimension	Ultimaker dimension	MakerBot dimension	%Error Objet 30	%Error Ultimaker	% Error MakerBot
R_1	21.00	20.96	20.88	20.95	0.19	0.60	0.24
R_2	2.50	2.46	2.45	2.44	1.68	1.98	2.40
R_3	43.20	43.23	42.94	44.04	0.07	0.60	1.94
R_4	7.80	7.79	7.76	7.99	0.19	0.52	2.44
Average % error					0.53	0.92	1.75
Maximum % error					1.68	1.98	2.44
STDEV (%)					0.77	0.70	1.04

3.2.5 Measurement of roundness, cylindricity and flatness

The form errors (flatness and cylindricity) were evaluated by using the standard, ASME Y14.5M-1994. For checking the circularity, cylindricity and flatness errors present in the component fabricated by FDM and PolyJet process, CONTURA G-2 coordinate measuring machine was used. Circularity and cylindricity in the connecting rod were measured at a cylindrical portion (big end). Flatnessof the flat surface of connecting rod was also measured through CMM. The probe size of 3 mm was used for the measurement of form errors.Table 3.6shows the measured value of form errors (roundness, cylindricity and flatness) present in the selected component. Figure 3.6 (a) shows the graphical representation of roundness in big end of the connecting rod of Objet30. Figure 3.6 (b) and Figure 3.6 (c) shows roundness in the component printed by Ultimaker and MakerBot respectively. The next sub-section highlights about the measurements of surface roughness.

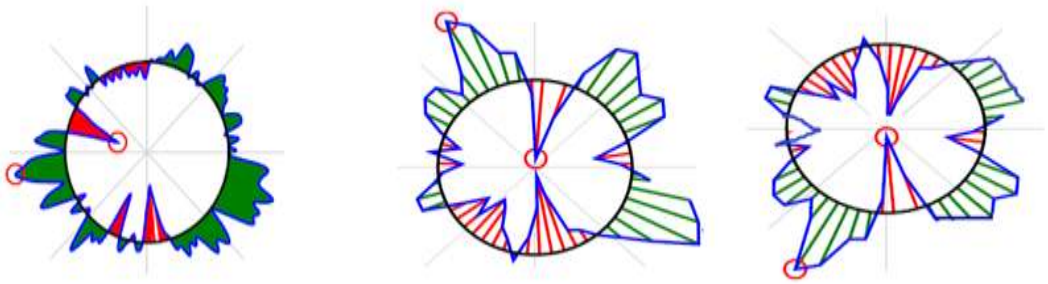

(a) (b) (c)

Figure 3.6: (a) Roundness of the big end of the connecting rod of Objet 30
(b) Roundness of big end of the connecting rod of Ultimaker
(c) Roundness of big end of the connecting rod of MakerBot

Table 3.6: Measurement of roundness, cylindricity and flatness

S.N.	Measurement	Objet30 (PolyJet)	MakerBot(FDM)	Ultimaker (FDM)
1	Roundness (mm)	0.0686	0.1673	0.2917
2	Cylindricity (mm)	0.0001	0.3426	0.0330
3	Flatness (mm)	0.1630	0.3692	0.1678

3.2.6 Investigation of surface roughness

The measurement of SR was performed by using optical profilometerMicroXAM-100 3D shown in Figure 3.7. Surface roughness of connecting rod was measured on the top surface only. All the SR parameters R_a, R_z and R_q were measured for both PolyJet and FDM printed components. Table 3.7 shows the measured value of surface roughness. Figure 3.8 (a) shows the SR and Figure 3.8 (b) shows the 3D surface of SR for the component fabricated through MakerBot printer. Figure 3.8 (c) demonstrates the 3D surface of the surface roughness of component manufactured through Objet-30 printer. Figure 3.8 (d) represents the surface roughness of the Objet-30 printed component. Figure 3.8 (e) shows the surface roughness of the component fabricated through Ultimaker printer. Figure 3.8 (f) shows the 3D surface profile the SR of Ultimaker component. The details of results of measurements of form errors are discussed in the nest-section.

Table 3.7: Measured surface roughness parameters

S.N	Roughness Parameters	Objet 30	MakerBot	Ultimaker
1	Average roughness height R_a (nm)	214.4	332.4	505.9
2	Mean roughness height R_q (nm)	290.1	478.3	613.1
3	Average peak to valley height R_z (nm)	1043.3	2304.2	2600.7
4	Peak roughness height R_p (nm)	3423.3	2634.6	2331.3
5	Peak valley height R_v (nm)	619.7	2530.7	1241.3
6	Peak height to peak valley height R_t (nm)	4043.0	5165.3	3572.6

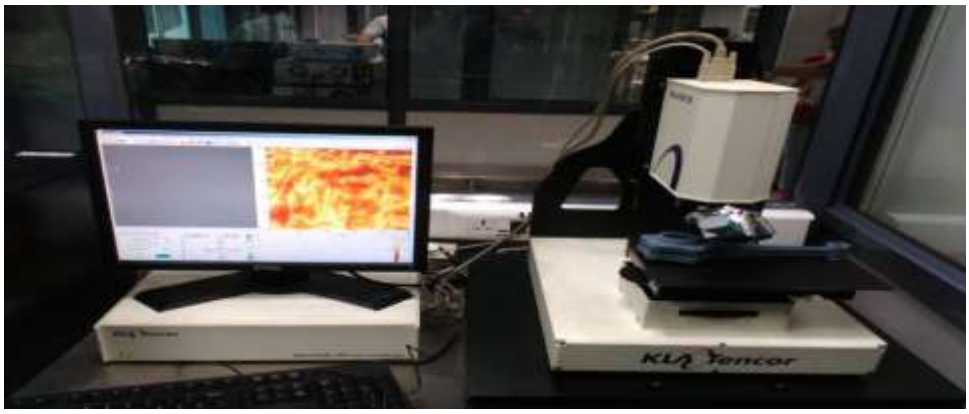

Figure 3.7: Optical profilometer setup for the measurement of surface roughness

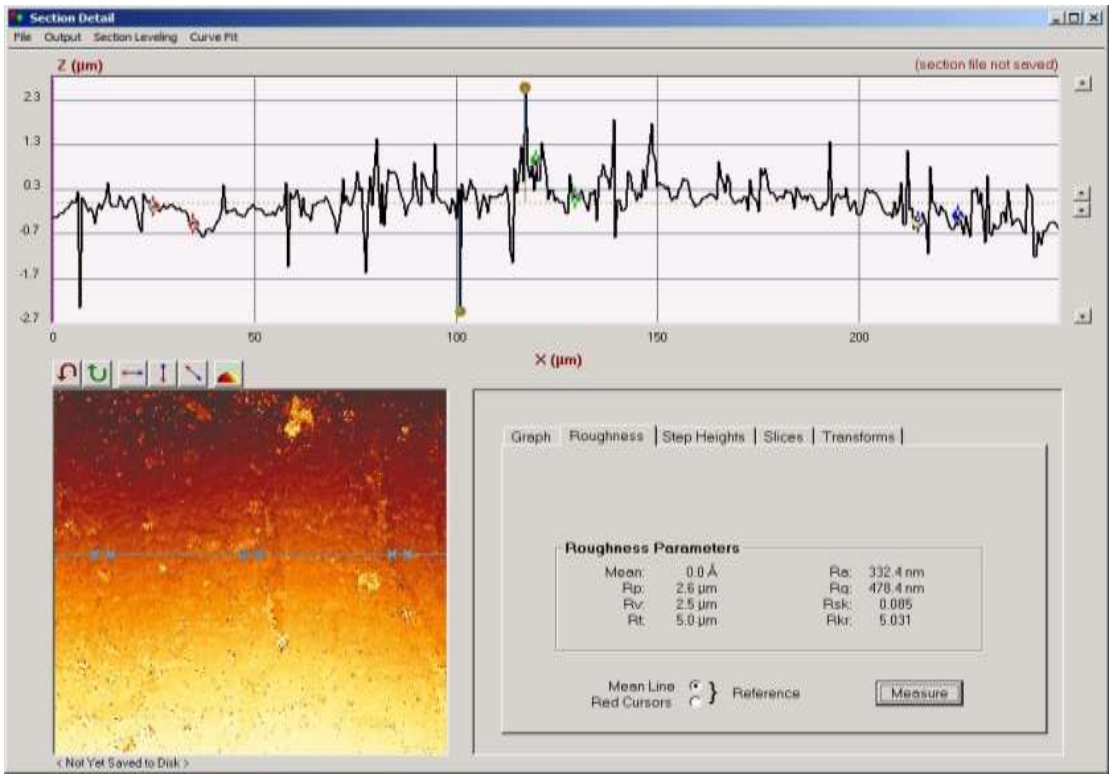

Figure 3.8(a): Surface roughness of MakerBot component

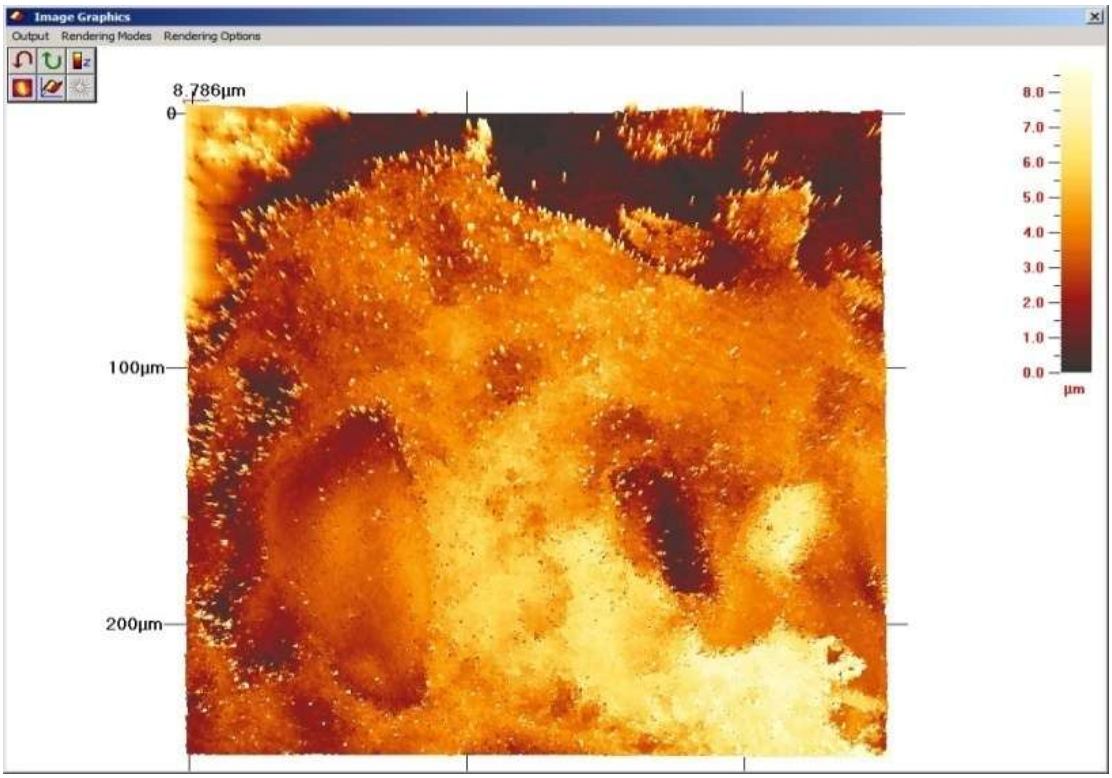

Figure 3.8(b): 3D surface of measured surface roughness for MakerBot component

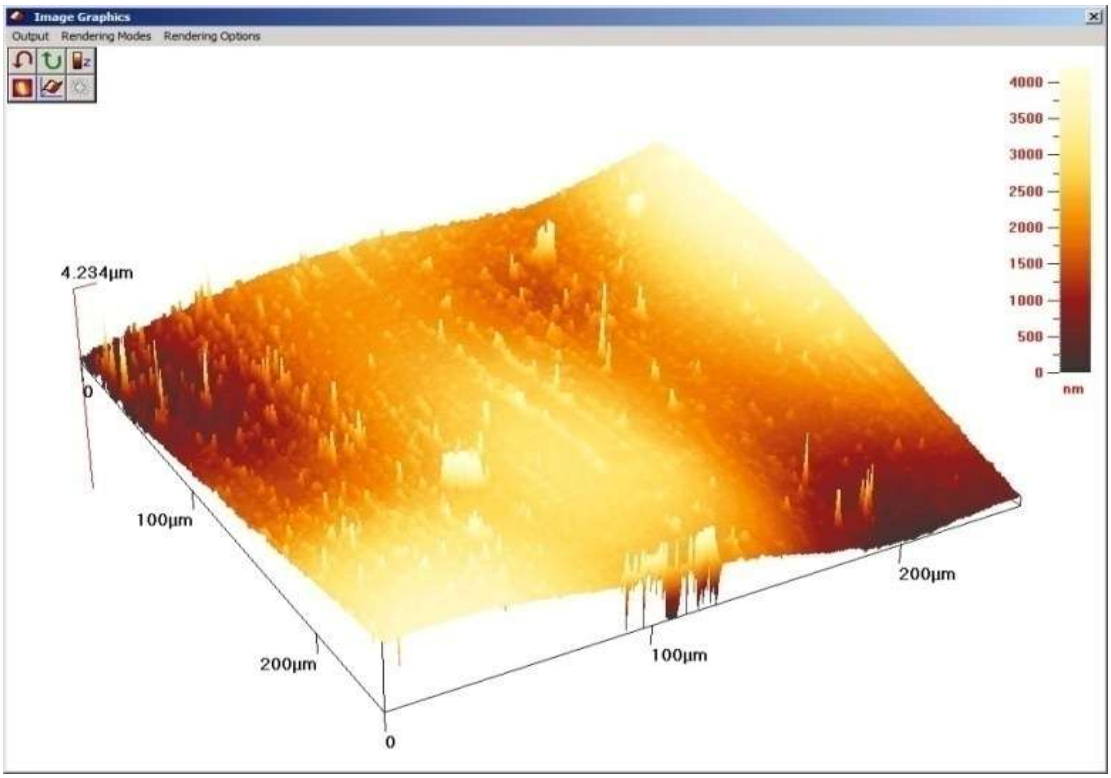

Figure 3.8(c): 3D surface of measured surface roughness of component printed through Objet 30 printer

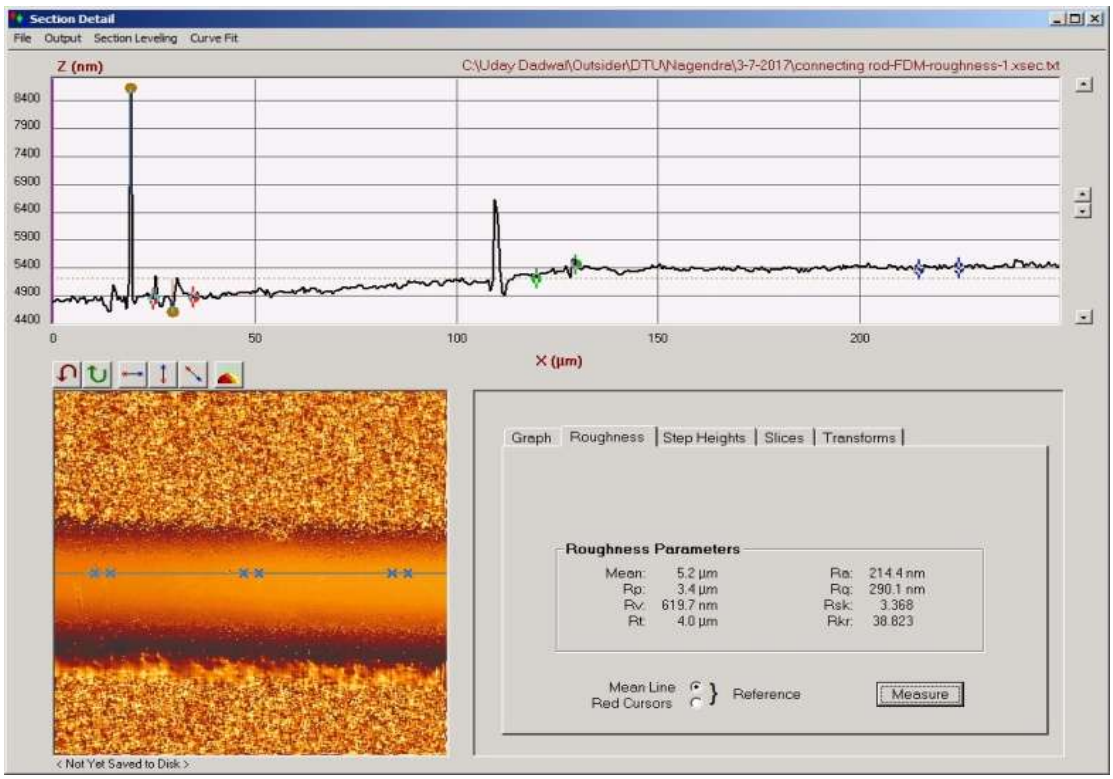

Figure 3.8(d): Surface of measured surface roughness for Objet 30 component

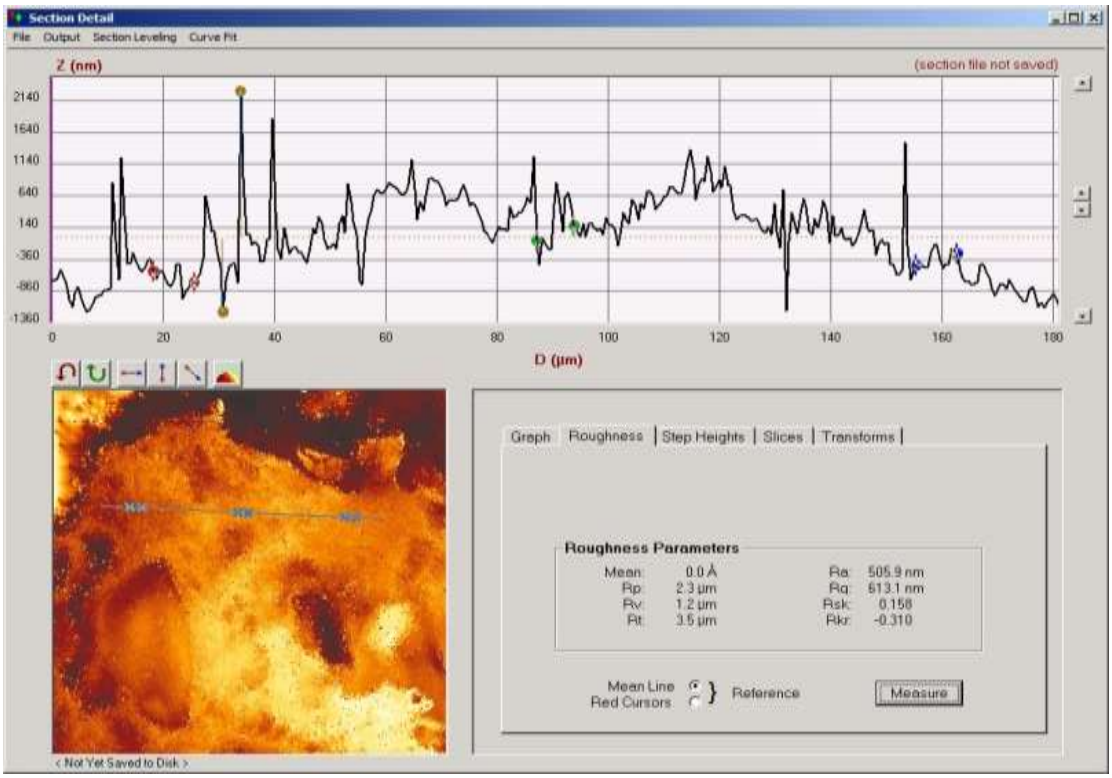

Figure 3.8(e): Surface roughness of Ultimaker component

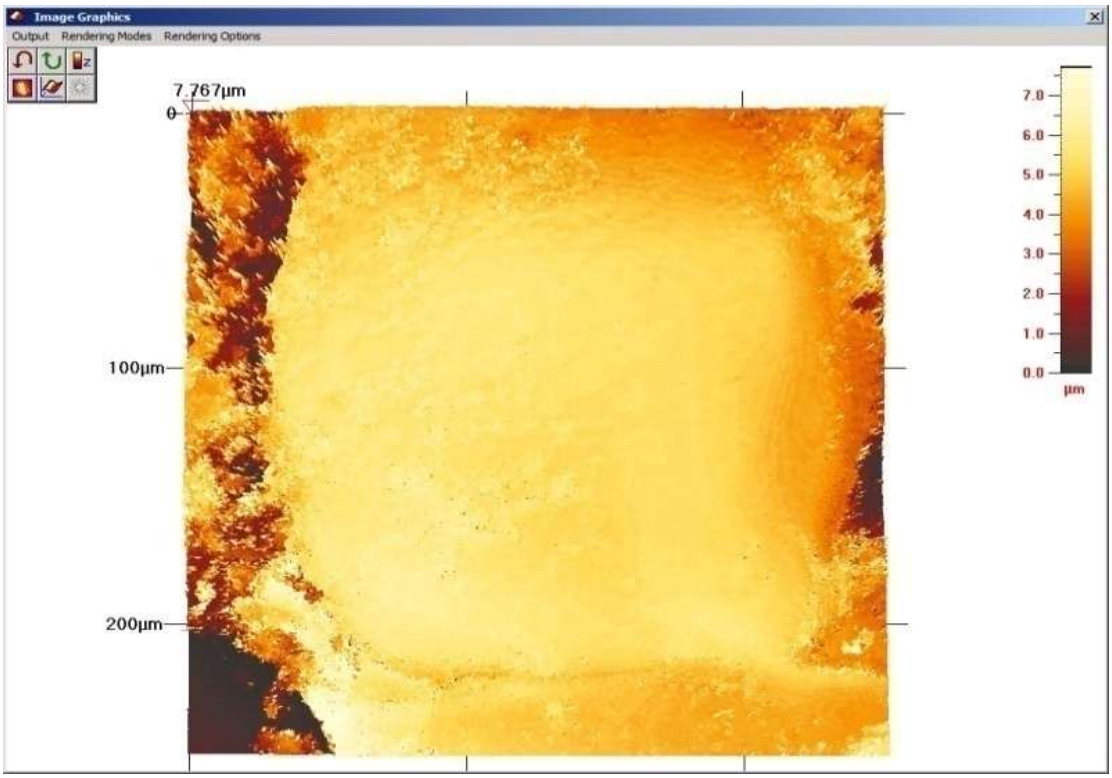

Figure 3.8(f): 3D surface of measured surface roughness for Ultimaker component

3.3 Results and discussion

3.3.1 Analysis of dimensional accuracy (DA)

Figure 3.9 shows the comparative analysis of average percentage error in DA of PolyJet and FDM technology. Four different types of dimensions were selected for the analysis i.e. linear dimensionsalong X-Y plane, linear dimensionsalong Y-Z plane, radial dimensions and circular dimensions.

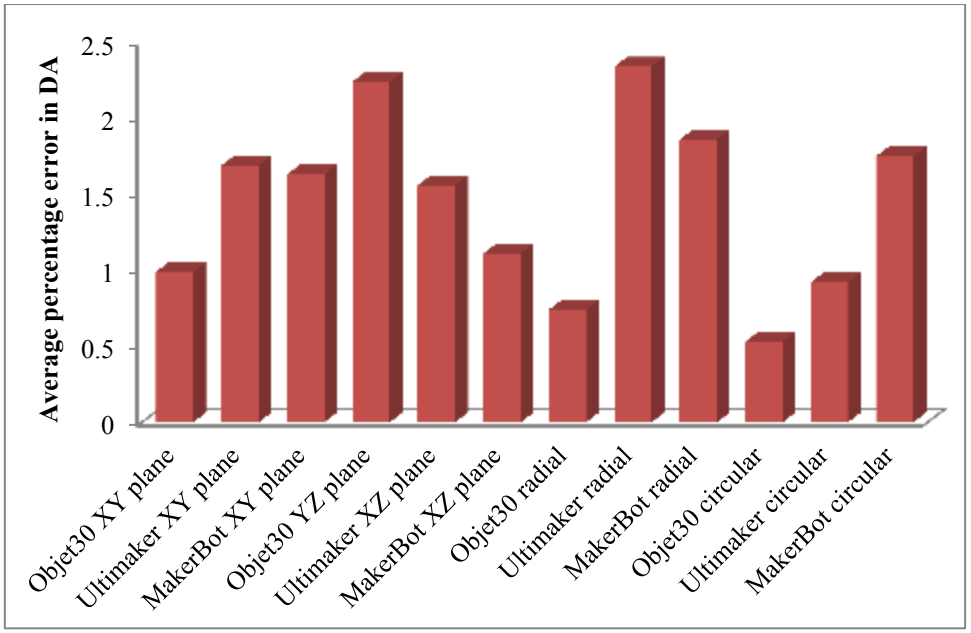

Figure 3.9: Comparison of average percentage error in dimensions of PolyJet and FDM

Tables (3.2 - 3.5) show the measured dimensions in terms of average percentage error. It is observed that the DA of component generated through PolyJet was better than the component fabricated through FDM printers. However, dimensional accuracy of the component fabricated through FDM printer along the Y-Z plane was found to be better as compared to PolyJet printer. It was also noticed that most of the dimensions were smaller than the actual model dimensions, due to the shrinkage occurs during the sintering of component. In FDM process, shrinkage was found more as compared to PolyJet technology. The component printed through FDM process are having air gapes,which

lead to the more shrinkage. However, along the Y-Z plane, PolyJet printed component always produce dimension more than the actual dimension. It forms a base on platform, which stick with the building geometry and assist in producing larger size. The average percentage error in radial and circular dimension in the component produced by Objet-30 printer was very less as compared to Ultimaker and MakerBot printers.

3.3.2 Analysis of form error

Figure 3.10 highlights the comparison of form error (circularity, cylindricity and flatness) in the selected component generated by Objet-30, Ultimaker and MakerBot printers. Experimental results ravelled that PolyJet technology have minimum form error as compared to the FDM. The measured value of form error is reported in Table 3.6. For perfect cylinder the value of cylindricity is '0'. In our analysis it was found that cylindricity in the component fabricated by Objet 30 is 0.0001, which is close to '0'. However, it was also observed that the components printed along inclined plane through PolyJet process are having more significant form errors, due to the shape distortion error.

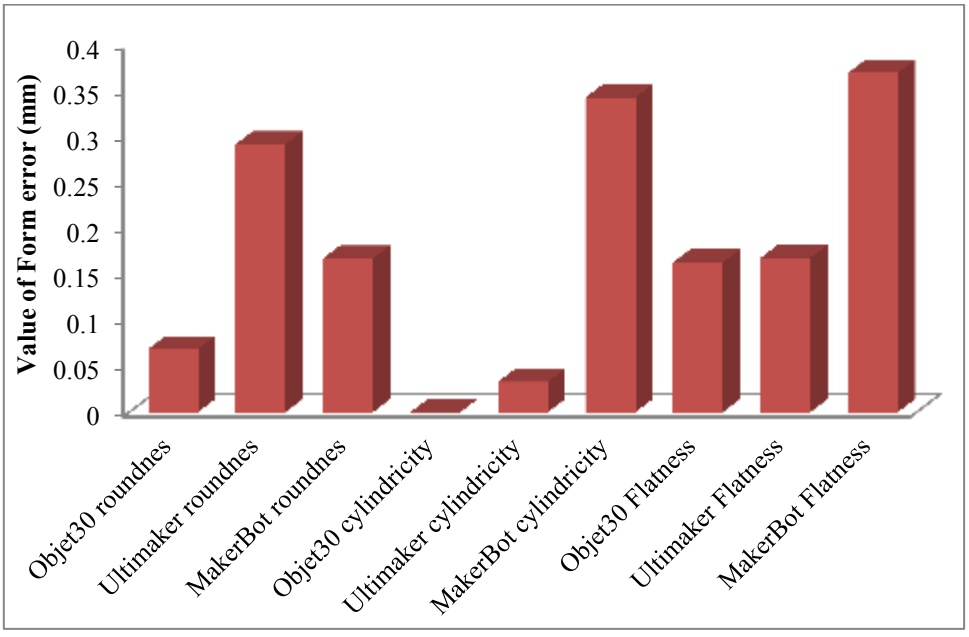

Figure 3.10: Form error comparison of PolyJet and FDM technology

3.3.3 Analysis of surface roughness parameters

Table 3.7 illustrates the measured value of variousSR parameters viz., R_a, R_q and R_z. The variation of SR and 3D plots of the surface roughness parameters were shown in Figures 3.8 (a-f). The comparative analysis of the measured surface roughness is represented in Figure 3.11. The experimental results revealed that component generated through PolyJet technology has superior surface quality than FDM components. It was observed that theSR parameter R_z was more significant than the other roughness parameters R_a and R_q value. It indicates that the surface irregularities were very high in components fabricated by using additive manufacturing technology. It is recommended that for superior surface quality PolyJet process is better in comparisonto FDM process. The next section presents the cost analysis of FDM and PolyJet process.

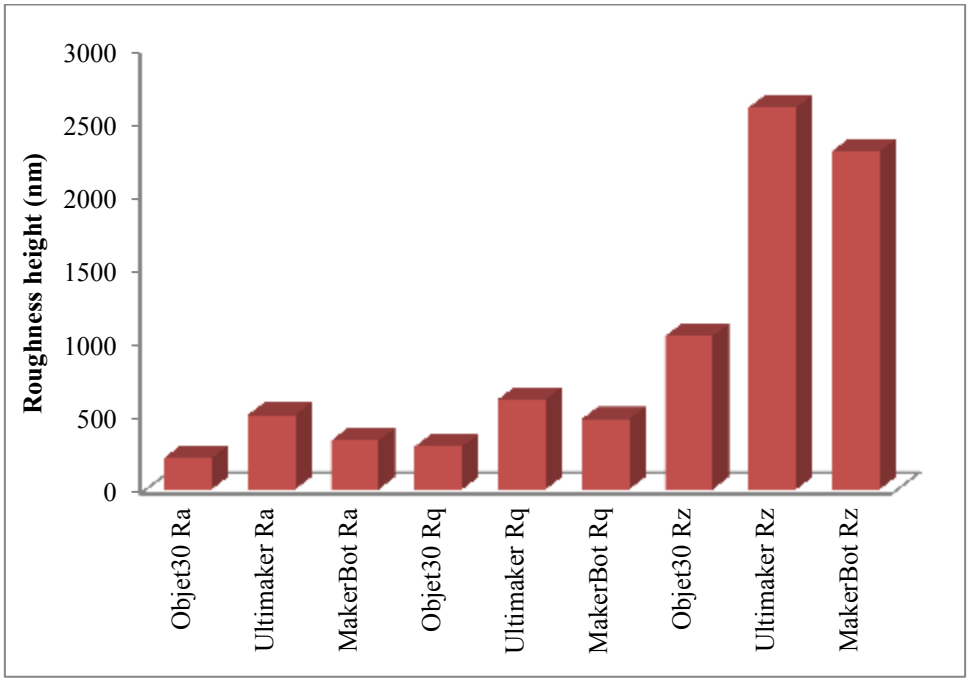

Figure 3.11: Roughness parameters comparison of PolyJet and FDM technology.

3.4 Cost analysis

Cost analysis of additive manufacturing is essential parameters for the designers while selecting the RP technology for printing components. Cost analysis is challenging for any RP technology because it depends on the number of factors, which varies locally & from place to place. However, in this work, cost analysis was calculated as per the Indian scenario. The factors, which mainly influence the cost are amount of materials (build and support) consumed, machine cost and labours cost. Total cost was calculated by using Eq.3.1.

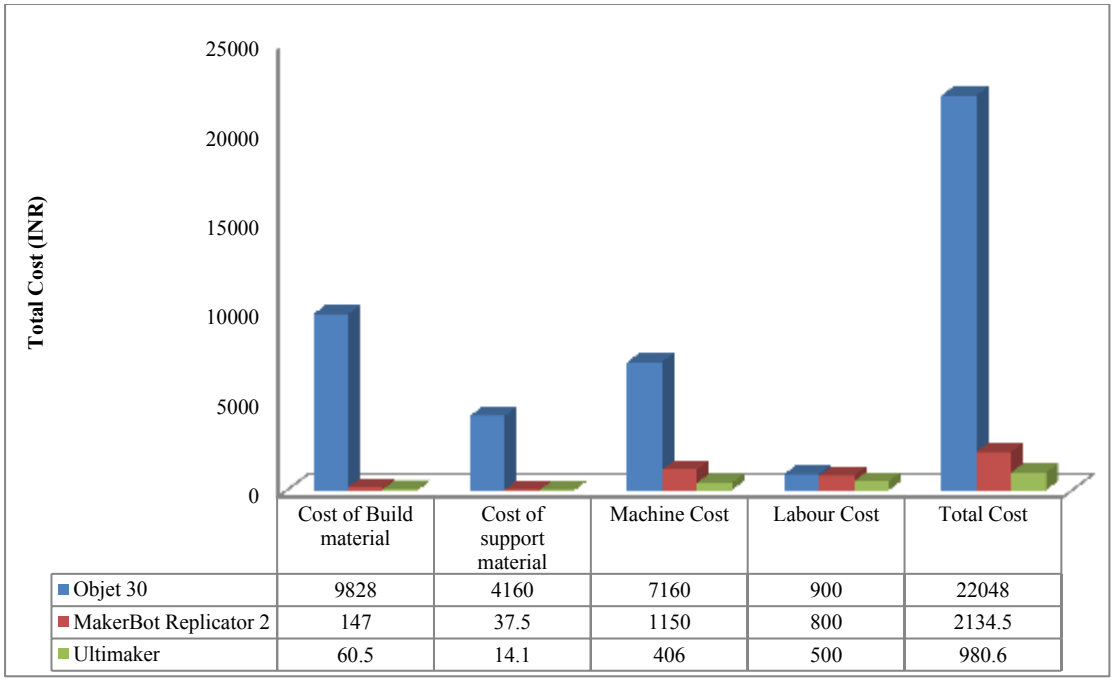

	Cost of Build material	Cost of support material	Machine Cost	Labour Cost	Total Cost
Objet 30	9828	4160	7160	900	22048
MakerBot Replicator 2	147	37.5	1150	800	2134.5
Ultimaker	60.5	14.1	406	500	980.6

Figure 3.12: Cost comparison of prototype fabricated by different 3D printers

Figure 3.12 shows the summary of cost analysis report of this work.

$$T_c = C_b \times A_b + C_s \times A_s + (t_{pre} + t_{post})\, C_{lc} + t_{pre} \times C_m \quad (3.1)$$

Where (Tc) is the total cost in (INR), C_b is the unit cost per kg of build material in (INR), C_s is the unit cost per kg of support material in (INR), A_b is the amount of build

material consumed in (Kg), A_s is the amount of support material consumed in (Kg), t_{pre} is the preprocessing time in (hrs), t_{post} is the post-processing time in (hrs), C_{lc} is the labour cost, and C_m is the machine cost in (INR).

3.5 Summary of the chapter

In this *chapter*, a comparative analysis of FDM and PolyJet technology was carried out. An automotive component, i.e. connecting rod was fabricated through FDM and Poly-Jet method. Comparative study was conducted based on linear and radial dimensions, flatness, cylindricity, surface roughness and cost of fabricated prototype models. Results of measurements depicted that dimensional accuracy and form error in PolyJet component were less as compared to FDM process. However, the cost of PolyJet component was very high as compared to FDM process. *Chapter 4* provides the optimization of process variables for the flatness, cylindricity and DA of the component fabricated by FDM process.

Chapter 4

Experimental Analysis of Flatness, Cylindricity and Dimensional Accuracy of Automotive Components

Chapter 4

Experimental Analysis of Flatness, Cylindricity and Dimensional Accuracy of Automotive Components

4.1 Introduction

In this *chapter*, various details are being presented regarding experimental analysis of flatness, cylindricity and dimensional accuracy. The methodology of the proposed scheme is also presented to give an idea of the whole methodology. It will cover the application of the experimental analysis for each analysis scheme to achieve the results. Multi-objective optimisation technique based on Utility theory is also applied to get the optimum results, which optimise all the response variables. Also, methodologies for the calculation of IT Grades are presented.

4.2Material and methodology of experiments

The aim of this study was to systematically measure the DA, flatness& cylindricity errors present in the fabricated prototype component by FDM technology and find out the optimum level of process parameters for the FDM process. Scaled radial engine connecting rod was selected as a specimen. Material used in this study was PLA plastic for both build and support. In this work, experimental studies were performed to investigate the influence of important FDM process variables like layer height, infill pattern infill density and orientation on DA, flatness and cylindricity at constant raster angle (45 degree). Taguchi method was employed for the conduction of the experiment. The next sub-section will emphasise the Taguchi approach.

4.2.1 Taguchi approach

In this research work, the Taguchi method is employed to optimise the FDM process variables. Taguchi design is a robust design, which uses orthogonal array (OAs) for the study of a significant number of process variables with a few experiments. This method suggests two different ways for the analysis of results. In the first route, the main effect and ANOVA analysis are executed for analysis of experimental data of single run or average value of multiple runs. In second route, S/N ratio is utilized for the experimental data analysis. In this study, effect of decision variables viz., layer thickness, infill pattern, orientation and infill density on response factors, i.e. percentage error in linear dimension, percentage error in radial dimension, flatness and cylindricity was experimentally investigated. Each decision variable has three levels. Every three levels of process parameters have one degree of freedom. The total degree of freedoms required for all four-decision variables at three levels is 4. In Taguchi method, total DOF required for the analysis of (OAs) must be greater than or equal to the required degree of freedom for the design variables.

4.2.2 Selection of specimen geometry

In this present work, the used dimensions for 3D modelling of connecting rod are similar, which is described in *chapter 3* shown in Figure 4.1. The selected component has linear dimension, radial dimension and cylindrical as well as flat surface.

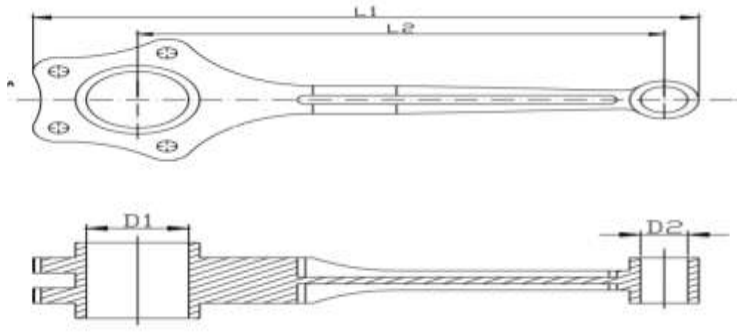

Figure 4.1: Selected linear and radial dimensions of the component

4.2.3 Design of experiment

The analysis of printing parameters' impact on dimensional accuracy and shape deviation was executed by Taguchi method. It reduces the number of samples and allow for good approximation. To ensure the repeatability of results, three samples were generated for the each set of experiments and the average value of each group was used for the analysis. Total of 27 samples were fabricated, three samples for each group of experiments. Four process variables and three levels of each process variables were used for all process variables. Levels of process variables in present study were layer thickness (100 µm, 200 µm and 300 µm), infill pattern (linear, hexagonal and Moroccan star fill), orientation (flat, edge and inclined at 45°), and infill density (20%, 40% and 60%). Table 4.1 illustrates the process variables and their levels. The experimental plan for each trial was reported in Table 4.2.

For 3D modelling standard modelling software, CATIA V6 was used. CAD model was converted into .STL file, which is required for the all 3D printing technology. Two linear dimension $L_1 = 202.56$ mm, $L_2 = 160.26$ mm and two radial dimension $D_1 = 31.20$ mm (big end of connecting rod), $D_2 = 14.40$ mm (small end of connecting rod) were selected for the measurement of percentage error in dimensional accuracy of FDM components. For measurement of cylindricity, big end and a small end holes were selected. For evaluation of cylindricity (big end hole and small end hole of connecting rod) was selected. Flatness was measured on the top surface of connecting rod. The next sub-section will provide the selection of FDM printer and fabrication of specimen.

Table 4.1: Process parameters & levels

S.N	Process parameters	Level1	Level 2	Level 3
1	Layer thickness (µm)	100 µm	200 µm	300 µm
2	Infill Pattern	Linear	Hexagonal	Moroccan star fill
3	Orientation	Flat	Edge	Inclined at 45°
4	Infill density (%)	20	40	60

Table 4.2: Taguchi's L_9 orthogonal array

Exp. No.	Layer thickness (µm)	Infill Pattern	Orientation	Infill density (%)
1	100	Linear	Flat	20
2	100	Hexagonal	Edge	40
3	100	Moroccan star fill	Inclined at 45°	60
4	200	Linear	Edge	60
5	200	Hexagonal	Inclined at 45°	20
6	200	Moroccan star fill	Flat	40
7	300	Linear	Inclined at 45°	40
8	300	Hexagonal	Flat	60
9	300	Moroccan star fill	Edge	20

4.2.4 Fabrication of samples

Components were fabricated by the MakerBotReplicator-2, a 3D desktop printer. To ensure the repeatability of results, three samples were manufactured for all sets of experiment and the average value of each group was used for the analysis. Total of 27 samples were fabricated with three samples for each group of experiment. Figure 4.2 (a) demonstrates the linear infill pattern, Figure 4.2 (b) demonstrates the hexagonal pattern and Figure 4.3(c) shows the Moroccan star fill pattern used for the fabrication of the component. The part orientation while fabrication is illustrated in Figures 4.3 (a-c). The fabricatedprototype model of connecting rod is shown in Figure 4.4. The next sub-section will provide the measurement process and experimental result of dimensional accuracy, flatness and cylindricity.

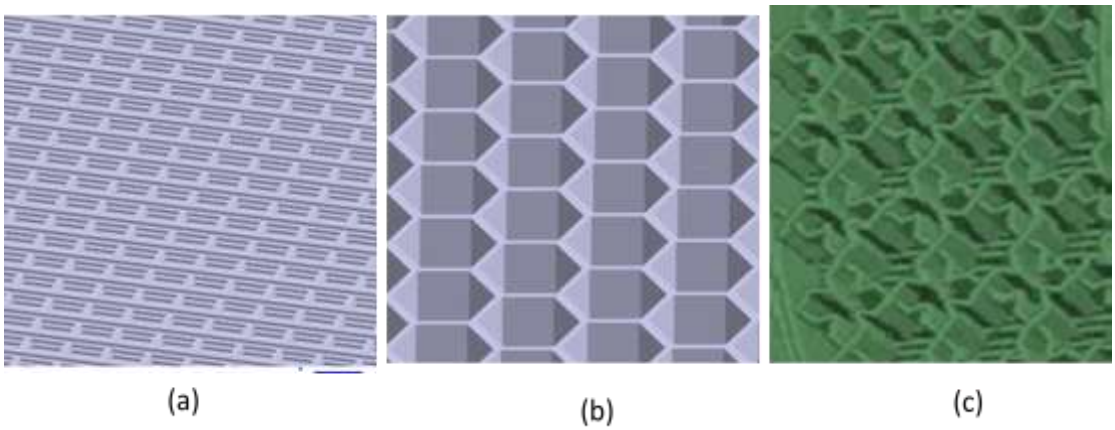

Figure 4.2: Type of infill pattern (a) Linear (b) Hexagonal (c) Moroccan star fill

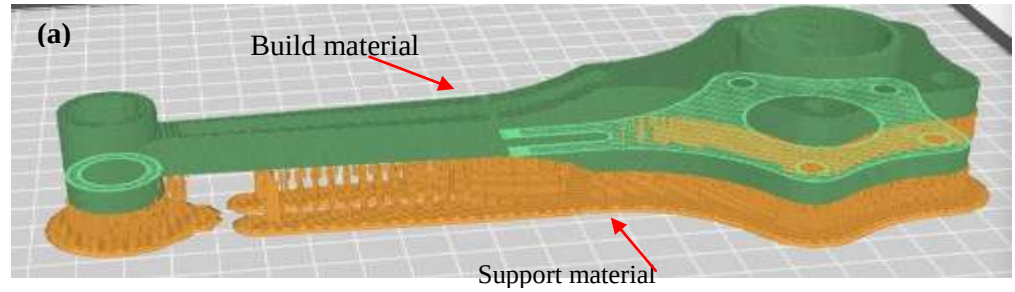

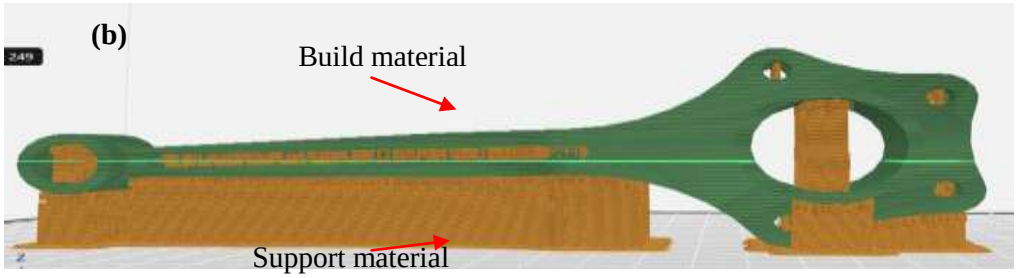

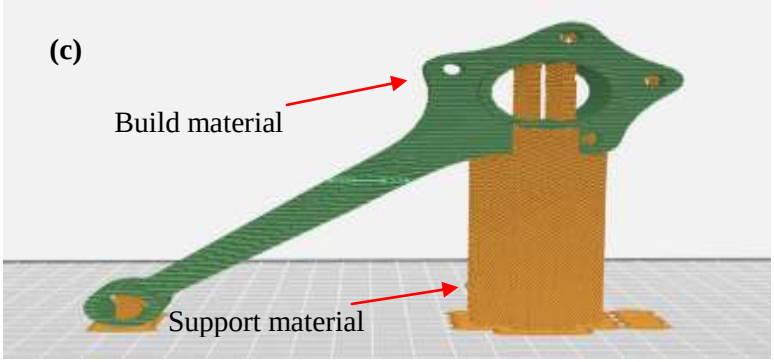

Figure 4.3: Orientation of specimens on FDM platform: (a) Flat orientation (b) Edge orientation (c) Inclined at *45°*

Figure 4.4: Prototype scaled model of connecting rod fabricated through the FDM process

4.2.5 Measurement of cylindricity, flatness and dimensional accuracy of FDM components

Cylindricity, flatness and dimensional accuracy of FDM manufactured products are major & very significant aspects, which are considered by researchers. The cylindricity is a three-dimensional tolerance which indicates roundness and straightness both along the entire length of a part. The value of '0' mm cylindricity represents an ideal cylinder case [90]. A perfectly flat surface is the one along which all points lie in a single plane. The flatness, cylindricity were evaluated by using the standard ASME Y14.5M-1994 [1]. In metrology, CMM is being used to automate the process of inspection, which has huge inspection capabilities. Flatness, cylindricity, radial dimension and linear dimension evaluation of automotive components (connecting rod) were performed by using CMM. In this research work, CONTURA G-2 CMM machine was used for the measurement. All axes of this machine are having 4-sided Carl Zeissair bearings for precise measurement. CONTURA G-2 is also equipped with C99 controller. It provides CAA for real-time dynamic correction. Selected linear and radial dimensions used for the measurement are highlighted in Figure 4.5.CMM has remarkably improved the confidence levels in forecasting of quality at the inspection

stage. The software associated with CMM does not directly provide many features like lines, planes, cylinders, circles etc. However, it gives data in the form of cloud points. The measured value of linear dimension, radial dimension, flatness and cylindricity are reported in Table 4.3.

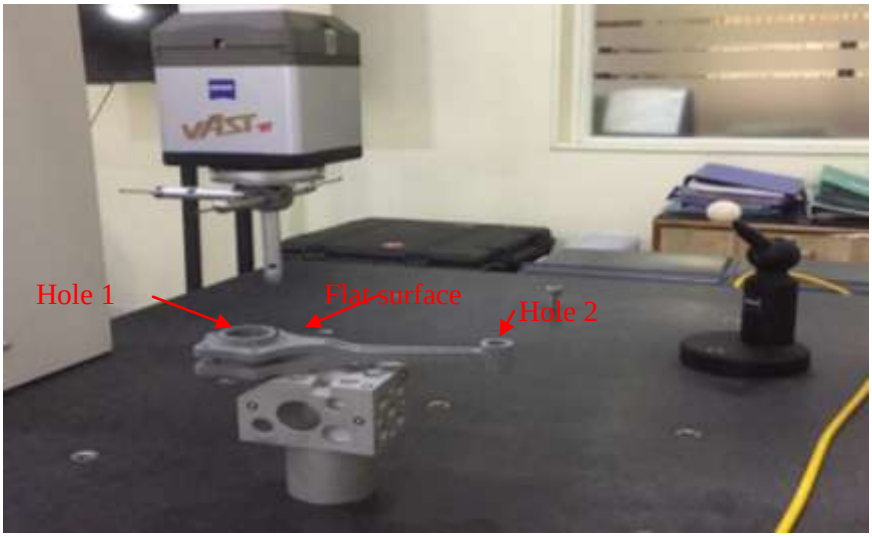

Figure 4.5: Measurement of flatness and cylindricity using CMM

Table 4.3: Measured value of the selected dimensions and form error

CADDimension / **Exp.no**	**No ofreplicate**	**Linear dimension (mm)**		**Radial dimension (mm)**		**Flatness (mm)**	**Cylindricity(mm)**	
		L_1 202.56	**L_2 160.26**	**D_1 31.20**	**D_2 14.40**	**Fy**	**Cy_1**	**Cy_2**
1	3	200.09	159.03	30.64	14.02	0.100	0.08	0.14
2	3	200.14	159.68	30.61	13.91	0.163	0.06	0.28
3	3	200.77	159.66	30.61	13.95	0.210	0.09	0.37
4	3	200.40	159.25	30.75	13.91	0.199	0.18	0.32
5	3	200.84	159.69	30.71	14.01	0.096	0.16	0.34
6	3	200.41	158.79	30.66	13.81	0.105	0.13	0.31
7	3	200.93	159.49	30.64	13.99	0.135	0.33	0.35
8	3	199.82	159.04	30.52	13.75	0.109	0.16	0.30
9	3	198.99	159.71	30.50	13.87	0.040	0.19	0.31

4.3 Statistical analysis of measured data

Experimentally measured data of Table 4.3 was analyzed for the linear dimension, radial dimension, flatness and cylindricity by using statistical software Minitab @14. The data analysis process is discussed in the next sub-section.

4.3.1 Signal to noise (S/N) ratio analysis

To examine the effect of process variables caused by each factor, the S/N ratio was used. It was observed that the experimental results varied linearly when they were presented in S/N ratio. The quality characteristic 'smaller is the better' was considered for the data analysis. S/N ratio (η) can be obtained by using Eq. 4.1*(Sood et al. [112]).*

$$\eta = -10\log(MSD) \tag{4.1}$$

$$MSD = \sigma^2 - (Y_{ave} - Y_0)^2 \tag{4.2}$$

Where *MSD* stands for Mean-Square Deviation, $\sigma^2$is the variance, Y_0isthe target value (0 in this design) and Y_{ave} is the average value of (n) data points. The value of MSD can be determined by using Eq. 4.2. For each run of the experiments, the S/N ratio was determined and reported in Table 4.4.The optimum factor level was selected by using the Main effect plot of S/N ratio. Significance of individual factor was also calculated by the comparison of calculated *F-value* found from experimental data with standard tabulated *F-value* at 95% CI level. The effect of the individual process parameters can be determined by ANOVA Eqs. (4.3)-(4.6).

$$S_T = (\eta - \overline{\eta}) \tag{4.3}$$

Where (S_T) stands for a total sum of square, η_0 is the overall mean of (S/N) ratio, and n is the total no of experiment [113].

$$SS_j = \sum_{i=1}^{l} (\eta_{ji} - \bar{\eta})^2 \tag{4.4}$$

$$V_j = \frac{SS_j}{f_j} \tag{4.5}$$

$$F_j = \frac{V_j}{V_e} \tag{4.6}$$

Table 4.4: S/N ratio analysis of the measured value

Exp.No.	Average value of flatness	Average value of cylindricity	Average % error in linear dimension	Average % error in radial dimension	S/N ratiofor flatness	Value of S/N ratio		
						Cylindricity	Linear dimension	Radial dimension
1	0.100	0.11	0.99	2.22	20.0	19.2	0.09	-6.93
2	0.163	0.17	0.78	2.65	15.8	15.4	2.16	-8.46
3	0.210	0.23	0.63	2.51	13.6	12.8	4.01	-7.99
4	0.199	0.25	0.85	2.42	14.0	12.0	1.41	-7.68
5	0.096	0.25	0.60	2.14	20.4	12.0	4.44	-6.61
6	0.105	0.22	0.99	2.91	19.6	13.2	0.09	-9.28
7	0.135	0.34	0.64	2.32	17.4	9.4	3.88	-7.31
8	0.109	0.23	1.06	3.35	19.3	12.8	-0.51	-10.50
9	0.040	0.25	1.05	2.96	28.0	12.0	-0.42	-9.43

The higher *F-value* signifies that the process response is getting affected by the factor. The *F-values* for the DA, flatness and cylindricity for this study was reported in Tables (4.6 -4.9) respectively. The main effect plot of signal to noise ratio for DA, flatness and cylindricity are shown in Figures 4.6 (a-d).

4.3.2 Development of an empirical model for the dimensional accuracy, flatness and cylindricity

Empirical model was derived by using the least square multivariable linear regression analysis. The response function *Y* for the DA, flatness and cylindricity in

terms of four input process parameters (X_1, X_2, X_3 and X_4) can be expressed by Eq. 4.7.

$$Y = f(X_1, X_2, X_3, X_4) \qquad (4.7)$$

The linear equation for the experimental data can be defined by Eqs. (4.8- 4.13)

$$Y = \beta_0 + \beta_1 \times X_1 + \beta_2 \times X_2 + \beta_3 \times X_3 + \beta_4 \times X_4 \qquad (4.8)$$

$$\sum_{i=1}^{n} Y_i = n\beta_0 + \sum_{i=1}^{n} \beta_1 \times X_1 + \sum_{i=1}^{n} \beta_2 \times X_2 + \sum_{i=1}^{n} \beta_3 \times X_3 + \sum_{i=1}^{n} \beta_4 \times X_4 \qquad (4.9)$$

$$\sum_{i=1}^{n} Yi \times X_1 = \sum_{i=1}^{n} \beta_0 X_2 + \sum_{i=1}^{n} \beta_1 \times X_1^2 + \sum_{i=1}^{n} \beta_2 \times X_1 \times X_2 + \sum_{i=1}^{n} \beta_3 \times X_1 \times X_3 + \sum_{i=1}^{n} \beta_4 \times X_1 \times X_4 \qquad (4.10)$$

$$\sum_{i=1}^{n} Y_i \times X_2 = \sum_{i=1}^{n} \beta_0 \times X_2 + \sum_{i=1}^{n} \beta_1 \times X_1 \times X_2 + \sum_{i=1}^{n} \beta_2 \times X_2^2 + \sum_{i=1}^{n} \beta_3 \times X_2 \times X_3 + \sum_{i=1}^{n} \beta_4 \times X_2 \times X_4 \qquad (4.11)$$

$$\sum_{i=1}^{n} Y_i \times X_3 = \sum_{i=1}^{n} \beta_0 \times X_3 + \sum_{i=1}^{n} \beta_1 \times X_1 \times X_3 + \sum_{i=1}^{n} \beta_2 \times X_2 \times X_3 + \sum_{i=1}^{n} \beta_3 \times X_3^2 + \sum_{i=1}^{n} \beta_4 \times X_3 \times X_4 \qquad (4.12)$$

$$\sum_{i=1}^{n} Y_i \times X_4 = \sum_{i=1}^{n} \beta_0 \times X_4 + \sum_{i=1}^{n} \beta_1 \times X_1 \times X_4 + \sum_{i=1}^{n} \beta_2 \times X_2 \times X_4 + \sum_{i=1}^{n} \beta_3 \times X_3 X_4 + \sum_{i=1}^{n} \beta_4 \times X_4^2 \qquad (4.13)$$

Where (n) is the total no of experiment, and β_0, β_1, β_2, β_3&β_4 are the regression coefficient. Y_i is the output response, and X_1, X_2, X_3 and $X_4$are the input parameters. The value of the unknown coefficient of the regression Eq. (4.8) can be determined by using Eqs. (4.9-4.13). In this study, the output variables were flatness, cylindricity, percentage error in linear dimension and percentage error in radial dimension. The input parameters were layer height, infill pattern, orientation and infill density. The obtained Regression equation for the flatness (F_y), cylindricity (C_y), percentage error in linear dimension *(%ΔL)* and percentage error in radial dimension *(%ΔR)* are as shown in Eqs. (4.14- 4.17).

$$Fy = 0.816 - 0.000315X_1 - 0.01317X_2 + 0.021173X_3 + 0.002350X_4 \quad (4.14)$$

$$Cy = 0.0044 + 0.000517X_1 + 0.0000X_2 + 0.0433X_3 + 0.000833X_4 \quad (4.15)$$

$$\%\,\Delta L = 1.09 + 0.000583X_1 + 0.0317X_2 - 0.195X_3 - 0.00083X_4 \quad (4.16)$$

$$\%\,\Delta R = 1.90 + 0.00208X_1 + 0.237X_1 - 0.252X_4 \quad (4.17)$$

Where X_1 stands for the layer thickness (µm), X_2 stands for the infill pattern (1 for linear, 2 for hexagonal and 3 for Moroccan star fill), X_3 is the orientation (1 for flat, 2 along edge and 3 for inclined at 45°) and X_4 is the infill density (%).The above developed empirical model predicts the DA, flatness and cylindricity for any combination of process parameters within the experimental domain. *F-test* was carried out for checking the accuracy of models. The optimum condition for the flatness and cylindricity is reported in Table 4.5.

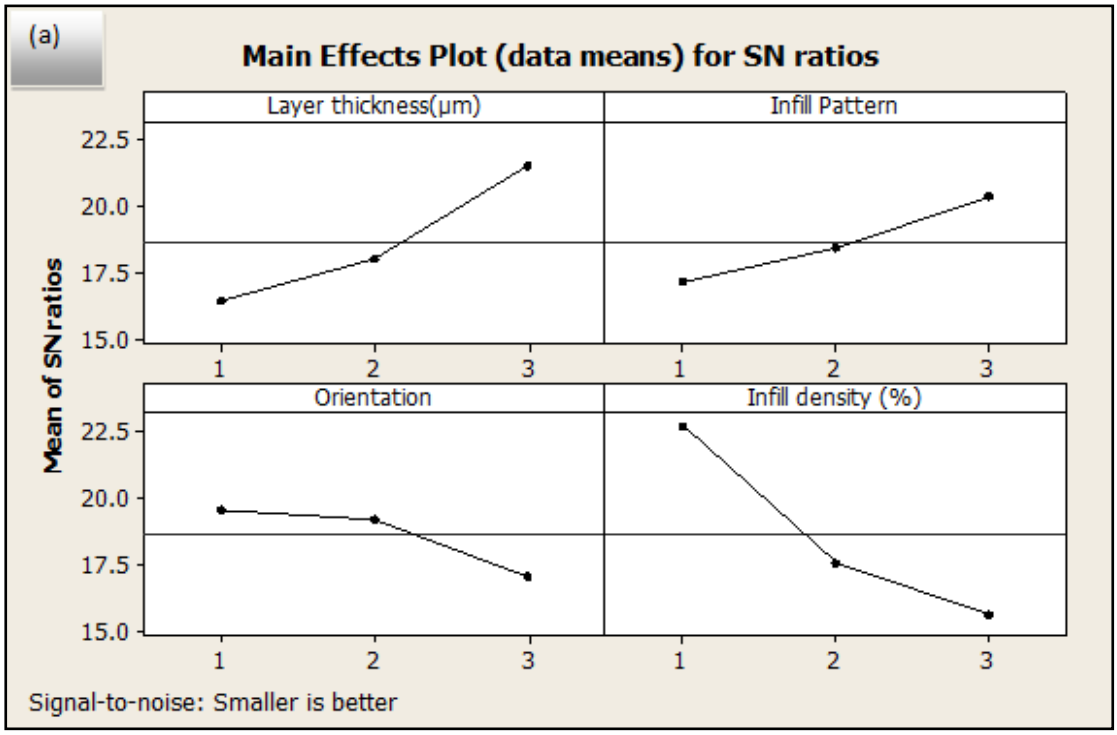

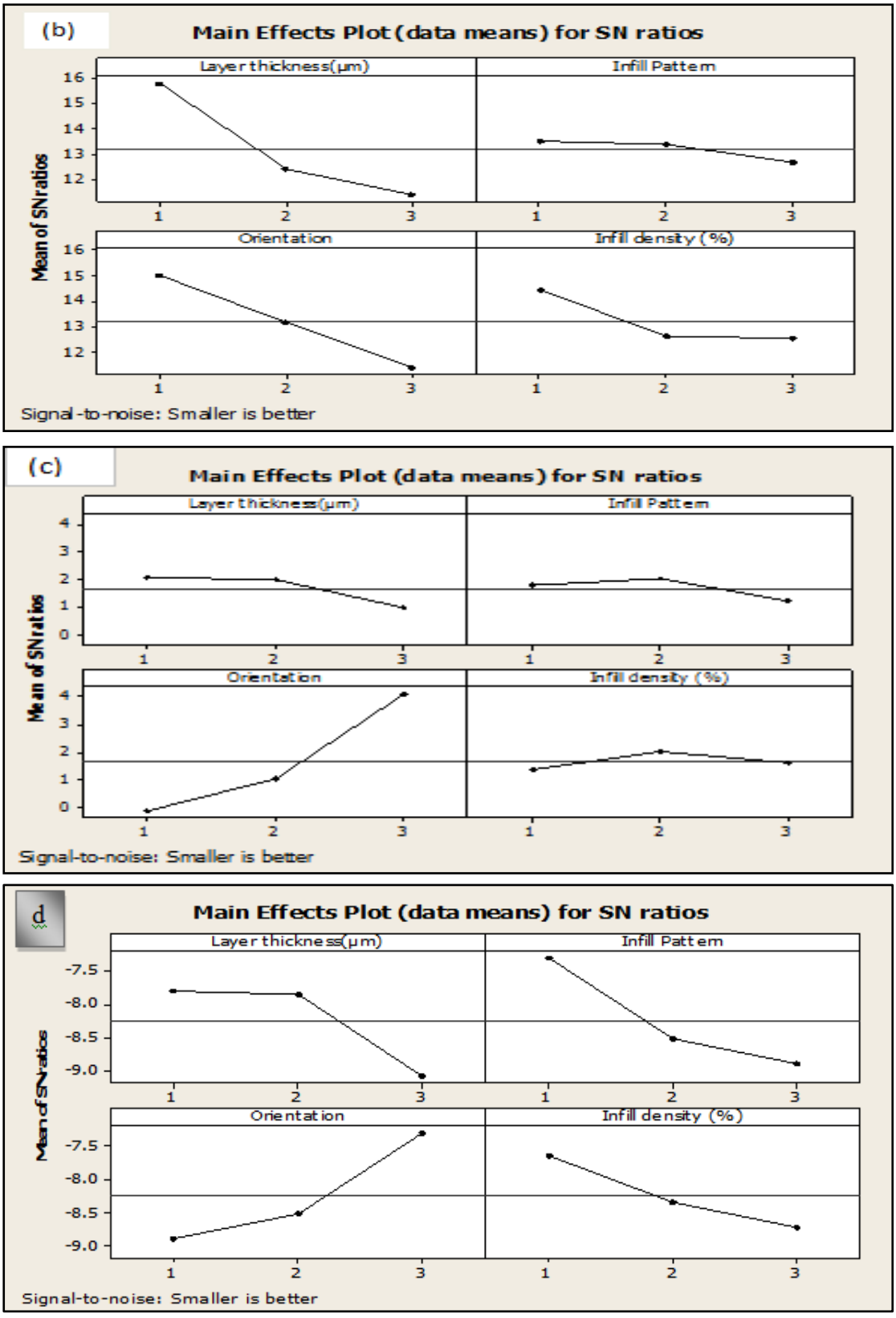

Figure 4.6: (a) Main effect plot of SN ratio of flatness (b) Main effect plot of SN ratio of cylindricity (c) Main effect plot of SN ratio of percentage error in linear dimension (d) Main effect plot of SN ratio of percentage change in radial dimension

Table 4.5: Optimum condition for minimum fatness, cylindricity, dimensional accuracy in the linear and radial direction

S.N	Shape error	Layer thickness	Infill pattern	Orientation	Infill density	Calculated from model
1	Flatness	300 µm	Moroccan star fill	Flat	20	0.0158 mm
2	Cylindricity	100 µm	Linear	Flat	20	0.116 mm
3	Percentage error in linear dimension	100 µm	Hexagonal	Inclined at 45°	40	0.5935 %
4	Percentage error in radial dimension	100 µm	Linear	Inclined at 45°	20	1.749 %

4.4 Results and discussion

The measured value of dimensional accuracy, flatness and cylindricity are illustrated in Table 4.4. The present study includes the evaluation of percentage error in linear dimension *(%ΔL)*, percentage error in radial dimension *(%ΔR),* flatness *(F_y)* and cylindricity *(C_y).* Results of measurement depicted that actual dimensions of the fabricated components were smaller than CAD dimension due to the shrinkage of material during solidification. Figures 4.6 (a-d) show main effect plots of S/N ratio for the DA, flatness and cylindricity. A regression model was developed for the forecasting of DA, flatness and cylindricity in terms of input process parameters. ANOVA technique was performed for checking the adequacy and fitness of these regression models. The *P-value* (probability value) of the suggested regression models were less than *0.05* and F-value of regression models were higher than tabulated *F-value* in the confidence interval of *95%*. The fitting accuracy of the regression models are decided by correlation coefficient R^2. Generally, a high value of R^2 (approaching to 1.0) indicates a good fit of developed mathematical model for the response variables. In the above model, value of R^2 was *0.976* for flatness Eq. *4.14*, value of R^2 was *0.9234* for the cylindricity Eq. (4.15), R^2 is *0.906* for percentage error

in linear dimension Eq. (4.16) and *0.893* for the percentage error in radial dimension Eq.(4.17), which indicates that there was a definite co-relation between actual and predicted value. The ANOVA analysis for response factors is shown in Tables 4.6 – 4.9. Higher value of percentage contribution indicates more significant process parameters in output response. In Table 4.6 corresponding to the process parameters layer thickness and orientation percentage contribution was high for the cylindricity evaluation. From Table 4.7 it can be concluded that flatness is highly affected by process variables infill density and layer thickness. It can be observed from Table 4.8 that percentage error in linear dimension is mainly influenced by the process parameter orientation. However, Table 4.9 demonstrates that percentage errors in radial dimension are affected by all the selected response variables.

Table 4.6: ANOVA table for the cylindricity

Source	**df**	**Seq SS**	**Seq MS**	**F-value**	**P-value**	**% contribution**	**Remarks**
Regression	4	0.0289	0.007238	12.03	0.017		
Layer thickness	1	0.0160	0.016017	26.63	0.007	51.08	
Infill pattern	1	0.000	0.000000	0.00	1.000	0.00	$F_{0.025,4,4} = 9.6045$
Orientation	1	0.0113	0.011267	18.73	0.012	35.93	$F > F_{0.025,4,4}$
Infill density	1	0.0016	0.001667	2.77	0.171	5.32	Model is adequate
Error	4	0.0024	0.000601			7.67	
Total	8	0.0313					

Table 4.7: ANOVA table for the flatness

Source	**df**	**Seq SS**	**Seq MS**	**F-Value**	**P-Value**	**%Contribution**	**Remarks**
Regression	4	0.022936	0.005734	42.29	0.002		
Layer thickness	1	0.005954	0.005954	43.91	0.003	25.36	
Infill pattern	1	0.001040	0.001040	7.67	0.050	4.43	$F_{0.025,4,4} = 9.6045$
Orientation	1	0.002688	0.002688	19.82	0.011	11.45	$F > F_{0.025,4,4}$
Infill density	1	0.013254	0.013254	97.75	0.001	56.45	Model is adequate
Error	4	0.000542	0.000136			2.31	
Total	8	0.023478					

Table 4.8: ANOVA table for the percentage error in linear dimension

Source	**df**	**Seq SS**	**Seq MS**	**F-Value**	**P-Value**	**% Contribution**	**Remarks**
Regression	4	0.256250	0.064063	9.65	0.025		
Layer thickness	1	0.020417	0.020417	3.08	0.154	7.22	
Infill pattern	1	0.006017	0.006017	0.91	0.395	2.13	$F_{0.025,4,4} = 9.6045$
Orientation	1	0.228150	0.228150	34.37	0.004	80.68	$F > F_{0.025,4,4}$
Infill density	1	0.001667	0.001667	0.25	0.643	0.59	Model is adequate
Error	4	0.026550	0.006638			9.39	
Total	8	0.282800					

Table 4.9: ANOVA table for the percentage error in radial dimension

Source	**df**	**Seq SS**	**Seq MS**	**F-Value**	**P-Value**	**% Contribution**	**Remarks**
Regression	4	1.1301	0.28253	8.38	0.032		
Layer thickness	1	0.2604	0.26042	7.73	0.050	20.59	
Infill pattern	1	0.3361	0.33607	9.97	0.034	26.57	$F_{0.05,4,4} = 6.3882$
Orientation	1	0.3800	0.38002	11.28	0.028	30.04	$F > F_{0.05,4,4}$
Infill density	1	0.1536	0.15360	4.56	0.100	12.14	Model is adequate
Error	4	0.1348	0.03370			10.66	
Total	8	1.2649					

It has been noticed from the above Tables 4.6-4.9 that dimensional accuracy and cylindricity is affected by layer thickness significantly. Figure 4.6(a) shows that the value of flatness is minimum at a layer thickness of 300 µm. According to *Wu et al. [65]* at layer height of 300 µm, FDM component has maximum mechanical properties. As tensile strength of the component increases, value of flatness automatically decreases. Figures 4.6 (b and d) show that the dimensional accuracy and cylindricity are better at smaller layer thickness of 100 µm. Dimensional error in radial direction and cylindricity are produced due to triangulation of circular geometry. At thickness of 100 µm, triangulation errors are

minimum, which result better cylindricity. Figure 4.6(c) shows that layer thickness is insignificant process parameters for the dimensional error in linear dimension.

Infill pattern plays a significant role in the mechanical behaviour and porosity in the FDM component. Hexagonal patterns have a maximum tensile strength *(Aljohani and Desai [114]*. However, it was observed that the infill pattern was not the significant process parameter for the flatness and dimensional error in linear dimension. Figure 4.5 (a) shows that the Moroccan star fill pattern has the lowest value of flatness. Figures 4.6(b and d) illustrate that linear pattern have the lowest cylindricity and dimensional error in radial dimension. It was observed that infill pattern has significant effect on dimensional error in radial direction.

Figures 4.6(a-b) show that along flat orientation, value of flatness and cylindricity were minimum. Figures 4.6(c-d) demonstrate that dimensional accuracy of the fabricated components was better along 45° orientation. It was observed that orientation has a significant effect on linear as well as radial dimension of the fabricated component. The effect of infill density was very high for the flatness. Figures 4.5(a – b, d) show that at 20% infill density, dimensional accuracy in radial dimension and form error in fabricated PLA component were minimum. Figure 4.6(c) shows that infill density was the insignificant process parameter for the dimensional accuracy in linear dimension.

4.5 Optimization of process parameters

The overall performance analysis of any machine is evaluated based on the number of output response. Table 4.5 shows that optimum condition for DA, flatness and cylindricity were different. Hence it was required to find out the best process parameter condition, which optimizes DA, flatness and cylindricity. So multi-objective

optimization technique was required. In this work, utility theory was employed for the optimization. The next sub-section will provide the utility theory in brief.

4.5.1 Utility theory

Utility theory is a powerful tool used for the multi-objective optimization of the decision variables. This theory converts multiple response factors into a single objective function. It presumed that a decision was taken to maximize the utilization of utility *Jayadithya et al. [115]*. According to utility theory, the mathematical expression of common utility is expressed below.

$$U\,(Z_1,Z_2,Z_3,Z_n)= f(U_1(Z_1),U_2(Z_2),U_3(Z_3)\ldots U_r(Z_n)) \tag{4.18}$$

Where $U_i(Z_i)$is the utility of the i^{th} attribute. The mathematical terms and greek symbols used from Eqs. (4.19 - 4.28) are described in the nomenclature of the thesis. The sum of individual utility makes the overall utility function. For an independent attribute, the utility function is given below:

$$U(Z_1,Z_2,Z_3....Z_n)=\sum_{i=1}^{n} U_i(Z_i) \tag{4.19}$$

The overall utility in terms of weight function can be calculated as:

$$U(Z_1,Z_2,Z_3....Z_n)=\sum_{i=1}^{n} W_iU_i(Z_i) \tag{4.20}$$

Where W_i is the weight function. Logarithmic scale is used for evaluating the performance scale.

$$P_i = A\times\log\left(\frac{Z_i}{Z_1}\right) \tag{4.21}$$

Where Z_i is the value of quality characteristics of i^{th} attribute, A is the constant and Z_1 is the minimum acceptable value. The value of the constant term can be evaluated with the help of optimal condition.

If $Z_i = Z^*$ (where Z^* is the optimal value) and $(P_i=9)$ for this case.

$$P_i = A \times \log\left(\frac{Z_i}{Z^*}\right) \tag{4.22}$$

The following expression gives the value of overall utility

$$U = \sum_{i=1}^{n} W_i P_i \tag{4.23}$$

The overall utility value can be used as a single objective function. Optimization is carried out by using the 'more significant is the better' quality characteristics. However, in this work, equal weight function (1/4) is considered for all response factors.

4.5.2 Construction of performance scale

The following performance scale scale has been constructed:

i. Performance scale of flatness

Performance scale for the response factors can be calculated by using Eqs.4.21 and 4.22. Optimum value of the process parameter was shown in Table 4.5 and value of minimum acceptable values of response factors is highlighted in Table 4.3. Z_f^* is the optimum value of flatness.

Z_f^* = 0.0158mm optimum value of flatness

Z_{1f} =0.21mm minimum acceptable value of flatness

A_f= - 8.01

$$P_{Fy} = -8.01\log\left(\frac{Z_{Fy}}{0.21}\right) \tag{4.24}$$

ii. Performance scale of cylindricity

Zc^* = 0.158mm optimum value of cylindricity (refer Table 4.5)

Zc_1=0.34mm minimum acceptable value of cylindricity (refer Table 4.3).

Ac= -27.25

$$P_{Cy} = -27.25 \log\left(\frac{Z_{Cy}}{0.21}\right) \tag{4.25}$$

iii. Performance scale of percentage error in linear dimension

Z_L^* = 0.5935% optimum value of percentage error in linear dimension (refer Table 4.5)

Z_{1L} = 1.06% minimum acceptable value of percentage error in linear dimension (refer Table 4.3).

A_L = -35.7

$$P\varepsilon l = -35.73 log\left(\frac{Z\varepsilon l}{1.06}\right) \tag{4.26}$$

iv. Performance scale of percentage error in radial dimension

Z_R^* = 1.749 % optimum value of percentage error in radial dimension (refer Table 4.5).

Z_{1R} = 3.35% minimum acceptable value of percentage error in radian dimension (refer Table 4.3).

A_R = -31.88

$$P\varepsilon r = -31.88 log\left(\frac{Z\varepsilon r}{3.35}\right) \tag{4.27}$$

4.5.3 Utility value calculation

Eq. 4.28 was used to evaluate the utility value of each group of experiment.

$$U = P_{Fy} \times W_{Fy} + P_{Cy} \times W_{Cy} + P\varepsilon l \times W\varepsilon l + P\varepsilon r \times W\varepsilon r \tag{4.28}$$

In this work, equal weight function (1/4) was used for evaluating overall utility value. Table 4.10 shows the summary of utility value and S/N ratio corresponding to an overall utility value. The quality characteristics 'larger is the better' is implied for the evaluation of the S/N ratio. Minitab @14 was used for evaluation of S/N ratio and main effect plot of S/N ratio. Figure 4.7 shows the best conditions of the selected process parameters for DA, flatness and cylindricity.

Table 4.10: Utility value and S/N ratio

Exp. No.	U_{Fy}	U_{cy}	$U_{\varepsilon l}$	$U_{\varepsilon r}$	$U_{overall}$	S/N ratio
1	2.58	13.4	1.05	5.69	5.68	15.1
2	0.88	8.20	4.75	3.24	4.27	12.6
3	0	4.62	8.07	7.24	4.98	13.9
4	0.18	3.63	3.42	4.50	2.93	9.3
5	2.72	3.63	8.83	6.20	5.35	14.6
6	2.41	5.15	1.06	1.94	2.64	8.4
7	1.53	0	7.83	5.08	3.61	11.2
8	2.28	4.62	0	0	1.73	4.8
9	5.76	3.63	0.14	1.73	2.82	9.0

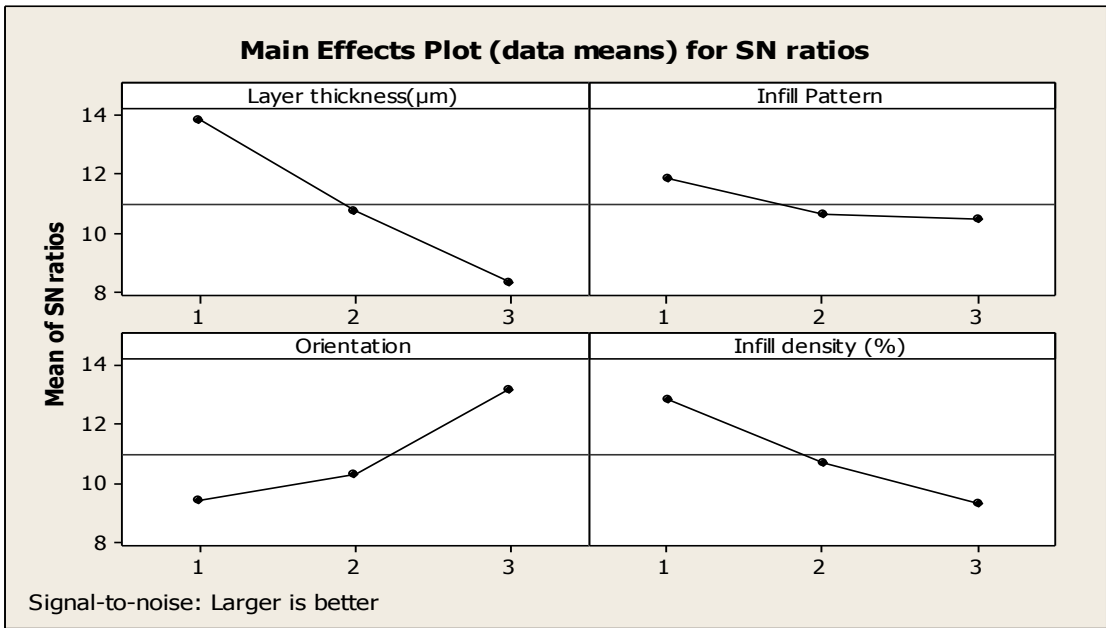

Figure 4.7: Main effect plot for S/N ratio

4.5.4 Confirmation test

A confirmation test was conducted corresponding to the best process parameter condition. The best values of process parameters were layer thickness (100 µm), infill pattern (linear), orientation (inclined at 45°) and infill density (20%).Owing to the uncertainty of the output response, three-component corresponding to the best process parameter condition were fabricated, and the average value of DA, flatness and cylindricity were reported in Table 4.11. Due to uncertainty output response was expected to fall in the range ofthe confidence interval (CI) [83]. The value of DA, flatness and cylindricity can be evaluated by using Eq. 4.29. Results of the conformation test depicted that the proposed models for the DA, flatness and cylindricity were adequate in the 95% of CI within the experimental domain.

$$\left.\begin{aligned}
&\text{Expected cylindricity} && = (Cy_{opt} \pm C.I)\\
&\text{Expected flatness} && = (Fy_{opt} \pm CI)\\
&\text{Expected \% error in linear dimension} && = (\%\Delta L_{opt} \pm CI)\\
&\text{Expected \% error in radial dimension} && = (\%\Delta R_{opt} \pm CI)
\end{aligned}\right\} \quad (4.29)$$

Table 4.11: Best value of process parameters for flatness and cylindricity

S.N	Shapeerror	Layer thickness	Infill pattern	Orientation	Infill density	Calculated from model	Experimental value
1	Flatness (mm)	100 µm	Linear	Inclined at 45°	20%	0.147±0.0173	0.154 mm
2	Cylindricity (mm)					0.185± 0.036	0.212 mm
3	% error in linear dimension					0.593 ± 0.121	0.649 %
4	% error in radial dimension					1.749 ± 0.122	1.683 %

4.6 Calculation of IT grade

For evaluation of International Tolerance Grade (IT grades) in the fabricated samples, ISO standard UNIEN 20286-I(16901) was considered [41]. IT grade was calculated based on tolerance unit '*n*', and tolerance unit was evaluated based on fundamental tolerance '*i*'. Tolerance unit and fundamental tolerance was calculated by using Eqs. 4.30 and 4.31 respectively [49]

$$i = 0.45\sqrt[3]{D} + 0.001D \tag{4.30}$$

$$n = \left(\frac{|D_n - Dm|}{i} \right) \tag{4.31}$$

The mathematical terms in Eqs. 4.30 and 4.31 are described in the nomenclature of the thesis. For present study, radial dimension (D_1= 32.2 mm) and linear dimension (L_1 = 202.56 mm) were used for the calculation of IT grades. The values of IT grade for the radial and linear dimension are reported in Table 4.12. It was noticed that the linear dimension has smaller IT grade as compared to the radial dimension.

Table 4.12: IT grade for the linear and radial dimension

Exp. No	L_1	n	IT grade	D_1	n	IT grade
1	200.09	853.2	IT14	30.64	358.7	IT13
2	200.14	835.9	IT14	30.61	378.0	IT13
3	200.77	618.3	IT13	30.61	378.0	IT13
4	200.40	746.1	IT14	30.75	288.3	IT13
5	200.84	594.1	IT13	30.71	313.9	IT13
6	200.41	742.7	IT14	30.66	345.9	IT13
7	200.93	563.0	IT13	30.64	358.7	IT13
8	199.82	946.5	IT14	30.52	435.6	IT14
9	198.99	1233.2	IT15	30.5	448.4	IT14

4.7 Summary of the chapter

In this *chapter*, studies were performed to calculate the impact of process variables viz., layer height, infill pattern, orientation and infill density on DA, flatness and cylindricity of FDM parts. Experiments were designed by using Taguchi orthogonal array L_9. A regression model was established to predict the DA, flatness and cylindricity. It can be concluded from experimental results that the process variables viz. orientation, layer height and infill density were the most significant process variables in the FDM process. Further, the multi-objective optimization technique utility theory was successfully employed to obtain the best level of process parameters, which optimized all the response factors. Also, International Tolerance Grades for the linear and radial dimensions were calculated. The next chapter of the thesis provides the influence of process parameters on DA, flatness and SR of the component manufactured by PolyJet process.

Chapter 5

Experimental Investigation of Dimensional Accuracy, Flatness and Surface Roughness of PolyJet Components

Chapter 5

Experimental Investigation of Dimensional Accuracy, Flatness and Surface Roughness of PolyJet Components

5.1 Introduction

In *chapter 3*,a comparative study of FDM and PolyJet process has been carried out. It was observed that the surface quality of the component produced by PolyJet process was better over the FDM component.In present scenario, AM is considered to produce the functional parts in a low volume.Investigations of effect of PolyJet process parameters are great interest for the researchers. This study focuses on impact of process variables on DA, flatness and SR of the component printed through the PolyJet process. The details of process variables and methodology are presented in the next section.

5.2Material and methodology

PolyJet technique includes several process parameters like surface type, orientation, support material, builds material, layer thickness, raster angle etc. The range of process parameters depends on machine type and materials. For printing superior quality products through PolyJet process, the knowledge of the effect of process parameters is required. Thus, these aspects are discussed in this investigation. The details of machine, material, process variables and levels are discussed in the next sub-section.

5.2.1 The details of PolyJet machine and material

PolyJet is a liquid-based technology, which is used to fabricate parts layer- upon- layer. It can produce a functional part directly from the CAD data. In this study, Objet30 (PolyJet) 3D desktop printer was chosen for the fabrication of the sample. The specification details of the printer are discussed in *chapter 3*. Figure 5.1 demonstrates

the diagram of machine used for the fabrication of samples. The schematic line diagram of PolyJet printer used in this investigation is shown in Figure 5.2.

Figure 5.1: Positioning of sample on objet 30 tray

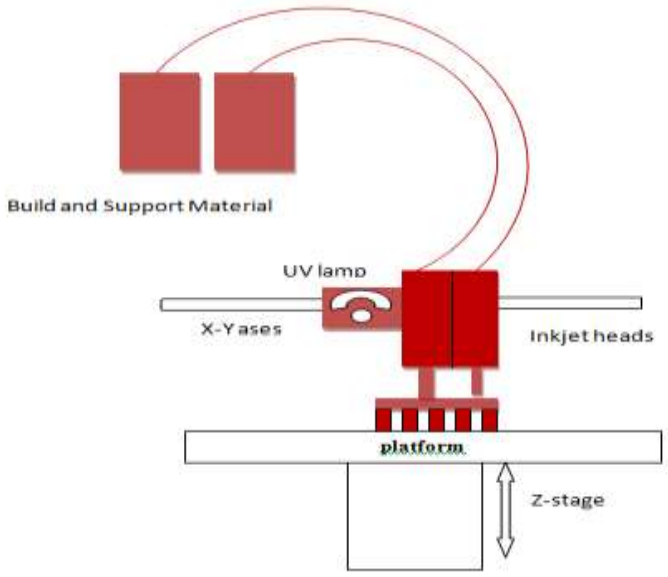

Figure 5.2: Schematic diagram of the PolyJet process

The working principle of PolyJet process is discussed in *chapter 1*. In thiswork, RGD840 material was used for the manufacturing of samples and SUP705 was used as a support

material. The properties details of the build and support material are discussed in *chapter 3.* The next sub-section provides the details of specimen geometry.

5.2.2 Selection of specimen geometry and process parameters

In order to analyse the impact of process variables on DA, flatness and SR, specimen of tensile test ASTM D-638 have been chosen for experimentation. The selected specimen had features of flat surface, linear and radial dimensions. Sample was symmetrical about both X and Y axis, and thickness along the Z-axis was kept constant (4 mm). *Melaka et al.[6]* used similar object to observe the DA of 'MakerBot' (FDM) 3D printer. Study shows that orientation and surface type had more impact on the SR of PolyJet component *(Kumar et al.[33]).* This study deals with the process parameters namely raster angle (*0°, 30°, 60° & 90°),* orientation (Flat and on-edge) and type of finish (Glossy and Matte). Owing to the limitation of the machine, levels of selected process parameters were not same. Table 5.1 illustrates the process variables and their levels. Dimension and geometry of ASTM model is shown in Figure 5.3. Standard CAD modelling software (CATIA V6, Dassault Systems) was used for 3D modelling of specimen. The 3D model of the selected specimen is shown in Figure 5.4. CAD model was converted into the standard file format '.STL', which is suitable for all the RP processes and imported into the objet studio software. This software has control over the selection of process parameters viz., raster angle, orientation, surface finish and spacing between the adjacent parts etc.

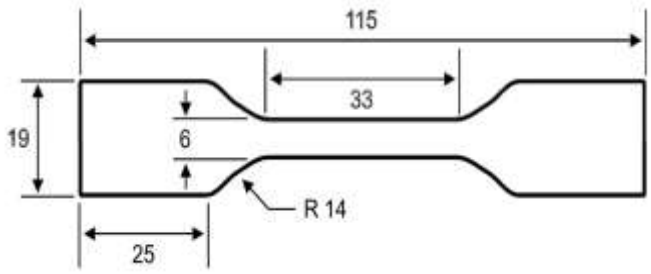

Figure 5.3: Dimension of the test specimen

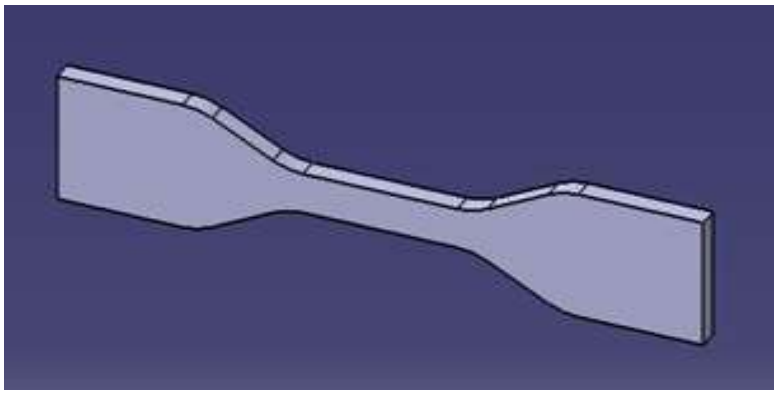

Figure 5.4: 3D CAD model of the specimen.

Table 5.1: Process Parameters and their levels for analysis of surface roughness, dimensional accuracy and flatness of PolyJet component

S.N	Factors	Level 1	Level 2	Level 3	Level 4
1	Raster angle (F_1)	*0°*	*30°*	*60°*	*90°*
2	Orientation (F_2)	Flat	on-edge	-	-
3	Surface Finish (F_3)	Glossy	Matte	-	-

5.2.3 Fabrication of samples

In this investigation, mixed levels Taguchi design was selected to find the optimum levels of process variables. Table 5.2 shows the experimental plan for the Taguchi design array (L_8) with three parameters and mixed levels. Raster angle was used at four levels whereas orientation and surface types were chosen at two levels due to the machine limitation. This design has used single block, single replicate and eight runs. The details about the Taguchi approach is discussed in *chapter 4.*

In Taguchi's design, the degree of freedom for process parameters (df= number of levels-1) may be ascertained by the evaluating total degree of freedom for the process parameters as 5[(4-1) +(2-1)+(2-1)]. According to Taguchi's principle, the total degree of freedom for the selected orthogonal array must be higher than the total degree

of freedom needed for the conduction of experiments. Table 5.3 shows the levels of the process variables used for each run of the experiment. The levels of process parameter raster angle (F_1) are shown in column 1. Column 2 and 3 show the levels of process parameters, i.e. orientation (F_2) and surface type (F_3), respectively. Figure 5.5 shows the fabricated samples used for this investigation.

Table 5.2: Design table for the experimentation

Experiment No	Raster angle (F_1)	Orientation (F_2)	Surface Finish (F_3)
1	1	1	1
2	1	2	2
3	2	1	1
4	2	2	2
5	3	1	2
6	3	2	1
7	4	1	2
8	4	2	1

Figure 5.5: Fabricated ASTM D638 tensile test specimen

5.2.4 Measurements of surface roughness

In this study, measurement of surface roughness was performed on MicroXAM-100 3D optical surface profiler. This optical profilometer uses light source rather than direct physical contact to the surface. It is an entirely non-destructive type of measurements. It provides precise, non-contact, high-resolution, and 3D profiles of both smooth and rough surfaces. It can measure 100 × 100 μm to the 2 × 2 millimetres depending on lens used. It can quickly measure 3D topography of surfaces at the nanometer level with a z-scan range of 250 microns.

In this investigation,the surface roughness of the flat surface (top surface) was measured. Five surface roughness parameters viz., R_a, R_p, R_v, $R_t$and R_q were measured. Table 5.3 shows the results of measured surface roughness height. Figures 5.6(a-h) show the variation of surface roughness of each run of the experiment.

- R_a (arithmetic mean roughness height): It is defined as the absolute average roughness value alongthe sampling length. Sign of the ordinate is not considered *(Sachdeva et al. [40]).*

$$R_a = \frac{1}{l}\int_0^l |y(x)|\,dx \tag{5.1}$$

- R_p (peak roughness height): It is defined as the absolute maximum roughness height over the sample length.

$$R_p = Max\big(y(x)\big) \tag{5.2}$$

- R_v (peak profile valley): It is also known as maximum profile valley, which indicates the position of the lowest point in the profile curve.

$$R_v = Min|y(x)| \tag{5.3}$$

- R_t (total height of the profile): It is defined as the total distance between peak height to the peak valley in the sample length.

$$R_t = Max(R_p) + Max|R_v| \tag{5.4}$$

- R_q (root mean square deviation): It is defined as the root mean square in the sample length.

$$R_t = \sqrt{\frac{1}{l}\int_0^l y^2(x)dx)} \tag{5.5}$$

- R_z (average peak to valley deviation): It can be expressed as an average of five highest peaks to deepest valleys in the sample length.

$$R_z = \frac{y_{1p+}\, y_{2p+}\, y_{3p+}\, y_{4p+}\, y_{5p+}\, |y_{1v+} y_{2v+} y_{3v+} y_{4v+} y_{5v}|}{5} \tag{5.6}$$

Figure 5.7 shows the relative variations of SR parameters (R_a, R_q and R_z) for each run of the experiment. Results showed that experiment 1 have the minimum value of all roughness parameters. The next sub-section highlights about the measurement of dimensional accuracy and flatness of the component fabricatrdthrough Objet 30 printer.

Table 5.3: Experimental results of surface roughness

S.N	Raster angle (F_1)	Orientation (F_2)	Surface type (F_3)	Surface roughness parameter					
				R_a (nm)	R_p (nm)	R_v (nm)	R_t (nm)	R_q (nm)	R_z(nm)
1	0°	Flat	Glossy	39.9	348.4	204.0	552.4	59.9	377.4
2	0°	on-edge	Mat	173.6	842.6	951.9	1800.0	227.4	1084.9
3	30°	Flat	Glossy	45.8	563.3	1400.0	1900.0	96.0	842.0
4	30°	on-edge	Mat	172.3	972.3	974.9	1800.0	231.0	1386.3
5	60°	Flat	Mat	133.4	1600.0	476.5	2100.0	191.3	1312.0
6	60°	on-edge	Glossy	73.0	1600.0	226.0	1800.0	175.7	907.6
7	90°	Flat	Mat	92.3	466.7	355.2	821.9	120.8	703.0
8	90°	on-edge	Glossy	80.20	415.00	235.90	651.00	100.1	479.60
Mean Value				101.31	851.04	603.05	1428.1	150.3	886.61
Maximum Value				173.60	1600.0	1400.0	2100.0	231.0	1386.3
Minimum Value				39.90	348.40	204.00	552.40	59.90	377.40
Standard Deviation				52.75	508.49	448.61	635.53	64.69	364.71
Standard Deviation/Mean				0.52	0.60	0.74	0.44	0.43	0.41

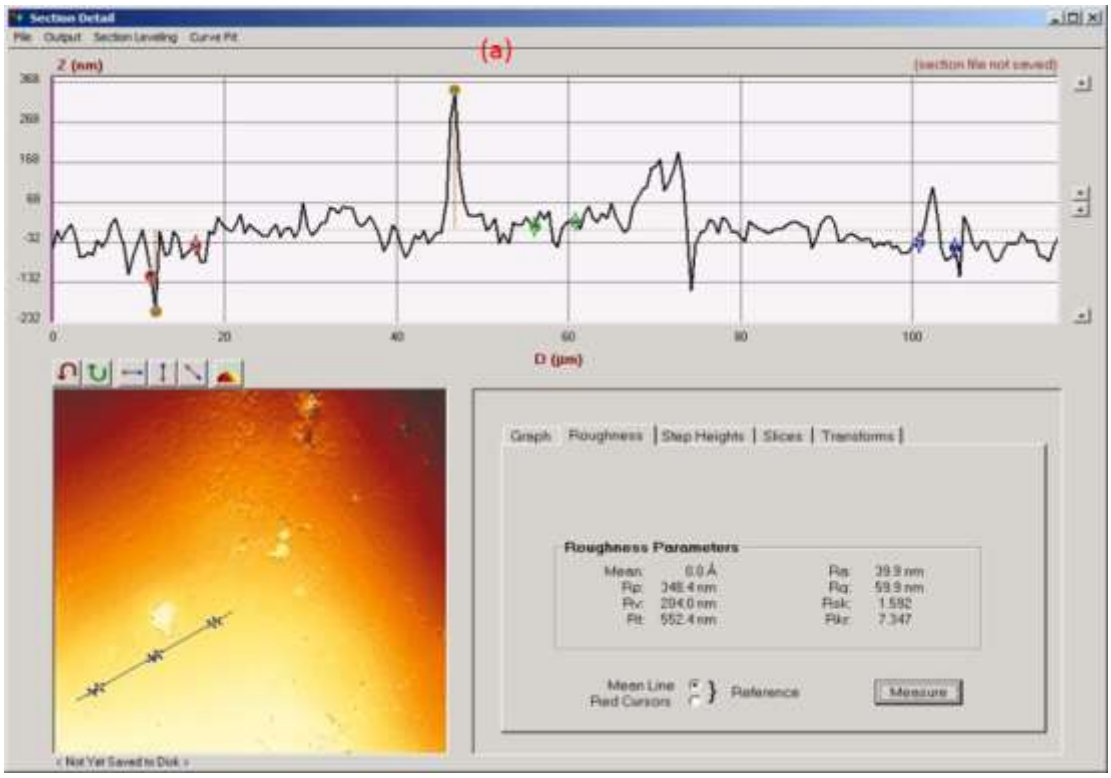

Figure 5.6(a): Surface roughness of experiment 1

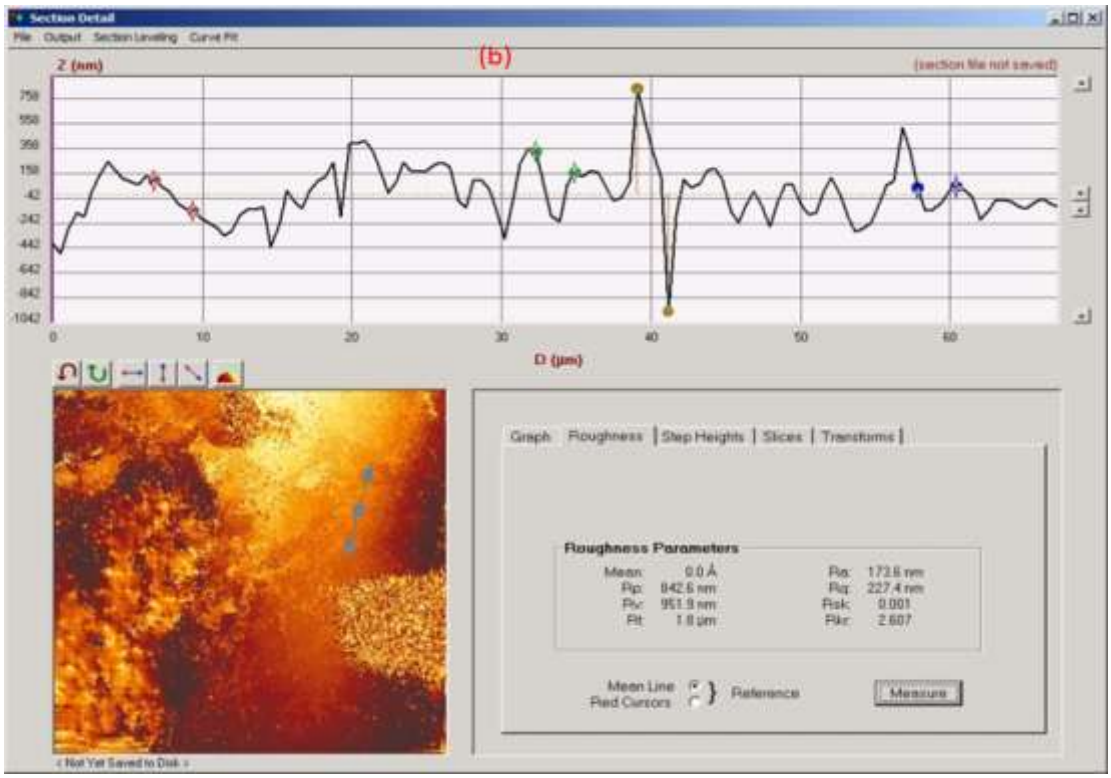

Figure 5.6(b): Surface roughness of experiment 2

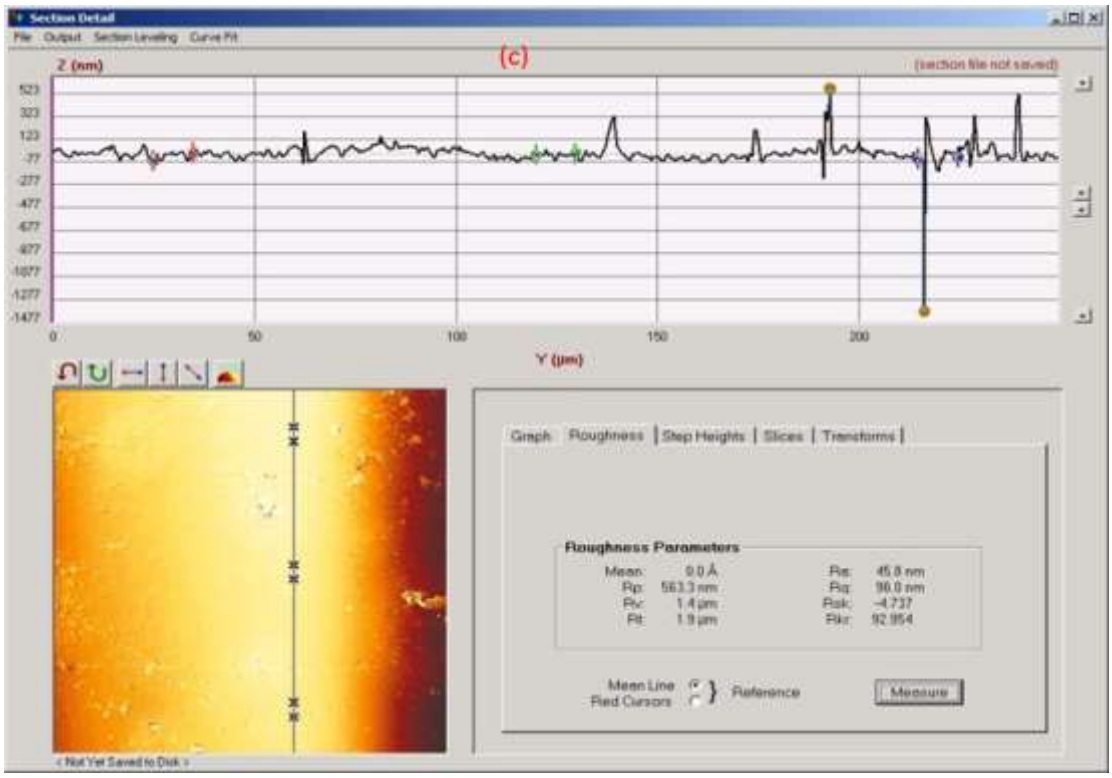

Figure 5.6(c): Surface roughness of experiment 3

Figure 5.6(d): Surface roughness of experiment 4

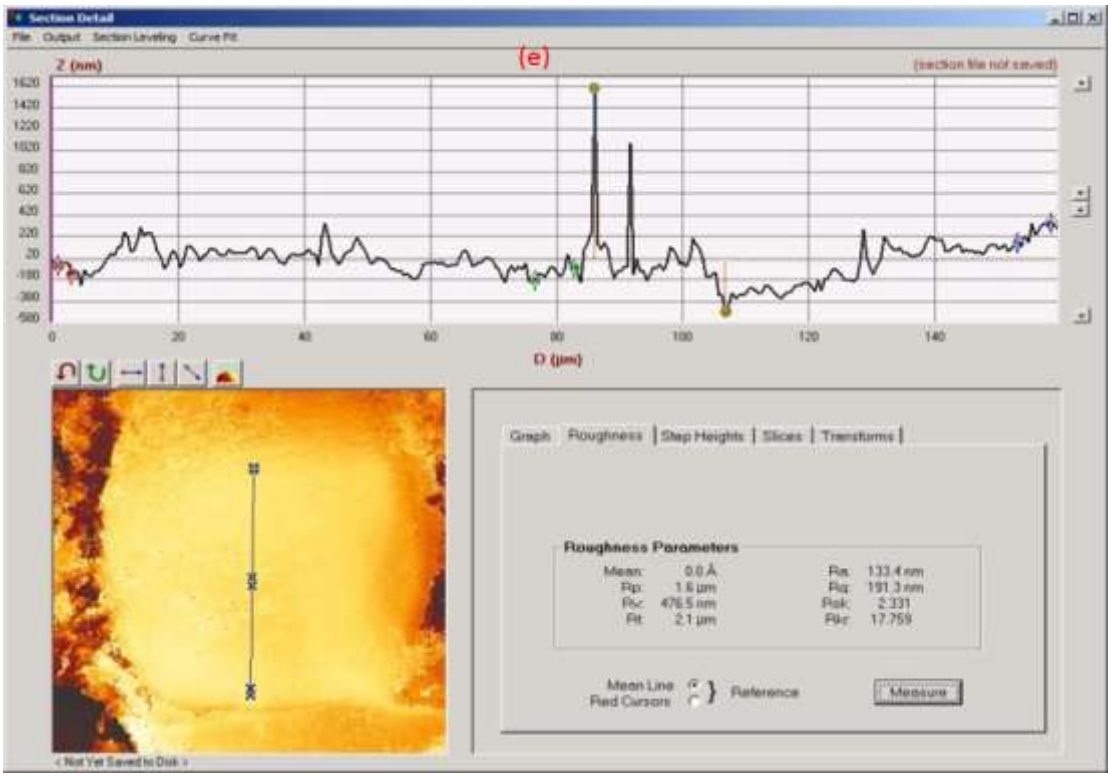

Figure 5.6(e): Surface roughness of experiment 5

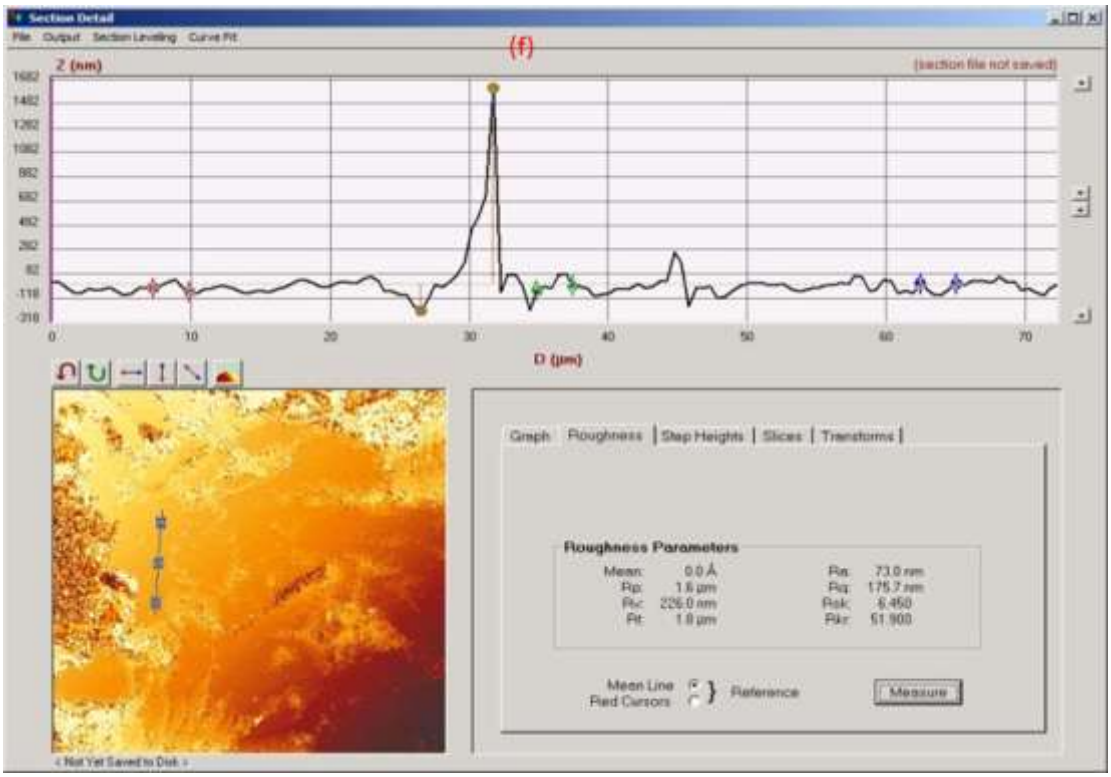

Figure 5.6(f): Surface roughness of experiment 6

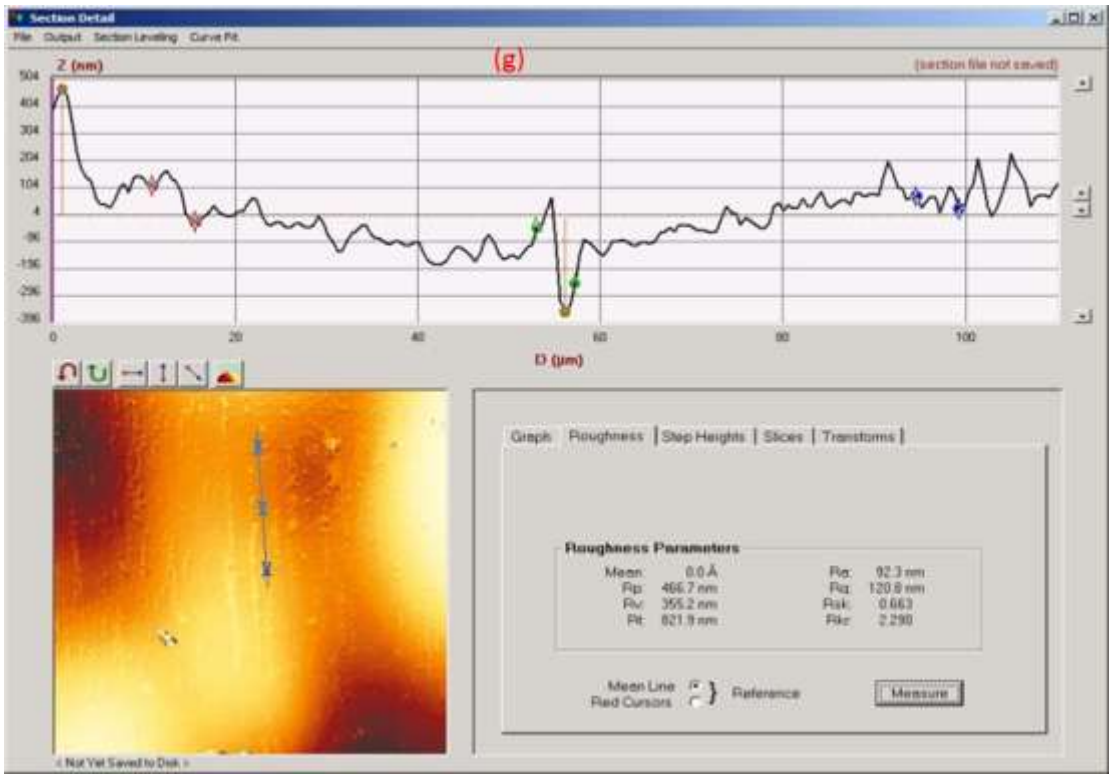

Figure 5.6(g): Surface roughness of experiment 7

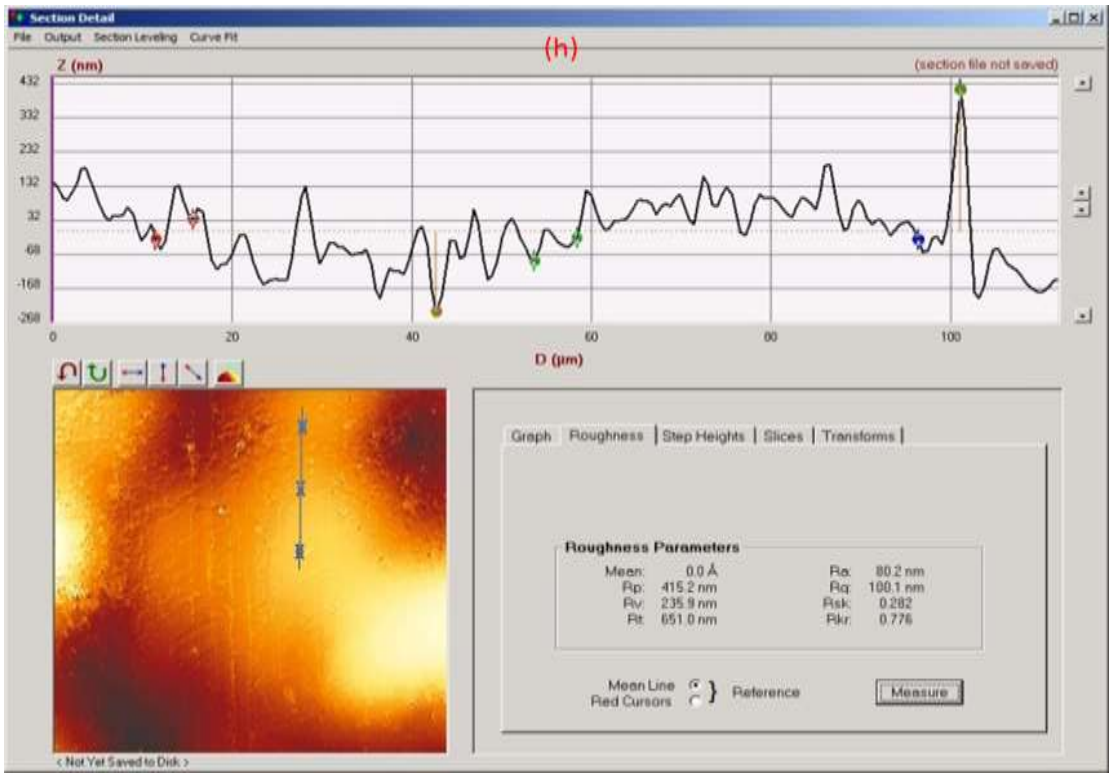

Figure 5.6(h): Surface roughness of experiment 8

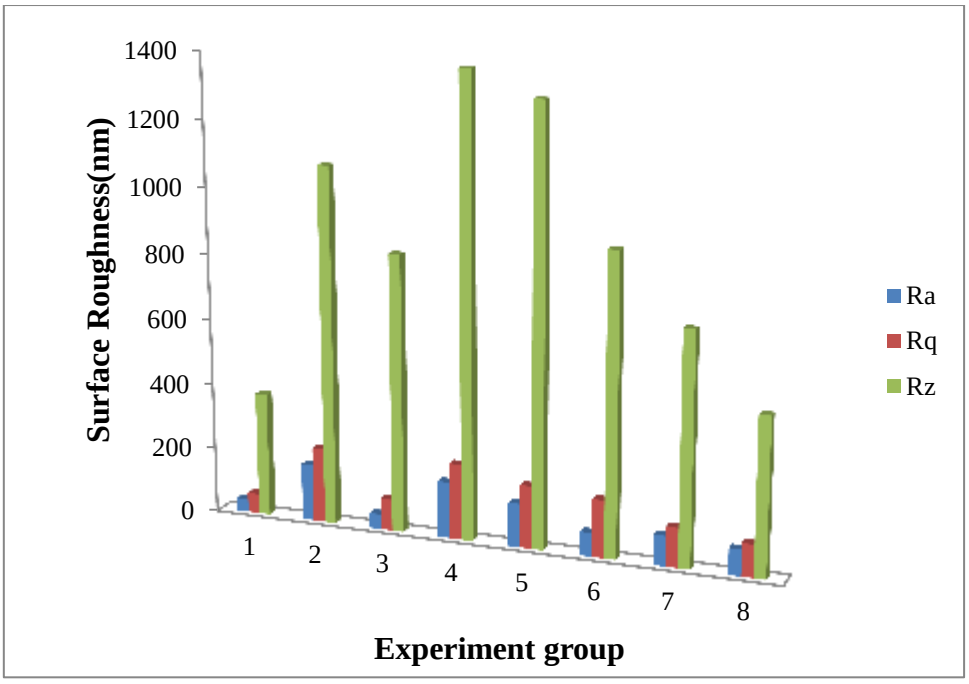

Figure 5.7: Measured surface roughness for each group of experiment

5.2.5 Measurement of dimensional accuracy and flatness

The DA and flatness of the surface was measured using CONTURA G-2 coordinate measuring machine (CMM). The details of the CMM machine is discussed in *chapter 4* of the thesis. For analysing the DA of the specimen, two dimensions L_1 (115 mm) & L_2 (25 mm) were measured along the length, two dimensions along width W_1 (19 mm) & W_2 (6 mm) and one along the thickness (t = 4 mm). Measured dimension and the percentage error are reported in Table 5.4. Figure 5.8 shows the percentage error in DA along length, width and thickness. The results reflect that the maximum dimensional error occurred in the thickness of the specimen. Flatness was measured along the top surface of the specimen.

Table 5.4: Measured value of specimen dimension and % error

CAD dimension / Exp. No.	L_1	L_2	W_1	W_2	t	|% Dimensional error|			Flatness (mm)
	115(mm)	25(mm)	19(mm)	6 (mm)	4(mm)				
	Actual specimen dimension					Length	Width	Thickness	
1	115.03	24.91	19.00	5.97	4.48	0.04	0.12	12.00	0.05
2	114.92	24.86	19.27	6.03	4.18	0.16	1.20	4.50	0.09
3	114.94	24.87	19.05	6.01	4.69	0.14	0.24	17.25	0.05
4	115.04	25.21	19.45	6.86	4.33	0.18	5.24	8.25	0.06
5	115.01	25.04	19.25	6.11	4.58	0.04	1.44	14.50	0.02
6	114.89	24.85	19.45	6.00	4.08	0.19	1.80	2.00	0.10
7	114.85	24.94	19.29	6.18	4.51	0.15	1.88	12.75	0.05
8	114.88	24.86	19.50	6.04	4.34	0.19	2.16	8.50	0.11
Average	114.95	24.94	19.28	6.15	4.40	0.13	1.76	9.97	0.07
Maximum value	115.04	25.21	19.50	6.86	4.69	0.19	5.24	17.25	0.11
Minimum value	114.85	24.85	19.00	5.97	4.08	0.04	0.12	2.00	0.02
SD	0.07	0.13	0.18	0.29	0.21	0.06	1.59	5.13	0.03

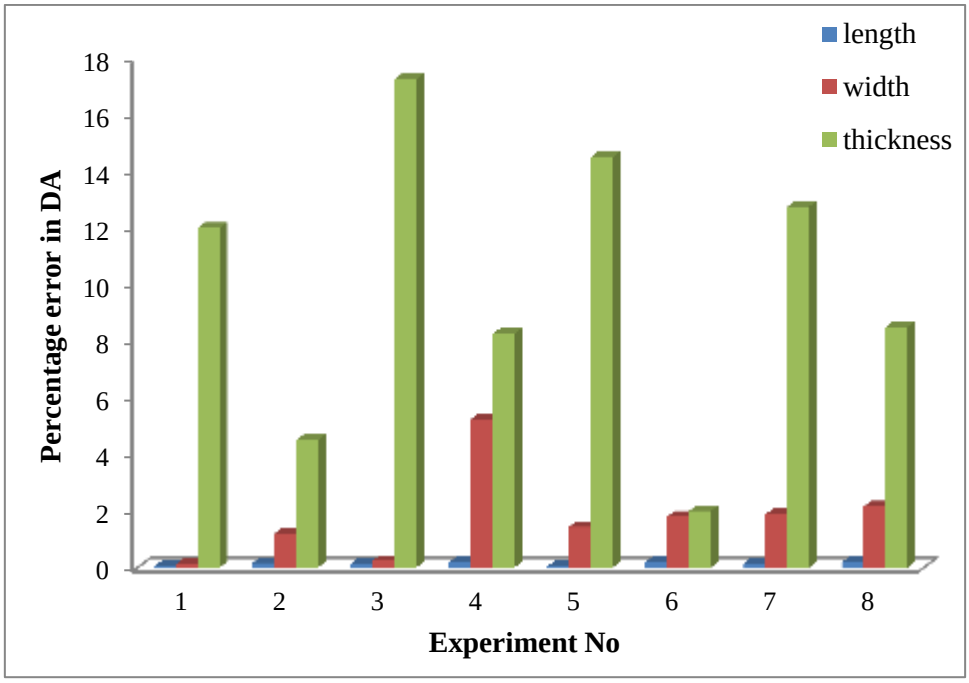

Figure 5.8: Percentage errors in DA along the length, width and thickness

5.3 Results and discussion

5.3.1 Analysis of surface roughness

All SR parameters (R_a, R_q & R_z) were analysed by using S/N ratio. Table 5.5 shows the S/N ratio of the SR parameters. Signal to noise ration use mean square deviation as a single measure, which includes both standard deviation and mean value with the same priority. Experimental results were linearly varied when they were presented in terms of S/N ratios. In this analysis, quality characteristic 'smaller is the better' was considered for the data analysis. The detailed analysis of the SR is discussed in the next sub-section.

Table 5.5: S/N ratio analysis of surface roughness

S.N	Raster angle (F_1)	Orientation (F_2)	Surface type (F_3)	S/N ratio R_a	S/N ratio R_q	S/N ratio R_z
1	0°	Flat	Glossy	-32.0195	-35.5485	-51.536
2	0°	on-edge	Mat	-44.791	-47.1358	-60.7084
3	30°	Flat	Glossy	-33.2173	-39.6454	-58.5062
4	30°	on-edge	Mat	-44.7257	-47.2722	-62.8371
5	60°	Flat	Mat	-42.5031	-45.6343	-62.3587
6	60°	on-edge	Glossy	-37.2665	-44.8954	-59.1579
7	90°	Flat	Mat	-39.304	-41.6413	-56.9391
8	90°	on-edge	Glossy	-38.0835	-40.0087	-53.6176

i. Arithmetic mean roughness height (R_a)

Linear model was used to fit the experimental data for the roughness parameter (R_a). The fisher value (F) of the predicted model was 31.86 and probability (p) value was 0.003, which indicates that the linear model is adequate to approx the surface roughness in the range of experimental domain *(Senthilkumaran et al.[116]).* Table 5.6 shows the ANOVA of the regression model. Model is adequate to evaluate the SR in the confidence limits of 99%. The values of R^2 and R^2-*adj* for the predicated model are 0.96

and 0.93, respectively. These values confirm anexcellent agreement between R^2 and R^2-*adj*. Eq. 5.7 shows the regression model of the roughness parameterR_a in terms of process parameters.

The *p-value* of the process parameters is found to be higher than 0.10, which implies that process parameters were insignificant *(Sachdeva et al. [40]).* The *F- value* of the raster angle was 0.72 while p-value is 0.624. It indicated that these factors are less significant process parameters. The lower *F- value* and higher *p-value* indicate that variations are random. It may happen due to noise factors. The effect of orientation is the second-highest dominant factor after the surface type. *F-value* of surface type is 46.42 and *p-value*is 0.021. It reveals that surface type factor is highly significant. The main effect plots for S/N ratio and percentage contribution of individual factors are reported in Figure 5.9(a) and Figure 5.9(b) respectively. Normal probability distribution plots in Figure 5.9(c) shows that residuals were linearly distributed.

$$R_a = - 83.7 - 0.225F_1 + 46.9F_2 + 83.2F_3 \quad (5.7)$$

Where F_1 is the raster angle, $F_2$is orientation and F_3 is the surface type

Table 5.6:ANOVA and adequacy of the regression equation for roughness (R_a)

Source	**df**	**Seq SS**	**Adj MS**	**F**	**P**	**Percentage contribution**	**$F_{0.01,3,4}$=16.694**
Regression	3	18693.7	6231.2	31.86	0.003		
Raster angle (F_1)	3	639.8	213.3	0.72	0.628	3.285069	$F > F_{0.01,3,4}$ Model is adequate in the confidence limit of ($\alpha = 0.01$)
Orientation (F_2)	1	4403.9	4403.9	14.77	0.062	22.61193	
Surface type (F_3)	1	13836.2	13836.2	46.42	0.021	71.04231	
Error	2	596.2	298.1			3.061204	
Residual Error	4	782.3	195.6				
Total	7	19476.0					

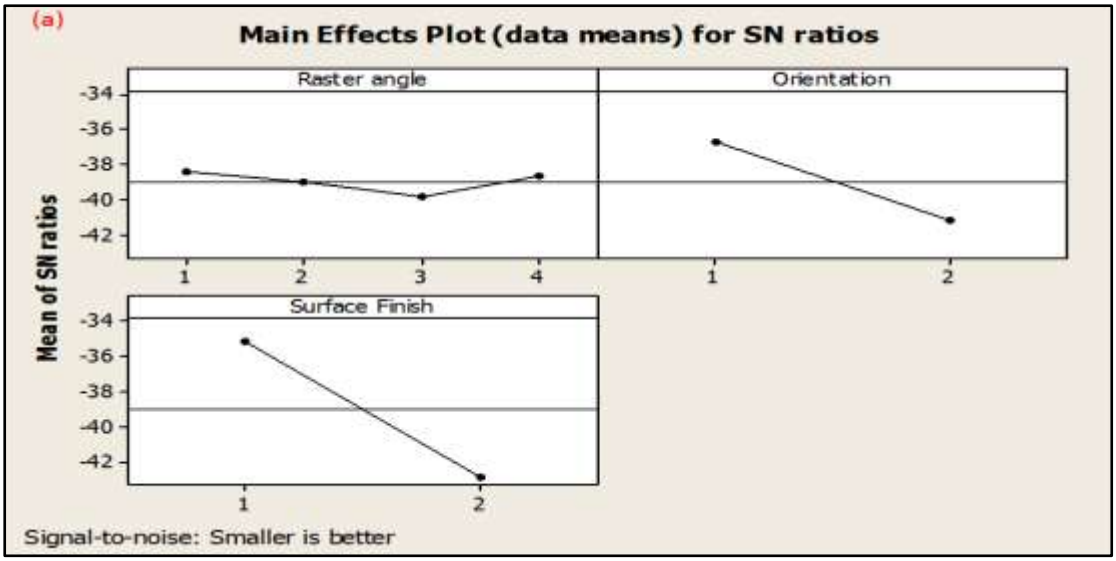

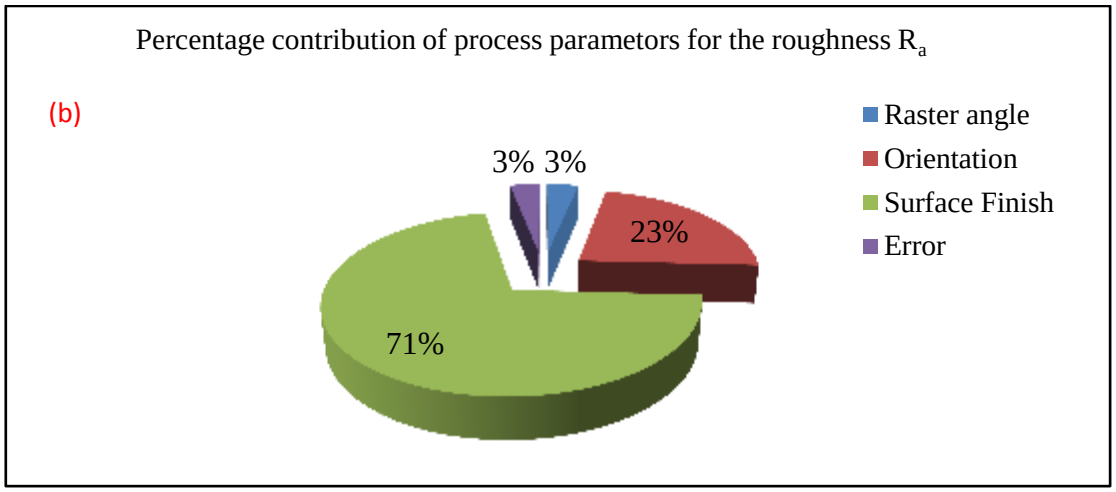

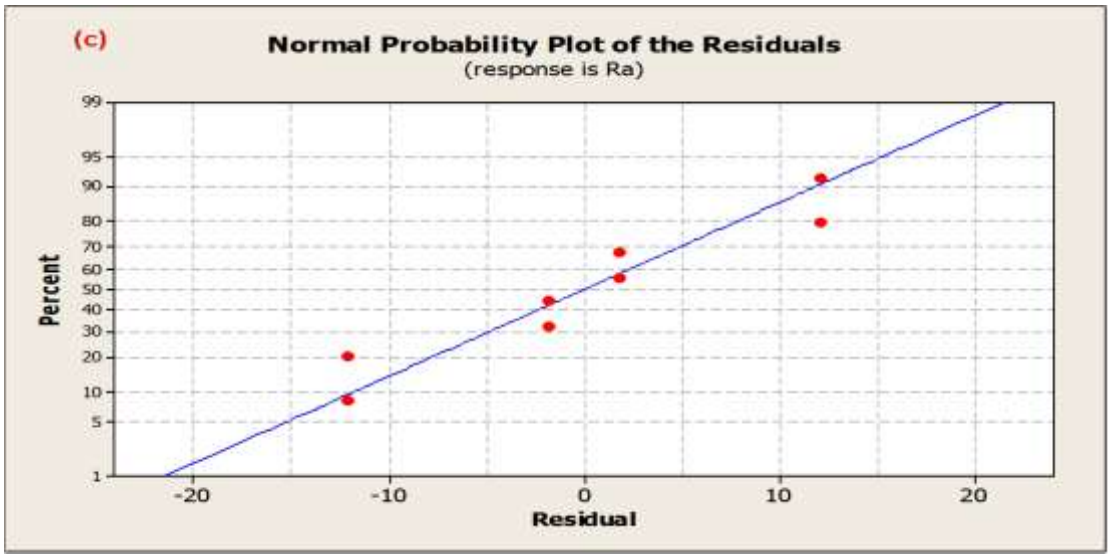

Figure 5.9:(a) Main effect plots for the (S/N) ratio for the (R_a) (b) Percentage contribution of process parameters for the (R_a) (c) Normal Probability plots of the residuals for roughness (R_a)

ii. Root mean square deviation (R_q)

Table 5.7 shows the ANOVA of the regression model for the response factor R_q. This model fits in the confidence limit of 90%. The results depicted that the *F-value* of the regression model and individual factor were more significant than the tabulated value. The *p-value* isfound to be 0.061, which implies that the model was significant. The values of R^2 and R^2-*adj* are 0.814 and 0.67, respectively. Figure 5.10(a) demonstrates the main effect plots for the SR parameterR_q. Figure 5.10(b) shows the percentage contribution of process parameters.The normal probability distribution plots of residual are shown in Figure 5.10(c). Fitted residuals also varied linearly. Eq.5.8 is the final model for the surface roughness (R_q) in terms of the actual value of the process variable. The effect of raster angle is noticed to be less significant process variable for the PolyJet technology.

$$R_q = -64.7 - 0.265F_1 + 66.6F_2 + 84.7F_3 \quad (5.8)$$

Table 5.7: ANOVA of the regression model for roughness (R_q)

Source	**df**	**Seq SS**	**Adj MS**	**F**	**P**	**Percentage contribution**	**$F_{0.1,3,4}$= 4.19086**
Regression	3	23840	7947	5.83	0.061		
Raster angle (F_1)	3	5817.4	1939.1	14.33	0.066	19.85	$F > F_{0.1,3,4}$ Model is adequate in the confidence limit (α= 0.1)
Orientation (F_2)	1	8857.8	8857.8	65.48	0.015	30.23	
Surface Finish (F_3)	1	14348.2	14348.2	106.06	0.009	48.98	
Error	2	270.6	135.3			0.92	
Residual Error	4	5454	1364				
Total	7	29294.0					

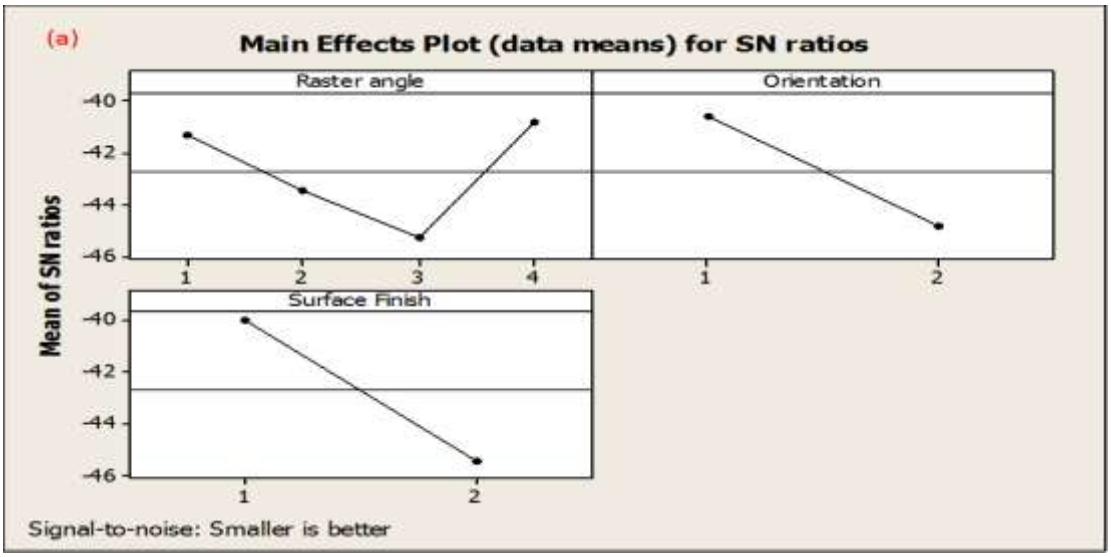

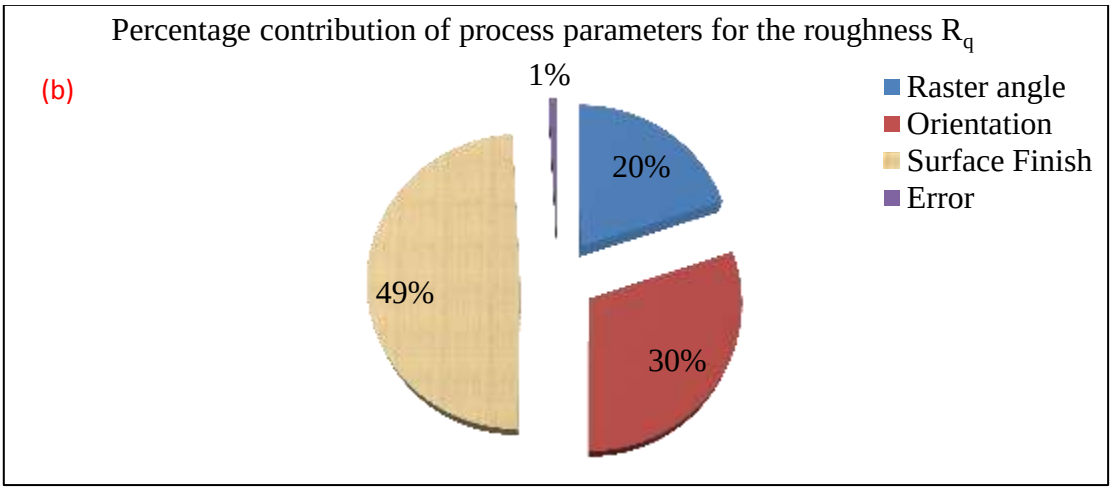

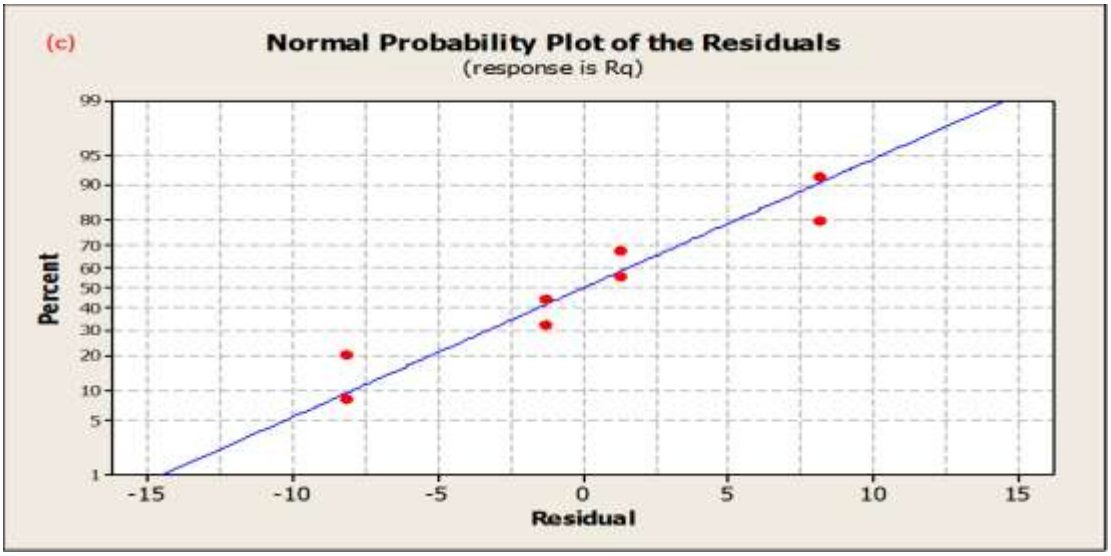

Figure 5.10:(a) Main effect plot for S/N ratio of roughness (R_q)(b) Percentage contribution of process parameters(c) Normal probability plots of the residuals for the (R_q)

iii. Average peak to valley deviation (R_z)

Table 5.8 illustrates the ANOVA of the roughness parameter (R_z) for the regression Eq.5.9. The*p-value* and *F-value* of the developed model were not adequate. The error due to noise factor dominated for the forecastaboutroughness parameter (R_z). The values of R^2 and R^2-*adj* were 0.546 and 0.205, respectively. Figure 5.9 (a) demonstrates the main effect plot for S/N ratios of the surface roughness $R_z$and Figure 5.11(b) shows normal probability plot of residual visualised that errors are not fitted along the straight line. It was observed that process parameter surface type (glossy) had minimum surface roughness.

$$R_z = 54 - 42F_1 + 156F_2 + 470F_3 \quad (5.9)$$

Table 5.8: ANOVA of the regression model for roughness (R_z)

Source	**df**	**SS**	**MS**	**F**	**P**	**$F_{0.01,3,4}$= 4.19086**
Regression	3	508313	169438	1.60	0.322	
Raster angle (F_1)	3	425903	141968	19.11	0.050	
Orientation (F_2)	1	48684	48684	6.55	0.125	$F < F_{0.01,3,4}$ Model is lack of fit
Surface Finish (F_3)	1	441650	441650	59.46	0.016	
Error	2	14855	7428			
Total	7	931093				

5.3.2 Effect of process parameters on surface roughness

From main effect plots of S/N ratio Figures (5.9(a), 5.10(a) and 5.11(a)) it can be concluded that surface type and orientation has more significant effects on the SR. It was observed that by increasing the value of raster angle up to *60°*, SR value was increased. However, beyond an increase of *60°* in raster angle, SR value further decreases. Surface roughness is found to be minimum at *90°* raster angle.

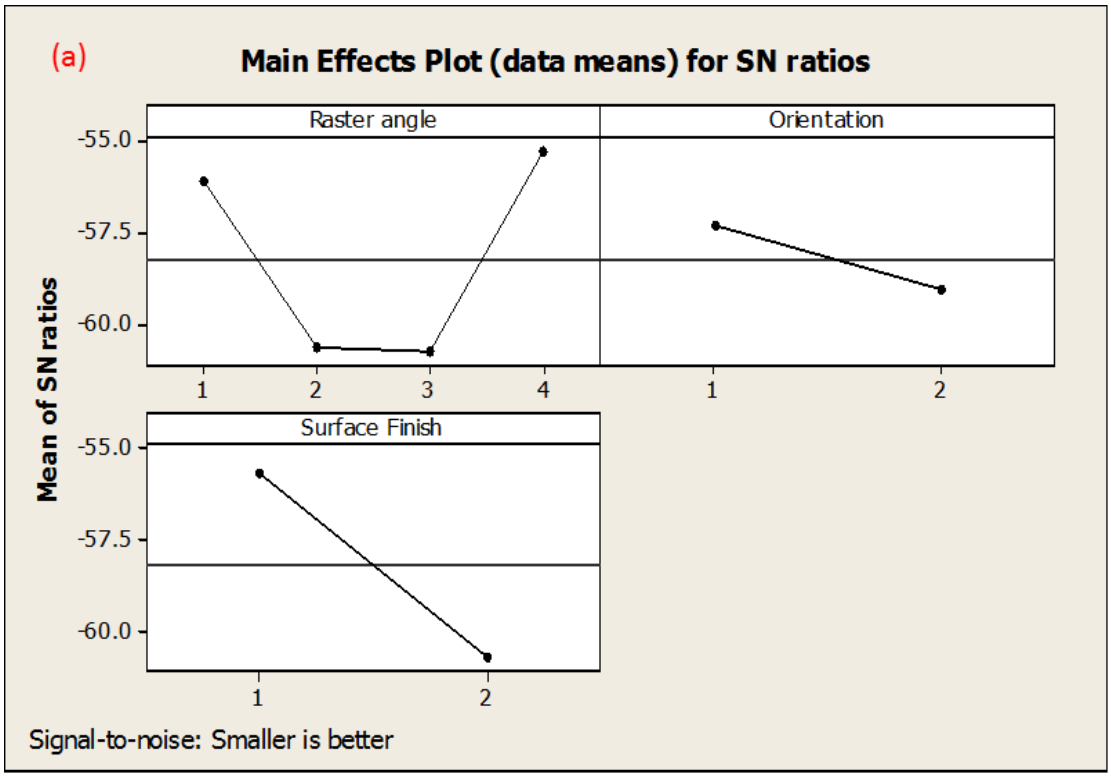

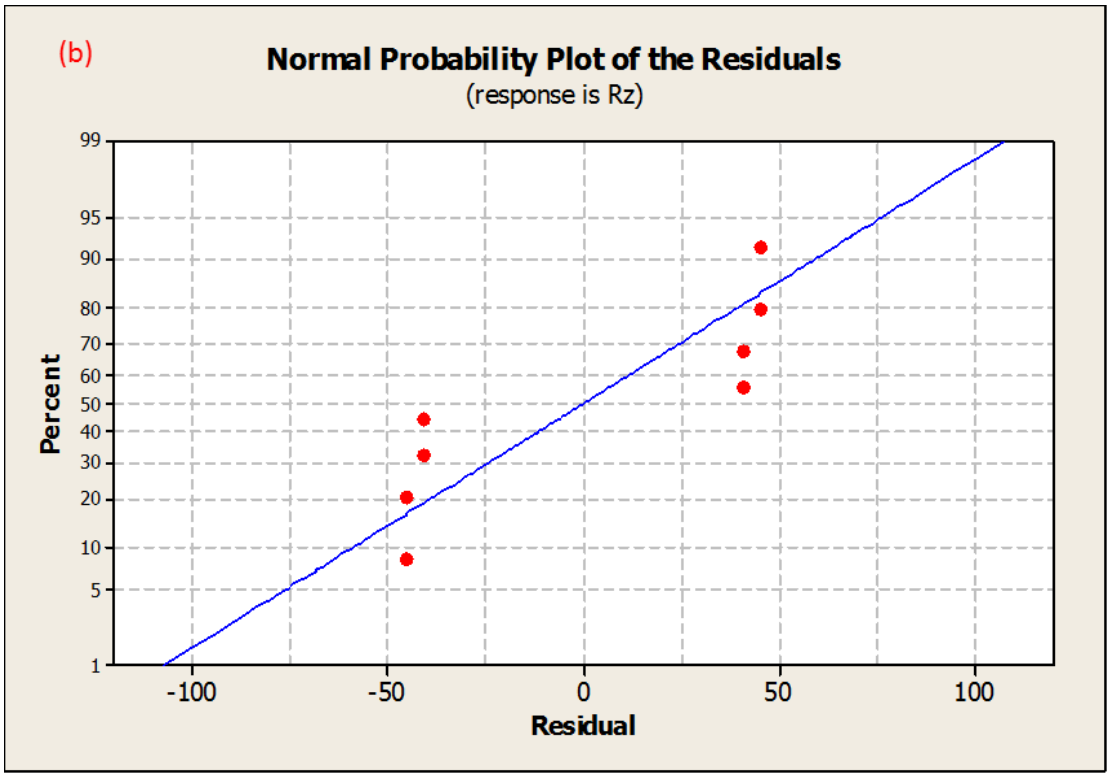

Figure 5.11:(a) Main effect plot for the S/N ration of roughness R_z (b) Normal probability plot of the residual R_z

Interaction plot Figure 5.12 shows that raster angle and orientation have not much impact on the glossy surface. However, the matte finish type strongly affects the surface quality of the fabricated component. A significant interaction was noticed between the raster angle and surface type. The surface finish type 'glossy' and 'matte' will decides whether the upward-facing surface has support materials or not. In the absence of support material, model material droplets freely expand and form a smooth surface. This result was consistent with the observation made by *(Kumar et al. [33])* for the Vero Clear Fullcure 720 material. Support material remains stick with the build material during the post-processing of 'matte' finish surface. Support material creates burrs on the surface of build geometry during removal of supports in the post-processing operation.

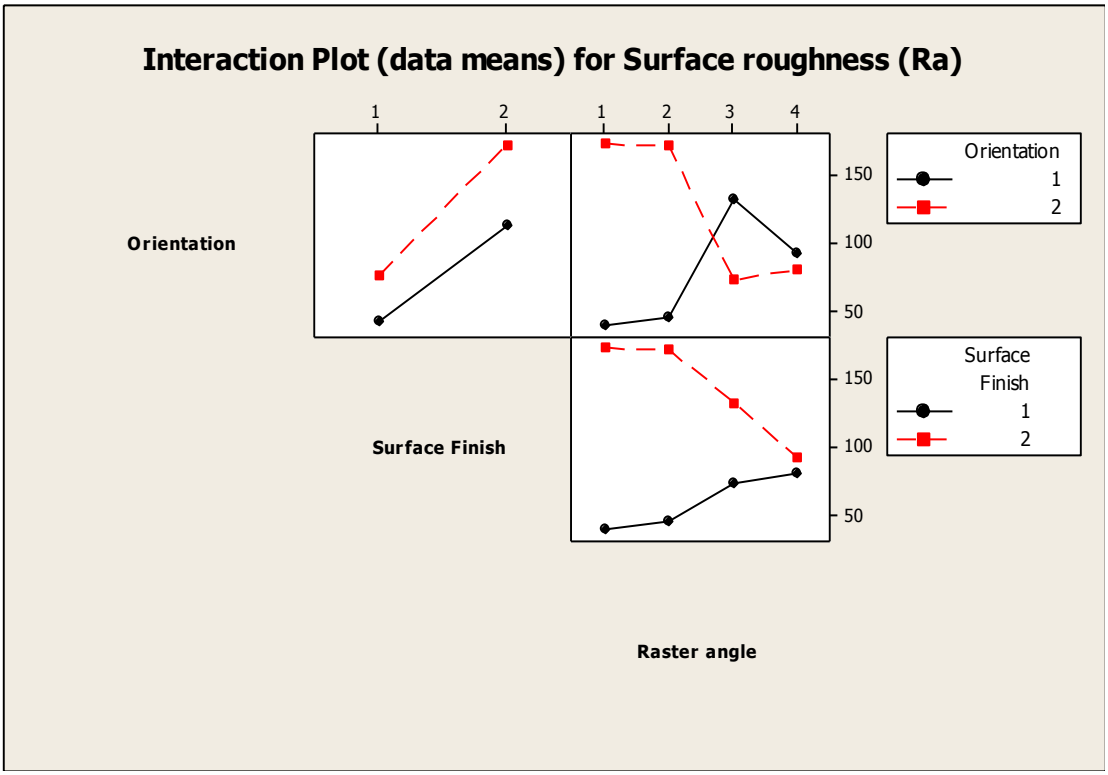

Figure 5.12: Interaction plots for the surface roughness

The significant findings of this investigation are as follows:

- The influence of raster angle on SR parameters R_a,R_q and R_z are less significant. Optimised condition of raster angle for the surface roughness is found to be 90°.
- Orientation is the second-highest dominant process parameter. Surface roughness was minimum corresponding to the orientation condition 'flat'. Since the flat condition has not required the support material, hence better surface finish has been achieved.
- Surface type is the significant process parameters for the surface roughness. Glossy surface produces a better surface finish.

5.3.3 Analysis of dimensional accuracy

Experimental results for the DA along the length, width and height are presented in Table 5.5. The results depicted that the deviation of actual dimensions along length and width from CAD dimension was not significant. Average percentage deviation in the dimension along length was found to be 0.13% whereas deviation along the width is 1.76%. These variations are within the range of company user manuals guideline [117]. Hence, these two dimensions of the specimen do not need anyoptimisation. On the other side, the percentage deviation in DA along the thickness of the specimen is found to be 9.97% from the CAD dimension. Therefore, optimisation is required to minimise the percentage error in DA along the thickness of the sample. S/N ratio is used to find the optimum setting of process variable for the DA.

Figure 5.13 (a) shows the main effect plot of S/N ratio for the DA along with the thickness of specimen. Figure 5.13 (b) represents the percentage contribution of the

process variables. It is observed that the effect of surface finish was negligible on DA. After neglecting the insignificant process parameter, a regression model is developed to predict the DA. The value of R^2 for this predicated model was 0.75 whereas the value of R^2-*adj* is 0.65. *F-value* of this regression model ishigher than the *F-tabulated*. The *P-value* for the regression Eq.5.10 was 0.03, which is less than 0.05 and hence, it is desirable. The developed regression model was found to be good enough to predict the DA along the thickness of the specimen within the experimental range. Table 5.9 shows ANOVA of the regression Eq.5.10 for the DA. The *F-value* corresponding to process parameter 'orientation' was very high, which has yielded that this factor was the most dominating process parameters.

$$\%\Delta_t = 21.8 + 0.262F_1 - 0.831F_2 \tag{5.10}$$

Where $\%\Delta t$ is the percentage error in DA along perpendicular direction from build tray.

Table 5.9: ANOVA table for the regression model of DA

Source	**DF**	**SS**	**MS**	**F**	**P**	**$F_{0.05,2,5}$ = 5.7861**
Regression	2	138.88	69.442	7.71	0.03	F > F0.05,2,5 model is adequate in the range of 95% of confidence interval
Raster angle (F_1)	3	28.148	9.383	1.60	0.35	
Orientation (F_2)	1	138.195	138.19	23.5	0.017	
Error	3	17.586	5.862			
Residual Error	5	45.045	9.00			
Total	7	183.930				

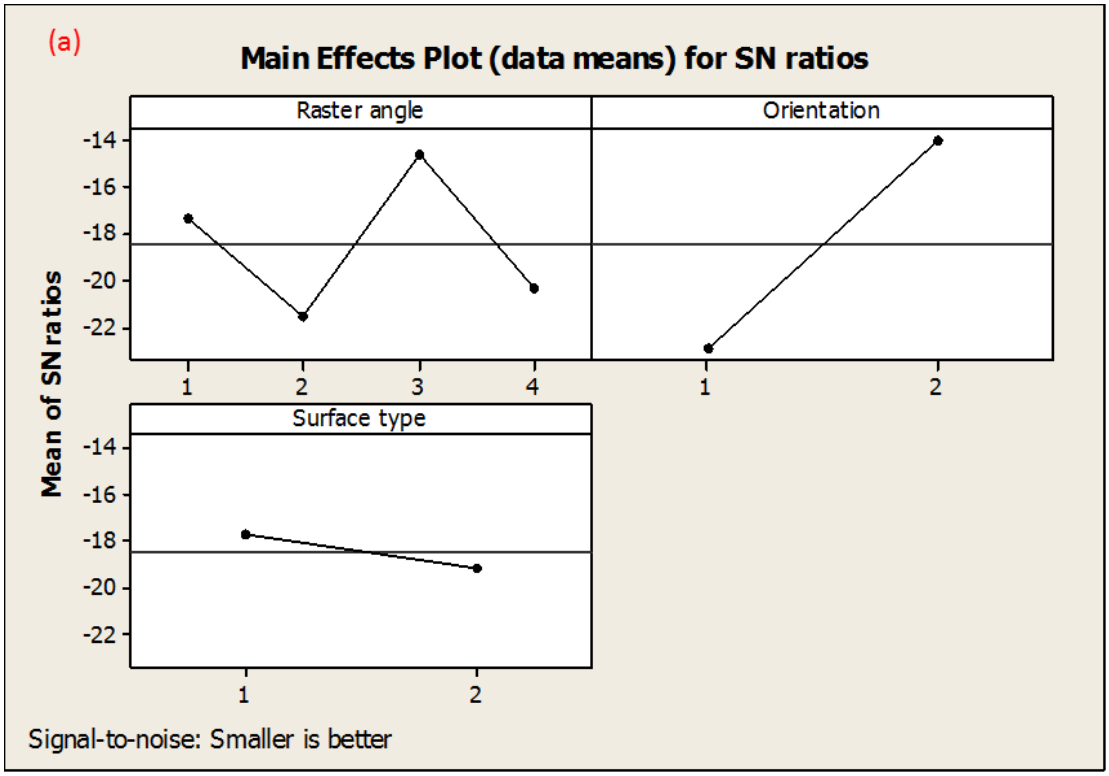

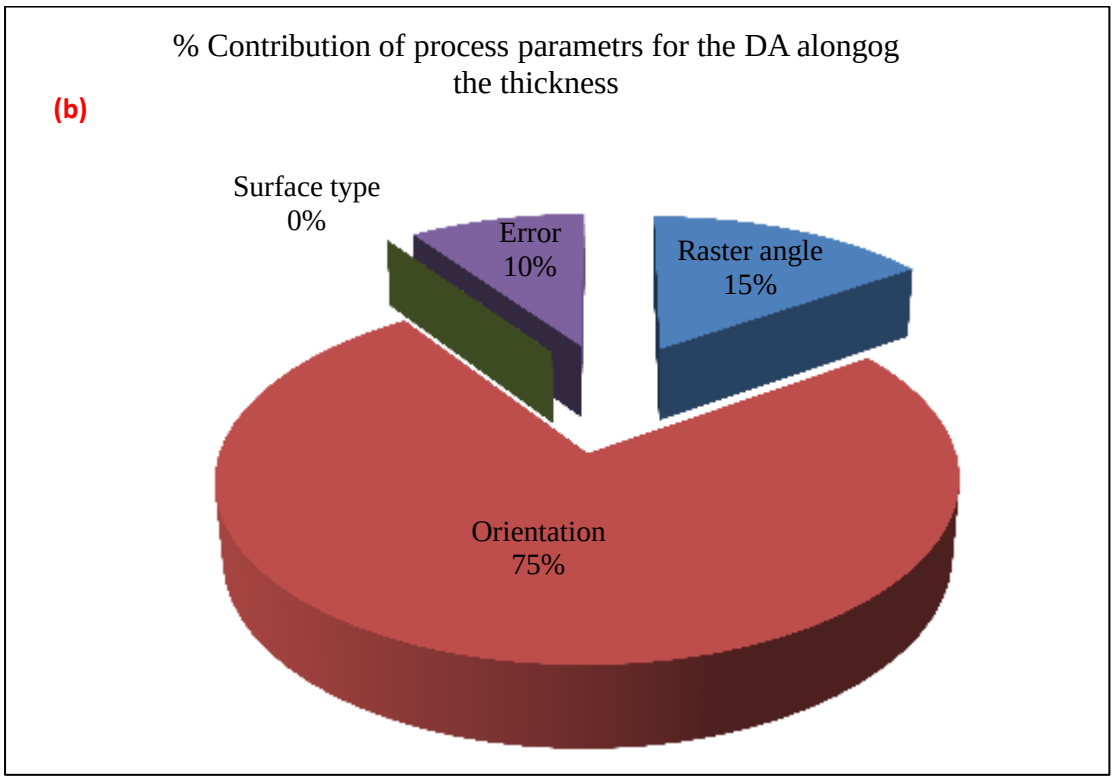

Figure 5.13:(a) Main effect plot for S/N ratio analysis for the DA along the thickness (b) Percentage contribution of process parameters for the DA

5.3.4 Effect of process parameter on dimensional accuracy

From Figure 5.13(b),it has been observed that the process parameter 'orientation' has the highest contribution (*75%*) on the DA of the printed component. Raster angle is the second-highest contributing factors (*15%*) after orientation. However, surface type does not affectthe DA of the component. Figure 5.13(a) shows that percentage contribution of error terms is high (*10%*), which might be due to an unidentified region. From Table 5.5, it can be concluded that along the X-Yplane (parallel to the bed) direction, percentage errors in the linear dimension are minimum. Maximum percentage error is found in the Y-Z plane (perpendicular to the bed) direction.

Results of measurements have depicted that the shrinkage was predominant along the length of the component. Positive deviation was observed along the width and thickness of the component. Shrinkage along the length of components occurredbecause of stress development as a resultof the contraction of material during cooling of material at some stage in curing *(Sood et al.[112]).* In the PolyJet process,non-uniform temperature gradient is caused due to high cooling rate. Non-uniform temperature gradient causes thermal stress in the component. It was one of leading cause of the dimensional inaccuracy. In PolyJet process, heat is dissipated by the forced convection and conduction. Due to the high value of the temperature gradient, material quickly solidifies. The increase of thickness has mainly occurred due to an anticipation of shape error and positive slicing method.

5.3.5 Analysis of flatness

The measurement of flatness was carried out to investigate the impact of process variables. Table 5.10 shows ANOVA summary of the regression Eq.5.11. Figure

5.14(a) demonstrates the percentage contribution of the process parameter on the flatness. Figure 5.15(b) represents the main effect plot of process parameter. The results showed that the effect of orientation was the highest important process parameter. The developed model was adequate to predict the flatness within the limits of a *95%* confidence interval. The value of R^2 was *0.857*, and the value of R^2*-adj* was *0.75*. The *F-value* for the predicated model was 8.01. The low *F-value* of raster angle implied that this factor was insignificant.

$$F_y = 0.0235 + 0.000117F_1 + 0.0475F_2 - 0.0225F_3 \quad (5.11)$$

Where F_y is the value of flatness (mm).

Table 5.10: ANOVA for the regression model of flatness

Source	**DF**	**SS**	**MS**	**F**	**p**	$F_{0.05,3,4} = 6.5914$
Regression	3	0.0056475	0.0018825	8.01	0.036	$F > F_{0.05,3,4}$ model is adequate to predict flatness in the range of 95% of CI
Raster angle (F_1)	3	0.0007375	0.0002458	1.51	0.422	
Orientation (F_2)	1	0.0045125	0.0045125	27.77	0.034	
Surface Finish (F_3)	1	0.0010125	0.0010125	6.23	0.130	
Error	2	0.0003250	0.0001625			
Residual Error	4	0.0009400	0.0002350			
Total	7	0.0065875				

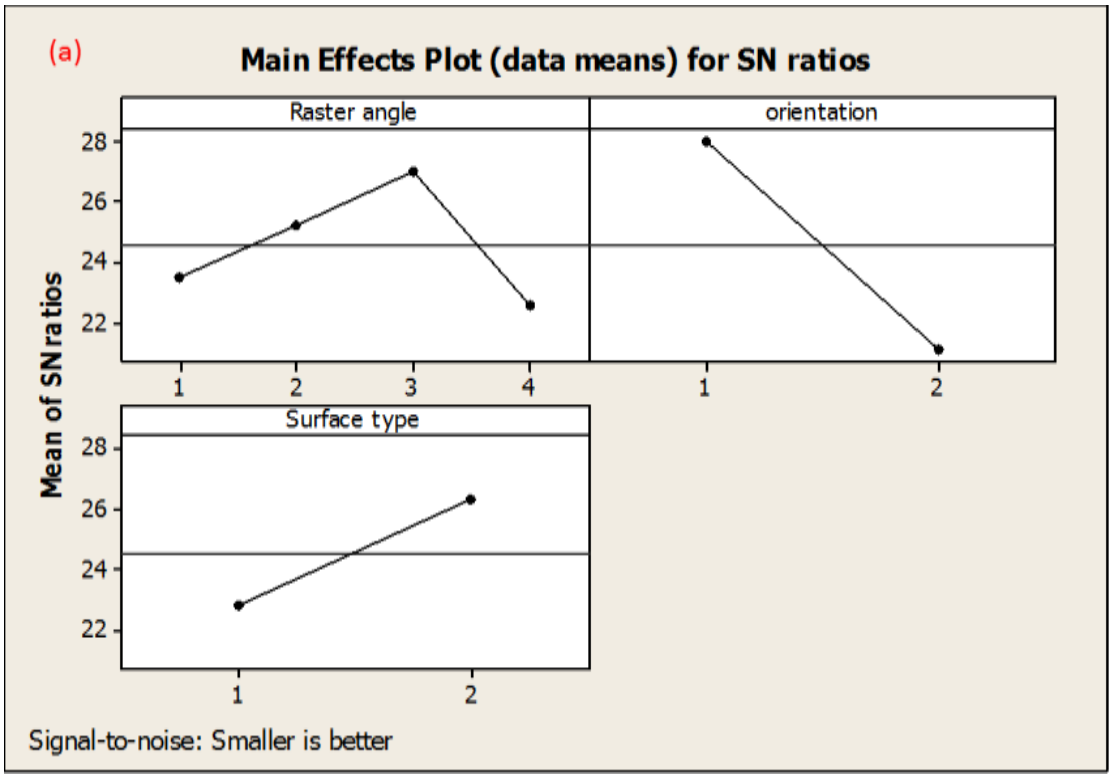

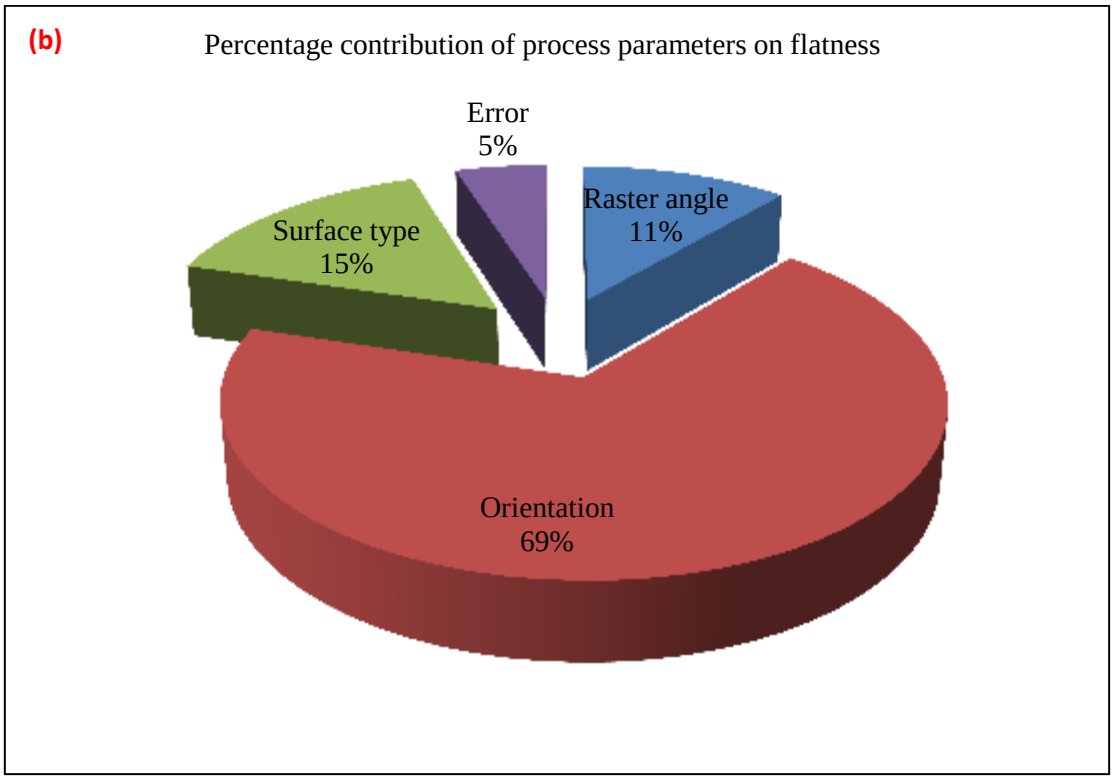

Figure 5.14: (a) Percentage contributions of process parameters on flatness (b) Main effect plot for the S/N ratio for the flatness.

5.3.6 Effect of process parameters on flatness

Figure 5.14(a) demonstrates that the impact of process parameter 'orientation' has the highest contribution (*68%*) on the flatness. However, other process parameters like raster angle and surface type contributions are *11% & 15%* respectively. Figure 5.15(b) shows that increase in raster angle up to *60°* results into flatness decrement. However, such behaviour changed beyond *60°* orientation. After this value the flatness further increases. Surface type is found to be the second important process parameter after orientation. Matte surface has the lowest value of flatness.

Cazon et al. [89] have suggested that the printed part along the horizontal orientation had the maximum tensile strength. The higher value of tensile strength of material restricts the distortion of components, which yields lesser value of flatness. The optimum contrition for the flatness is found to be the raster angle at *60°*, matte surface type and flat orientation.

5.3.7 Confirmation test

Finally, a confirmation test was executed to validate the developed model for roughness (R_a), DA and flatness at optimum conditions. Table 5.11 shows the optimum condition for process variables. It was noticed that optimum conditions were different for the response factors. Due to noise factor present in the system, it was expected that the result would fall in the range of confidence limits. Experimental result for the SR at optimum process condition is shown in Figure 5.15. The value of roughness (R_a) is *28.2* nm, which is close to the model value. Average error for the DA along the thickness is found to be *9.97%*. At optimum condition, percentage error is *5.96%*, which is *40.6%* smaller than the average percentage error in DA. The measured value of flatness is *0.0303* mm, which lies within range of the predicated value.

Table 5.11: Optimum process condition for the response

Response	Raster angle	Orientation	Surface type	Optimum value	Experimental value
Roughness (R_a)	90°	Flat	Glossy	26.15(nm)	28.2 (nm)
Dimensional accuracy (DA)	60°	Edge	Glossy	5.96%	6.12%
Flatness (F_y)	60°	Flat	Mat	0.03302(mm)	0.0403

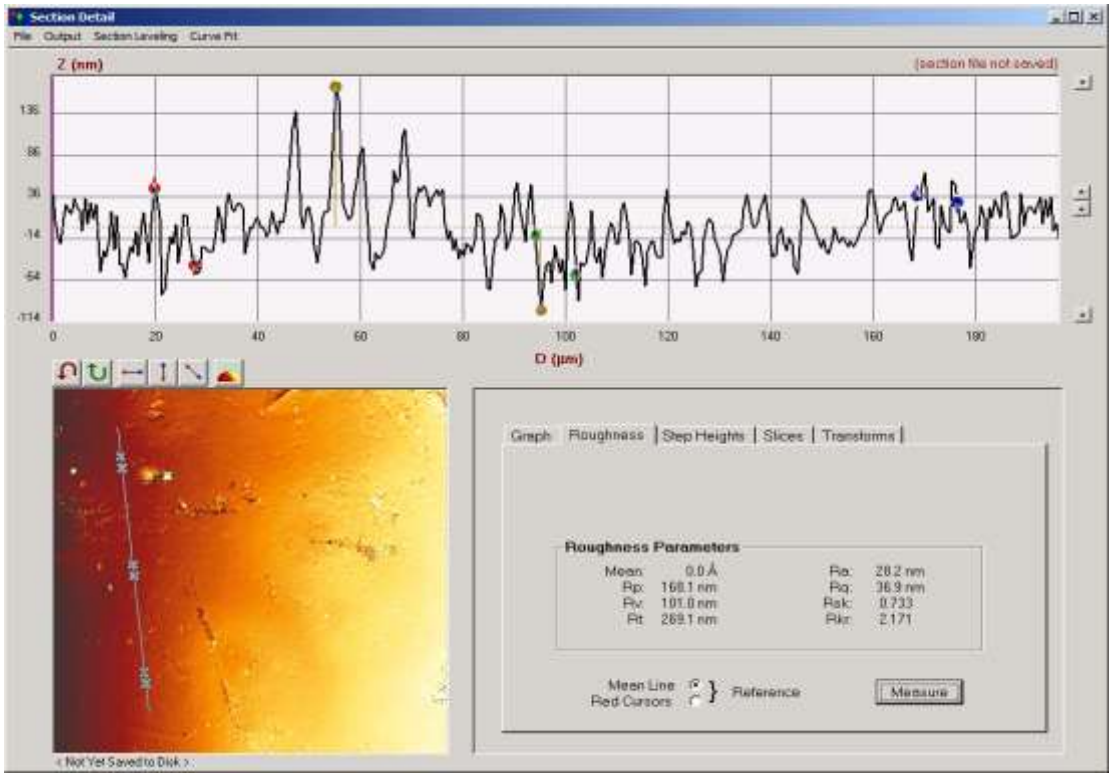

Figure 5.15: Measured surface roughness at the optimum setting condition.

5.4 Summary of the chapter

The purpose of this research work was to examine the impact of process variable on SR, DA and flatness of the component printed by the PolyJet process. This work deals with three SR parameters R_a, R_q and R_z for examination of SR. The process variables used in this analysis were raster angle, orientation and surface type. A linear regression model was developed to evaluate SR, DA and flatness. ANOVA technique was employed to

forecast the effect of individual process parameters. The adequacy of the model was checked by performing the *F-test*. The developed models are adequate within the CI of *95%*. The next *chapter* of the thesis present a methodology for improving part strength of the FDM and PolyJet component.

Chapter 6

Experimental and Computational Analysis for Evaluating Part Strength through FDM and PolyJet Components

Chapter 6

Experimental and Computational Analysis for Evaluating Part Strength through FDM and PolyJet Components

6.1 Introduction

Recent development in the field of additive manufacturing is to fabricate heterogeneous material by using multi-material. In this *chapter*, an attempt is made to investigate the effect of unidirectional reinforcement of PETG material on mechanical behaviour of ABS and PLA material. Computational analysis of effect of reinforcement material is also carried out. Further, effects of PolyJet process variable on mechanical properties of RGD 840 material are investigated. An attempt is also made to evaluate the plastic strain of the material through both experimentally and computationally. Control methodology for the clearance analysis is presented. The next section provides the experimental plan.

6.2Experimental plan for FDM component

The present study, unidirectional reinforcement composite, has been developed through FDM process. In additive manufacturing softer material is referred as matrix material and harder material is referred as reinforcement material [118]. Development of AM for the fabrication of multi-material has improved the mechanical properties, specific functional requirement and design feature for the new product design. In this work, effect of unidirectional reinforcement of PETG material on mechanical properties of ABS and PLA material is investigated. The next

subsection will provide the details of the matrix and reinforcement material used in this investigation.

6.2.1 Matrix and reinforcement material

In this work, two separate cases were considered for selection of matrix material. In first case, ABS was considered as matrix material and PETG was used as reinforcement material. In second case, PLA filament was used as matrix material and PETG was considered as reinforcement material. Three different reinforcement percentages were used for the preparation of test samples viz., *15%, 25%* and *35%*. ABS was the weakest material and PETZ was the stronger material among all the three material. The schematics arrangement of matrix and reinforcement material is shown in Figure 6.1. The characteristics of ABS, PLA and PETG materials are shown in Table 6.1.

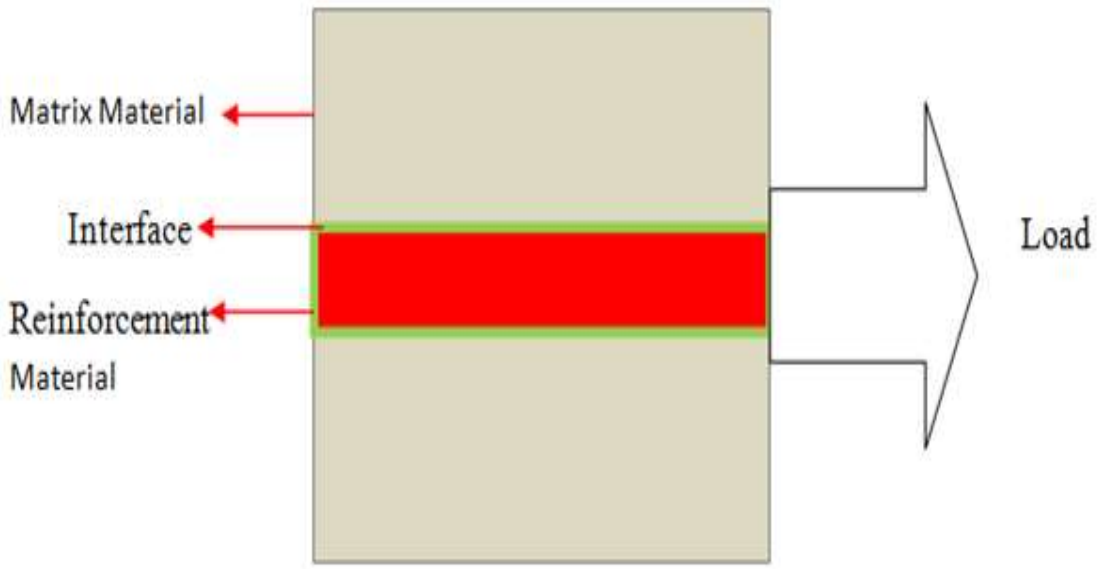

Figure 6.1: Reinforcement direction of fibre and matrix material

Table 6.1: Characteristic of ABS, PLA and PETG

Properties	**ABS**	**PLA**	**PETZ**
Nozzle temperature (^{o}C)	245	200	245
Filament diameters (mm)	1.75	1.75	1.75
Tensile strength (MPa)	27	37	53.08
Temperature resistance	Resistant to hightemperature	Poor resistant to high temperature	Poor resistant to high temperature
Environmental friendly/recyclable	Recyclable, but not environmental friendly, based on petroleum	Environmental friendly, made from corn & sugarcane, recyclable	Recyclable
Heated bed temperature (^{o}C)	100-110	50-60	60-70

6.2.2 Selection of specimen geometry and 3D modelling

For the evaluation of mechanical properties of the material ASTM has fixed some standards for testing [119]. The D638 series corresponds for tensile testing of plastic and polymers [120]. Figure 6.2 shows the ASTM D638 Type-IV specimen which was fabricated through FDM printer. ASTM D638 specimen has the dog bone-like structure. Specimen has shoulders at both ends, which are wider than other portion of the structure. In this work, Autodesk Fusion @360 was used for the 3D modelling of the specimens shown in Figure 6.2. Figure 6.3 illustrates the CAD model of the test specimen. The next section will give the fabrication method of test specimens.

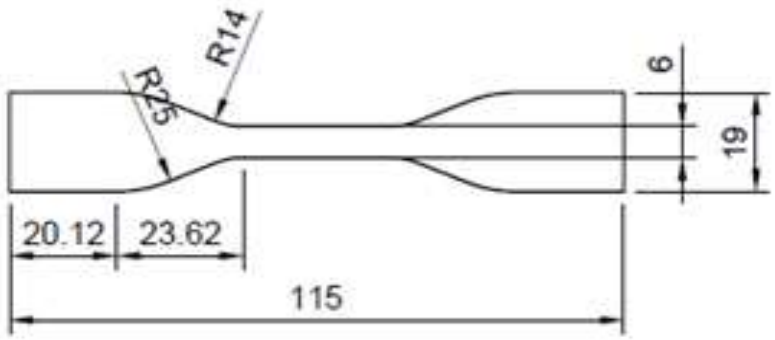

Figure 6.2: Drawing of ASTM D638 type-IV specimen

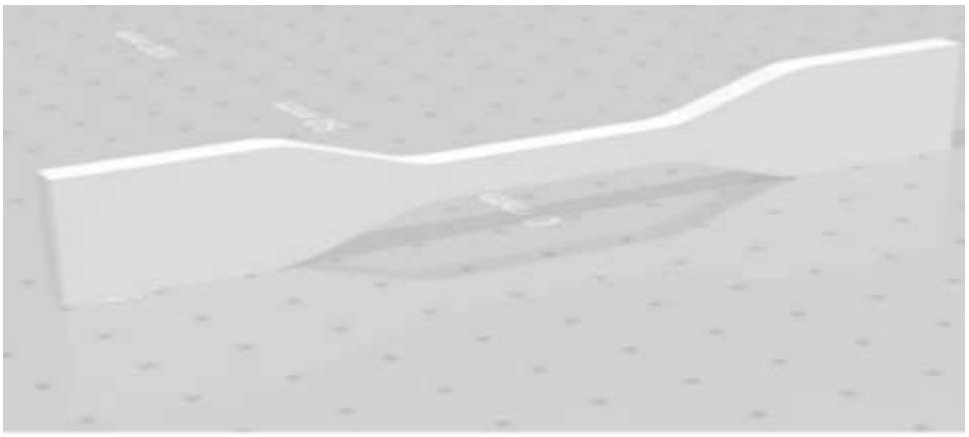

Figure 6.3: CAD design of specimen in .STL format

6.2.3 Fabrication method

Fused deposition modeling additive manufacturing technique was used in this research work for the preparation of test specimens. Three different materials were used for the fabrication of the specimen viz., ABS, PLAand PETG. Printer used for the fabrication of test specimens was PRUSA MK3. This printer can manufacture the component of single material only. Additional machine mosaic pallet 2 was attached with PRUSA MK3 for fabrication of multi-materials samples. Optimum level of process variables were selected for the manufacturing of test specimen. The process variables used for the fabrication of samples are shown in Table 6.2. Three different reinforcement percentages were used for the preparation of test samples viz., 15%, 25% and 35%. Figure 6.4 shows the research methodology used for improving part strength in the flow diagram. Experimental plan used in this research work is presented in Table 6.3. Figure 6.5 shows the schematic representation of a dual extrusion nozzle used to fabricate test specimen. Figure 6.6 demonstrates the fabricated samples, with and without reinforcement.

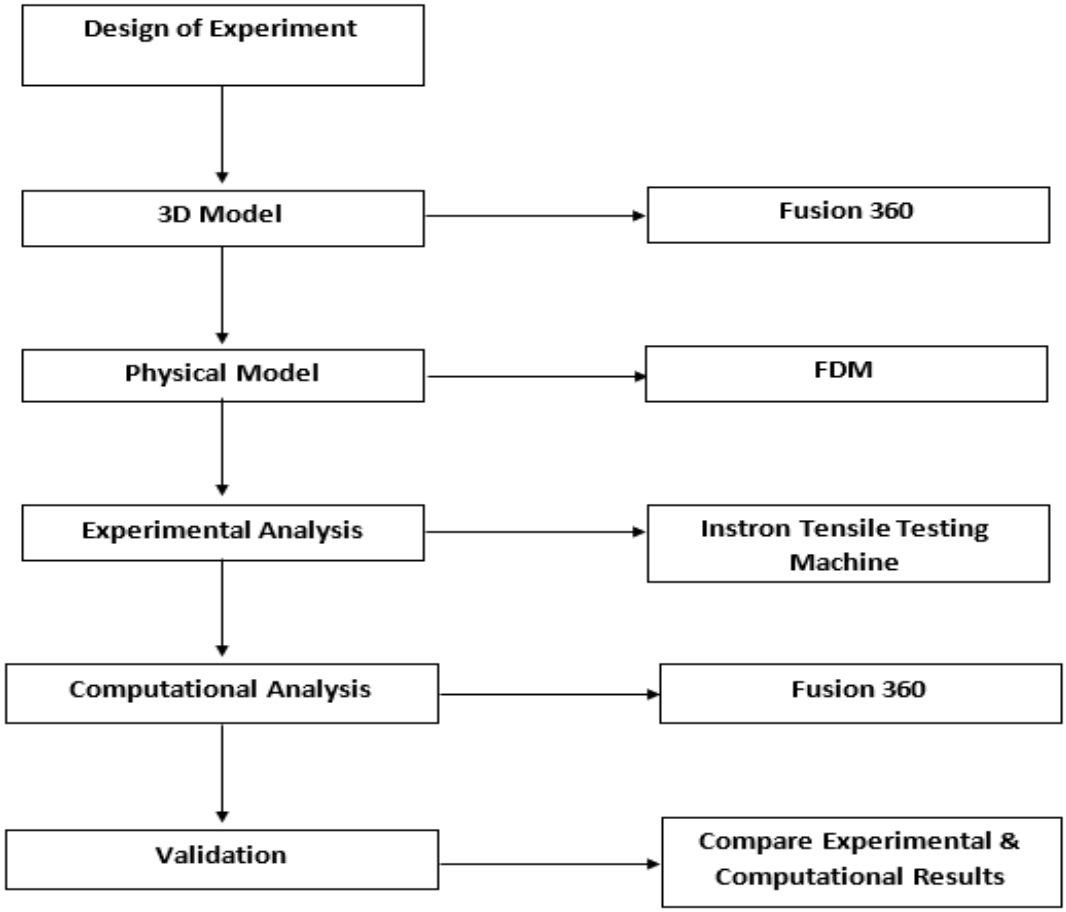

Figure 6.4: Flow diagram of the research methodology

Table 6.2: Process parameters used for the sample fabrication

Process parameters	**Value**
Nozzle diameter	0.4 mm
Infill density	100%
Print speed	60mm/s
Raster angle	45°
Orientation	0° from x-axis
Layer thickness	0.2 mm
Infill pattern	Hexagonal

Table 6.3: Experimental plan for part strength

Experiment No	Matrix material	Reinforcement fiber material	Reinforcement percentage	Tensile strength (MPa)
1	ABS	-	0%	24.05
2	PLA	-	0%	43.50
3	PETG	-	0%	49.50
4	ABS	PETG	15%	38.44
5	ABS	PETG	25%	39.42
6	ABS	PETG	35%	40.64
7	PLA	PETG	15%	45.26
8	PLA	PETG	25%	46.72
9	PLA	PETG	35%	46.85

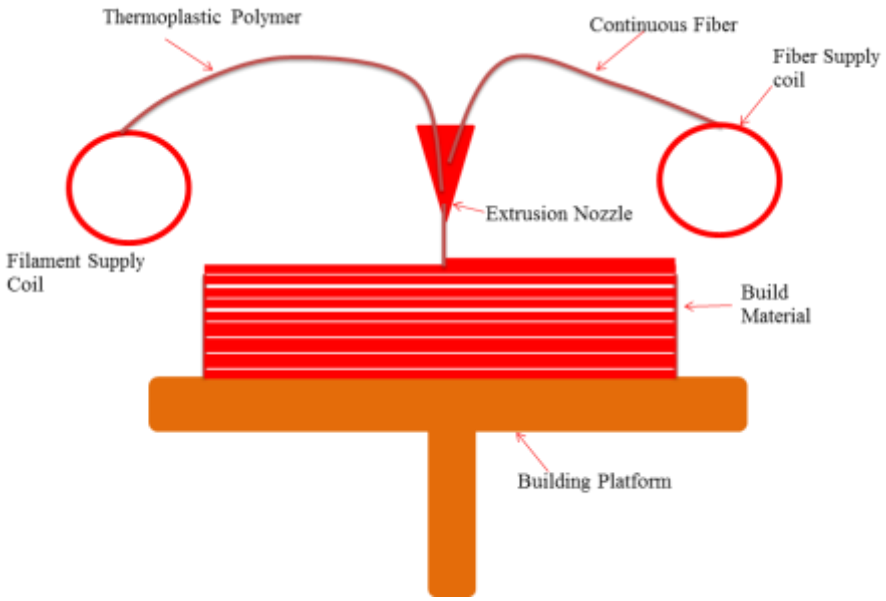

Figure 6.5: Schematic layout of FDM printing process

Figure 6.6: Fabricated specimen along the flat orientation

6.2.4 Experimental setup for tensile test

The tensile test of the fabricated specimen was conducted on universal testing machine Instron. The actual experimental set-up image is shown in Figure 6.7. The specimen held between the crosshead of UTM machine and axial tensile load was applied on the material at the one end. The corresponding stress-strain diagram was traced on computer according to the load conditions. The specimens were tested at a rate of *1.5* mm/min, for the conduction of the tensile test.

Figure 6.7: UTM Instron tensile testing machine

6.2.5 Results and discussion

The average value of tensile strength for PLA, ABSand PETG materials with and without reinforcement has been calculated using three samples each. The impact of PETG reinforcement on the tensile behaviour of PLA and ABS materials can be seen in Figure 6.8. Due to the reinforcement of PETG material, tensile strength of ABS and

PLA material has significantly improved. Due to the uncertainty of experimental results, tensile strength is shown within the range of *5%* error bar chart. The tensile strength of ABS and PLA material was improved by about *70%* and *8%* respectively.

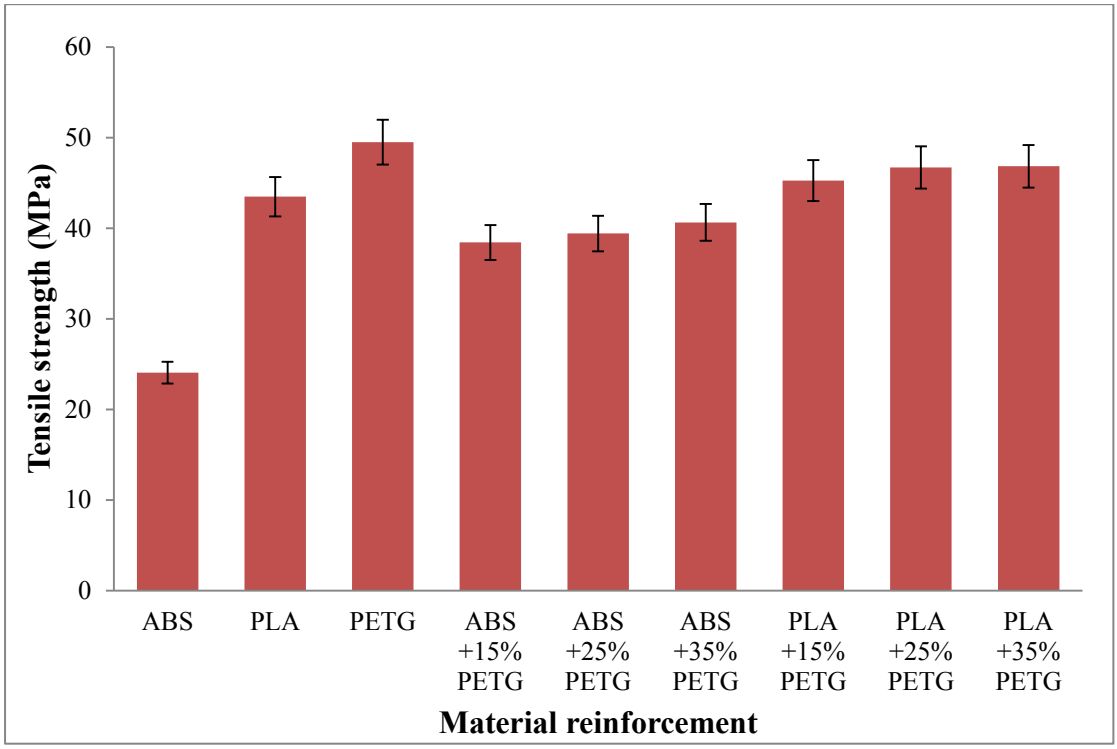

Figure 6.8: Effect of reinforcement on mechanical properties

Analysis of surface morphology, SEM test was performed. Figure 6.9 (a) shows the SEM image of ABS sample fabricated along flat orientation and Figure 6.9(b) shows the SEM image of ABS samples prepared along the edge orientation. However, air gaps were present between the two layers in both the samples. It may be seen that the surface produced along the flat orientation was better as compared to edge orientation. Voids were present in the component fabricated along the edge orientation, which yields low tensile strength. For analysis of tensile test all the samples were fabricated along the flat orientation.

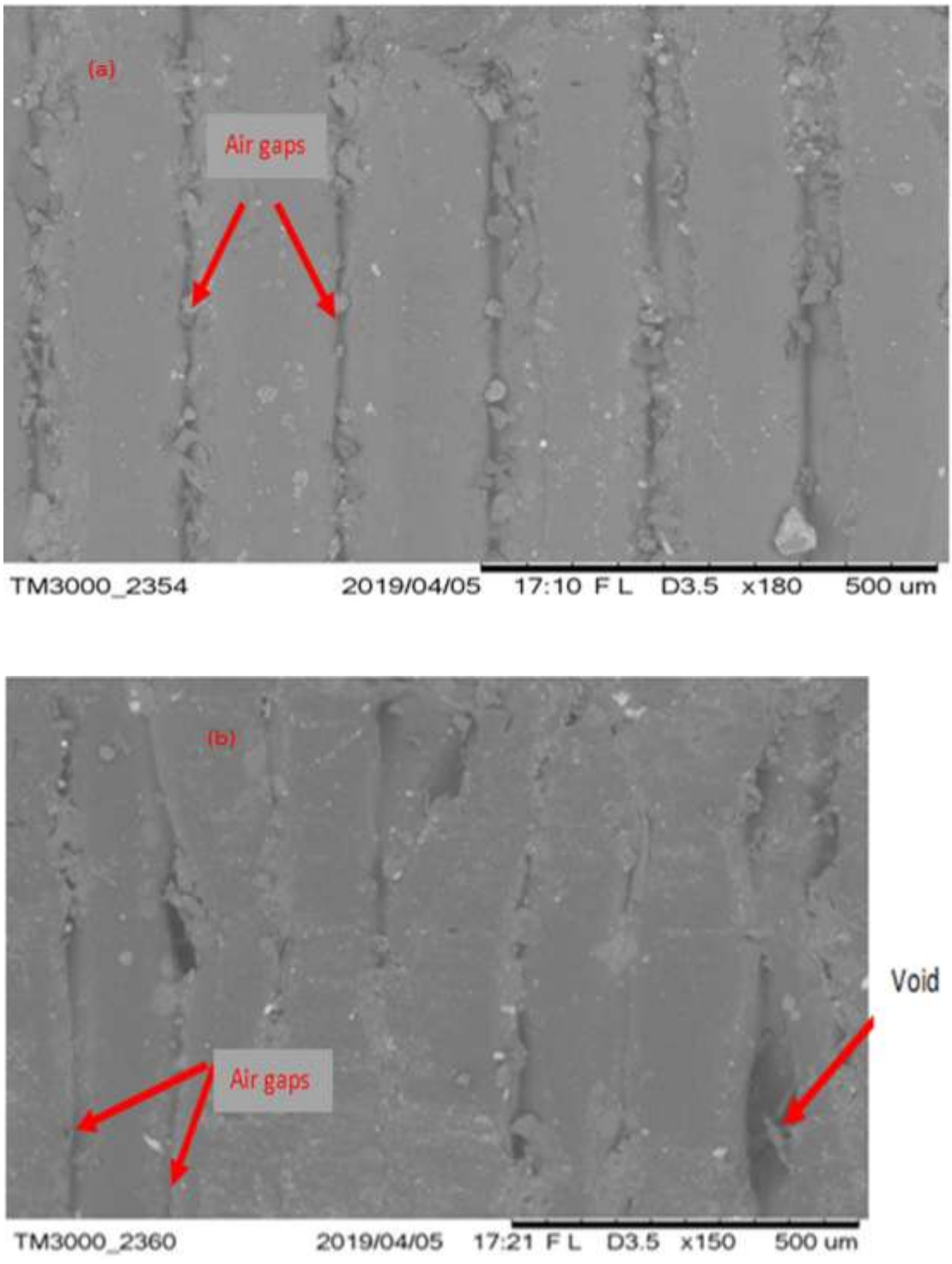

Figure 6.9: SEM image of ABS samples (a) Flat orientation (b) Edge orientation

6.3 Computational analysis of part strength of FDM component

For computational analysis, 3D CAD model of ASTM-D638 was created by using Autodesk Fusion 360 software. Autodesk Fusion360 software was used for the numerical simulation of CAD model. An 8-node linear brick element was used for meshing of test specimen. After performing several mesh convergence studies 7284 elements with 1.0 seed size has been chosen for current simulation as shown in Figure 6.10.The bottom end of the specimen is fixed with the boundary condition U_x, U_y, U_z, R_x, R_y, $R_z = 0$, where U_x, U_y, and U_z are the displacement in *x*, *y* and *z*-direction respectively. Further, R_x, R_y and R_z are the rotation in *x*, *y* and *z*-direction respectively. A velocity of 1.5 mm/min has been applied at the top surface of the specimen as shown in Figure 6.11. A tie constraint has been applied to assemble the PLA and PETG in a standard specimen for providing the mix effect of properties.

Total nine simulations were carried out to investigate the impact of reinforcement on the mechanical behaviour of ABS and PLA materials. First three simulations were carried out without reinforcement to check the Von mises stress in the ABS, PLA and PETG material respectively. In this study, two cases were considered for the analysis. In case–I, ABS material was considered as matrix material, and PETG was treated as reinforcement material. Unidirectional reinforcement material was placed between the matrix materials. The direction of reinforcement was considered in the loading direction. Three different reinforcement percentage was used, i.e. *15%, 25%* and *35%*. In case-II, PLA was considered as matrix material and PETG material was considered as reinforcement material. However, the reinforcement percentage was used similar to case-I.

Table 6.4 shows the material properties used for the simulation of the test specimen. For simulation of samples without reinforcement, material was considered as single solid geometry. Two materials system were defined; one for matrix material and other for reinforcement material.

Table 6.4: Mechanical properties for FEA simulation

Material	**Elastic modulus (E)**	**Shear Modulus (G)**	**Poisson's ratio (μ)**
ABS	2110MPa	14605 MPa	0.39
PLA	30140 MPa	2310MPA	0.33
PETG	2300MPa	1640MPa	0.38

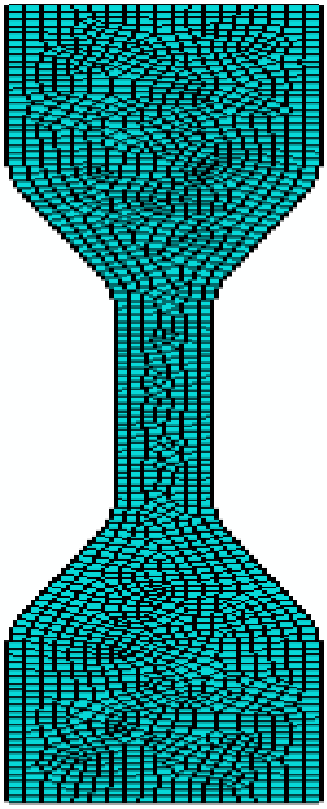

Figure 6.10: Mesh geometry of tensile test specimen

Figure 6.11: Loading condition of the test specimen

6.3.1 Computational result analysis

Figure 6.12 demonstrates the Von-mises stress of ABS and PLA materials with and without reinforcement of PETG material. It can be observed that the tensile strength of PLA and ABS materials was improved due to the reinforcement. Results of computational study depicted that ABS samples was failed at a load of *577.2 N*. The value of Von-mises stress was observed *25.37* MPa at failure point. Specimen of PLA material was failed at a load of 1044 N and value of Von-mises stress was found to be *46.61* MPa. Sample of PETG material was failed at a load of 1188N and value of Von mises stress was observed *53.06* MPa. Figure 6.13 (a), (b) and (c) shows the Von-mises stress in the specimen of ABS, PLA and PETG materials, respectively. The value of Von-mises stress was observed maximum in PETG material.

The effect of PETG reinforcement on mechanical properties of PLA was simulated with different reinforcement percentage. Figure 6.14 shows the effect of reinforcement on Von-mises stress of reinforced composite. Result shows that due to the

reinforcement, the value of Von-mises stress for the PLA composite material was found to be *50.51* MPa at *35%* of PETG reinforcement. It can be concluded that the tensile strength of PLA material was improved by about *8%* due to the reinforcement.

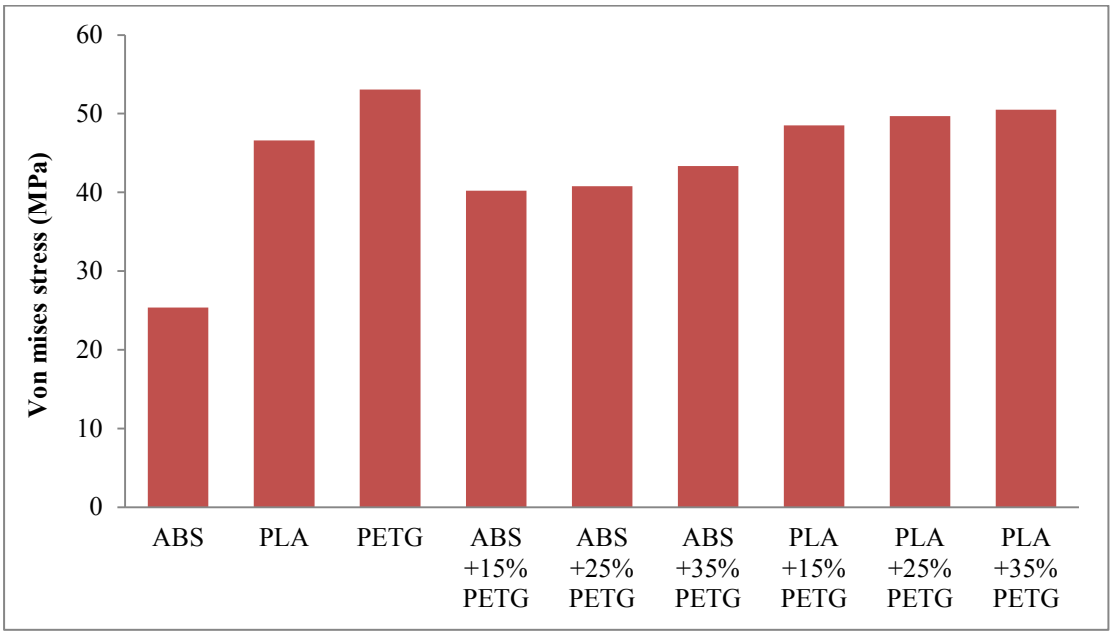

Figure 6.12: Von mises stress in ABS and PLA materials

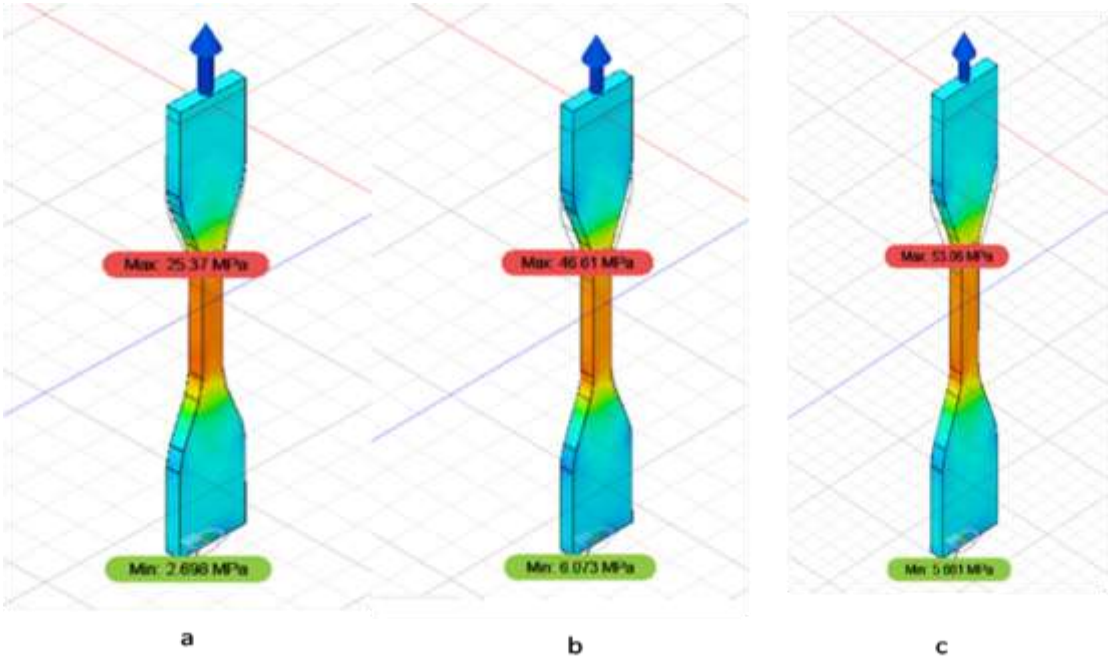

Figure 6.13: Von mises stress without reinforcement (a) ABS material (b) PLA material (c) PETG material

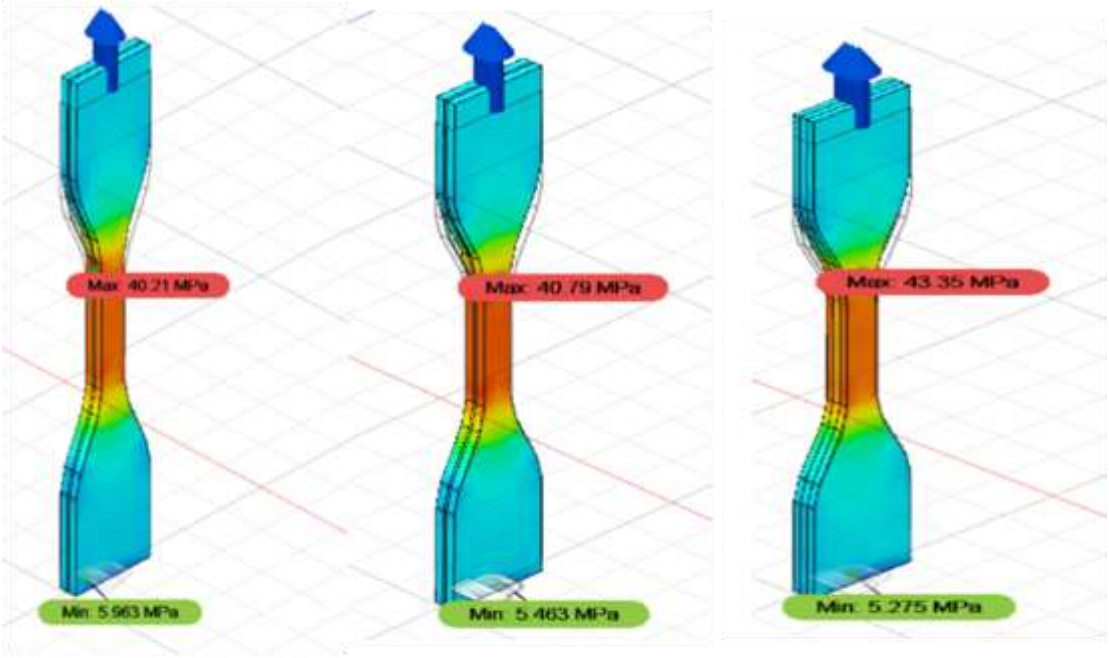

Figure 6.14: Von mises stress of PETG reinforced ABS composite (a) *15%* PETG reinforcement(b) *25%* percent PETG reinforcement(c) *35%* PETG reinforcement

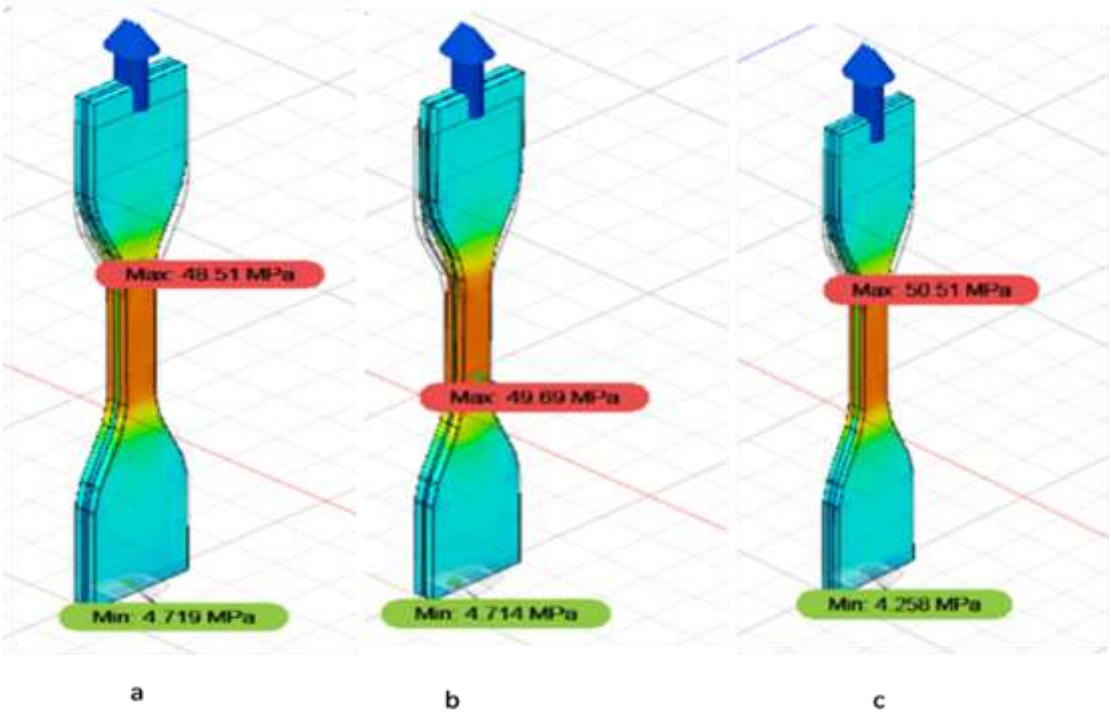

Figure 6.15: Von mises stress of PETG reinforced PLA composite (a) *15%* PETG reinforcement (b) *25%* percent PETG reinforcement (c) *35%* percent PETG reinforcement

Figure 6.15 shows the effect of PETG reinforcement on Von-mises stress of ABS material. Owing to reinforcement of PETG material, maximum value of Von-mises stress of ABS was observed about *43.35* MPa at reinforcement of *35%*. Result depicted that the mechanical properties of ABS material was significantly improved. Owing to the reinforcement mechanical properties of ABS was improved by about 70%.

6.3.2 Comparison of experimental and computational results

Figure 6.16 demonstrates the results of computational and experimental analysis. It can be concluded that results of computational analysis was a close approximation to the experimental results. However, the experimental value of tensile strength was found to be less as compared to computational results. From SEM analysis, it was observed that there were some air gaps and voids present in the fabricated samples, which yields lower tensile strength.

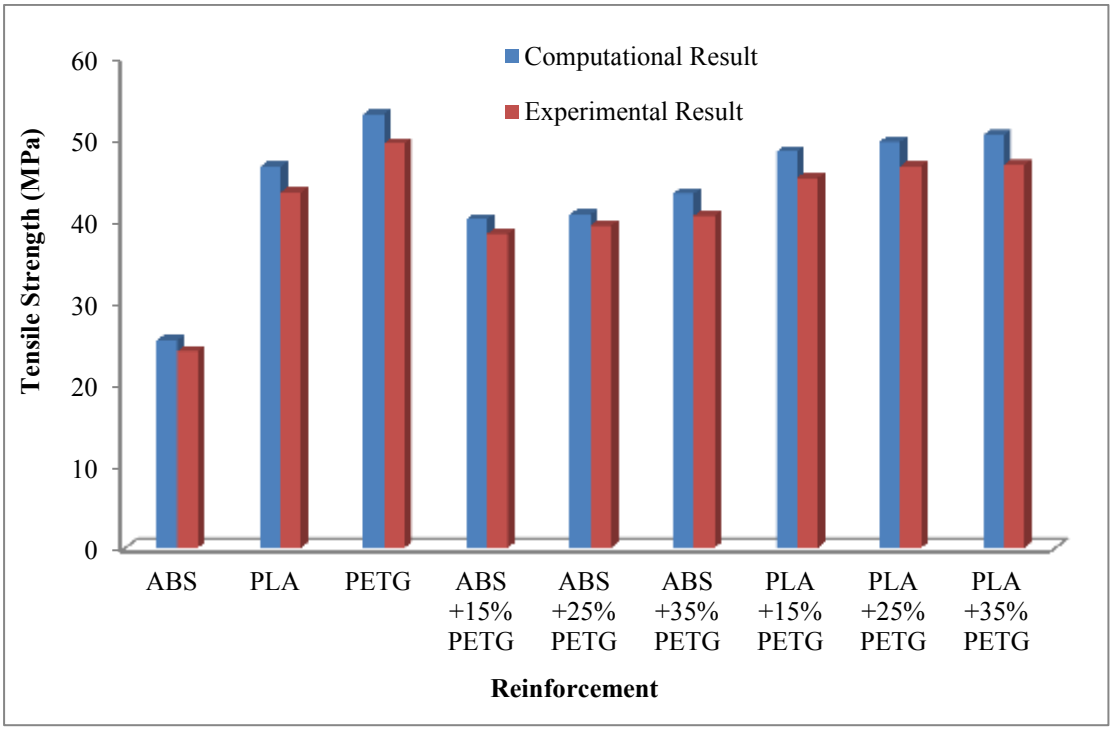

Figure 6.16: Comparison of experimental and computational results

6.4 Experimental plan for PolyJet component

6.4.1 Materials and method

For the evaluation of tensile behaviour of the RGD840 material specimens were fabricated according to ASTM D638 standards*[121]*. Test specimen for tensile test has been designed by using CATIA V6 software and converted into.STL file by using 0.0001 convergence tolerance. The dimensional details and 3D-CAD model of test specimen are presented in *Chapter 5*. Samples were manufactured by using Objet 30 PolyJet machine. The details of PolyJet machine is discussed in *chapter 3* of the thesis. In present investigation, RGD-840 Vero bluematerial was used as a building material, whereas SUP-705 was used as support material. A constant layer thickness of *28* µm was considered to fabricate all samples. The next sub-section will provide the details of the experimental plan.

6.4.2 Process parameters and their levels

Present study deals with the three factors viz., raster angle, orientation and surface type to conduct the experiment. Complex relation between UV irradiation patterns and manufacturing strategy recommends the presence of non-linear effects. However, possible interaction between the process parameters should be challenging to avoid. Keeping these facts into account, one factor at a time was selected for the manufacturing of test specimen. Modern approach provides an independent analysis of each process variables. Table 6.5 illustrates the process variables and their levels. In this study, raster angle was considered at four levels, i.e. *0°*, *30°*, *60°* and *90°*. Process parameter (orientations) was considered at two levels only, due to the height limitation

along 'Z' direction. The levels of process parameter (orientations) used in these studies were flat orientation and on-edge orientation.

Process parameter surface type was also considered at two levels only, due to the machine limitation. In this machine, only two types of finish product can be obtained namely glossy and matte finish type. Two experiment series is planned to conduct the experiments.

Table 6.6 illustrates the process variables of series one experiment. In this series, process parameter raster angle was varied between *0º* to *90°*. Due to the involvement of symmetry, orientation of component on the tray can be varied only up-to 90°. To check the repeatability of results, four samples were taken for each trial, and average value of four samples was considered. Hence, total 16 samples were fabricated for series one experiment. Figure 6.17 shows the raster direction on PolyJet build tray. Angles are measured from the X-axis. Raster angle represents the printing direction of the component on the build platform. Figure 6.18 shows the raster angle orientation of fabricated samples on Objet 30 PolyJet machine tray. Figure 6.19 shows the type of surface finish of the manufactured samples through Objet 30 PolyJet machine.

Table 6.5: Factor and their levels

S.N	Factors	Level 1	Level 2	Level 3	Level 4
1	Raster angle	*0°*	*30°*	*60°*	*90°*
2	Orientation	Flat	on-edge	-	-
3	Surface Finish	Glossy	Matte	-	-

Table 6.6: Experimental plan for ultimate tensile strength and percentage elongation of series one experiments

S.N	Fixed process parameters		Variable process parameter	Ultimate tensile strength (MPa)	Modulus of elasticity (MPa)	Percentage elongation
	Orientation	Surface type	Raster angle			
1	Flat	Glossy	0°	26.87	2658.5	21.65
2	Flat	Glossy	30°	22.54	2219.4	20.00
3	Flat	Glossy	60°	24.46	2165.6	23.38
4	Flat	Glossy	90°	27.85	2891.5	12.08

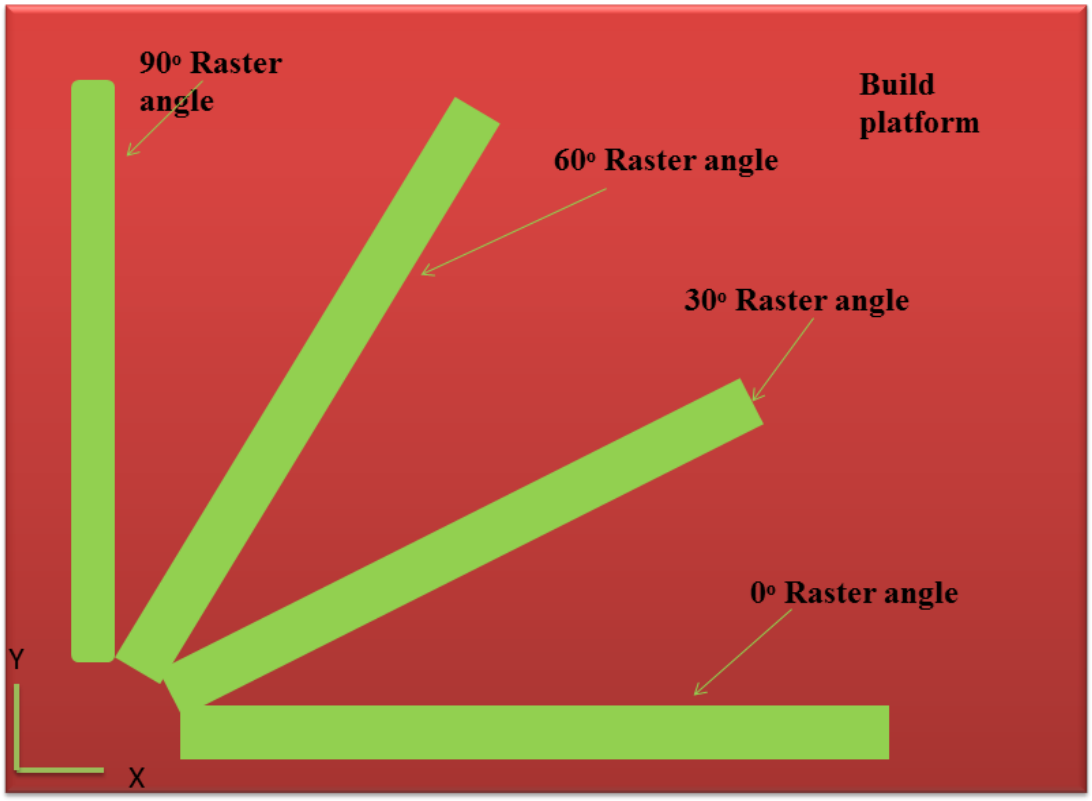

Figure 6.17: Raster directions on PolyJet platform

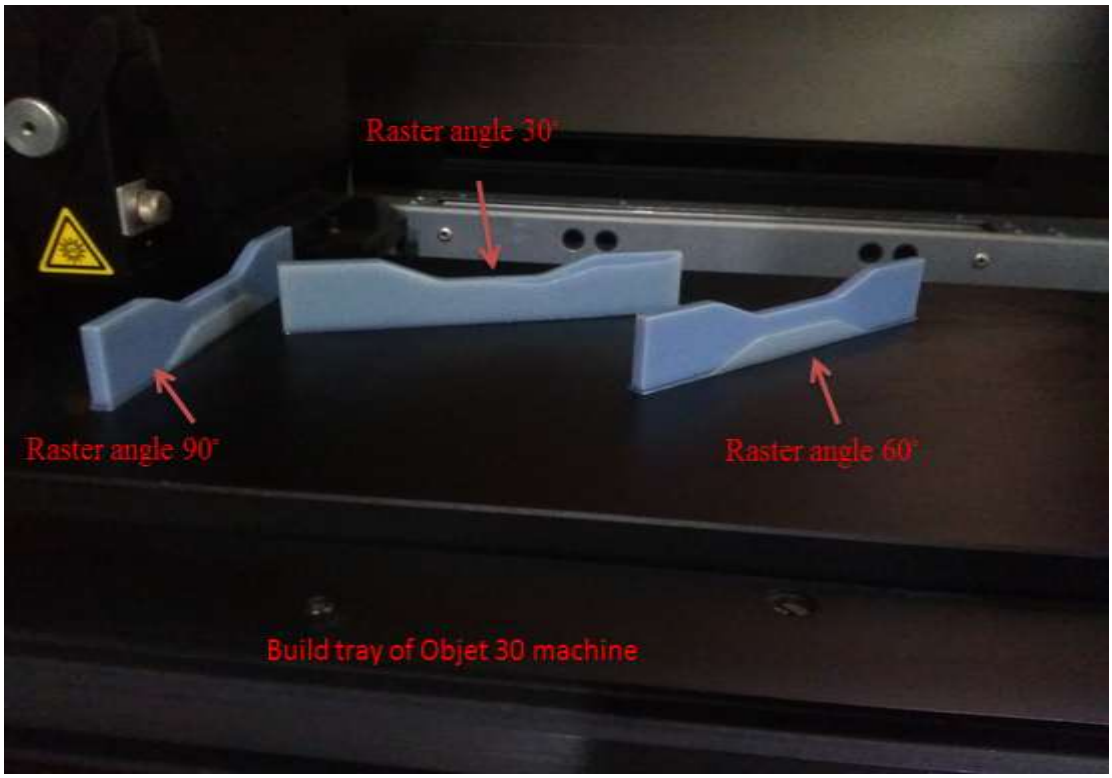

Figure 6.18: Raster angle on Objet 30 PolyJet machine tray of the fabricated samples

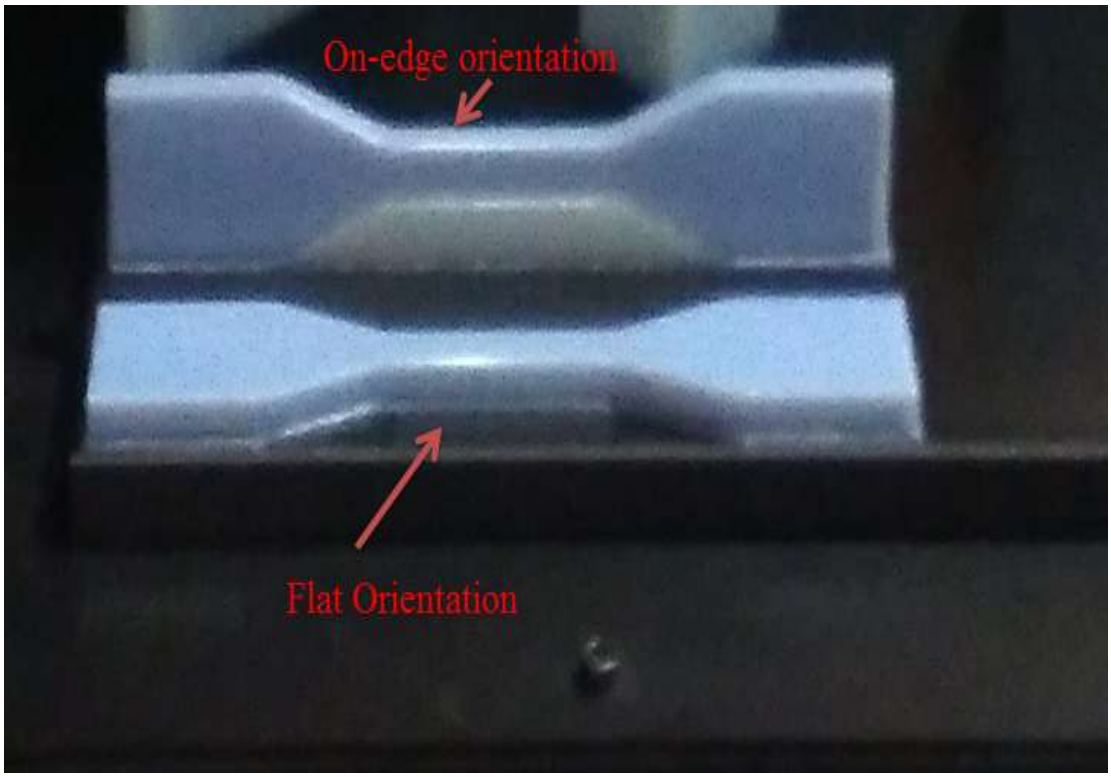

Figure 6.19: Orientation of fabricated samples on Objet 30 PolyJet machine tray

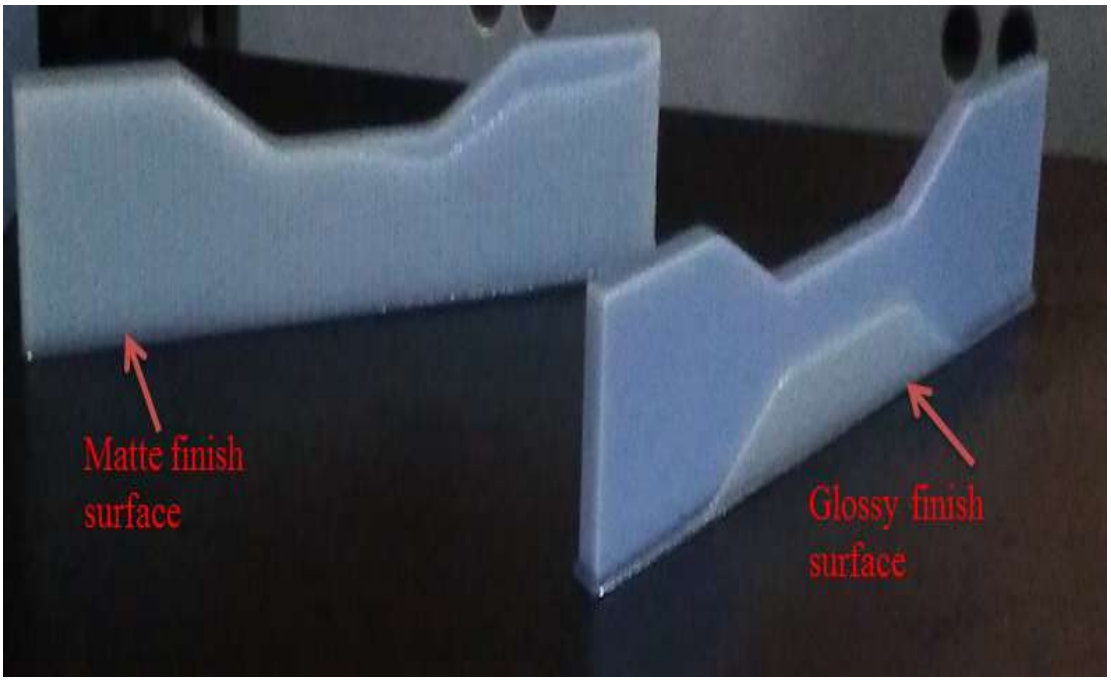

Figure 6.20: Type of surface finish of fabricated samples on Objet 30 PolyJet machine tray

Table 6.7 shows the process parameters and their levels of series 2 experiment. In this series,impact of orientation and type of surface finish on the mechanical behaviour of RGD-840 Vero blue material was investigated. Due to the size limitation of the Objet 30 machine, along the Z-direction perpendicular to the tray, fabrication is allowed in two directions. Orientations used in this investigation were flat and on-edge. Due to the uncertainty of experimental results, four samples were prepared on each orientation.

Only two types of surface, i.e. glossy and matte can be manufactured through Objet 30 machine. In glossy surface, support material does not stick on the surface of the fabricated samples. From Figure 6.20, it can be visualised that matte finish surface contains support material on its surface. In removal process, support material leaves burrs on the surface of fabricated sample, which results poor surface quality in the fabricated component. Total 16 samples were prepared in the second series of experiment. However, raster angle was kept constant, i.e. 0^o in series 2 experiment.

Table 6.7: Experimental plan for ultimate tensile strength and percentage elongation of series two experiments

S.N.	Raster angle	Surface type	Orientation	Ultimate tensile strength (MPa)	Modulus of elasticity (MPa)	Percentage elongation
1	0°	Glossy	Flat	26.13	2658.5	21.65
2	0°	Matte	Flat	23.56	2533.9	15.83
3	0°	Glossy	On-edge	20.58	1878.4	18.55
4	0°	Glossy	Flat	20.78	1628.2	21.98

6.4.3 Evaluation of mechanical properties

The ultimate tensile strength has been considered as response parameter to evaluate the mechanical properties of RGD 840 machine. Computerized UTM Logic Controller was used to conduct the tensile test of the specimen. The equipment can apply a constraint rate of strain. In this study, an instantaneous constant strain rate, i.e. *0.1mm/min*, was used. All the experiments were performed under controlled environment *20 °C*.

6.4.4 Results and discussion

i. First series: effect of raster angle within the tray

The average value of four samples of elastic modulus, ultimate tensile strength and percentage elongations were calculated on each orientation. In first series, impact of raster angle on elastic modulus, ultimate tensile stressand percentage elongation were analysed. Rest of the other process variables were considered as a constant. Figure 6.21 shows the effect of raster angle on elastic modulus of the fabricated component through PolyJet process. It can be observed that elastic modulus of RGD 840 material was significantly affected by the raster angle. Results of experimental studies showed that the value of elastic modulus was found to be maximum 2891.5MPa in the component fabricated along 90^{o} raster angle. The value of elastic modulus was found to be

minimum *2165.6MPa* at *60º* raster angle. Figure 6.22 shows the influence of raster angle on ultimate tensile strength of the material. The average value of four samples on each raster angle is reported in Table 6.6. The ultimate tensile strength of the material was found to be maximum of *27.88* MPa at *90º* raster angle.

Figure 6.23 shows that the percentage elongation of the fabricate samples manufactured by PolyJet process. It can be observed that percentage elongation was found to be maximum in the component fabricated along 60º raster angle. However, minimum percentage elongation was observed at 90º raster angle. Figure 6.24 demonstrates the stress-strain graph of tensile test for the sample fabricated along 0º raster angle. Figure 6.25 illustrates the stress-strain graph of tensile test corresponding to raster angle *30º*. Figure 6.26 shows the stress-strain curve of the samples manufactured along *60º* raster angle. Moreover, Figure 6.27 represents the stress-strain curve corresponding to the *90º* raster angle orientation. The influence of raster angle orientation on stress-strain graph of the fabricated samples is shown in Figure 6.28.

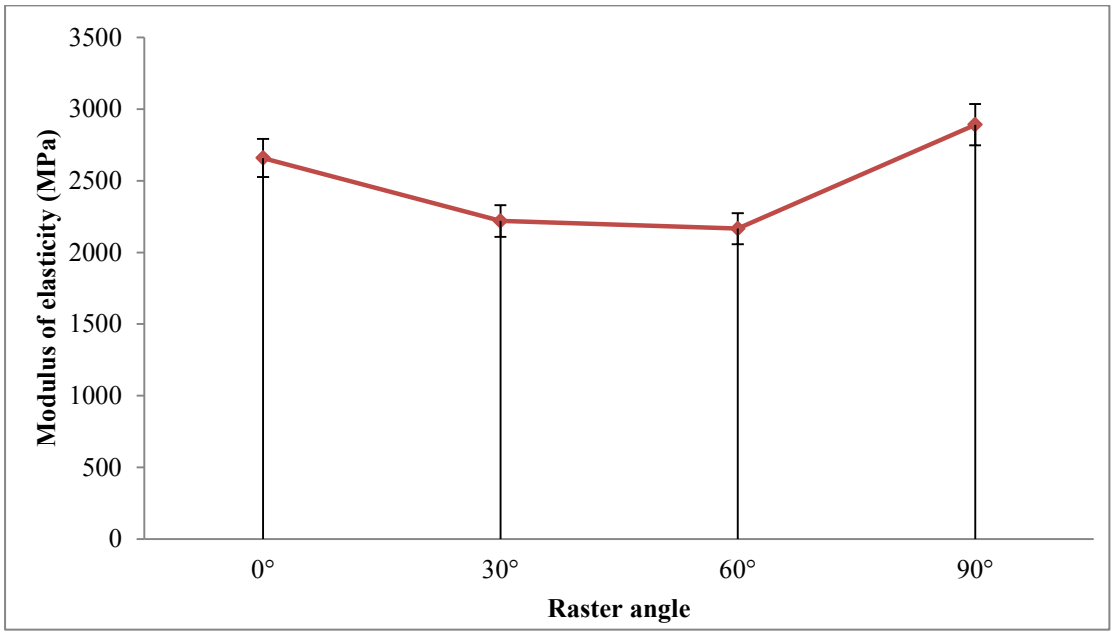

Figure 6.21: Effect of raster angle on the elastic modulus of the material

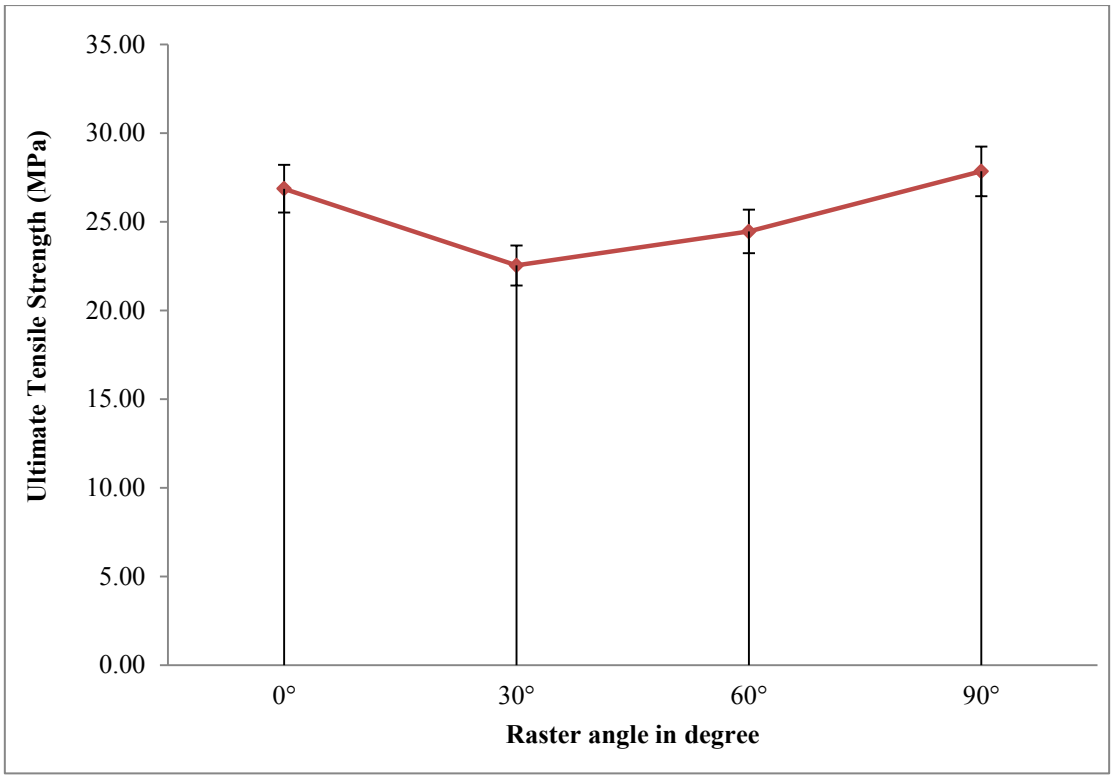

Figure 6.22: Effect of raster angle on ultimate tensile strength of the material

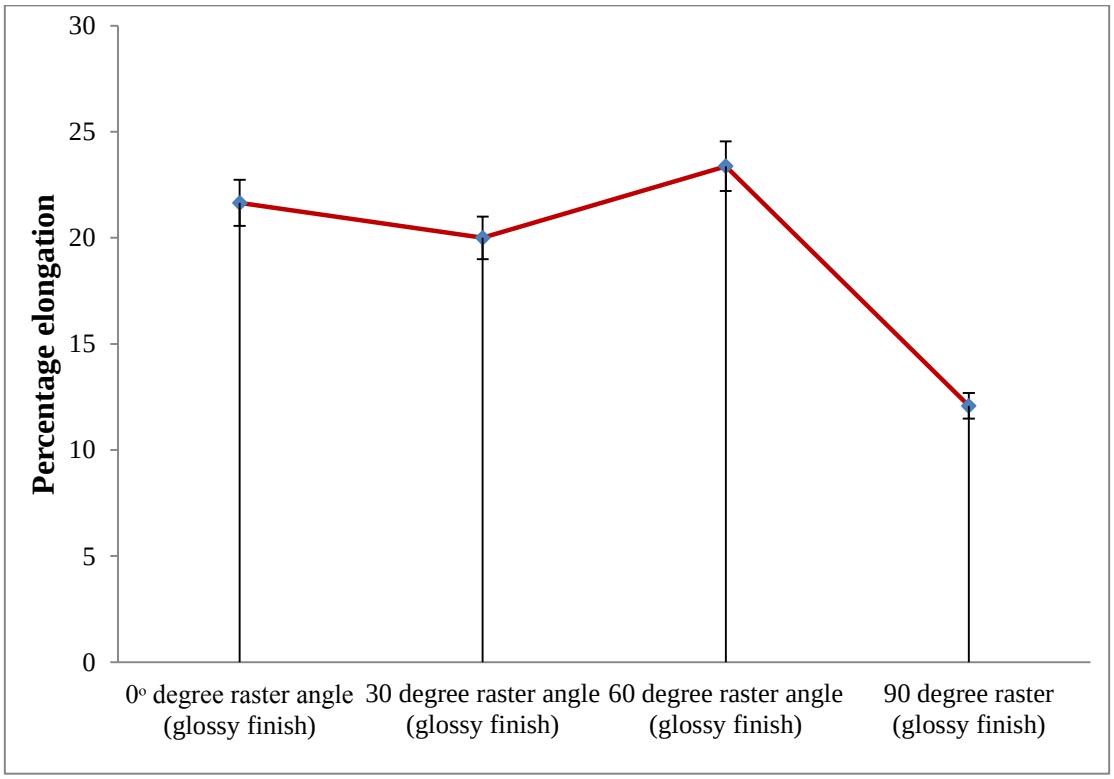

Figure 6.23: Effect of raster angle on percentage elongation of materials

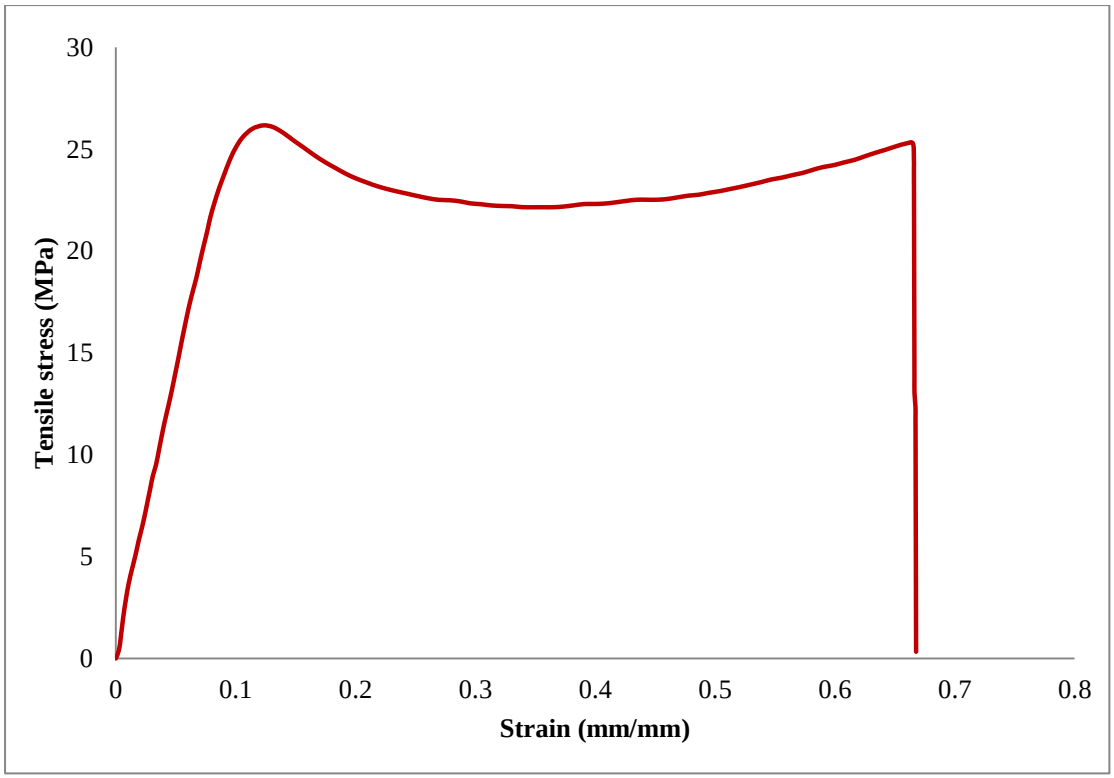

Figure 6.24: Stress-strain curve at *0°* raster angle

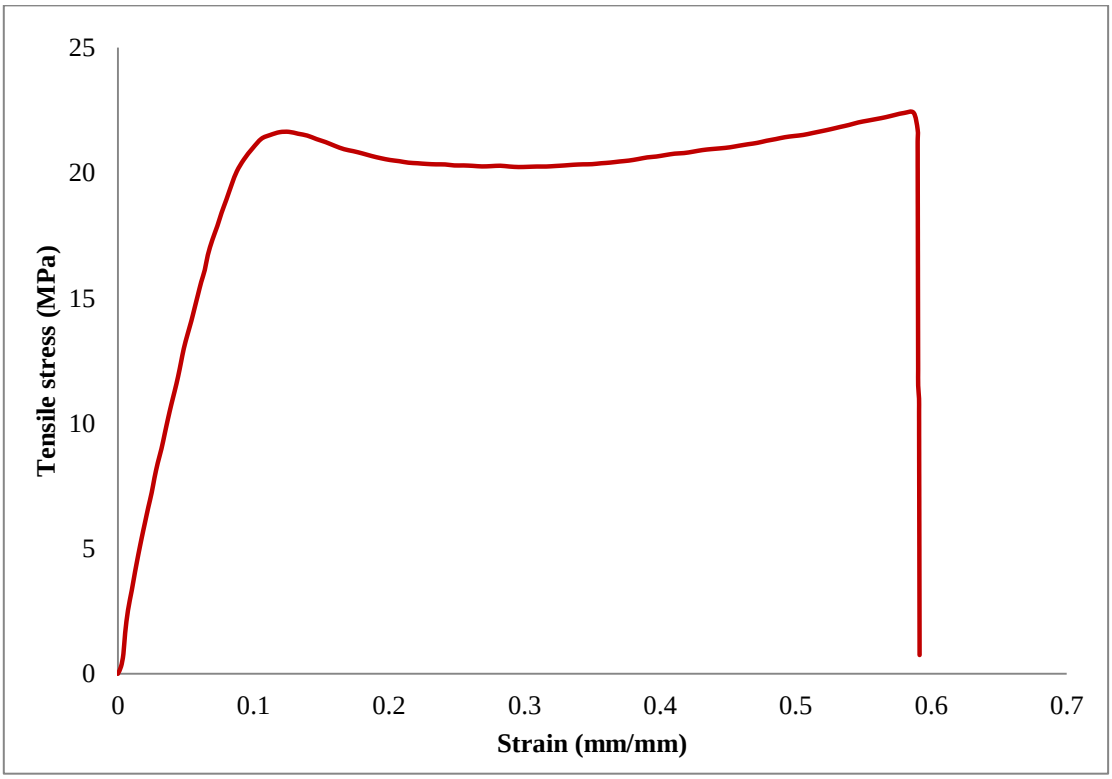

Figure 6.25: Stress-strain curve at *30°* raster angle

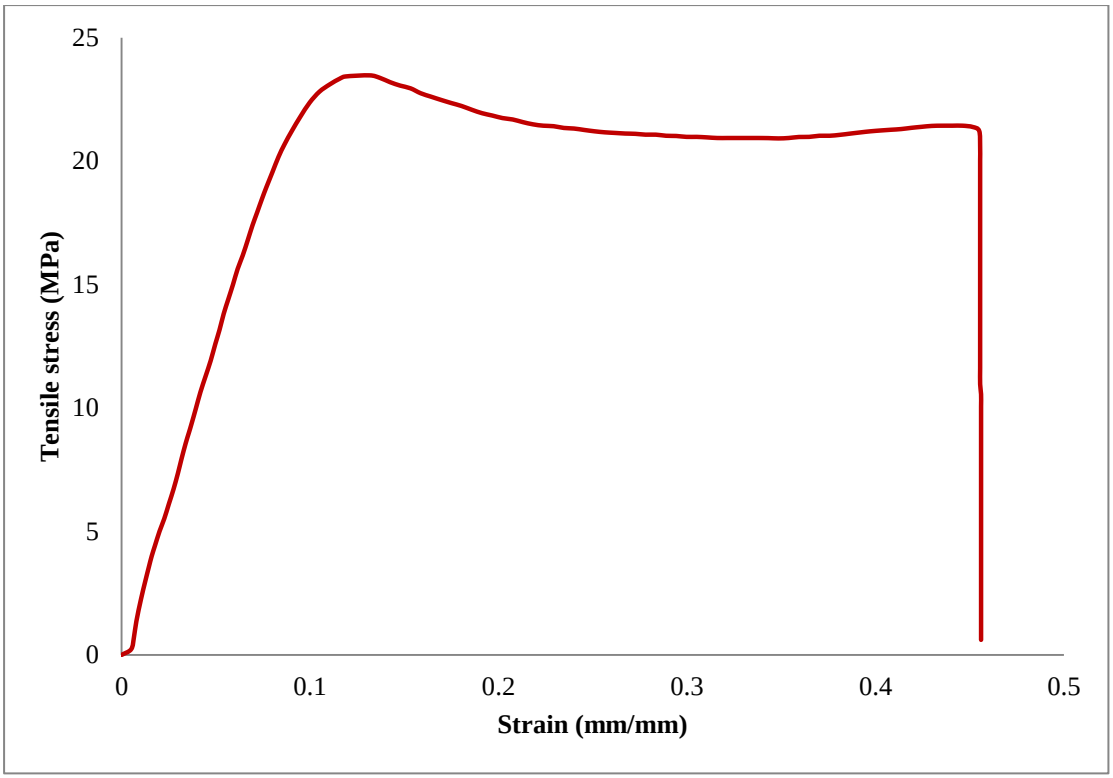

Figure 6.26: Stress-strain curve at *60º* raster angle

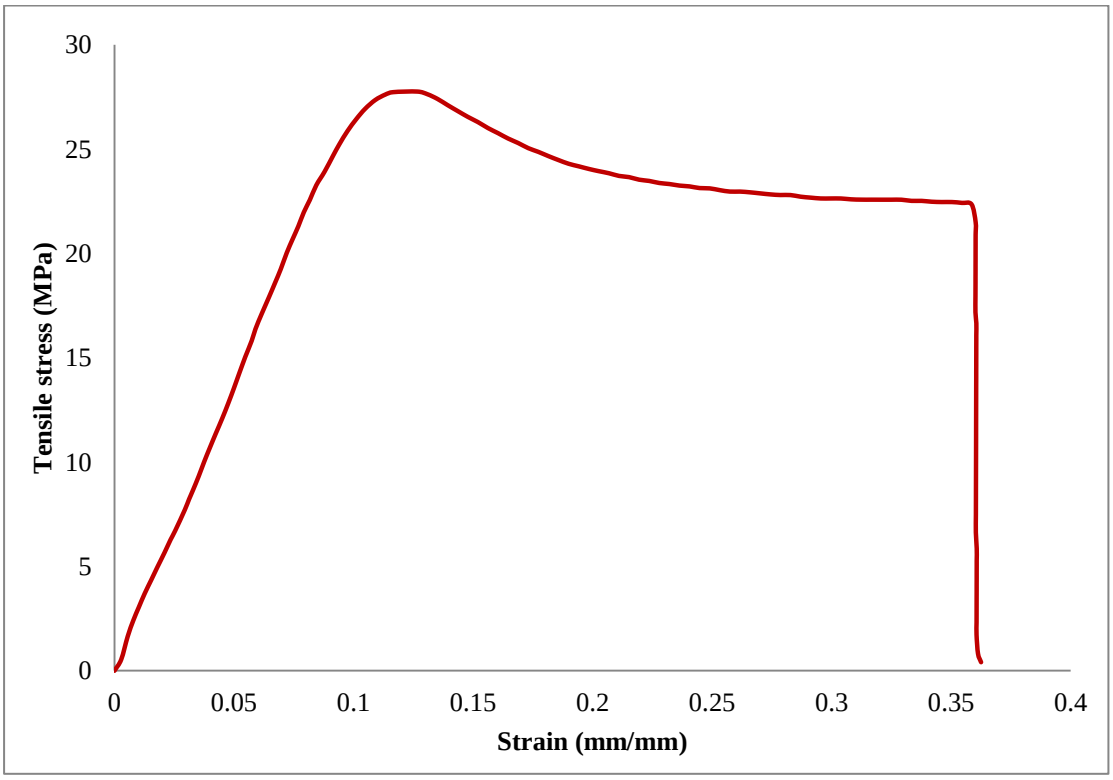

Figure 6.27: Stress-strain curve at *90º* raster angle

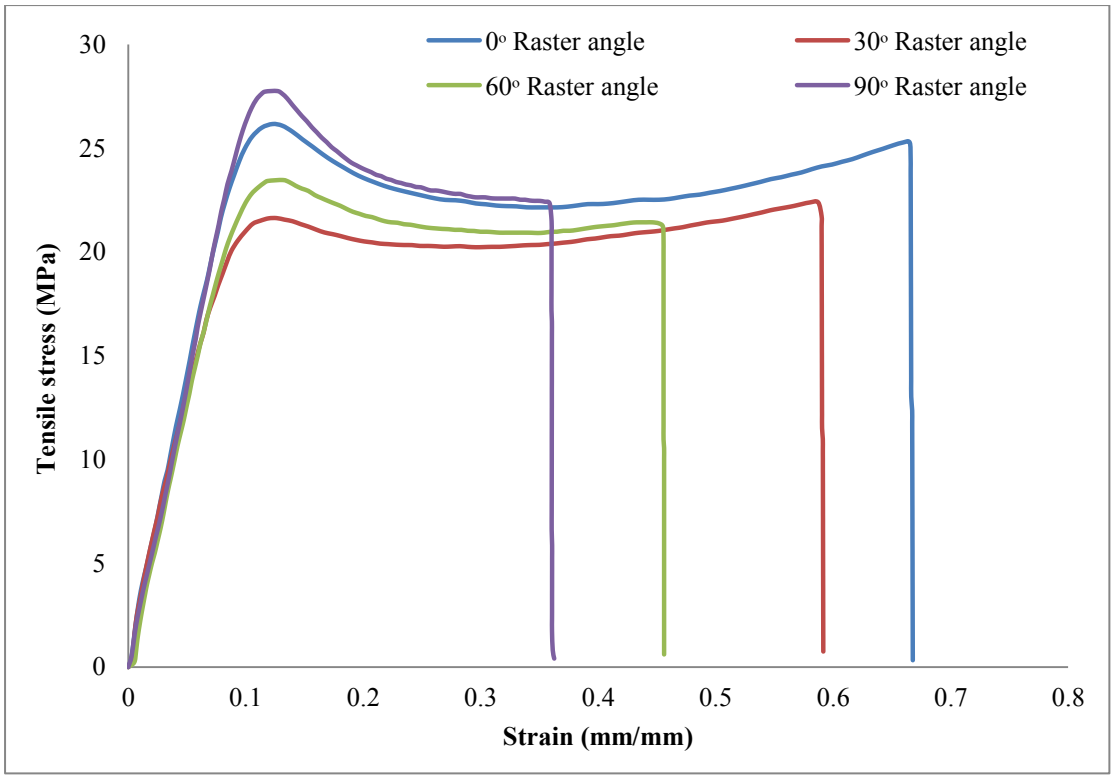

Figure 6.28: Combined stress-strain curve for all raster angle

ii. Second Series: effect of orientation of part within the tray and type of surface finish

The value of elastic modulus, ultimate tensile stress and percentage elongation of second series experiments are also calculated by taking the average value of four samples. In this series effect of part orientation on tray and type of surface finish was calculated. Figure 6.29 shows the effect of part orientation and type of surface finish on elastic modulus of RGD840 material fabricated through PojyJet technique. Results depicted that value of elastic modulus was found to be maximum *2658.5* MPa corresponding to process parameters flat orientation and glossy finish type surface. However, raster angle was kept constant, i.e. *0°* in the second series experiments. The value of elastic modulus was found to be minimum *1628.2* MPa at process variable on-edge orientation and matte finish type surface. It can be observed that process parameter

surface type have very less effect on elastic modulus of the material. However, the elastic modulus was significantly affected by the process parameter orientation. The average value of four samples of elastic modulus, ultimate tensile strength and percentage elongation are shown in Table 6.7.

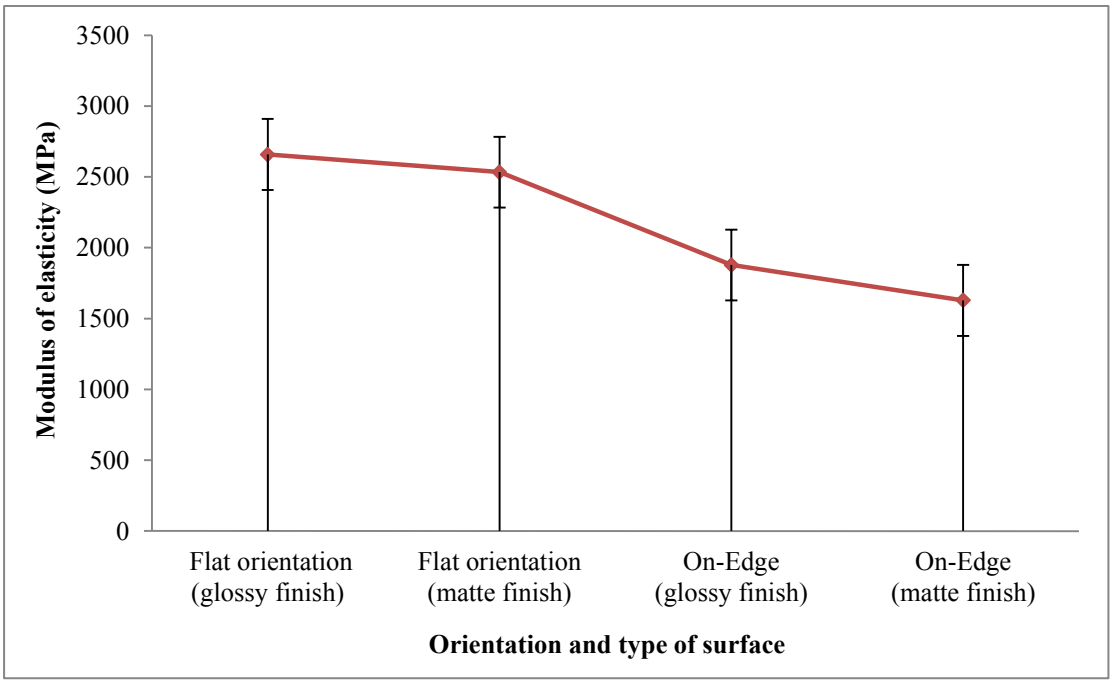

Figure 6.29: Effect of orientation and type of surface finish on modulus of elasticity of a material

Figure 6.30 shows the effect of process variables, i.e. orientation and type of surface finish on ultimate tensile strength of RGD840 material. Studies revealed that ultimate tensile was significantly affected by process parameter orientation. However, surface type has less effect on fracture strength of the material. The value of ultimate fracture strength was found to be maximum *26.13* MPaat flat orientation and glossy finish type surface.

Figure 6.31 shows the effect of orientation and type of surface finish on percentage elongation of RGD840 material. Studies revealed that orientation and type of

surface finish both have significant effect on percentage elongation of the material. The value of percentage elongation was found to be minimum at flat orientation and matte finish type of surface. Matte finish surface leaves burrs on the surface of build material during the post-processing process, which results in less deformation before fracture.

Figure 6.32 represents the stress-strain behaviour of material corresponding to parameters viz., flat orientation and glossy type of surface finish. Figure 6.33 demonstrates the stress-strain graph of the fabricated specimens corresponding to process parameters, i.e. flat orientation and matte type of surface finish. Figure 6.34 demonstrates the stress-strain curve of the material at process parameters level; on-edge orientation and glossy type of surface finish. Figure 6.35 it is evident from the stress-strain curve at process parameters level, i.e. on-edge orientation and matte finish type of surface. Figure 6.36 portrays the combined stress-strain curve for RGD 840 material in series two experiments.

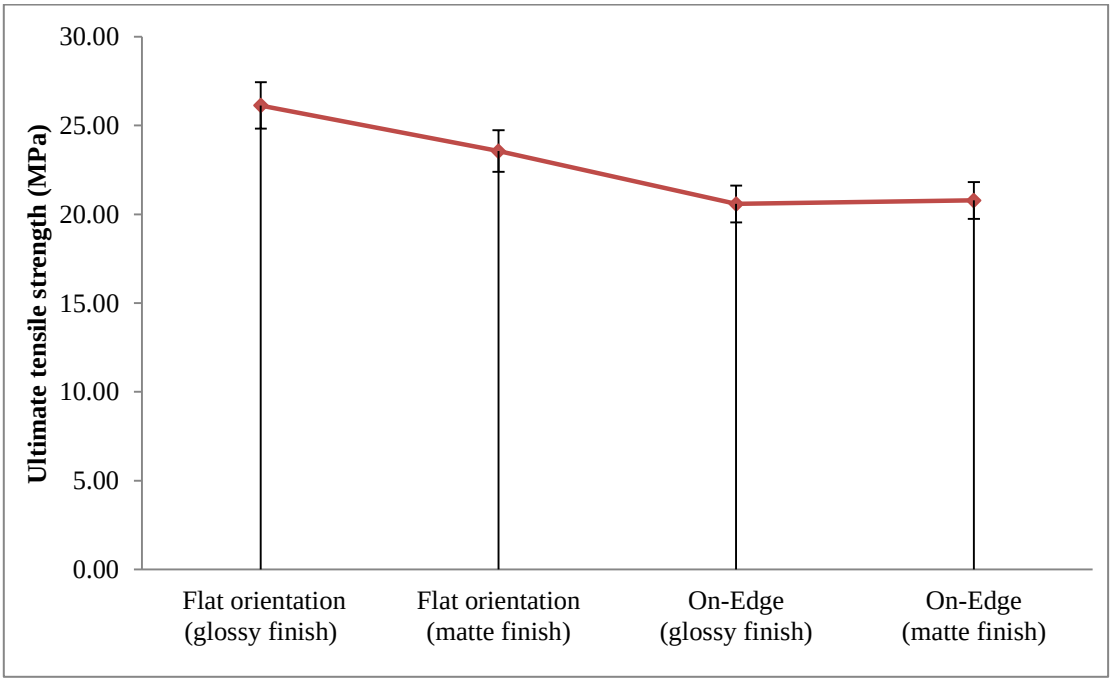

Figure 6.30: Effect of orientation and type of surface finish on ultimate tensile strength ofthe material

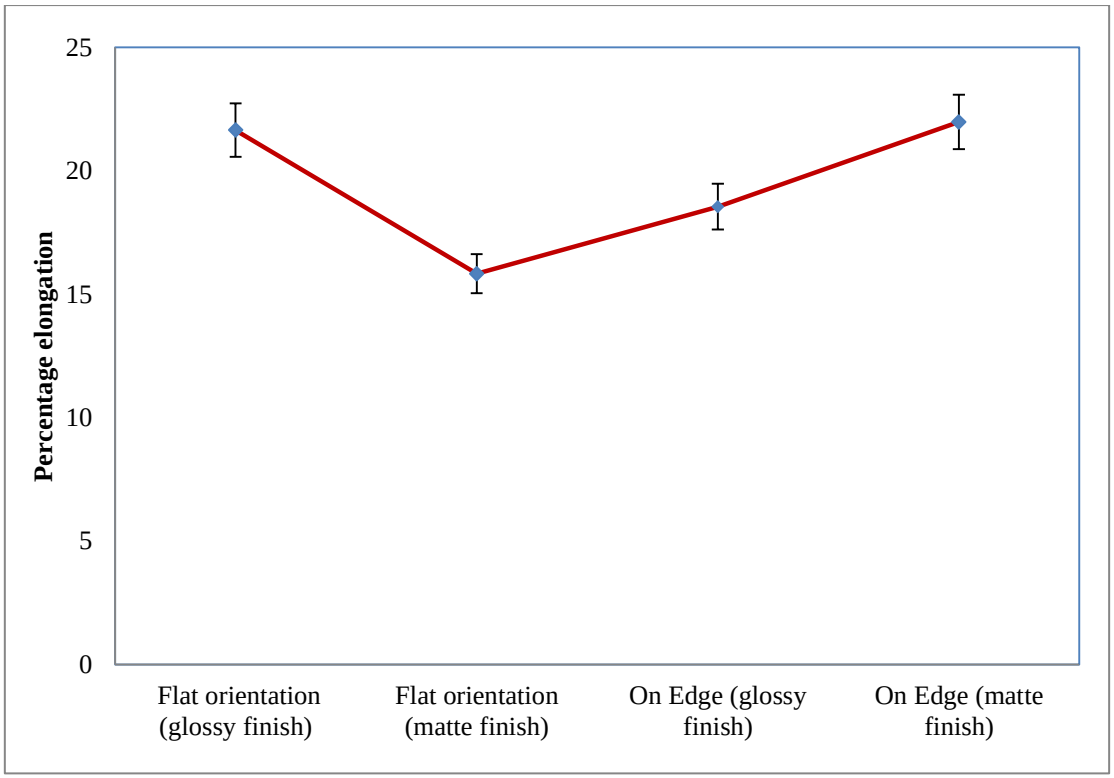

Figure 6.31: Effect of orientation and type of surface finish on percentage elongation of material

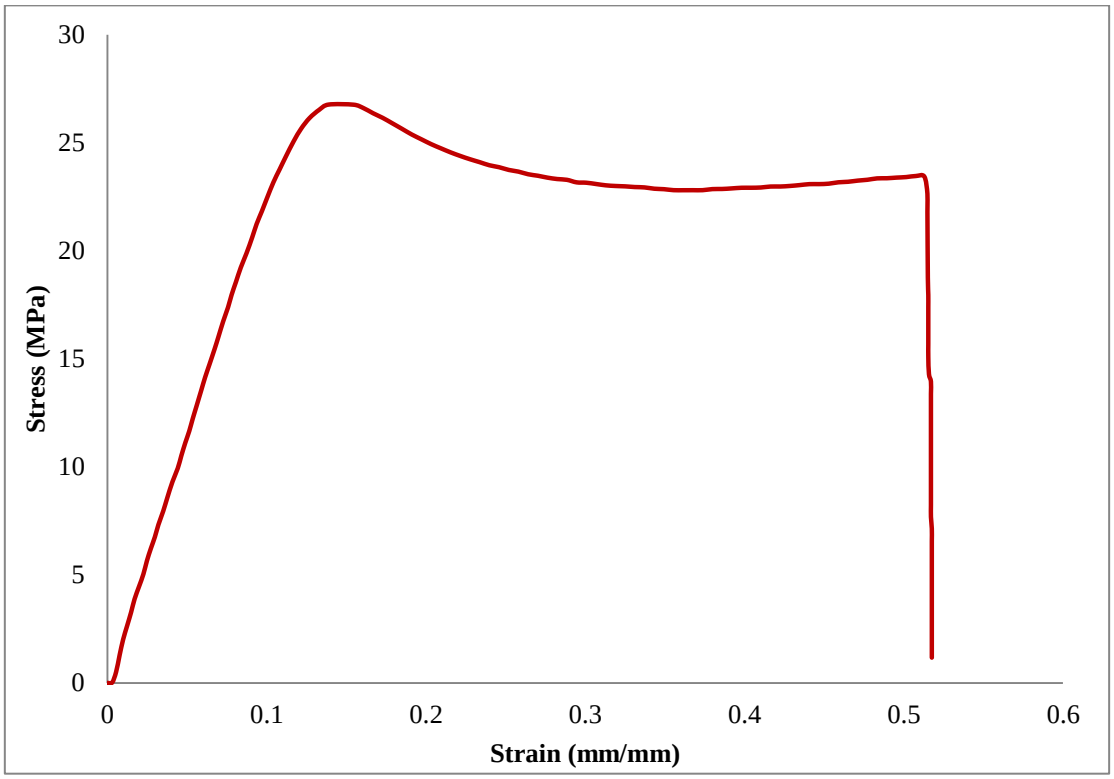

Figure 6.32: Stress-strain curve of flat orientation and glossy finish surface

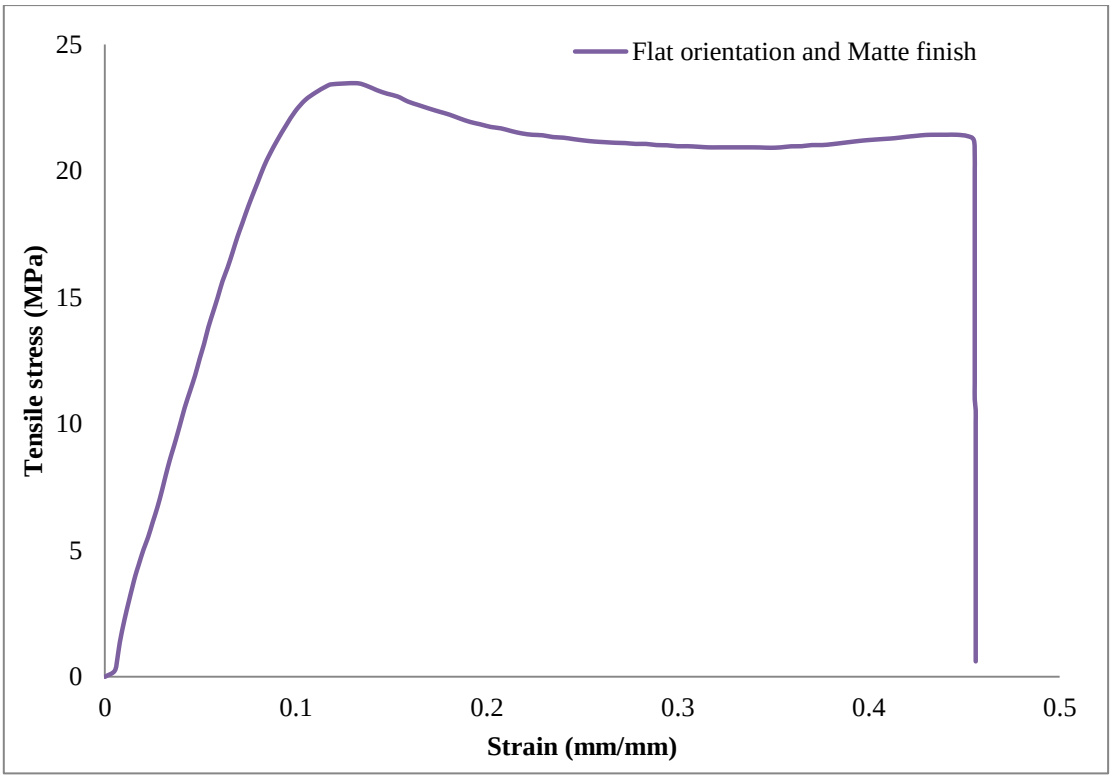

Figure 6.33: Stress-strain curve of flat orientation and matte finish surface

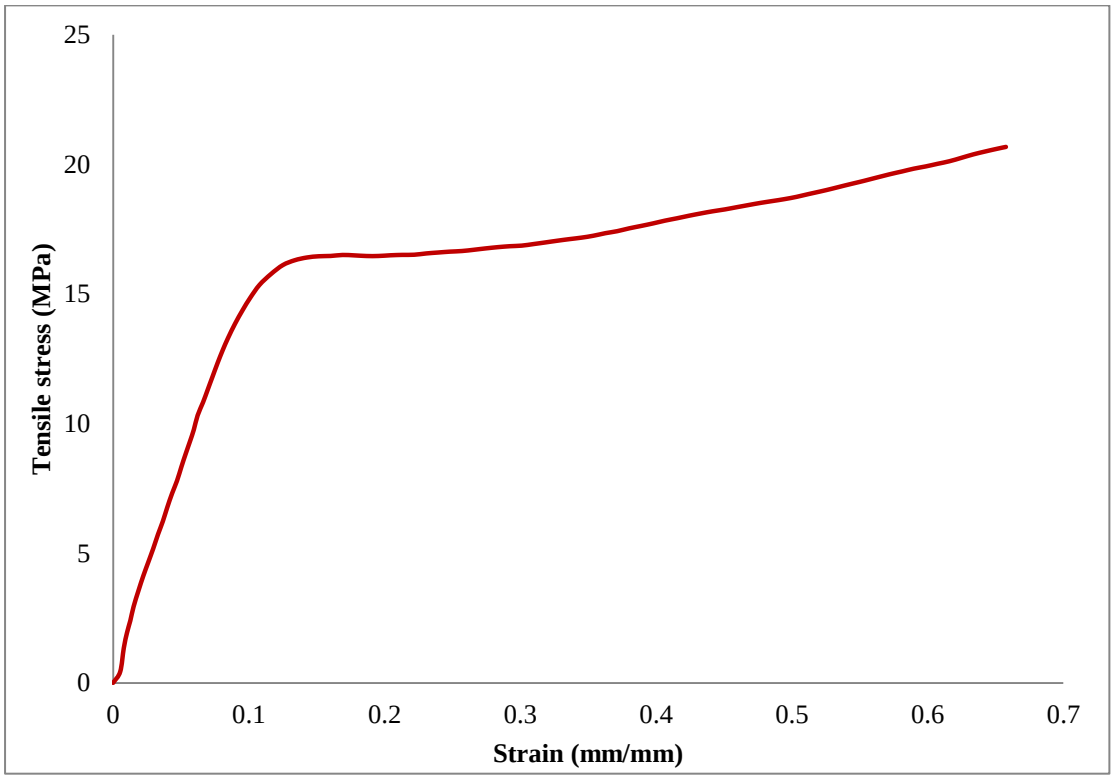

Figure 6.34: Stress-strain curve of on edge orientation and matte, glossy finish type surface

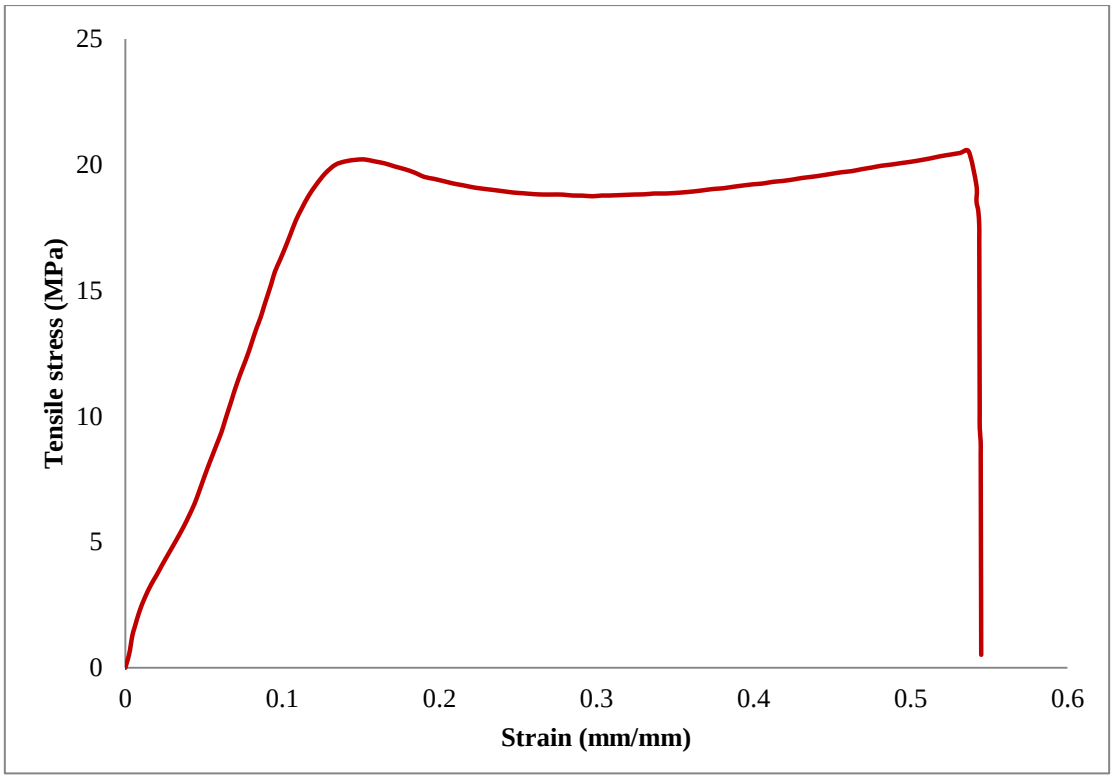

Figure 6.35: Stress-strain curve of on-edge orientation and matte finish surface

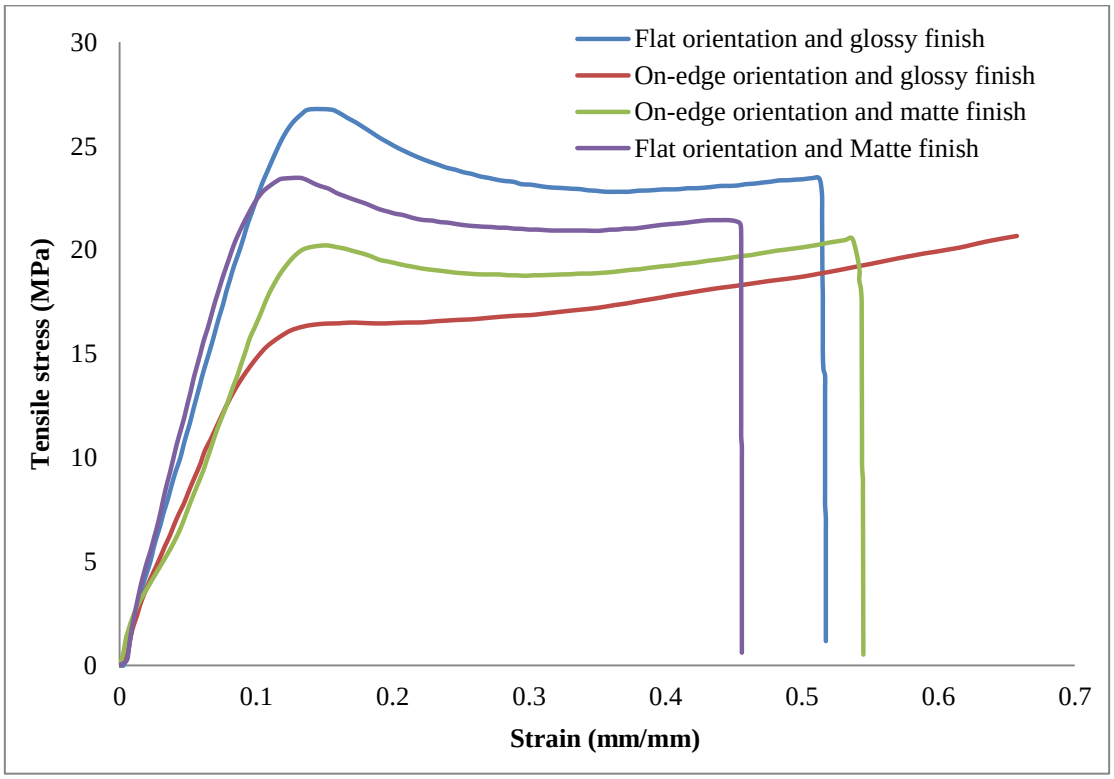

Figure 6.36: Combined stress-strain curve of second series experiment

6.5 Analysis of plastic strain of RGD 840 material

Plastic strain was evaluated by experimentally as well as computationally both. For this purpose ASTMD-638 tensile test specimen was used to evaluate the plastic strain. FEA software ABAQUS was used to investigate the plastic strain computationally. A constant displacement of *0.1* mm/min was applied. The details of experimental and computational studies are discussed in next sub-section.

6.5.1 Experimental investigation of plastic strain

Plastic strain behaviour of RGD840 material was investigated from the experimental data of load-deflection diagram. The load-deflection curve of the material corresponding to process parameter, i.e. raster angle *0*°, orientation flat and surface finish type glossy is shown in Figure 6.37. The methodology adopted for the calculation of plastic strain is presented in Figure 6.38. The value of engineering strain was evaluated by dividing the extension length with a gauge length of the specimen.

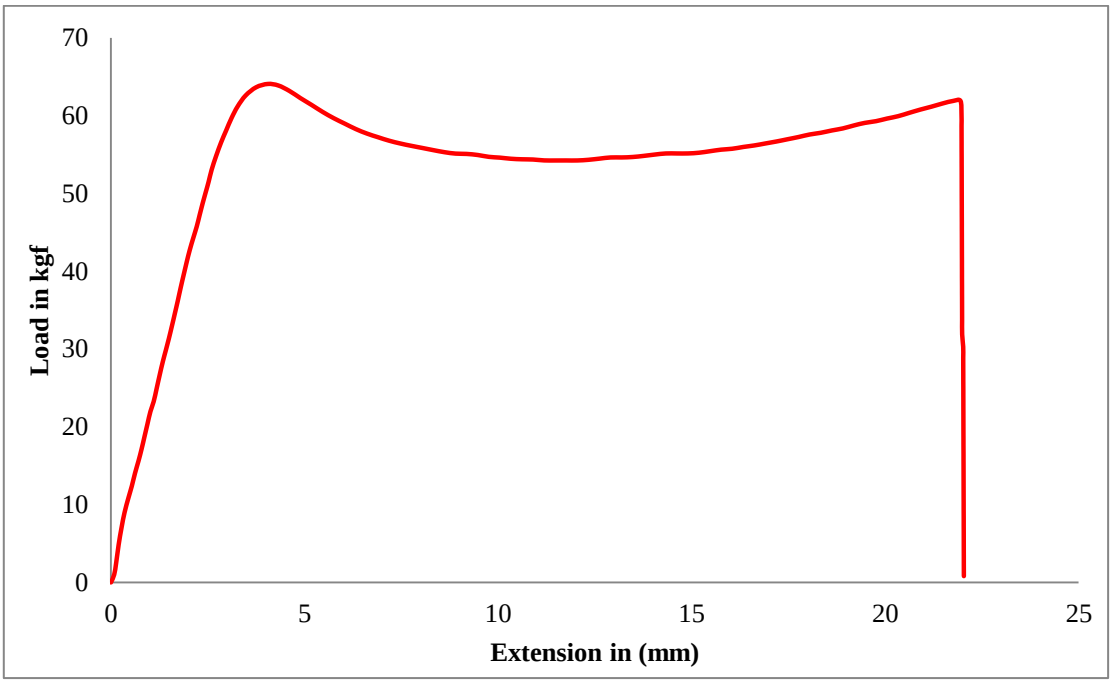

Figure 6.37: Load deflection curve of the material

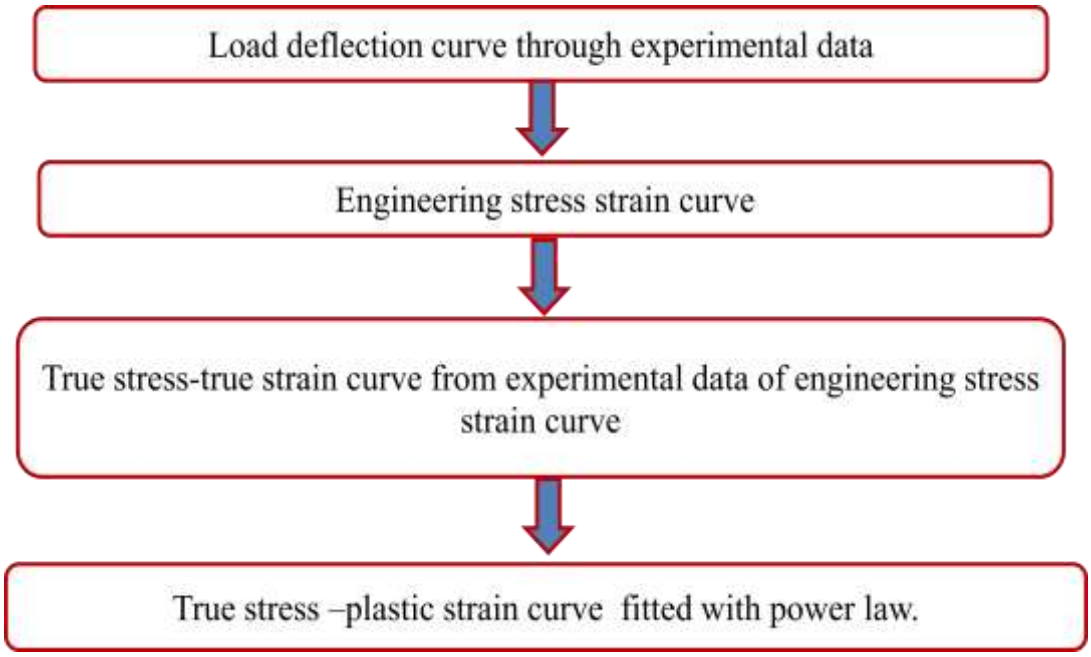

Figure 6.38: Flow chart for the calculation of true stress-plastic strain

The value of true stress and true strain were calculated by using Eqs. 6.1 and 6.2 respectively. Plastic strain was calculated by using power law from the true strain data. The Eq. 6.3 is used for the calculation of plastic strain. Relation between true stress and plastic strain is shown in Eq. 6.4. Figure 6.39 illustrates the true stress-true strain curve.

$$Truestress(\sigma_T) = \sigma_T \times ln(1 + \varepsilon_E) \tag{6.1}$$

$$Truestrain(\varepsilon_T) = ln(1 + \varepsilon_E) \tag{6.2}$$

$$\varepsilon_T = \varepsilon_E + \varepsilon_P \tag{6.3}$$

$$Truestress(\sigma_T) = K \times \varepsilon_P^{n1} \tag{6.4}$$

Where σ_T is true stress (N/mm^2), σ_E is engineering stress(N/mm^2), ε_E is engineering strain (mm/mm), ε_T is true strain (mm/mm), ε_E is engineering strain (mm/m), K is strength coefficient (MPa), n_1 is strain hardening exponent, and ε_p is plastic strain.

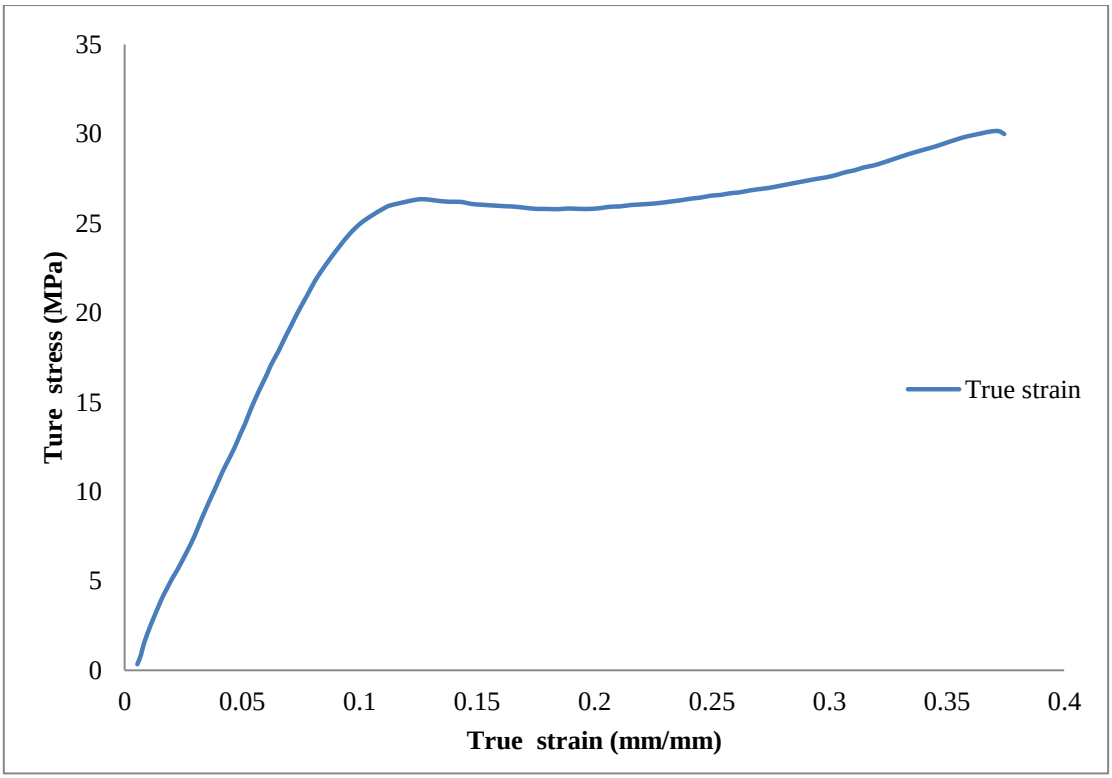

Figure 6.39: Experimental true tensile stress-true tensile strain curve of the RGD 840 material

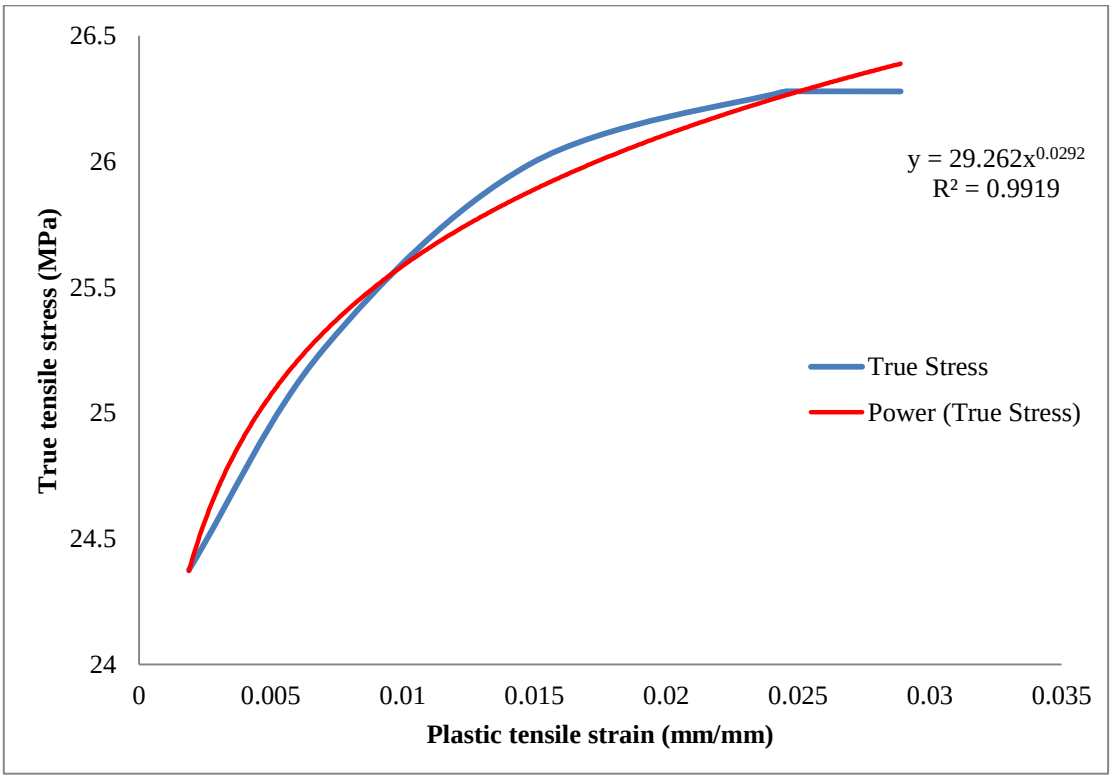

Figure 6.40: Experimental true stress-plastic tensile strain curves

Figure 6.40 demonstrates the experimental true tensile stress- plastic strain graph. The value of strength coefficient (K = 29.26 MPa) and strain hardening coefficient (n_1 = 0.029) were determined by using graphical method. The value of R^2 of fitted curve represents the accuracy of the fitted curve. In curve fitting power law was chosen to fit the experimental data because calculation of plastic strain was based on power law. The value of the R^2 of the fill line is 0.991 closed to *1*. It indicates that the fitted line is good enough to predict the plastic strain.

6.5.2 Computational investigation of plastic strain

Explicit 3D ASTM D-638 models consist of flat dog bone shape shown in Figure 6.2. For computational analysis of plastic strain finite element analysis software, ABAQUS was used.

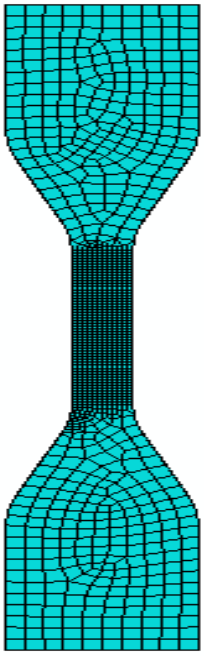

Figure 6.41: Mesh geometry of ASTM D638 tensile test specimen

A continuum 3-D,eight-node linear brick element C3D8R element was used to simulate the material in a virtual environment. The mesh density was considered high.

The mesh size at gauge length section was selected as *0.5* mm, and the rest of the section mesh size was used *2* mm. Total *9368* element was used in this analysis. Figure 6.41 shows the mesh geometry of the ASTMD638 specimen.

Figure 6.42 shows the boundary condition for tensile test specimen simulation. Boundary condition was applied similar to tensile test on UTM. Degree of freedom at the bottom section *(U_x= 0,U_y = 0, U_z= 0, $M_{t/x}$ = 0,$M_{t/y}$ = 0, $M_{t/z}$ = 0)* was considered as zero. A displacement *(Uy = 0.1* mm/min) along Y- axis load was applied at the top of the specimen. The other boundary contestation *(Ux = 0, Uz =0)* was applied at the top section.

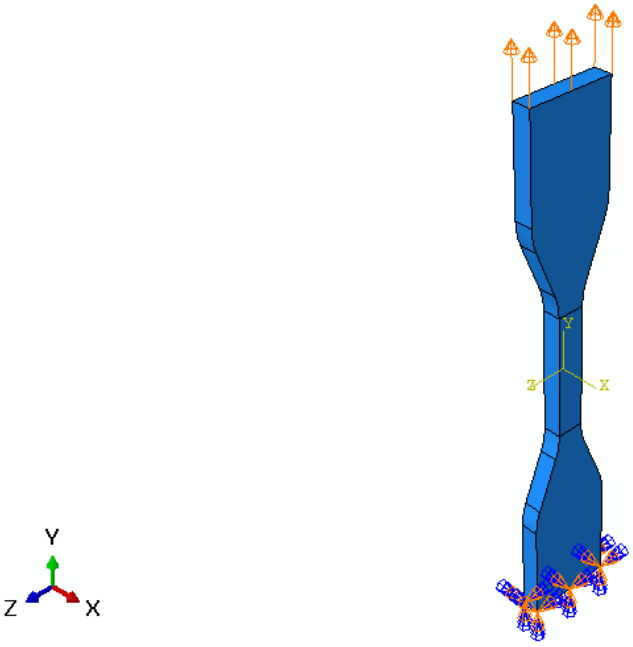

Figure 6.42: Boundary condition and load application on specimen for investigation of plastic strain.

Figure 6.43 represents the contour plot of plastic strain of the tensile test specimen.It can be observed that maximum plastic strain is occurred in the gauge length section due to high value of tensile stress at the section. The value of true stress is maximum at gauge section because smaller cross-sectional area. It is shown

in Figure 6.44 the contour plot of plastic strain of gauge length section. In experimental study deformation of test specimen is measured only for the gauge length section. Hence FEA analysis of gauge length section becomes a critical observation.

In ABAQUS software for analysis of plastic strain, materialproperties viz., modulus of elasticity, passion's ratio value of K and n_1 were required. The value of E = *2.65 GPa* and μ*=0.49* was used in this investigation. The value of strength coefficient (K = *29.26 MPa*) and strain hardening coefficient (n_1 = *0.029*) were used for the computational analysis. The value of strength coefficient and strain hardening coefficient was calculated from the experimental value of true stress and plastic strain curve fitting by applying power law. The fitted value of the strength coefficient and strain hardening coefficient is shown in Figure 6.40. Figure 6.45 shows the true stress-plastic strain curve.

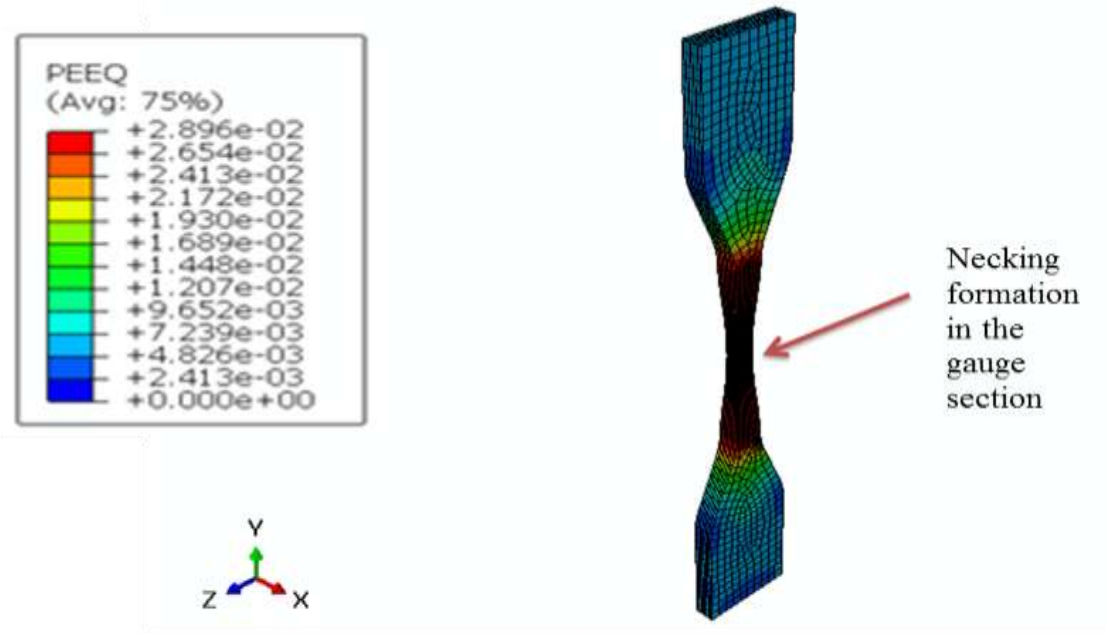

Figure 6.43: Contour plot of plastic strain of the test specimen

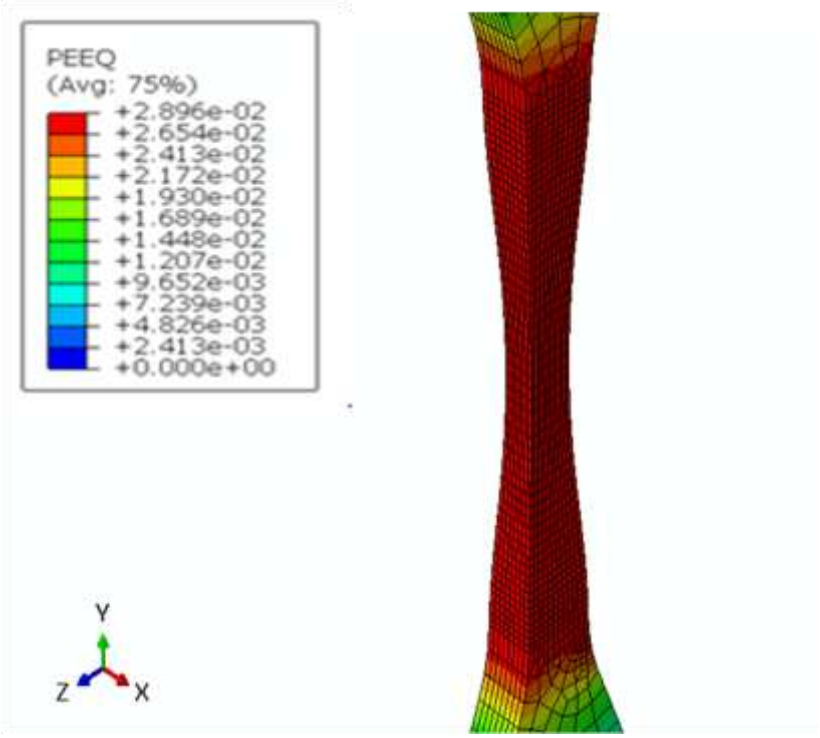

Figure 6.44: Contour plots at the gauge length section

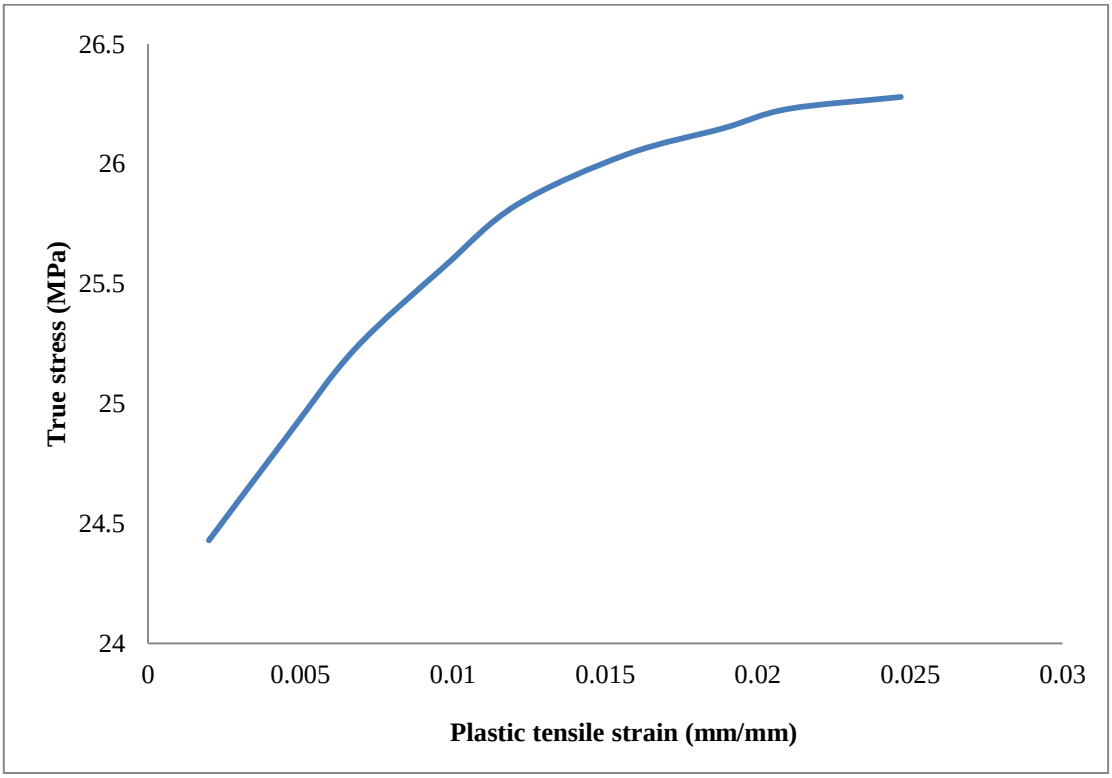

Figure 6.45: FEA true tensile stress-plastic strain

6.5.3 Comparison between experimental and computational results of plastic strain

Figure 6.46 distinguish the experimental and computational observation of plastic strain behaviour of RGD 840 material under tensile loading condition. It is concluded from the graph, FEA analysis is close approximation of the experimental results. The value of plastic strain of computational result is within the range of *5%* of the experimental results. FEA results deviate from experimental results at some point due the approximation error of strength coefficient and strain hardening coefficient. In case of strain analysis convergence of FEA results over predict. Hence, a result observed from numerical simulation is correlating the convergence criteria. The next subsection presents the methodology for clearance analysis between the mating parts of the automotive components.

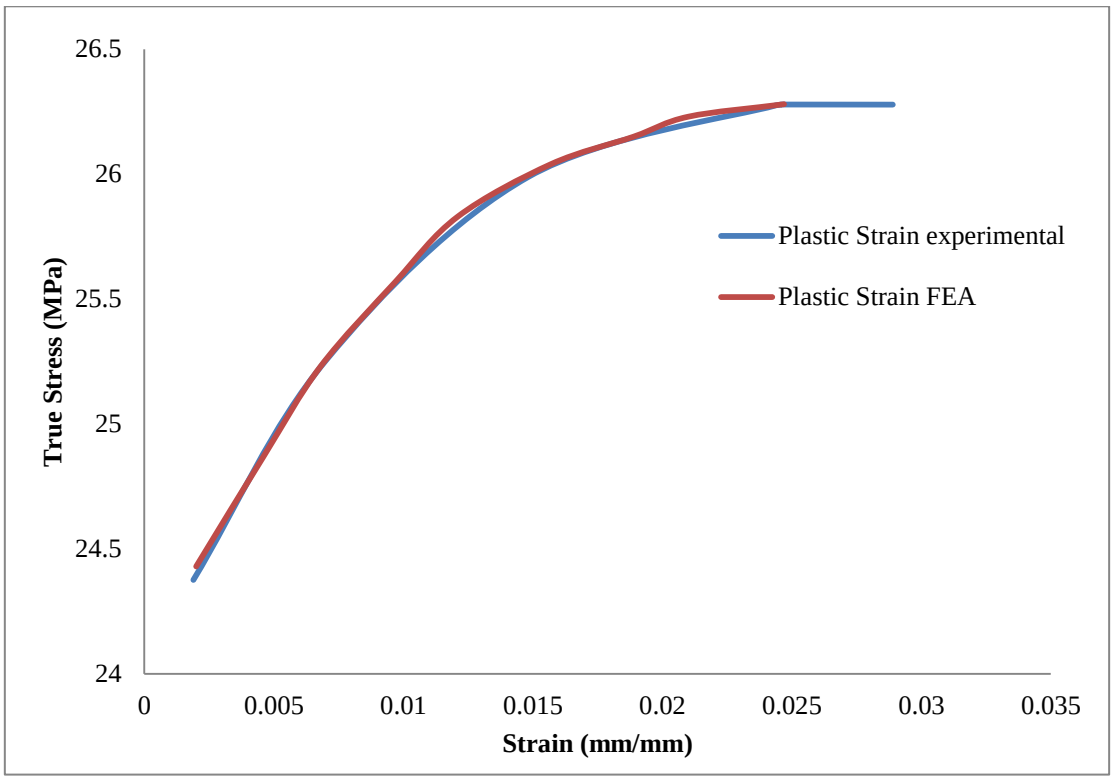

Figure 6.46: Comparison of experimental and FEA analysis of true stress-plastic strain curve

6.6 Control methodology for clearance between mating parts

Through the various literature available, it has been observed that the actual dimension of the component fabricated through RP process was slightly less than the actual dimension, due to some shrinkage of material during the solidification process. The shrinkage phenomena is not uniform; it depends on number of factor like direction, material, size of the component etc. It was also observed that shrinkage phenomena in solid section and hollow section were different. In the hollow object, shrinkage was found to be more as compared to solid object. In this research work, an assembly of piston, connecting rod and cylinder was fabricated through FDM process to analyse the clearance between mating parts. In evaluation process of clearance a regression model proposed by Ragunath and Pandey [40] was used. It accommodates the shrinkage factor. Figure 6.47 shows the dimension of cylinder used for the 3D modelling and Figure 6.48 indicates that the dimension of piston used for the 3D modelling.

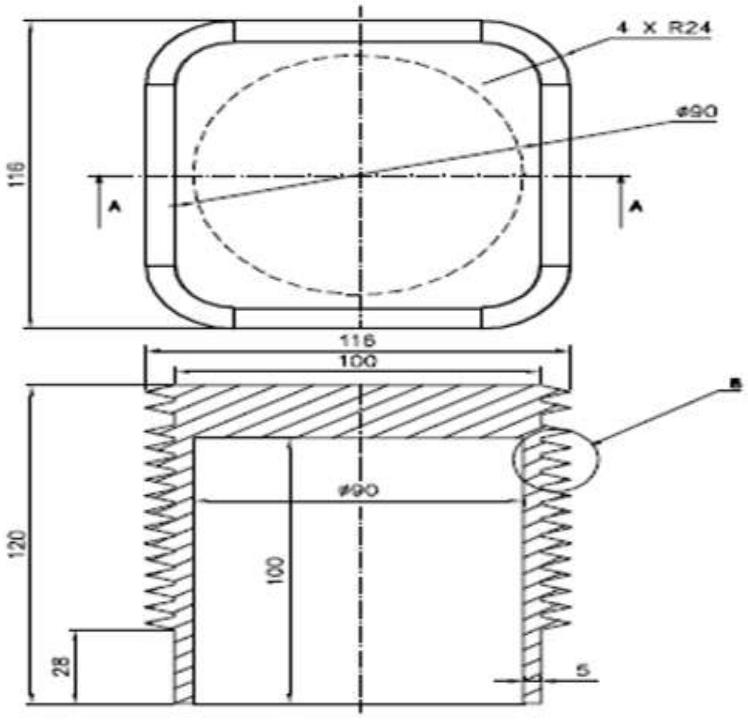

Figure 6.47: Dimension of the cylinder

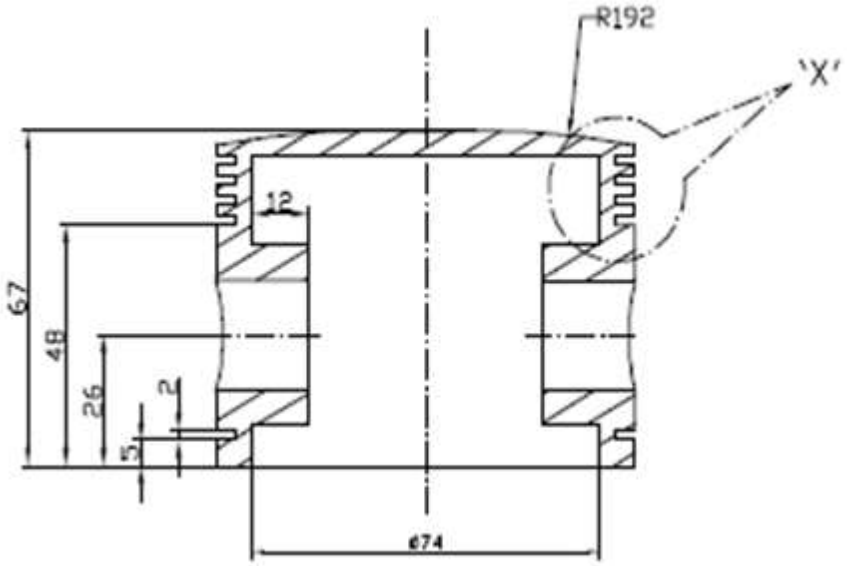

Figure 6.48: Dimension of piston

6.7 Summary of the chapter

In this *chapter* of the thesis, a methodology for improving part strength of the FDM and PolyJet printed component was presented. For FDM process, a high strength reinforcement material is placed between the ABS and PLA material. In this study, effects of reinforcement of PETG material on ultimate tensile strength of ABS and PLA materials have been experimentally investigated. Computational analysis was also carried out to validate the experimental results. It was depicted through surface morphology that components fabricated along the flat orientation have less defects as compared to edge orientation. Unidirectional reinforcement of PETG material has improved the tensile strength of ABS material by about *70%*, and strength of PLA material was improved by about *8%*. From Figure6.16 it can be concluded that computational results were a close approximation to the experimental results. However, computational results were slightly more as compared to experimental results which may be due to the presence of void and air gap between the layers of fabricated samples.

Further, the effect of process parameters viz., raster angle, orientation and type of surface finish on fracture strength, elastic modulus and percentage elongation of the component manufactured by PolyJet process were evaluated. It was observed that ultimate tensile strength was found to be maximum of *26.87* MPa corresponding to process parameters raster angle *0°*, orientation flat and glossy finish surface type. The value of elastic modulus was found to be maximum *2891.58* MPa corresponding to process parameter raster angle *90°*, flat orientation and glossy finish surface. The mechanical properties of the PolyJet component significantly changed on variation of process parameter. At the optimum level of process parameter true strain and plastic strain and true stress were also evaluated. The experimental value of plastic strain was validated through FEM software ABAQUS. It has been concluded that the computational investigation of plastic strain was the close approximation of the experimental results.

In the last part of this chapter, a control methodology for the clearance analysis between the matting part was discussed. It was observed that the shrinkage phenomena in the solid part and hollow section were different. The amount of shrinkage in the hollow part was found to be more as compared to the solid section.

Chapter 7
Conclusions and Future Directions

Chapter 7
Conclusions and Future Directions

7.1 Conclusions

This thesis has presented an experimental and computational investigation of the effect of various design process variables on the quality of component fabricated through FDM and PolyJet process. In this work, a comparative study of FDM and PolyJet printed component was carried out. Further,effect of process variables on flatness, cylindricity, linear and radial dimension and IT grade of the components fabricated through MakerBot Replicator-2 (FDM) printer were analysed. A multi-objective optimisation technique was successfully employed to obtain the best level of parameters. Moreover, influence of PolyJet process variables on DA, flatness andSR were investigated. Methodology for improving part strength of the FDM and PolyJet printed component were also presented. Control methodology for clearance analysis between the mating components was discussed.

Chapter 1 of the thesis highlighted about the motivation behind this research work, development of various rapid prototyping technology, classification & working principle of various RP processes. Engineering and medical application of RP technology were also discussed. Further, the contribution of thesis and thesis scope has been discussed. In *Chapter 2,* an overview of research workcarried out by various researchers related to form errors and mechanical property were highlighted. The significantfinding of the literature review were as follows:

- Selection of process parameters plays avital role in the mechanical behaviour of all rapid prototyping technology. Before printing, one should take care of the optimum process parameter setting for the selected printer.

- From the reported work, it was revealed that the significant attention of the researchers was to explore the tensile strength, impact strength and elastic modulus of the component only. However, less work has been reported related to other mechanical properties like stiffness, creep deformation, fatigue and hardness etc.
- It was observed that PolyJet technology was better than other RP technology concerning mechanical properties and form error. However, it is less in use due to high material cost. Hence, more work is needed to develop new low-cost material suitable for PolyJet technique.
- Researchers have mainly focused on observing the surface roughness and dimensional accuracy. However, very less work has been reported in regards to other critical form errors like flatness, cylindricity and perpendicularity of the component.
- Most of the research work was carried out by considering one response factor at a time. However, it was noticed that the optimum process parameter for different response factors were different. Hence, multi-objective optimisation technique will be more suitable for optimising multiple response factors at a time.
- The demand of RP technology in medical field has increased very rapidly due to its capability to prepare physical model directly from the CT scan or MRI data. Reported work revealed that medical model generated through RP has better DA than other manufacturing methods.
- In the case of mould design, RT has significantly shortened the lead time of the product development cycle.

Chapter 3 presented the comparative study of FDM and PolyJet technology. In this study, a prototype automotive component (connecting rod) was printed by both the technology. Objet30 printer was used for the manufacturing of prototype part by PolyJet technique.MakerBot Replicator-2 and Ultimaker were used to fabricate component through the FDM process. Components were fabricated at the optimum levels of process parameter of the printer. Comparisons were carried out based on dimensional accuracy, flatness, cylindricity, roundness, surface roughness and cost of the component. The significant finding of this research work is illustrated below.

- The average percentage error in DA along XY plane for printers Objet30, Ultimaker and MakerBot were found to be *0.99%, 1.69%* and *1.63%* respectively. However, Objet30 had minimum percentage error along the XY plane.
- The average percentage error in DA along YZ plane for printers Objet30, Ultimaker andMakerBot were found to be *2.24%, 1.56%* and MakerBot *1.11 %*. MakerBot had got minimum percentage error along the YZ plane.
- In the case of radial dimension, average percentage error of DA forObjet30, Ultimaker and MakerBot printer was *0.53%, 0.92%* and *1.75%*.
- Average percentage error in circular dimension of Objet30, Ultimaker and MakerBotprinter was obtained to be *0.74%, 2.34%* and *1.86%*.
- Component generated through PolyJet technology (Objet30) had minimum form error. The measured value of form errors for Objet-30 was roundness (*0.0686* mm), cylindricity (*0.0001* mm) and flatness (*0.1630* mm).

Chapter 4 of the thesis has elucidated the effect of FDM process variables, i.e. layer thickness, infill pattern, orientation and infill density on the dimensional accuracy,

flatness and cylindricity. Experiments were design based on Taguchi's theory. A regression models were developed for the flatness, cylindricity, percentage error in the linear dimension and percentage error in the radial dimension. The developed regression models were fitted within the CI of *95%*. It was observed that the optimum level of process parameters for the response variables were different. A multi-objective optimisation technique based on the 'Utility theory' was successfully applied to obtain the best level of process variables in terms of FDM process variables. The significant findings of the work carried out are demonstrated below.

- Infill density, orientation and layerheight were the most significant process parameters for the flatness. However, infill pattern had less significance on the flatness.
- From the (S/N) analysis for the flatness, it was found that layer thickness *300* µm, infill pattern (Moroccan star fill), orientation (flat) and infill density (*20%*) were the optimal process parameters.
- The optimum conditions of process parameters for cylindricity were layer thickness (*100 µm*), infill pattern (linear), orientation (flat) and infill density (*20 %*).
- The empirical models developed for the DA, flatness and cylindricity was adequate in the range of *95%* of confidence interval.
- The optimum conditions of the process parameters for DA, flatness and cylindricity were different. Multi-objective optimisation (utility theory) was successfully employed to find out the best level of process parameter.
- The best condition for the DA, flatness and cylindricity were layer thickness (100 µm), infill pattern (linear), orientation (inclined at 45°) and density (*20 %*).

- International tolerance grades (IT-grades) were also calculated, and it was found that IT grades are consistent. The higher IT grades IT13 and IT14 indicates that RP FDM products have high deviation from its target value.

Chapter 5 of the thesis has shown the effect of PolyJet process parameters on flatness, dimensional accuracy and surface roughness of the component. As Objet30 machine was considered to fabricate the specimen for tensile test as per ASTMD638 standard. Flatness and dimensional accuracy were measured by using the CONTURA G-2 coordinate measuring machine. SR of the fabricated samples was measured through MicroXAM-100 3D optical surface profiler. In this study, all the SR parameters, i.e. R_a, R_p, R_v, R_t and R_q, were measured. The process parameters used in these investigations were raster angle, orientation and surface type. A regression model for the surface roughness parameters R_a, R_z and R_q, flatness and dimensional accuracy in terms of PolyJet process parameters were developed. The developed model was good enough to forecast the SR value, flatness and DA at the level of *95%* CI within the experimental domain.Experimental results can be concluded as follows:

- Effect of orientation on surface roughness parameter R_a was the main influencing process parameter. Glossy surface had produced abetter surface finish in comparison to matte surface.
- For the SR parameter R_q, the regression model was significant within the CI of *90 %*.
- The optimum condition of process parameters for the roughness R_a, R_q and $R_z$were raster angle (90°), orientation (flat) and surface type (glossy).

- In the case of DA, average percentage error obtained along the length, width, and thickness of the specimen was *0.13%, 1.76%* and *9.97%* respectively. The percentage error in DA along the length and the width of specimen were within the range of manual provided by the printer developer.
- Effect of orientation was the most significant process parameter for DA along with thickness of the specimen. However, it was found that surface type was insignificant process parameter. Derived mathematical model for DA was significant after neglecting the insignificant process parameter.
- It was observed that the flatness was mainly affected by process parameter orientation. Regression model of flatness was sufficient within the range of *95%* CI.
- Results of the confirmation test for the surface roughness parameter R_a, DA and flatness had revealed that the developed model was adequate to predict the response for the process parameter.

Sixth chapter of the thesis has investigated an experimental and computational methodology for improving part strength of the FDM and PolyJetcomponent. In the analysis of FDM component,the effect of unidirectional reinforcement of PETG material on ultimate tensile strength of ABS and PLA material was evaluated.

- It was depicted through surface morphology that components fabricated along the flat orientation have less defects as compared to edge orientation.
- Owing to unidirectional reinforcement of high strength PETG material, tensile strength of ABS and PLA material had significantly improved.

- Unidirectional reinforcement of PETG material had improved the tensile strength of ABS material by *70%*, and strength of PLA material was improved by *8%*.
- It was observed that the results of computational analysis for the Von Mises stresses were close to the fracture strength of the experimental results. It can be concluded that the FEM results were close approximation of the experimental results.
- However, computational results were slightly more as compared to experimental results. This may be due to the presence of voids or air gap between the layers of fabricated samples.

Effect of PolyJet process parameter on elastic modulus, percentage elongation and fracture strength on the RGD840 material were experimentally investigated. Also, true stress, true strain and plastic strain were experimentally investigated. Computational investigation of plastic strain was also carried out by using ABAQUS software to validate the experimental results. The major highlights of this research work are given below:

- Experimental investigation of the effect of process parameters on mechanical properties, i.e. tensile strength and modulus of elasticity were investigated.
- The value of elastic modulus was found to be maximum of *2.65* GPa at process parameter, i.e. flat orientation, glossy surface and *0°* raster angle.
- The value of elastic modulus was found to be minimum of 1.*878* GPa corresponding to process parameter level on-edge orientation, glossy finish and *0°* orientation.

- The value of fracture strength was found to be maximum about *26.87* MPa corresponding to process parameter flat orientation, glossy surfaceand *0°* orientation.
- Corresponding to the optimum level of process parameter of fracture strength, plastic strength was also investigated experimentally.
- Computational analysis of plastic strain was carried out by using ABAQUS software to validate the experimental result.
- Results depicted that FEA results of plastic strain were close approximation to the experimental results.

Finally, a controlled methodology for clearance analysis between the matting components was also discussed. For the clearance approximation, mathematical model suggested by the researcher for shrinkage allowance were used for the calculation of clearance between matting components. From the literature, it was found that the shrinkage phenomenon in RP technology depends on the number of variables like process parameters, material, geometry of component etc.

7.2 Future directions

In this thesis, an effort was made to find out the optimum selection of process parameters for the FDM and PolyJet process to manufacture automotive components. However, these processes were limited to the prototyping and concept proof only. The future directions in the area of rapid prototyping are discussed below.

- Recently some of the 3D printers can fabricate the metallic part via 3D printing, which can be experimentally tested or utilisedas an end-use product.

- In present work, the effect of unidirectional reinforcement on tensile strength of the ABS and PLA material was carried out. However, presented methodology can be applied to the other biodegradable materials in future.
- A mathematical model for the DA, SR and flatness was developed for the FDM and PolyJet process. These models were valid within the range of selected process parameters. However, these response factors also depend on some other process variables. The presented methodology can be applied to include other process variables to obtain a more holistic model.
- Methodology presented for evaluation of true stress, true strain and plastic strain can be used for the other materials.
- For the numerical simulation of plastic strain, it was assumed that material is isotropic. However, orthotropic or anisotropic behaviour needs to be simulated.
- Ceramic particles and agro waste can be used as a reinforcement to improve the tensile strength and hardness of the fabricated RP component.

References

References

[1] Senthilkumaran, K., Pandey, P. M., Rao P.M.V. (2012), Statistical modeling and minimization of form error in SLS prototyping. *Rapid Prototyping Journal*. 18(1), 38 – 48.

[2] World Economic Forum (WEF) (2018), Global manufacturing index January.

[3] Global Manufacturing Competitiveness Index, 2016.

[4] Keo, C.C., Su, S. J. (2013), A simple method for improving surface quality of rapid prototype. *Indian journal of engineering & material science* 20, 465-470.

[5] Keo, C. C., Shi, Z. S. (2012), Fabrication of high precision silicon rubber mold for replacing wax patterns of cylinder heads. *Indian journal of engineering & material science*, 19, 157- 162.

[6] Melenka, G. W., Schofield, J. S., Dawson, Jonathon, R., Carey, J.P. (2016), Evaluation of dimensional accuracy and material properties of the MakerBot 3D desktop printer. *Rapid Prototyping Journal*, 21(5), 618 – 627.

[7] Narang, R., Chhabra, D. (2017), Analysis of process parameters of fused deposition modeling (FDM) technique. *International Journal on Future Revolution in Computer Science & Communication Engineering*, 3 (10), 41-48.

[8] Paul, R., Paul, S., (2015), Optimization of layered manufacturing process for reducing form errors with minimal support structures. *Journal of Manufacturing Systems*, 36, 231-243.

[9] Chen, Y. (2001), Computer-aided design for rapid tooling, methods for mold design and design-for-manufacturing. Ph.D. Thesis 56-61.

[10] Zoran, A. (2015), The 3D printed flute, digital fabrication and design of musical instruments. *Journal of New Music Research*, 40(4), 379-387.

[11] Lee, K. H., Woo. H. (2000), Direct integration of reverse engineering and rapid prototyping. *Computers & Industrial Engineering*, 38, 21- 38.

[12] Perinka, N., Kim, C. H., Kaplanova, M., Bonnassieux, Y. (2013), Preparation and characterization of thin conductive polymer films on the base of PEDOT,PSS by ink-jet printing. *Physics Procedia*, 44, 120 – 129.

[13] Kechagias, J. (2007), An experimental investigation of the surface roughness of parts produced by LOM process. *Rapid Prototyping Journal*, 13(1),17 – 22.

[14] Lusic, M., Schneider, K., Hornfeck, R. (2016), A case study on the capability of rapid tooling thermoplastic laminating moulds for manufacturing of CFRP components in autoclaves. *Procedia CIRP*, 50, 390 – 395.

[15] Afonso, D., Pires, L., Sous, R.A.D., Torcato, R. (2017), Direct rapid tooling for polymer processing using sheet metal tools. *Procedia Manufacturing*, 13, 102–108.

[16] Noble, J., Walczak, K., Dornfeld, D. (2014), Rapid tooling injection molded prototypes, a case study in artificial photosynthesis technology. *Procedia CIRP*, 14, 251 – 256.

[17] Rahmati, S., Dickens, P. (2007), Rapid tooling analysis of Stereolithography injection mould tooling. *International Journal of Machine Tools & Manufacture*, 47, 740–747.

[18] Ding,Y., Lan, H., Hong, J., Wu, D. (2004), An integrated manufacturing system for rapid tooling based on rapid prototyping, *Robotics and Computer-Integrated Manufacturing*, 281–288.

[19] Jiang, J., Xun, U., Stringer. J. (2019), Effect of Extrusion temperature on Printable threshold Overhang in additive manufacturing, 52nd CIRP Conference on Manufacturing Systems. *Procedia CIRP*, 81, 1376-1381.

[20] Chen, H., Gu, D., Xiong, J., Xia, M. (2017), Improving additive manufacturing processability of hard-to-process overhanging structure by selective laser melting. *Journal of Materials Processing Technology*, 250, 99-108.

[21] Allaire, G., Dapogny, C., Estevez, R., Faure, A., Michailidis, G. (2017), Structural optimization under overhang constraints imposed by additive manufacturing technologies. *Journal of Computational Physics*, 351, 295-328.

[22] VanKoevering, K.K., Morrison, R.J., Prabhu, S.P, Torres, M.F., Mychaliska, G.B., Treadwell, M.C., Hollister, S.J., Green, G.E. (2015), Antenatal three-dimensional printing of aberrant facial anatomy, *Pediatrics*,136, 1382-1385.

[23] Durfee, W. K., Iaizzo, P.A. (2019), Medical Applications of 3D Printing, Engineering in Medicine, *Chapter 21*, 527-543.

[24] Santis, R.D., Gloria, A., Russo,T., Ronca, A., Amora, U.D., Negri,G., Ronca, D., Ambrosio, L., (2016), Viscoelastic properties of rapid prototyped magnetic nanocomposite scaffolds for osteochondral tissue regeneration. *The second CIRP conference on biomanufacturing, Procedia CIRP*, 49, 76 – 82.

[25] Nizam, A., Gopal, R.N., Naing, L., Hakim, A.B., Samsudin, A.R. (2006), Dimensional Accuracy of the Skull Models Produced by Rapid Prototyping Technology Using Stereolithography Apparatus, *Archives of Orofacial Sciences*, 1, 60-66.

[26] Martínez-Vázquez, F.J., Cabañas, M.V., Paris, J.L., Lozano, D., Vallet-Regí, M. (2015), Fabrication of novel Si-doped Hydroxyapatite/Gelatine scaffolds by rapid prototyping for drug delivery and bone regeneration. *Acta Biomaterialia*, 15, 200-209.

[27] Kanazawa, M., Minakuchi, S. (2012), Evaluation of a complete denture trial method applying rapid prototyping, *Dental Materials Journal*, 31(1), 40–46.

[28] Bustamante, S., Bose, S., Bishop, P., Klatte, R., Norris, F. (2014), Novel Application of Rapid Prototyping for Simulation of Bronchoscopic Anatomy. *Journal of Cardiothoracic and Vascular Anesthesia*, 28(4), 1122-1125.

[29] Boyer, C.J., Ballard, D. H., Weisman, J.A., Hurst, S., McGee, D. J., Mills, D. K., Woerner, J.E., Jammalamadaka, U., Tappa, K., Alexander, J.S. (2018), Three-Dimensional Printing Antimicrobial and Radiopaque Constructs. *3D Printing and Additive Manufacturing*, 5(1), 29-35.

[30] Zopf, D.A., Hollister, S.J., Nelson, M.E., Ohye, R.G., Green, G.E. (2013), Bioresorbable airway splint created with a three-dimensional printer. *The New England Journal of Medicine*, 368, 2043-2045.

[31] Salmi, M., Paloheimo, K.S., Tuomi, J., Wolff, J., Makitie, A. (2013), Accuracy of medical models made by additive manufacturing (rapid manufacturing). *Journal of Cranio-Maxillo-Facial Surgery*, 41, 603-609.

[32] Liu,W., Wang, D., Huang, J., Wei, Y., Xiong, J., Zhu,W., Duan, L., Chen, J., Sun, R., Wang, D. (2017), Low-temperature deposition manufacturing, A novel and promising rapid prototyping technology for the fabrication of tissue-engineered scaffold. *Materials Science and Engineering C*, 70, 976–982.

[33] Kumar, K., Kumar, G.S. (2015), An experimental and theoretical investigation of surface roughness of poly-jet printed parts. *Virtual and Physical Prototyping*, 10(1), 23–34.

[34] Ahna, D., Kweon, J.H., Choi, J., Lee, S. (2012), Quantification of surface roughness of parts processed by laminated object manufacturing, *Journal of Materials Processing Technology*, 212, 339– 346.

[35] Kechagias, J.(2007), An experimental investigation of the surface roughness of parts produced by LOM process, *Rapid Prototyping Journal*, 13(1),17 – 22.

[36] Galantucci, L.M., Lavecchia, F., Percoco, G. (2009), Experimental study aiming to enhance the surface finish of fused deposition modeled parts. *CIRP Annals - Manufacturing Technology*, 58,189–192.

[37] Galantucci, L.M., Lavecchia, F., Percoco, G. (2010), Quantitative analysis of a chemical treatment to reduce roughness of parts fabricated using fused deposition modelling, *CIRP Annals - Manufacturing Technology*, 59 , 247–250.

[38] Guerra, M.G., Volpone, C., Galantucci, L.M., Percoco, G. (2018), Photogrammetric measurements of 3D printed microfluidic devices, *Additive Manufacturing*, 21, 53–62.

[39] Nigel, J., Kent, L., Jolivet, P.N., Dermot, B. (2017), An evaluation of components manufactured from a range of materials, fabricated using PolyJet technology. *Advances in Materials and Processing Technologies*.3(3), 318-329

[40] Sachdeva, A., Singh, S., Sharma,V.S (2013), Investigating surface roughness of parts produced by SLS process. *Int J Adv Manuf Technol*, 64, 1505–1516.

[41] Singh, J., Singh, R., Singh, H., (2017), Experimental investigations for dimensional accuracy and surface finish of polyurethane prototypes fabricated by indirect rapid tooling, a case study. *Prog Addit Manuf*, 2, 85–97.

[42] Shi, D., Gibson, I. (1999), Improving surface quality of selective laser sintered rapid prototype parts using robotic finishing. *Proc Instn Mech Engrs Part B.* 214, 197-203.

[43] Satyanarayana, B., Prakash K. (2015), Component replication using 3D printing technology. Procedia Materials Science.2015, 10,263 – 269.

[44] Lee, W.C., Wei, W.C., Chung, S.C. (2014), Development of a hybrid rapid prototyping system using low-cost fused deposition modeling and five-axis machining, *Journal of Materials Processing Technology*, 214, 2366–2374.

[45] Pohit, G., Kumar, K., (2012), Virtual manufacturing of various types of gears and validation of the technique using rapid prototype. Virtual and Physical Prototyping, 7(2),153-171.

[46] Senthilkumaran, K., Pandey, P.M., Rao, P. V. M., (2008), Shrinkage compensation along single direction dexel space for improving accuracy in selective laser sintering. Automation Science and Engineering (CASE). IEEE International Conference, DOI: 10.1109/COASE.2008.4626479 .

[47] Jain, P., Kuthe, A.M. (2013), Feasibility study of manufacturing using rapid prototyping, FDM Approach. *Procedia Engineering* , 63,4-11.

[48] Garrett, W., Melenka, J. S., Schofield, M., R. Dawson, J. P. C. (2015), Evaluation of dimensional accuracy and material properties of the MakerBot 3D desktop printer. *Rapid Prototyping Journal*, 21 (5), 618 – 627.

[49] Singh, R. (2011), Process capability study of polyjet printing for plastic components. *Journal of Mechanical Science and Technology,* 25(4), 1011-1015.

[50] Panda, B.N., Bahubalendruni, M.V.A.R., Biswal, B. B., Leite, M.(2016) A CAD-based approach for measuring volumetric error in layered manufacturing. *Proc IMechE Part C, J Mechanical Engineering Science. 231(13), 2398–2406*

[51] Brajlih, T., Valentan, B., Balic, J., Drstvensek, I. (2011), Speed and accuracy evaluation of additive manufacturing machines. *Rapid Prototyping Journal* , 17(1), 64 – 75.

[52] Dimitrov, D., Van, Schreve, W.K., Beer, N.D. (2014), Investigating the achievable accuracy of three dimensional printing. *Rapid Prototyping Journal*, 12(1) , 42 – 52.

[53] Chang, D.Y., Huang, B.H. (2011), Studies on profile error and extruding aperture for the RP parts using the fused deposition modeling process. *Int J Adv Manuf Technol*, 53,1027–1037.

[54] Chaudhari, M., Jogi, B.F., Pawade, R.S. (2018), Comparative study of part characteristics built using additive manufacturing (FDM). *Procedia Manufacturing*, 20, 73-78.

[55] Knoop, F., Schoeppner, V. (2017) , Geometrical accuracy of holes and cylinders manufactured with fused deposition modeling. Solid Freeform Fabrication 2017, *Proceedings of the 28th Annual International Solid Freeform Fabrication Symposium – An Additive Manufacturing Conference.*

[56] Saqib, S., Urbanic, J., (2011), An Experimental Study to Determine Geometric and Dimensional Accuracy Impact Factors for Fused Deposition Modelled Parts. *In: ElMaraghy H. (eds) Enabling Manufacturing Competitiveness and Economic Sustainability. Springer, Berlin, Heidelberg.* DOI https://doi.org/10. 1007/978-3-642-23860-4_48

[57] Durgun, I., Ertan , R. (2014), Experimental investigation of FDM process for improvement of mechanical properties and production cost. *Rapid Prototyping Journal*, 20 (3), 228 – 235.

[58] Bellini, A., Guceri, S. (2003), Mechanical characterization of parts fabricated using fused deposition modeling. *Rapid Prototyping Journal*, 9(4), 252–264.

[59] Cantrell, J., Sean, R., Damiani, D., Gurnani, R., DiSandro, L., Anton, J., Young, A., Jerez, A., Steinbach, D., Kroese, C., Ifju, P. (2016), Experimental Characterization of the Mechanical Properties of 3D-Printed ABS and Polycarbonate Parts, *Rapid Prototyping Journal*,. 23(4), 811-824.

[60] Mohamed, O.A., Masooda, S.H., Jahar Lal Bhowmik, 2017, Process parameter optimization of viscoelastic properties of FDM manufactured parts using response surface methodology. *Materials Today, Proceedings* 4, 8250–8259.

[61] Raut, S., Jatti, V. K. S., Khedkar, N. K., Singh, T .P. (2014), Investigation of the effect of built orientation on mechanical properties and total cost of FDM parts. *Procedia Materials Science.* 6, 1625 – 1630.

[62] Ravari, M. R. K., Kadkhodaei, M., Badrossamay, M., Rezaei, R. (2014), Numerical investigation on mechanical properties of cellular lattice structures fabricated by fused deposition Modeling. *International Journal of Mechanical Sciences,* 88, 154-161.

[63] Onwubolu, G.C., Rayegani, F. (2014),Characterization and Optimization of Mechanical Properties of ABS Parts Manufactured by the Fused Deposition Modelling Process. *International Journal of Manufacturing Engineering*. http,//dx.doi.org/10.1155/2014/598531.

[64] Dawoud, M., Taha, Ebeid, S,J. (2016), Mechanical behaviour of ABS, An experimental study using FDM and injection moulding techniques. Journal of Manufacturing Processes, 21, 39–45.

[65] Wu, W., Geng, P., Li, G., Zhao, D., Zhang, H., Zhao, J.(2015), Influence of Layer Thickness and Raster Angle on the Mechanical Properties of 3D-Printed PEEK and a Comparative Mechanical Study between PEEK and ABS, *Material*, 8, 5834-5846.

[66] Mohamed, O. A., Masood, S. H., Bhowmik, J. L.(2017), Experimental investigation of time-dependent mechanical properties of PCABS prototypes processed by FDM additive manufacturing process. *Materials Letters*, 193, 58-62.

[67] Espin, M. D., Forcada, J. M. P., Granada, A., Garcia, A., Llumà, J., Borros, S., Reyes, G. (2015), Mechanical property characterization and simulation of fused deposition modeling Polycarbonate parts. *Materials & Design* 83, 670–677.

[68] Espin, M.D., Borros, S., Agullo, N., Granada, N.A.G., Reyes, G. (2014), Influence of Building Parameters on the Dynamic Mechanical Properties of Polycarbonate Fused Deposition Modeling Parts. *3D Printing Mary Ann Liebert, INC,* 1(2),70-77.

[69] Szykiedans, K., Credo, W., (2016), Mechanical properties of FDM and SLA low-cost 3-D prints. *Procedia Engineering*, 136, 257 – 262.

[70] Chacon, J.M., Caminero , M.A., Garcıa-Plaza, E., Nunez, P.J. (2017), Additive manufacturing of PLA structures using fused deposition modelling, effect of process parameters on mechanical properties and their optimal selection. *Materials and Design, 124,143-157*

[71] Anderson, I. (2017), Mechanical Properties of Specimens 3D Printed with Virgin and Recycled Polylactic Acid. *3D Printing and Additive Manufacturing*, 4(2), 110-115.

[72] Vicente, M.F., Calle, W., Ferrandiz, S., Conejero, A., (2016) , Effect of Infill Parameters on Tensile Mechanical Behavior in Desktop 3D Printing. *3D Printing and Additive Manufacturing*, 3(3)183-192.

[73] Kashdan, L., Seepersad, C.C., Haberman, M., Wilson, P.S. (2012), Design, fabrication, and evaluation of negative stiffness elements using SLS. *Rapid Prototyping Journal*, 18 (3) 194–200.

[74] Athreya, S.R.,Kalaitzidou, K., Das, S. (2011), Mechanical and microstructural properties of Nylon-12/carbon black composites, Selective laser sintering versus melt compounding and injection molding. *Composites Science and Technology*, 71, 506–510.

[75] Bassoli, E., Gatto, A. (2011), Joining mechanisms and mechanical properties of PA composites obtained by selective laser sintering. *Rapid Prototyping Journal*, 18 (2), 100 – 108.

[76] Spierings, A.B., Herres, N., Levy, G. (2011), Influence of the particle size distribution on surface quality and mechanical properties in AM steel parts, *Rapid Prototyping Journal*, 17 (3) , 195 – 202.

[77] Sudarmadji, N., Tan, J.Y., Leong, K.F., Chua, C.K., Loh, Y.T. (2011), Investigation of the mechanical properties and porosity relationships in selective laser-sintered polyhedral for functionally graded scaffolds. *Acta Biomaterialia*, 7 , 530–537.

[78] Starr, T. L., Gornet, T.J., Usher, J. S. (2011), The effect of process conditions on mechanical properties of laser-sintered nylon. *Rapid Prototyping Journal*, 17(6) , 418–423.

[79] Song, Bo., Dong, S., Zhang, B., Liao, H., Coddet, C. (2012), Effects of processing parameters on microstructure and mechanical property of selective laser melted Ti6Al4V. *Materials and Design*, 35, 120–125.

[80] Majewski, C., Zarringhalam, H., Hopkinson, N. (2008), Effect of the degree of particle melt on mechanical properties in selective laser-sintered Nylon-12 parts. Institution of Mechanical Engineers, 222 (9), 1055–1064.

[81] Shi, Y., Wang, Y., Chen, J., Huang, S. (2006), Experimental Investigation into the Selective Laser Sintering of High-Impact Polystyrene. *Wiley InterScience*, 108, 535–540.

[82] Zheng, H., Zhang, J., Lu, S., Wang, G., Xu, Z., (2006), Effect of core–shell composite particles on the sintering behaviour and properties of nano-Al_2O_3/polystyrene composite prepared by SLS. *Materials Letters*, 60 , 1219–1223.

[83] Jain, P.K., Pandey, P.M., Rao, P.M.V. (2008), Experimental investigations for improving part strength in selective laser sintering. *Virtual and Physical Prototyping* , 3(3),177-188.

[84] Farzadi, A., Waran, V., Solati-Hashjin, M., Rahman, Z. A. A A., Asadia, M., Osmana, N. A. A. (2015), Effect of layer printing delay on mechanical properties and dimensional accuracy of 3D printed porous prototypes in bone tissue engineering. *Ceramics International* , 41,8320–8330.

[85] Santos, E.C., Osakada, K., Shiomi, M., Kitamural, Y., Abe, f. (2004), Microstructure and mechanical properties of pure titanium models fabricated by selective laser melting. *Proceedings of the Institution of Mechanical Engineers, Part C, Journal of Mechanical Engineering Science*, 218(7), 711-719.

[86] Sugavaneswaran, M., Arumaikkannu, G. (2015), Analytical and experimental investigation on elastic modulus of reinforced additive manufactured structure. *Materials and Design*, 66, 29–36.

[87] Moore, J.P., Williams, C. B. (2015), Fatigue properties of parts printed by Polyjet material jetting. *Rapid Prototyping Journal* 21(6) , 675 – 685.

[88] Blanco, D., Fernandez, P., Noriega, A. (2014), Nonisotropic experimental characterization of the relaxation modulus for PolyJet manufactured parts. *Materials Research Society* , 29(17),1876-1882.

[89] Cazon, A., Morer, P., Matey, L. (2014), PolyJet technology for product prototyping, Tensile strength and surface roughness properties. *Proc IMechE Part B, J Engineering Manufacture*, 228(12), 1664–1675.

[90] Yapa, Y.L., Yeong, W.Y. (2005), Shape recovery effect of 3D printed polymeric honeycomb. *Virtual and Physical Prototyping*, 10 (2), 91–99.

[91] Chockalingam, K., Jawahar, N. (2006), Influence of layer thickness on mechanical properties in stereolithography. *Rapid Prototyping Journal*, 12(2) , 106 – 113.

[92] Mansour, S., Gilbert, M., Hague, R. (2007), A study of the impact of short-term ageing on the mechanical properties of a stereolithography resin. *Materials Science and Engineering A* 447 , 277–284.

[93] Sabree, I., Gough, J.E., Derby, B. (2015) , Mechanical properties of porous ceramic scaffolds, Influence of internal dimensions. *Ceramics International*, 41(7), 8425-8432.

[94] Alharbi, N., Osman, R., Wismeijer, D. (2016), Effects of build direction on the mechanical properties of 3D-printed complete coverage interim dental restorations. *The journal of prosthetic dentistry*, 115 (6),760-767.

[95] Weng, Z., Zhou, Y., Lin, W., Senthil, T., Wu, Lixin. (2016), Structure-Property Relationship of Nano Enhanced Stereolithography Resin for Desktop SLA 3D Printer. Composite Part A, *Applied Science and Manufacturing*, 88, 234-242.

[96] Wu, Z., Liu, W., Wu, H., Huang, R., He, R., Jiang, Q., Chen, Y., Ji, X., Tian, Z., Wu, S. (2018), Research into the mechanical properties, sintering mechanism and microstructure evolution of Al2O3-ZrO2 composites fabricated by a stereolithography-based 3D printing method. *Materials Chemistry and Physics,* 207, 1-10.

[97] Vayrynen,V.O.E., Tanner, J., Vallittu, P. K. (2016), The anisotropicity of the flexural properties of an occlusal device material processed by stereolithography. *The Journal of Prosthetic Dentistry*, 116 (5), 811-817.

[98] Galeta, T., Raos, P., Stojsic, J., Paksi, I. (2016), Influence of structure on mechanical properties of 3D printed objects. *Procedia Engineering,* 149. 100 – 104.

[99] Rong-Ji, W., Xin-hua, L., Qing-ding, W., Lingling, W. (2009), Optimizing process parameters for selective laser sintering based on neural network and genetic algorithm. *Int J Adv Manuf Technol*, 42, 1035–1042.

[100] Sajan, N., John, T.D., Sivadasan, M., Singh, N. K. (2018), An investigation on circularity error of components processed on Fused Deposition Modeling (FDM). *Materials Today, Proceedings*, 5 , 1327–1334.

[101] Srivastava, M., Maheshwari, S., Kundra, T.K., Rathee, S., (2017), Multi-Response Optimization of Fused Deposition Modelling Process Parameters of ABS Using Response Surface Methodology (RSM)-Based Desirability Analysis. *Materials Today, Proceedings*,4, 1972–1977.

[102] Casalino, G., Campanelli, S.L., Contuzzi, N., Ludovico, A.D. (2015), Experimental investigation and statistical optimisation of the selective laser melting process of a maraging steel. *Optics & Laser Technology*, 65, 151–158.

[103] Calignano, F., (2014), Design optimization of supports for overhanging structures in aluminum and titanium alloys by selective laser melting. *Materials and Design*, 64, 203–213.

[104] Peng, A., Xiao, X., Yue, R. (2014), Process parameter optimization for fused deposition modelingusing response surface methodology combined with fuzzy inference system. *Int J Adv Manuf Technol*, 73, 87–100.

[105] Velu, R., Singamneni, R., (2015), Evaluation of the influences of process parameters while selective laser sintering PMMA powders. *Proc IMechE Part C, J Mechanical Engineering Science*, 229(4),603–613.

[106] Onwubolu, G.C., Rayegani, F. (2014), Characterization and Optimization of Mechanical Properties of ABS Parts Manufactured by the Fused Deposition Modelling Process. *International Journal of Manufacturing Engineering.* http,//dx.doi.org/10.1155/2014/598531

[107] Sood, A.K. (2011), optimization of process parameters in fused deposition modeling using weighted principal component analysis, *Journal of Advanced Manufacturing Systems*, 10(2), 241–259.

[108] Villalpando, L., Eiliata, H., Urbanic, R.J. (2014), An optimization approach for components built by fused deposition modeling with parametric internal structures. *Procedia CIRP*, 17, 800 – 805

[109] Wang, C.C., Lin, T.W., Hu, S.S. (2010), Optimizing the rapid prototyping process by integrating the Taguchi method with the Gray relational analysis. *Rapid Prototyping Journal*, 13(5) , 304–315.

[110] Vosniakos, G.C., Maroulis, T., Pantelis, D. (2007), A method for optimizing process parameters in layer-based rapid prototyping. *Proc. IMechE Part B, J. Engineering Manufacture*, 221, 1329-1340.

[111] Lee, B.H., Abdullah, J., Khan, Z.A. (2005), Optimization of rapid prototyping parameters for production of flexible ABS object. *Journal of Materials Processing Technology*, 169,54–61.

[112] Sood, A.K., Ohdar, R.K., Mahapatra, S.S. (2009), Improving dimensional accuracy of Fused Deposition Modelling processed part using grey Taguchi method. *Materials and Design*, 30, 4243–4252.

[113] Mahmood, S., Qureshi, A.J., Nazarbayev, D.T. (2018), Taguchi Based Process Optimization for Dimension and Tolerance Control for Fused Deposition Modelling. *Additive Manufacturing*, 21, 183-190.

[114] Aljohani, A., Desai, S.(2018), 3D Printing of Porous Scaffolds for Medical Applications. *American Journal of Engineering and Applied Sciences* , 11(3), 1076-1085.

[115] Jayadithya, R., Deekshith, B., Chaithnya, P.L., Rajyalakshmi, G. (2014), Multi Objective Optimization of WEDM through Tagchi Method and Utility Concept. *International Journal of Science and Applied Information Technology (IJSAIT)*, 3(4), 01 – 06.

[116] Senthilkumaran, K., Pandey, P.M., Rao, P.M.V. (2009), Influence of building strategies on the accuracy of parts in selective laser sintering, *Materials and Design*, 30, 2946–2954.

[117] Data Sulpt User's Manual stratasys @2015 Stratasys Direct, Inc.

[118] Cazon, A., Morer, P., Matey, L. (2014), Poly-jet technology for product prototyping, Tensile strength and surface roughness properties. *Proc IMechE Part B, J Engineering Manufacture*, 228(12), 1664–1675.

[119] Blanco, D., Fernandez, P., Noriega, A.(2014), Nonisotropic experimental characterization of the relaxation modulus for PolyJet manufactured parts. *Journal of Materials Research*, 29(17) 1876-1882 .

[120] Sosiati, H., Shofie, Y. A., Nugroho, A. W. (2018), Tensile Properties of Kenaf/E-glass Reinforced Hybrid Polypropylene (PP) Composites with Different Fiber Loading. *EVERGREEN Joint Journal of Novel Carbon Resource Sciences & Green Asia Strategy*, 05 (02),1-5.

[121] Gay, P., Blanco, D., Pelayo, F., Noriega, A., Fernández, P. (2015), Analysis of Factors Influencing the Mechanical Properties of Flat PolyJet Manufactured Parts. *Procedia Engineering*, 132, 70 - 77.

Publication from the Present Work

Publication from the Present Work

International Journals

1. **Nagendra Kumar Maurya**, Vikas Rastogi, Pushpendra Singh (2019), "Investigation of dimensional accuracy and international tolerance grades of 3D printed polycarbonate parts". *Materials Today: Proceedings*. https://doi.org/10.1016/j.matpr.2019.06.007

2. **Nagendra Kumar Maurya**, Vikas Rastogi , Pushpendra Singh (2019), "Experimental and Computational Investigation on Mechanical Properties of Reinforced Additive Manufactured Component" . *EVERGREEN Joint Journal of Novel Carbon Resource Sciences & Green Asia Strategy*, 06(03):207-214.

3. **Nagendra Kumar Maurya**, Vikas Rastogi , Pushpendra Singh (2019), "Comparative Study and Measurement of Form Errors for the Component Printed by FDM and PolyJet Process". *Instrumentation Mesure Métrologie,* 18(4): 353-359.

4. **Nagendra Kumar Maurya**, Vikas Rastogi , Pushpendra Singh (2018), "An Experimental Investigations for Improving Part Strength in Fused Deposition Modeling". *International Journal of Engineering & Technology, 7 (4.39):457-461.*

5. **Nagendra Kumar Maurya**, Vikas Rastogi , Pushpendra Singh, "An Overview of Mechanical Properties and Form Error in Rapid Prototyping". CIRP journal of manufacturing science and technology **(Minor Revision submitted).**

6. **Nagendra Kumar Maurya**, Vikas Rastogi , Pushpendra Singh, "Fabrication of Prototype Connecting rod of PLA plastic material using FDM Prototype Technology". *Indian journal of engineering & material science* **(Minor Revision submitted).**

7. **Nagendra Kumar Maurya**, Vikas Rastogi, Pushpendra Singh, "Effect of process parameters on surface roughness, dimensional accuracy and flatness of VeroBlue *RGD840* rigid opaque materials produced by polyjet". *Material testing* **(Under Review).**

8. **Nagendra Kumar Maurya**, Vikas Rastogi, Pushpendra Singh, "Feasibility Analysis of Manufacturing Using Rapid Prototyping : A Review". Annales de Chimie – Science des Materiaux **(Under Review).**

International Conferences

1. **Nagendra Kumar Maurya**, Vikas Rastogi, Pushpendra Singh, "Comparative Study of Various Types of 3D Printing & 3D Modelling of Automotive Component" Presented in 1st International Conference on New Frontiers in Engineering, Science & Technology 2018 (January 08-2018), New Delhi.

2. **Nagendra Kumar Maurya**, Vikas Rastogi, Pushpendra Singh, "Investigation of Dimensional Accuracy and International Tolerance Grades of 3D Printed Polycarbonate Parts". Presented in 2nd International Conference on computational and experimental methods in mechanical engineering (May 2019).